FOREWORD

This report was prepared by the University of Dayton Research Institute on Air Force Contract No. AF 33(616)-7838. This contract was initiated under Project No. 7381, "Materials Application," and Task No. 738103, "Materials Information Development, Collection, and Processing." The work was administered under the direction of the Air Force Materials Laboratory, Wright-Patterson Air Force Base, Ohio, with Lawrence N. Hjelm as the project engineer.

This report covers work conducted from February 1961 through January 1962.

The assistance and support of the AFML project engineer, L. N. Hjelm, throughout the contractual period is appreciated and hereby acknowledged.

ABSTRACT

A small arc-plasma-jet was suitably modified and utilized for the evaluation and screening of high temperature materials at heat flux levels ranging from 10 to 500 Btu/ft^2-sec. A "standard" evaluation procedure was employed to characterize a number of systems representing ablating, insulating, and heat sink type materials. Results of these tests are presented in terms of weight loss, density change, depth and volume of erosion, and front and back surface temperatures.

A metallographic analysis of coating failures in the XLR-99 thrust chamber of the X-15 research aircraft and the subsequent development of a thermal shock test with the plasma-jet for sprayed ceramic coatings are discussed. The results of an extensive evaluation of protective coatings and the field test verification of these results are presented.

Preliminary tests leading to the development of a dynamic oxidation test are discussed and the results of arc-plasma-jet tests of five silicide coatings on Mo-1/2% Ti are presented.

This technical documentary report has been reviewed and is approved.

W. P. Conrardy

W. P. CONRARDY, Chief
Materials Engineering Branch
Materials Applications Division
AF Materials Laboratory

TABLE OF CONTENTS

LIST OF FIGURES

LIST OF FIGURES (Cont'd)

LIST OF FIGURES (Cont'd)

LIST OF FIGURES (Cont'd)

LIST OF FIGURES (Cont'd)

LIST OF FIGURES (Cont'd)

LIST OF FIGURES (Cont'd)

LIST OF FIGURES (Cont'd)

LIST OF TABLES

LIST OF TABLES (Cont'd)

LIST OF TABLES (Cont'd)

SECTION 1

INTRODUCTION

The aerospace age has produced requirements for materials systems capable of service in extreme thermal environments in such typical applications as rocket nozzles, leading edges and nose caps. Many concepts of thermal protection and numerous materials systems have been developed and proposed for use in these areas.

A comprehensive evaluation of any materials system must include a study of the influence of variations in basic chemistry, differences in processing variables, and modifications of reinforcing or dispersed phases. To accomplish such an evaluation by full scale testing or in hyperthermal facilities capable of exact environmental simulation would be economically prohibitive. Fortunately the small arc-plasma-jet can, in many instances, provide realistic thermal simulation and has therefore found application as an environmental source for the rapid and economical preliminary evaluation and screening of experimental high temperature materials.

A 50 KW arc-plasma-jet was employed in this program to evaluate a number of materials systems. For the majority of these tests an evaluation procedure based upon the proposed standard screening test of the Refractory Composites Working Group was followed although, in certain phases of the program it was necessary to deviate from standard procedures to simulate a specific thermal environment. For example, in the evaluation of experimental coatings for the XLR-99 thrust chamber and the dynamic oxidation testing of refractory alloy coatings arc effluent composition, specimen geometry, thermal input and exposure time were selected to achieve, as closely as possible, anticipated service conditions.

A brief description of the arc-plasma-jet facility, a discussion of evaluation procedures, and the test results for a number of material systems tests are presented in this report.

Manuscript released by the authors March 1964 for publication as an RTD Technical Documentary Report.

SECTION 2

EQUIPMENT AND FACILITY

The arc-plasma facility utilized in the tests described in this report was a modified Plasmadyne Corporation Model L-40 Plasmatron with an N-4 head. Electrical power for the operation of this unit was supplied by four selenium rectifiers each rated at 12.5 KW maximum output and 70 volts open circuit potential. Suitable controls were provided for regulating the output power from these rectifiers at any desired level to a maximum of 50 KW.

The standard N-4 head supplied with the unit was modified to produce a 1/2 inch diameter discharge effluent of simulated air composed of 79% nitrogen and 21% oxygen by stabilizing the arc with water pumped nitrogen and introducing medical grade oxygen through a mixing chamber located downstream from the foot point of the arc. These gases were obtained from commercial sources in standard compressed gas cylinders and were regulated at the cylinder for delivery at 80 psig to a metering system comprised of a rotameter and a needle valve.

Untreated tap water, delivered at a pressure of 60 psig provided coolant to the entire system. The temperature rise of this coolant through the head and the individual components of the nozzle was measured with mercury-in-glass thermometers permanently installed in the coolant inlet and discharge lines.

A two station fixture, shown in Figure 1, which incorporated a cross-slider member, was used to introduce various measuring probes and test specimens into the discharge effluent. Probes and test specimens were clamped into holders which were interchangeable in either of the two slide positions. The fixture assembly was adjustable in the axial direction over a span of approximately nine inches.

A water cooled calorimeter, Figure 2, was utilized for measuring heat transfer rates from the arc effluent. The assembly consisted of a 1/2 inch diameter tube sealed at one end by a flat disc. By maintaining a steady flow of water across the inner face of this disc the rate of heat transfer through this surface was determined from a measurement of the coolant temperature rise and flow rate. To confine the heating by the arc effluent to the face of the calorimeter a water cooled guard ring was assembled around the tube. An air gap of 0.005 inches was maintained between the guard ring and the calorimeter to minimize heat transfer between the two elements. The body of the calorimeter was fabricated from phenolic reinforced with linen and carried thermocouple probes arranged in a differential circuit for the measurement of water temperature. The thermocouple probes consisted of ungrounded copper-constantan thermocouples insulated by MgO in 1/16 inch diameter stainless steel tubing.

A flat-faced pitot tube, Figure 3, was employed for measuring the stagnation pressure of the arc effluent. This pitot tube was a water cooled copper assembly with a 1/16 inch I.D. orifice. A 30 inch water manometer was used in conjunction with the pitot tube.

The facility was instrumented to provide continuous temperature-time histories of both front and back surfaces of specimens during test. A total radiation pyrometer was used to measure front surface temperature in the range of 1400° to 6000°F. Front surface temperature was also measured at periodic intervals during test with an optical pyrometer. Back surface temperature was sensed by either a contact thermocouple (Pt-Pt 13% Rh) spring loaded against the specimen, or by a two-color pyrometer. The output of both the total radiation pyrometer and the thermocouple were recorded on separate strip chart recorders.

During the contractual period, the power capability of the arc-plasma-jet facility was expanded to 100 KW to extend the range of attainable heat flux levels for materials evaluation studies beyond the present limit of 500 Btu/ft^2-sec. Sixteen Miller rectifiers rated at 12.5 KW maximum output and 70 volts open circuit potential were installed in four banks of four rectifiers each. The rectifiers in each bank were connected in parallel and the output of each bank connected in series. A Plasmadyne Corporation M-4 head, rated at 200 KW, was procured. A console containing controls and instruments necessary for operation of the unit was built and installed with provision for adding controls and recording equipment to monitor specimen surface temperature during test. This unit has been operated using water pumped nitrogen as the arc stabilizing gas. Stable operation was achieved over a range of power levels from 15 KW to 105 KW. Efficiency of the unit ranged from approximately 85% at low power levels to 62% at high levels.

A Plasmadyne Corporation SG-1 arc-plasma spray system was also procured during this period. It is anticipated that this unit, which is rated at 40 KW maximum input when operated on nitrogen gas, will be utilized in the application of coatings to test specimens, the fabrication of special experimental specimens, and as a rocket exhaust simulator for materials compatibility studies.

SECTION 3

STANDARD MATERIALS SCREENING TEST

A standardized high temperature materials screening test was proposed in December 1959 by a subcommittee of the Refractory Composites Working Group, of which the University of Dayton Research Institute is a member. It was intended that this test provide a unified approach to the preliminary screening of high temperature materials thereby establishing a common criterion for comparing test results and eliminating much duplication of testing among the various laboratories engaged in materials evaluation. The standardized test was proposed for use with a 50 KW arc-plasma-jet suitably modified to produce a 1/2 inch diameter effluent of simulated air. Test levels were selected as a function of heat flux to a specified cold wall calorimeter configuration and a flat plate measuring 2 x 2 x 1/2 inches was proposed as the standard specimen configuration. It was further proposed that tests be conducted with these samples oriented at 45° to the subsonic arc discharge to simulate flow over an aerodynamic surface. The materials screening test performed at the University of Dayton was developed to a major extent from the recommendations of the Refractory Composites Working Group.

Experimental Methods

Prior to the exposure of a test sample the properties of the arc effluent were determined from measurements of the following parameters:

a) Nitrogen and oxygen flow rate

b) Input power to the arc

c) Power losses to the coolant

d) Heat flux at the sample location

e) Stagnation pressure at the sample location.

From these measured values the following properties were calculated:

a) Effluent velocity at the sample

b) Effluent enthalpy at the nozzle exit

c) Effluent temperature at the nozzle exit.

Following this calibration procedure, samples which had previously been measured and weighed were introduced into the effluent for test. During test, the front and back surface temperatures of the sample were continuously recorded as a function of time. Front surface temperature was also monitored periodically with an optical pyrometer.

Immediately after test the calibration procedure was repeated as a

recheck of the initial measurements. Samples were photographed after test and the following physical measurements taken: depth and volume of erosion, density, and weight.

Details of the calibration, test, and sample measurement procedures are described in WADD TR 60-926 "Evaluation of Materials Systems for Use in Extreme Thermal Environments Utilizing an Arc-Plasma-Jet."

Results

Since many of the materials evaluated were of a proprietary nature only a general description of the material is presented with the test results and any reference to a specific manufacturer is by code letter.

The data of these tests are presented as a tabulation of the environmental test conditions and their effect upon each specimen. Supplementing these data are front and back surface temperature-time histories of each sample during test. The final front surface temperature reported in the tables was obtained with the optical pyrometer.

Unless otherwise noted, all tests were conducted in a simulated air effluent at a mass flow rate of 0.0082 lb/sec according to the following schedule:

Heat Flux (Btu/ft^2-sec)	Time (sec)
500	24
300	40
100	120

Manufacturer AC

Cork composition with a phenolic resin binder was evaluated at a heat flux of approximately 10 Btu/ft^2-sec. The specimens, consisting of 1/4 and 1/8 inch cork sheet bonded to 50 mil aluminum sheet, were evaluated in duplicate tests for exposure times sufficient to penetrate the cork. The results of these tests are shown in Table 1. To achieve the desired heat flux it was necessary to place the samples nearly six inches from the nozzle exit and operate the plasma-jet at its minimum stable power input. Since the normal nozzle to sample distance is 1-1/8 inches only those test parameters determined at the sample (stagnation pressure, effluent velocity, and heat flux) may be used in comparing these test results with other standard evaluations.

Thermal degradation was characterized by the formation of a lightly adherent char. Front surface temperatures were too low to be measured and therefore Figures 4 and 5 show only the back surface temperature history.

The cold wall heat flux reported for these tests is probably in error since the calorimeter utilized was designed for use in the 100 to 1000 Btu/ft^2-sec range and is rather insensitive to inputs below 50 Btu/ft^2-sec.

Manufacturer AD

A series of three foamed plastic materials designated A, B, and C were evaluated at 100 Btu/ft^2-sec. Test conditions and results are shown in Table 2. Since only one specimen of each type was available for evaluation, these results do not necessarily reflect the optimum test conditions. Even at this low heat flux level and short exposure time the performance of these three samples was poor. Front and back surface temperature-time histories are shown in Figures 6, 7, and 8. No back surface temperature was obtained for Sample A due to an instrumentation malfunction. The back surface temperature of Sample B remained low throughout the test as did the back surface temperature of Sample C until complete burn-through was imminent. Front surface temperatures were comparable and did not exhibit any unusual deviations.

Manufacturer C

Eight samples of a ZrB_2 . $MoSi_2$ composite from Manufacturer C were evaluated at heat fluxes of 500 and 100 Btu/ft^2-sec for exposures of 24 and 300 seconds respectively. Of the eight specimens, six were formed by hot pressing and two by a sintering process. Two of the hot pressed samples had a 5% BN addition. Two grades of silicon carbide, GRB and KT, were also evaluated to provide a base line for comparing the performance of the boride composites.

Test conditions and results for this evaluation are shown in Tables 3 through 6.

The hot pressed composites including those with BN experienced cracking failures during test. In general, the severity of these failures was directly proportional to both sample thickness, which ranged from 0.293 to 0.537 inches, and heat flux level. The most severe failure was the thermal shock failure of a 1/2 inch thick sample which shattered upon introduction into the plasma stream at 500 Btu/ft^2-sec and subsequently experienced some melting along a fracture line. Failures of the remaining samples were characterized by the appearance of surface cracks after 3 seconds at 500 Btu/ft^2-sec and the formation of deep fractures at 100 Btu/ft^2-sec after exposures ranging from 15 to 240 seconds. Despite these failures, samples were retained in the specimen grips and it was not necessary to terminate any test prematurely.

The sintered boride was practically unaffected by the 100 Btu/ft^2-sec exposure and at 500 Btu/ft^2-sec exhibited minor surface cracking upon cooling after test. A similar pattern of cracking after the 500 Btu/ft^2-sec exposure was noted for both silicon carbide samples. As with the sintered boride, neither grade of silicon carbide was appreciably affected by the 100 Btu/ft^2-sec test.

The temperature-time histories for these samples are shown in Figures 9 through 20..

From the temperature-time histories at 100 and 500 Btu/ft^2-sec it does not appear that the BN addition had any significant effect upon the thermal conductivity of the hot pressed composite.

Although surface temperatures of the SiC samples were significantly lower than the hot pressed samples at 500 Btu/ft^2-sec, the long term exposures at 100 Btu/ft^2-sec produced equilibrium temperatures which were comparable for both groups. It is believed that the low back surface temperature of the GRB silicon carbide at 500 Btu/ft^2-sec was due to a thermocouple malfunction since similar behavior was not noted in the corresponding 100 Btu/ft^2-sec exposure.

At both heat flux levels, surface temperatures of the sintered boride samples corresponded quite closely with the KT silicon carbide.

Manufacturer F

Specimens representing a filled silicon rubber were evaluated at 500 and 300 Btu/ft^2-sec. Test conditions and results are presented in Tables 7 and 8. Temperature-time histories for the specimens are shown in Figures 21 and 22.

Thermal degradation of the samples was characterized by the continuous formation of a soft, lightly adherent, foam-like residue, which provided some degree of protection for the virgin material. Erosion of the samples was severe, particularly at the higher heat flux level where "tunneling" of the surface residue was observed. At both test levels back surface temperatures remained at ambient.

Manufacturer G

A total of seven different materials representing four molding components and three laminates were submitted for evaluation. Since the composition of these materials was not provided, the manufacturer's code was used to identify the samples.

Two sets of specimens were returned to the ASD Project Engineer prior to testing. One set, 010-VI molding compound had exhibited a rather large weight loss in air over a 30 day period. The second set, 010-V24 end grain laminate of asbestos paper severely delaminated during this same period. The remaining samples, 010-V6 molding compound, 015 molding compound, 015-VI molding compound, 015-end grain laminate of 181 Fiberglas and 010-V24 end grain laminate of alternate plys of 181 Fiberglas and graphite cloth were evaluated at 100, 300, and 500 Btu/ft^2-sec in both nitrogen and simulated air effluents. The test conditions and results are listed in Tables 9 through 18 and the corresponding temperature-time histories are shown in Figures 23 through 52.

As expected, specimen erosion was less in nitrogen than in air with the greatest difference being noted at the 100 Btu/ft^2-sec heat flux level. Surface temperature behavior did not appear to be significantly influenced by effluent composition and only in those tests where the sample burned through was any significant rise in back surface temperature observed.

In general, little difference was noted in the performance of the 015 and 015-VI molding compounds with respect to erosion resistance. In comparison, the 010 molding compound was severely degraded at all heat flux levels. The same difference in erosion resistance was noted for the 015 and 010 laminates.

Manufacturer I

A group of specially prepared resins with various reinforcement media were evaluated. These resins were specifically intended to be excellent char formers, superior to conventional materials utilized for this purpose. A minimum of two tests at 500 Btu/ft^2-sec, one in simulated air, the other in a nitrogen effluent, were performed on each system. For certain members of this group additional tests were performed in air at 300 and 500 Btu/ft^2-sec. Test conditions and results are outlined in Tables 19 through 29 and temperature-time histories in Figures 53 through 78.

A number of the samples experienced severe delamination while others formed localized hot spots as their reinforcement melted and was removed from the specimen surface. This probably accounts for the erratic front surface temperature behavior of these materials. It is significant to note, however, that in no instance did the back surface temperature of any sample rise appreciably above ambient.

Degradation of the copolymerized alkylated phenyl polyamide and phenolic resin material was observed to increase with increasing heat flux. In nitrogen at 500 Btu/ft^2-sec erosion of these same systems was substantially reduced, and in many instances was less than that of the 300 Btu/ft^2-sec evaluation in air. Despite relatively severe delamination the least erosion of the copolymerized alkylated phenyl polyamide resin was obtained with refrasil as the reinforcement media.

The performance of the halogenated resins did not appear to be influenced by effluent composition. Furthermore, these samples, all reinforced with refrasil, did not display significant differences in individual specimen performance although variations in resin preparation were represented in the group.

Manufacturer J

Nine samples representing composites of asbestos felt saturated with phenolic resin and filled with one of three inorganic materials, titanium dioxide, potassium titanate or tungsten were evaluated.

Initial tests were performed at 500 Btu/ft^2-sec and 100 Btu/ft^2-sec for 24 and 120 seconds, respectively. After reviewing the data of these tests a second evaluation at 500 Btu/ft^2-sec was performed for 64 seconds to more clearly define the effect of filler material upon specimen performance. The test results are shown in Tables 30 through 32 and the corresponding temperature-time histories are shown in Figures 79 through 87.

Sample degradation, determined by percentage weight loss and erosion depth was the greatest for the potassium titanate material with the titanium dioxide and tungsten filled materials following in decreasing order. Despite deep erosion at the high heat flux level and relatively long exposures at the low level, none of the samples displayed a significant increase of back surface temperature.

Manufacturer V

Three samples of a graphite plated on one side with a cermet material were evaluated at 300 and 500 Btu/ft^2-sec for varying time periods. Test conditions

and results are summarized in Tables 33 and 34. Included with these data are the results of a similar evaluation of ATJ graphite. Temperature-time histories for these tests are shown in Figures 88 through 90.

At 300 Btu/ft^2-sec the sample was exposed until back and front surface temperatures attained "steady state" levels. This exposure, 300 seconds in duration, produced only minor degradation of the coating. The volume loss of the sample was attributed to oxidation of the unprotected areas of the samples as depicted schematically in Figure 91. This undercutting of the sample was observed in all three tests. The coating was unaffected by a 24 second exposure at 500 Btu/ft^2-sec. However, at the same heat flux level when the exposure time was increased to 120 seconds the coating failed in approximately 60 seconds. This failure can be readily seen in the front surface temperature behavior which exhibited a sharp decrease as the coating was penetrated and a cooler surface was presented to the pyrometer.

Discussion of Standard Materials Screening Test

Since the materials tested in this program have potential merit in a number of applications, an evaluation based upon their performance in a single test is rather difficult. The individual manufacturer who has developed a materials system to satisfy the performance criterion of a specific application is in most instances, the best judge of a material's behavior in test. Therefore, the discussion of test results will be restricted to a general evaluation of these materials, a comparison of their performance with others of their particular class, and a discussion of the test and its implications.

In each test, thermal inputs and exposure times were selected to correspond as closely as possible to the general type of thermal environment in which materials of a given class would be utilized. For insulating, nonablating systems such as the cork composition of Manufacturer AC, the foamed plastics of Manufacturer AD, and the filled silicone rubber of Manufacturer F, tests were conducted at low and moderate thermal inputs. The ablation cooled materials of Manufacturers G, I, and J were evaluated at moderate and high heat flux levels for relatively short exposure time. Moderate and high heat flux tests were performed on the samples of Manufacturers C and V and because of the refractory nature of these materials, exposure times were extended whenever possible to allow front and back surface temperatures to reach steady state levels.

With the possible exception of the filled silicone rubber, the insulating materials were intended for low thermal input applications. The test itself and the supporting instrumentation were intended for higher heat flux evaluations and therefore the data of these tests are somewhat incomplete. Furthermore, since different thermal inputs were used in the evaluation of each material a comparison of their performance is not possible.

Ablation cooled materials are generally utilized in extreme thermal environments to protect a back up structure for a specific time interval. The materials of Manufacturers G, I and J all were effective since they maintained back surface temperatures near ambient despite deep erosion and high heat flux inputs. However some members of this group, in particular both reinforced resins of Manufacturer G and most of the reinforced resins of Manufacturer I, experienced severe delamination or ply separation during heating which could

conceivably limit their application to low mass flow environments. Neither the linen and asbestos reinforced resins of Manufacturer I nor the asbestos reinforced phenolics of Manufacturer J experienced delamination.

Refractory composites such as those of Manufacturers C and V normally find application in hot structures and radiation cooled systems for which dimensional stability, oxidation resistance, and thermal shock resistance are essential.

Although the hot pressed boride composite of Manufacturer C displayed good oxidation resistance, it failed in thermal stress at all levels of heat flux. Sintering of this composite reduced this tendency toward thermal stress failure appreciably with no sacrifice of oxidation resistance. Transient temperature behavior, thermal shock resistance and oxidation resistance of the sintered composite compared favorably with KT silicon carbide. The cermet plated graphite of Manufacturer V exhibited good oxidation resistance for short term, high heat flux inputs. Coating adherence was excellent and protection of the graphite was achieved for exposures up to 60 seconds at 500 Btu/ft^2-sec at which time the coating melted. No evidence of thermal stress failures such as occurred with the hot pressed boride was observed for this composite. Temperature-time histories of the 24 second, 500 Btu/ft^2-sec exposure of KT silicon carbide, cermet plated graphite, and sintered boride composite were quite similar.

The screening test appears to be useful for sorting and ranking materials within a given class. It is sufficiently sensitive to distinguish between differences in filler materials, reinforcement media, or resin materials; and materials characteristics such as thermal shock sensitivity and oxidation resistance may be readily evaluated. On the other hand, as was illustrated in some of the tests, the influence of minor variations of chemistry or methods of processing were generally not evident from specimen performance.

To obtain a better understanding of the test with regard to its capabilities a series of 120 tests at heat fluxes of 100, 300 and 500 Btu/ft^2-sec was performed on samples of phenolic-nylon, 1020 steel and ATJ graphite. Hopefully, the data of these tests when analyzed statistically will provide valuable information regarding the reproducibility and sensitivity of this test.

SECTION 4

EVALUATION OF PROTECTIVE COATINGS FOR THE XLR-99 THRUST CHAMBER

In February 1961 a program was initiated to define the cause of premature failures of the liquid fueled XLR-99 thrust chamber of the X-15 research aircraft. The XLR-99 thrust chamber is a regeneratively cooled, tube wall type, brazed stainless steel structure. The interior of the chamber has a flame sprayed coating of Rokide Z over a Nichrome primer to protect the surface of the stainless steel and to prevent overheating of the fuel (ammonia and lox) during engine operation. In service, several chambers experienced excessive coating loss during very short term operation with tube bursting failures occurring in the regions of high coating loss. Sections from one such chamber were delivered to the University for a metallographic analysis.

Inspection of the coating in the throat section revealed a pattern of divergent white streaks running down the interior of the chamber (Figure 92). These white streaks appeared to correspond to the radial location of the fuel injectors and therefore the regions of maximum temperature. It was within these white areas that tube failures and extensive coating loss had occurred. Metallographic examination of several failed tubes revealed a complete loss of coating and substantial erosion of the tube surface as shown in Figures 93 and 94. The inside surface of the tubes contained a second phase apparently due to a reaction of the liquid ammonia with the stainless steel. This phase which can be seen in Figure 93 and even more clearly in Figure 95 appeared to be quite brittle and exhibited considerable cracking in the diffusion zone. Tubes adjacent to ones which had failed revealed some surface erosion of the stainless steel and a thinner diffusion zone on the inside surface as shown in Figure 96.

Examination of the white areas where the Rokide coating remained intact revealed some erosion of the Rokide Z (Figure 97). In this area, as well as in those where the coating was completely eroded, recrystallization of the stainless steel was observed on both the inside and outside diameters. Significantly, no evidence of the diffusion zone was observed in those areas where only partial erosion of the coating had occurred.

A white area away from the throat section is shown in the photomicrographs of Figure 98. In this area non-uniformity of the coating is quite evident as well as grain growth at the inside and outside diameters. No evidence of the diffusion zone was observed in this area.

It was concluded from the examination of the failure and of adjacent areas that Rokide loss resulted in the formation of a brittle diffusion zone, very susceptible to cracking. The internal cracking coupled with erosion of the stainless steel outer surface reduced the effective cross-sectional area of the tube to such an extent that it burst. It was further concluded that tube failures were the ultimate result of complete Rokide loss.

Although no effort was made to identify the diffusion zone, it is probably

a nitrided region resulting from chemical breakdown of the ammonia. This hypothesis would tend to strengthen the belief that this zone does not begin to form until the Rokide layer has failed.

No specific conclusions were drawn from the metallographic evidence as to why the Rokide coating eroded during the relatively short operation of the engine. It did appear however, that once the Rokide coating was lost subsequent engine failure resulted from the combined effects of erosion of the outer surface of the stainless steel tubing and the formation of a brittle diffusion zone, presumed to be a nitrided layer, on the inner surface.

On the basis of this analysis, it was recommended that a program be initiated with an organization competent in the area of sprayed ceramic coatings to develop a coating with improved adherence under normal engine operating conditions.

Plasmakote Corporation was requested by the Air Force under Contract AF 33(616)-7323 to develop a coating for the XLR-99 thrust chamber. The University of Dayton was requested to provide the necessary support for this program by developing a simple but realistic evaluation test for ceramic coatings.

From reported engine data it appeared that an arc-plasma-jet could be utilized for a reasonable simulation of the chemical and thermal environment of the thrust chamber. It was believed that the combustion products of the fuel could be satisfactorily simulated by operating the plasma-jet on a N_2-H_2 mixture. However, attempts to obtain stable operation of the arc with this mixture were unsuccessful and rather than undertake a lengthy program to develop compatible electrodes it was decided to perform the tests in nitrogen only. Thermal simulation presented no difficulties and the coating surface temperatures reported for the engine could be reproduced by operating the plasma-jet at moderate input power levels.

Test specimens consisted of tube clusters which were cleaned and recoated after being sectioned from actual thrust chambers. Typical test samples such as the one shown in Figure 99, measured approximately 4 by 8 inches and generally were sufficient in size to permit four thermal shock tests of each side. In test, the samples were cooled by passing water through the fuel passages and were subjected to thermal cycling until a failure was produced. A sample undergoing test is shown in Figure 100 The test consisted of a series of thermal cycles in which the specimen was heated in the plasma-jet for 10 seconds, and cooled in ambient air for 10 seconds, with visual inspection of the coating during each cooling cycle. Tests originally conducted at a constant thermal input produced extremely erratic results. To obtain more meaningful test data, the procedure was modified and specimens were subjected to 10 thermal cycles at each of several increasing levels of power input to the plasma-jet until a failure occurred.

Generally failures occurred as a partial separation and lifting of the coating from the substrate although other types of failure such as spalling, cracking and melting of the coatings were also observed in some tests.

To establish a base line for comparison of coating performance, a total of 31 tests were performed upon tube clusters which had been cleaned and recoated with Rokide Z by Reaction Motors Division of Thiokol Corporation (RMD). This coating, similar to that of the original XLR-99 thrust chamber, consisted of a 0.010 inch layer of Rokide Z (flame sprayed ZrO_2) over approximately 0.004 inches of Nichrome primer. The results of these tests were compared with tests of several graded and monolithic coatings applied by Plasmakote Corporation utilizing both the flame and arc-spray processes.

The Plasmakote graded systems consisted of a metallic primer, several layers of a metal-ceramic mixture, and a ceramic insulating layer. By controlling the amount of metal in each of the intermediate layers a smooth transition from metal to ceramic was achieved. Because of the improved thermal expansion match between substrate and coating, it was anticipated that this type of system would exhibit improved thermal shock resistance as compared to the monolithic or single layer ceramic coating. In Figure 101 a typical single layer coating (Rokide Z), a Nichrome graded ZrO_2 over molybdenum primer, and Nichrome graded ZrO_2 on a molybdenum primer with a titanium nitride topcoat are shown.

A complete description of the coatings evaluated and the results of the thermal shock tests are shown in Table 35. It should be noted that for the graded coatings the composition of each intermediate layer is specified in terms of the volumetric proportions of metal and ceramic delivered to the spray torch during application of the coating. Since deposition efficiency generally runs higher for metals than for ceramics, the actual coating probably contains a higher percentage of metal than is indicated.

The results of the thermal shock tests are presented in Figures 102 through 105 as the average number of thermal shock cycles required to produce a failure. In each of the figures RMD Rokide Z is compared with Plasmakote coatings which were grouped according to primer and grading metal. This comparison, however gives no indication of the reliability of the system and if failures occurred over a wide range of values as was the case for some coatings, the use of average failure levels could be misleading.

A clearer picture of coating reliability can be obtained from Figure 106 in which the thermal shock test results of the RMD Rokide and the graded ZrO_2 coatings are presented in terms of the percentage of failures which occurred at less than an indicated number of thermal shock cycles. For clarity of presentation coatings were grouped according to primer and grading metal and no distinction was made between differences in graded layer composition.

From these data the following tenative conclusions were drawn:

1) The thermal shock resistance of Rokide Z and metal graded ZrO_2 coatings is substantially improved by the use of molybdenum as a primer metal.

2) Minor variations in the percentage of metal in the intermediate layers of a graded ceramic have little effect upon thermal shock resistance.

3) Two and three layer graded systems perform equally well.

4) Nichrome is a more effective metal for grading ZrO_2 than either molybdenum or tungsten.

5) Tungsten is not an effective primer metal for this application.

In addition to the evaluation of the basic graded coatings, systems with topcoats of zirconium diboride and titanium nitride were evaluated to determine the feasibility of adding an erosion barrier to the ceramic coating. In evaluating these topcoats, tests were terminated when the topcoat failed and an evaluation of the remainder of the coating was not attempted.

No topcoat survived more than six thermal cycles and grading with ZrO_2 did not improve their performance. The TiN topcoats failed by melting and spalling whereas the ZrB_2 topcoats failed primarily by spalling.

The results of the laboratory evaluation of these coatings were verified by the Air Force in static test firings of an XLR-99 thrust chamber coated in segments with six experimental coatings. Short term firings of the engine and subsequent examinations of the throat area revealed that:

1) Coating retention in this area could be improved substantially by the use of Nichrome graded ZrO_2 over Mo primer.

2) Mo graded ZrO_2 over Mo primer and W graded ZrO_2 over W were less effective coatings.

3) Topcoats of TiN and ZrB_2 were not satisfactory for this application.

A program was initiated in conjunction with the thermal shock evaluation to study the effects of coating variables upon bond strength. Initially the effect of grit blast media upon bond strength was determined with samples sectioned from 2 x 2 inch Inconel panels grit blasted with corundum, silicon carbide, flint, or garnet and coated with 100% alumina or a mixture of 50% alumina and 50% nickel. These test specimens measured 0.9 x 0.9 inches and were carefully cut so as not to include original edges of the panels. These pieces were bonded between aluminum blocks with Shell Epon VIII adhesive and tested in tension using a double universal type of fixture to insure axial loading. The results of these tests are summarized in Tables 36 and 37 and are depicted in the bar graph of Figures 107 and 108. The results of the 50% Al_2O_3-50% nickel coating tests are somewhat inconclusive since the majority of specimens did not fail at the metal to ceramic interface. However, it is significant to note that these coatings exhibited much higher bond strengths than the 100% alumina coatings. Bond strength was probably influenced by the method of sample preparation. Had the samples been cut to size prior to coating, higher values would have probably been obtained.

The influence of edge preparation upon bond strength is graphically illustrated by the results of tensile tests upon a Nichrome graded ZrO_2 coating on 347 stainless steel primed with molybdenum. In one group (A) coatings were applied to one face of six 1-1/16 inch square plates which were subsequently ground to 1.0" x 1.0" ± 0.001". A second group of six samples (B) were

coated after the plates were finish ground to 1.0" x 1.0" ± 0.001". The results of these tests are shown in Table 38 and in the bar graph of Figure 109. One sample from each group failed at the ceramic/adhesive interface and one sample from Group B experienced a partial ceramic/adhesive failure. The remainder of the samples failed within the coating. Metallographic examination of a typical sample from each group revealed that this failure had occurred in the molybdenum primer. Excluding the three ceramic/adhesive failures, Group A specimens had an average bond strength of 2690 psi whereas the average bond strength of the Group B specimens was 3300 psi, approximately 23% higher.

SECTION 5

EVALUATION OF PROTECTIVE COATINGS FOR REFRACTORY METALS

Considerable effort is currently being directed by several organizations toward the development of protective coatings for refractory alloys so that the potential high temperature capabilities of these alloys may be utilized in oxidizing atmospheres. It is well known that excellent mechanical properties of the alloys of tantalum, molybdenum, tungsten and columbium are retained at temperatures in excess of 2500°F, however, in the presence of air at temperatures above 2000°F, rapid and sometimes catastrophic oxidation will occur accompanied to a lesser extent by nitrogen and hydrogen reactions which alter the mechanical properties of the alloy. Attempts to devise oxidation resistant alloys of refractory metals have not been successful and emphasis has shifted to the protective coatings concept.

A protective coating must satisfy a number of requirements. It should be somewhat elastic, tightly adherent, and must be mechanically and chemically compatible with the basis metal. But most important, it must inhibit the transport of oxygen to the substrate and/or the migration of metal ions into the coating.

An extremely important phase of any coating development program is the laboratory evaluation of experimental systems in oxidizing atmospheres over a range of elevated temperatures. Coating manufacturers over the years have developed evaluation procedures, each somewhat different and not necessarily representative of end use environments. As a result each manufacturer tends to develop coatings which perform best in his particular test. Correlation of test results from different laboratories is therefore difficult if not impossible due to a lack of a unified approach to coating evaluation.

The University initiated a program to define procedures and techniques for the screening and evaluation of protective coatings. It was intended that the evaluation provide comprehensive data pertaining to the oxidation protection of various coatings when subjected to different thermal environments. As originally conceived the evaluation consisted of three separate phases: a long term still air exposure at temperatures in the range of 1500°to 2000°F to determine any tendency towards pest-type failures; a short-term dynamic oxidation test in an arc-plasma-jet effluent to evaluate coating life at the proposed application temperature, and a high temperature test with the plasma-jet to evaluate the ultimate refractory capabilities of the coating.

Prior to the initiation of this study the Sylcor aluminide coating was evaluated in the plasma-jet facility. The purpose of these tests was to characterize in a dynamic oxidizing atmosphere the coating for a tantalum alloy (Ta-10% W) and to determine if similar coatings would be feasible for columbium, tungsten and molybdenum.

Two different tests were performed on these samples, which were made from 2" x 2" coated sheet stock. The first consisted of exposing the specimen in the arc effluent at a specific surface temperature as measured by an optical pyrometer. Surface temperatures were increased at five minute intervals

until a failure was produced. In the second test, specimens were cycled in the plasma effluent at specific surface temperatures. The thermal cycle consisted of heating for 30 seconds and cooling in ambient air for 10 seconds. At 15 cycle increments surface temperatures were increased and the thermal cycling continued. The results of these tests are presented in Tables 39 and 40.

Continuous exposure tests of the Ta-10% W alloy indicated the coating would provide substrate protection at temperatures to 3340°F for 5 minutes, despite considerable warpage of the specimen. Similar coatings provided comparable protection for molybdenum and tungsten, although a columbium specimen failed at 2820°F after very short-term exposure. Photographs of typical specimens after continuous exposure are shown in Figure 110.

Thermal cycling of the coated Ta-10% W specimens produced failures at about 2900°F in 5 of 6 specimens, the single exception being a failure at 3150°F. A single molybdenum specimen survived 15 thermal cycles at 3270°F, but failed on further heating to 3450°F. The condition of several of these specimens after thermal cycling is shown in Figure 111.

Shortly after the Sylcor coatings were evaluated a program was initiated to standardize this type of test. Five silicide coatings on 0.030" Mo-1/2 Ti were selected for preliminary testing. Two basic tests were performed in the arc-plasma-jet facility operating with simulated air at a mass flow rate of 0.0082 lb/sec. In one test, samples were cycled at 3000°F, the anticipated operating temperature of these coatings, for a maximum of four hours or until a failure occurred. The thermal cycle consisted of 15 minutes heating and 2 minutes cooling in ambient air. This particular test procedure was selected since it corresponded to similar tests of the same silicide coatings by the Air Force in an oxyacetylene facility and would permit a comparison of results using two different heat sources. In the second test the ultimate refractory capabilities of the coatings were determined by subjecting the specimens to five minute exposures at specific temperatures until a failure was produced. By controlling input power to the arc, test temperatures from an initial value of 2500°F were increased in 200°F increments until 2900°F was reached. Above 2900°F temperature was increased in 100°F increments. Between each change in temperature the specimen was cooled in ambient air for 2 minutes.

In both tests specimen temperatures were measured at the back of the sample with a two color pyrometer and periodically checked with an optical pyrometer. Samples were exposed at an angle of 45° to the arc effluent in a cast alumina holder and were positioned such that the edges, particularly those in contact with the holder, remained relatively cool during test. The results of these tests are compared with the results of oxyacetylene test by the Air Force in Table 41. Photographs of these samples after tests are shown in Figures 112 through 117.

It should be noted that the reported coating thickness was obtained from measurements of total sample thickness and should be considered approximate since only nominal values for substrate thickness were available.

A 50 hour oxidation test in still air at 2000°F was also performed on five silicide coatings. Although changes were noted in the physical appearance

of most of the samples, only one obvious failure was produced; an edge failure of the fluidized bed silicide at 25 hours. The results of this test are summarized in Table 42 and a photograph of the single coating failure is shown in Figure 118.

The arc-plasma-jet tests produced extremely erratic results with apparent coating life showing a wide variation in duplicate tests. In view of the relatively small spread of the oxyacetylene test data it is doubtful that sample variations were responsible for this spread in results. It is more likely that non-reproducibility of the test itself, stemming from inadequate environmental control and the inability of the test operator to visually detect small failures, was largely responsible for these erratic results. The test could probably be improved by modifing test procedures to provide more reasonable assurance that consistent and well defined environments are being achieved.

Since coating failures are believed to result from random defects, a proper evaluation will require the testing of a sufficient number of samples to apply statistical analyses to the results. The present test does not lend itself readily to the processing of large numbers of samples in the plasma-jet because of the time required to produce a failure. To accentuate the presence of coating defects to produce earlier failures several techniques could be employed such as: exposure of the sample in still air at elevated temperatures periodically during the dynamic oxidation test, the use of an air blast during the cooling portion of the thermal cycle, and the use of shorter thermal cycles. Long-term preconditioning of the samples at 1800°-2500°F in still air prior to dynamic oxidation testing may also be helpful.

SECTION 6

GENERAL DISCUSSION, CONCLUSIONS, AND RECOMMENDATIONS

Since the tests of specific materials systems have been treated in other sections of this report, this section will be restricted to a general discussion of the various test methods.

The screening test described in this report provided a rapid and economical means of characterizing and comparing the high temperature behavior of potential materials systems for a variety of applications. Tests of this nature, in which all classes of materials are evaluated in essentially the same thermal environment, produce data which emphasize the undesirable characteristics of a material such as inadequate insulating ability, thermal shock sensitivity, poor oxidation resistance, etc., but do not necessarily provide a direct index of the material's performance in its intended application. This is particularly true for those materials which may be utilized in applications for which the associated environmental parameters of a given thermal input such as mass flow, stagnation pressure or effluent chemistry cannot be realistically simulated by the test facility.

In certain instances the plasma-jet can provide sufficiently realistic environmental simulation so that laboratory test data can be applied directly to service conditions. For example, the results of laboratory tests on experimental sprayed coatings were correlated directly with full scale tests of the same coatings in the XLR-99 thrust chamber. Thus it was shown that simple bench test techniques could be successfully employed to screen, classify, and perhaps even optimize coating systems for this application and thereby significantly reduce the amount of costly and time consuming full scale engine testing inherent in development programs of this nature.

The plasma-jet would also appear to be ideally suited for the dynamic oxidation testing of coatings for the refractory alloys since desired sample temperatures are easily achieved, mass flow rates and effluent composition are variable over a wide range, and continuous operation of the device is possible. However, initial evaluations of five different silicide coatings on Mo-1/2 Ti in a dynamic oxidation test with the plasma-jet produced coating life data which appears to be excessively scattered when compared with test results for the same coatings obtained by other organizations in similar tests with an oxyacetylene torch facility.

It is unlikely that the scatter of these data is due to non-uniformity of the coatings. It is more probable that the inability of the test operator to detect a coating failure when it occurs and non-reproducibility of thermal inputs are responsible for much of this scattering of data. It is apparent that the usefulness of the test will be limited until more reproducible data can be obtained.

The utility of the arc-plasma-jet as a basic tool in the evaluation of high temperature materials could be increased if information were available regarding the reproducibility of specific environments and the sensitivity of the various tests with respect to materials performance. A program has been initiated to experimentally determine the reproducibility and sensitivity of the standard materials evaluation test. Studies of this nature will, in all probability, be extended to include the other tests.

With present techniques certain test parameters are defined at the specimen location while others are defined at the exit plane of the plasma-jet. It would be more desirable to specify all test conditions at the specimen location. Determinations of effluent properties at the exit plane of the plasma-jet are useful only as relative quantities since a significant redistribution of effluent energy, due primarily to air entrainment, will occur in the interval between the plasma-jet exit and the specimen. Several methods for measuring and/or calculating effluent properties at the specimen location are now being evaluated.

In accordance with the objectives of this program i.e., to characterize the behavior of high temperature materials systems the following recommendations are submitted:

1. The performance of materials in these tests and in actual end use environments should be correlated whenever possible.

2. Tests which yield data directly applicable to service conditions such as were employed in the X-15 program should be developed as required.

3. The reproducibility study of the standardized test should be concluded as quickly as possible.

4. Instrumentation should be developed to provide a more accurate and complete measure of environmental conditions in the arc effluent at the sample location.

5. A thermal shock test should be devised for use in conjunction with the standardized materials evaluation test.

6. The dynamic oxidation test for refractory alloy coatings should be refined and the scope of the program be expanded to include the development of techniques to completely characterize the physical properties of such coatings.

7. A correlation between the bond strength and thermal shock resistance of sprayed ceramic coatings should be attempted.

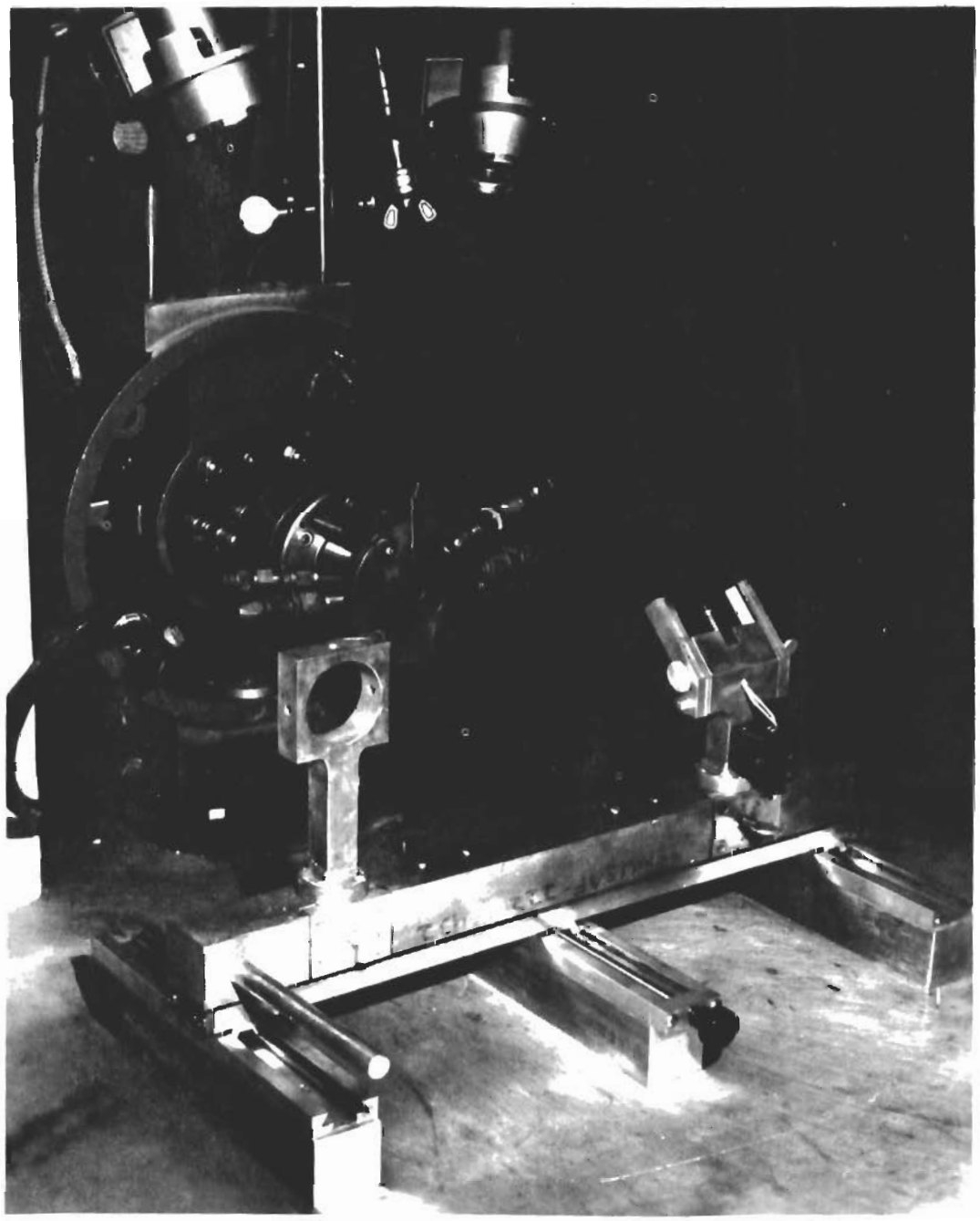

Figure 1. Two-Position Sliding Specimen Holder with Special Holders in Place and Arc-Plasma-Jet Front Orifice in Background.

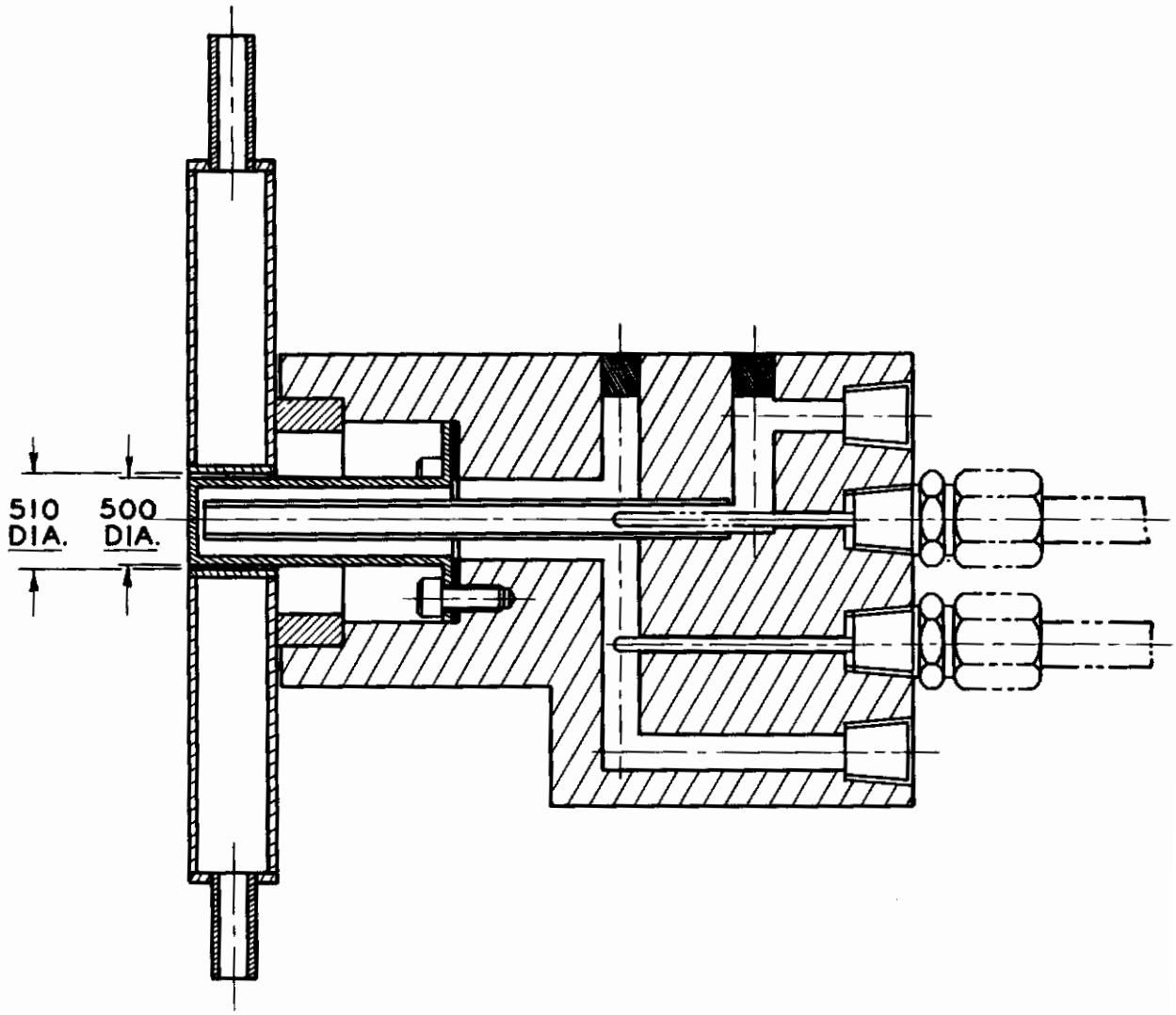

Figure 2. Water Cooled Calorimeter

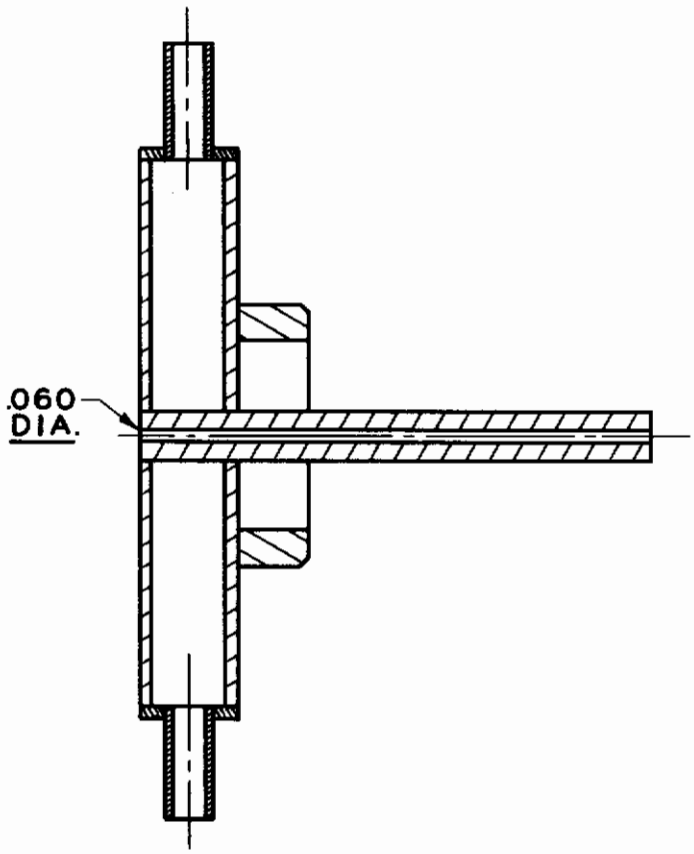

Figure 3. Flat-Faced Pitot Tube

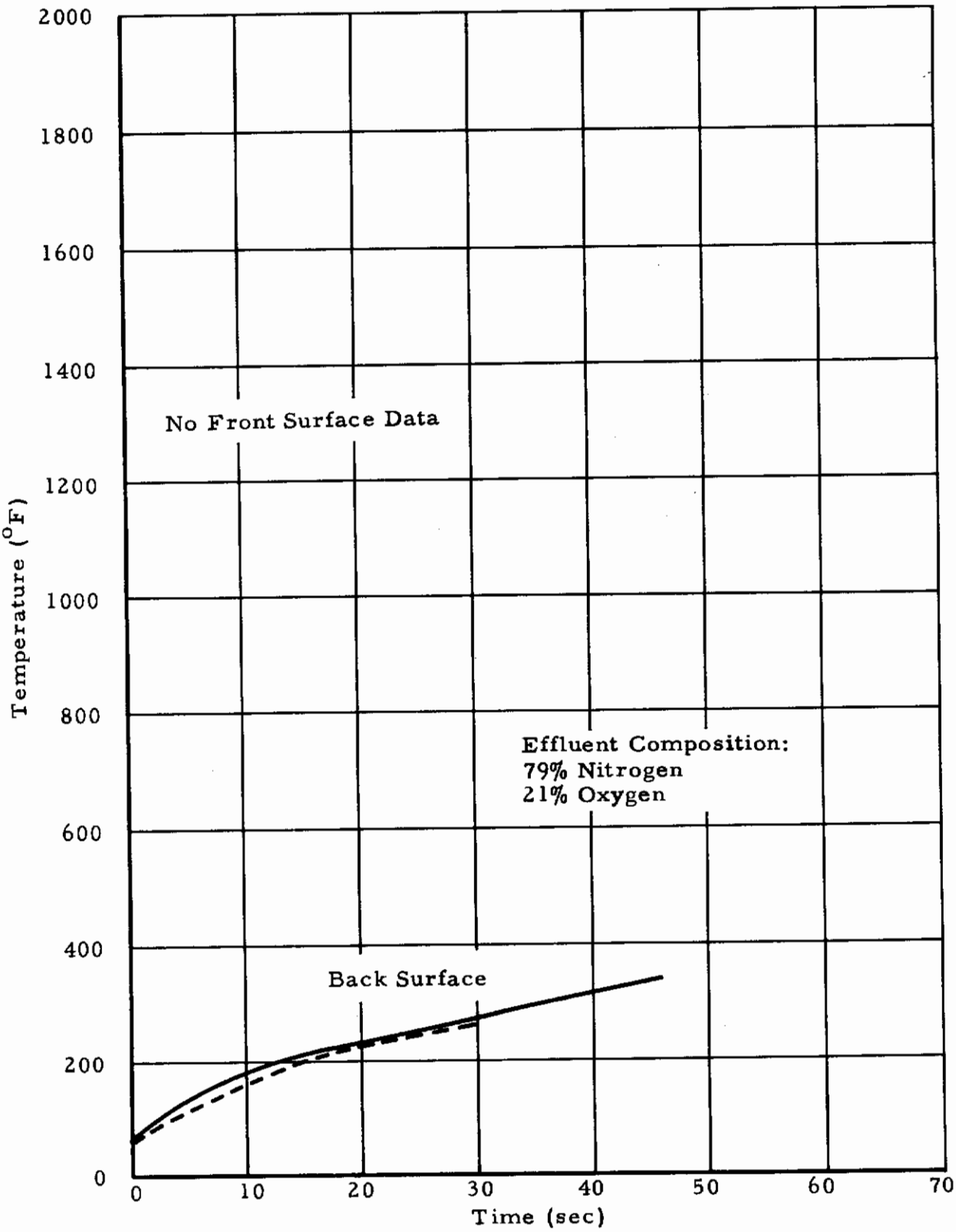

Figure 4. Temperature-Time History of 1/8 Inch Thick Cork Composition with Phenolic Binder Exposed to a 10.8 Btu/ft^2-sec Environment (Two Tests.)

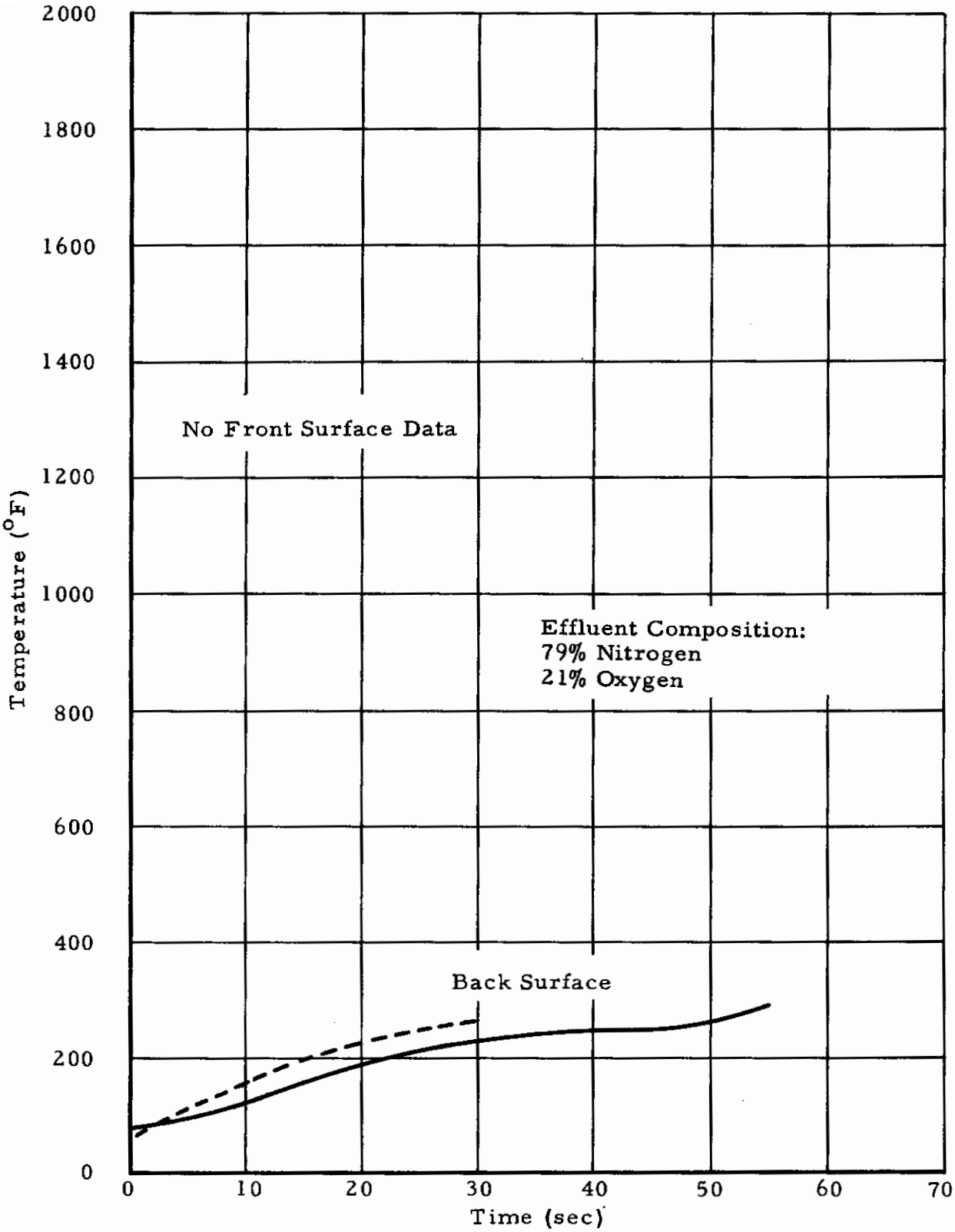

Figure 5. Temperature-Time History of 1/4 Inch Thick Cork Composition with Phenolic Binder Exposed to a 10.8 Btu/ft^2-sec Environment (Two Tests.)

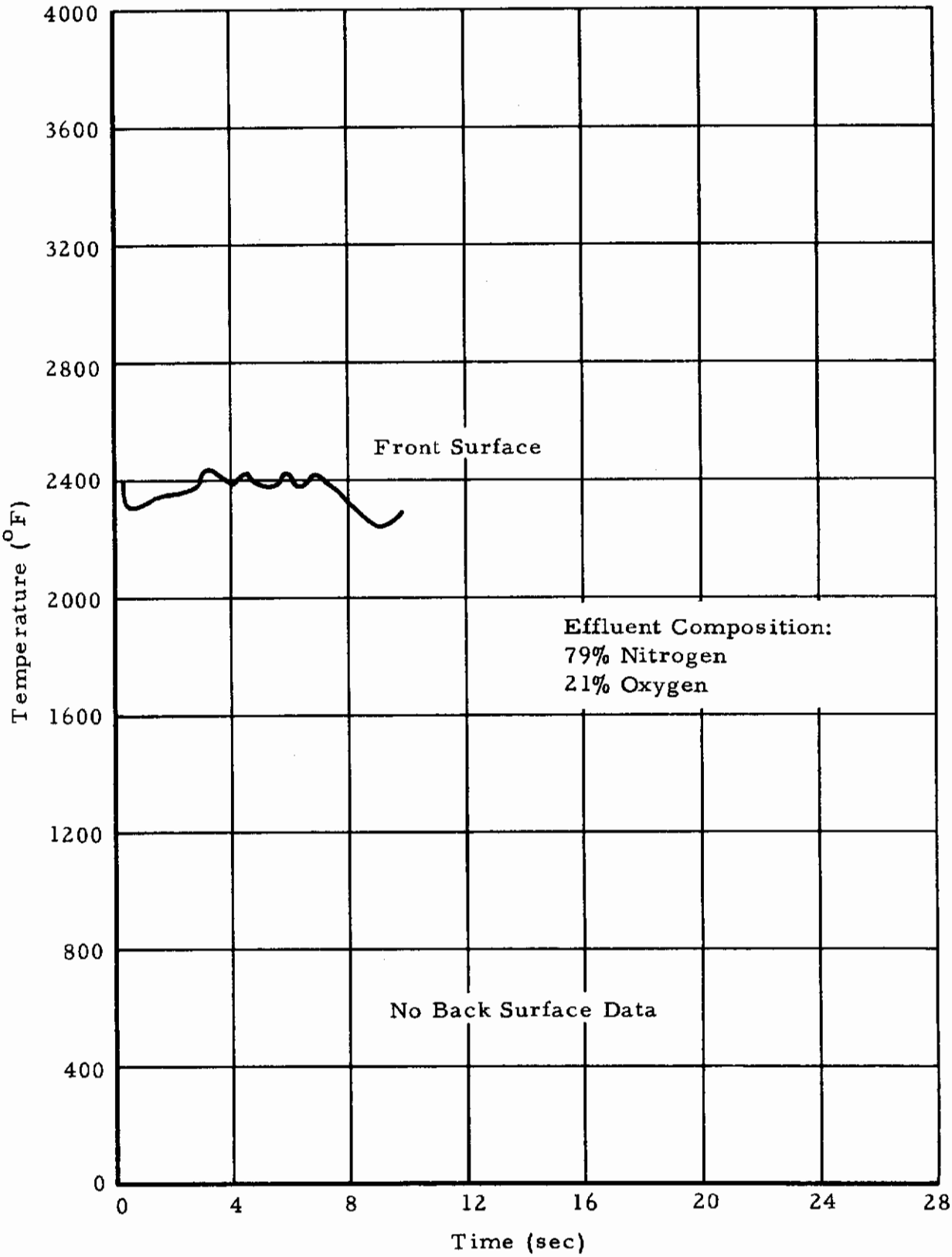

Figure 6. The Temperature-Time History of Foamed Plastic A Exposed to a 100 Btu/ft^2-sec Heat Flux Environment.

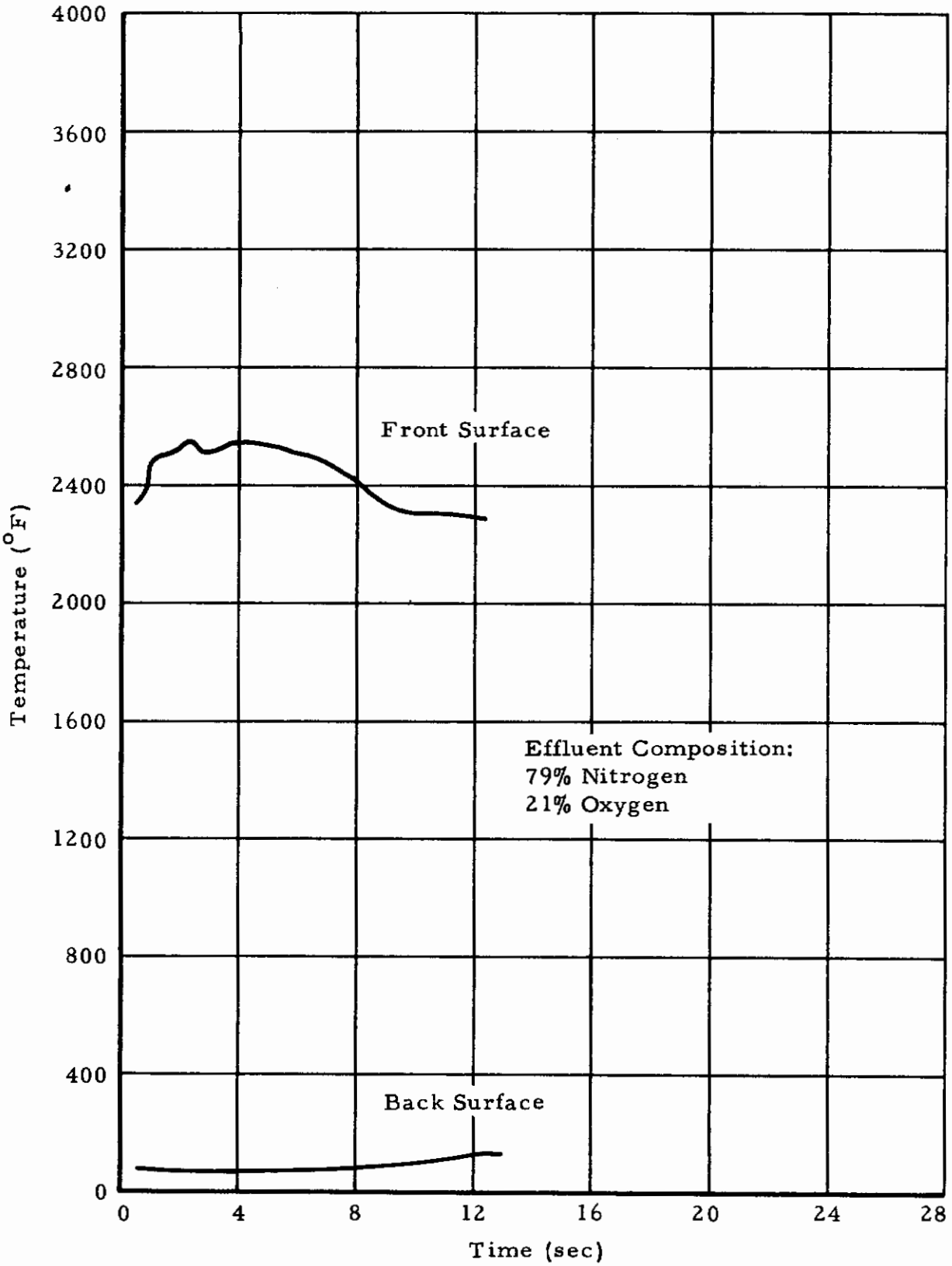

Figure 7. The Temperature-Time History of Foamed Plastic B Exposed to a 100 Btu/ft^2-sec Heat Flux Environment.

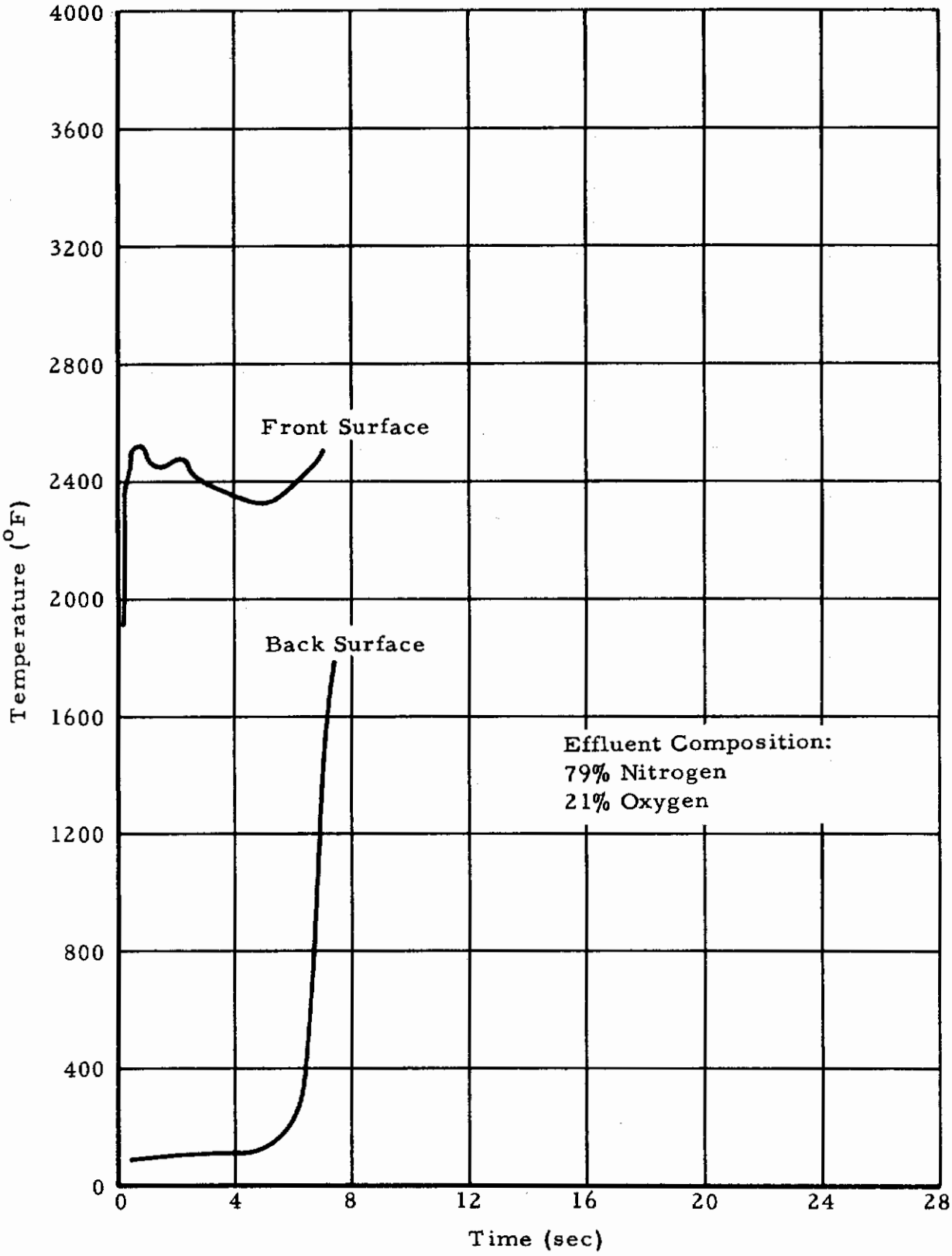

Figure 8. The Temperature-Time History of Foamed Plastic C Exposed to a 100 Btu/ft^2-sec Heat Flux Environment.

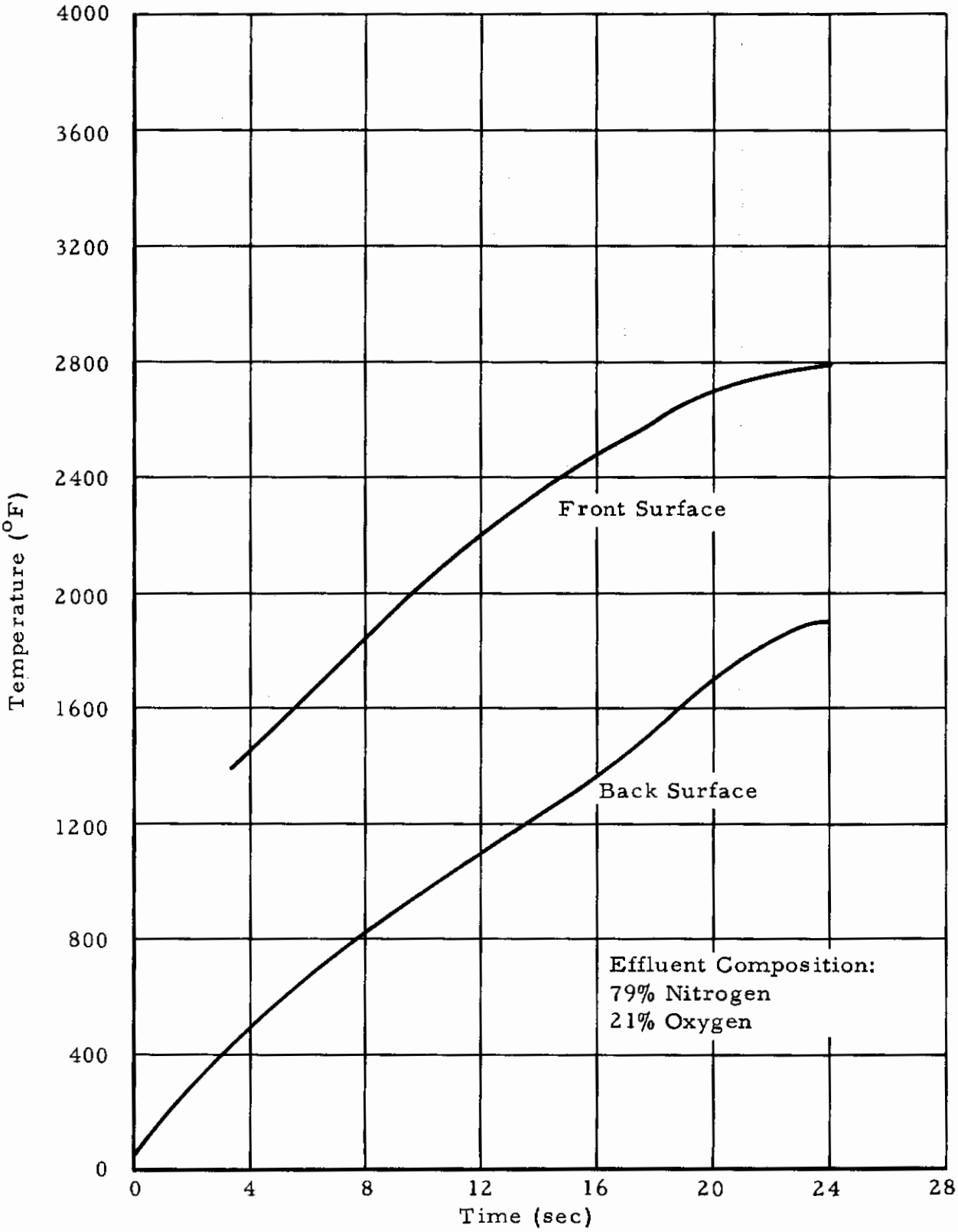

Figure 9. Temperature-Time History of Hot Pressed $ZrB_2 \cdot MoSi_2$ + 5% BN Exposed to a 493 Btu/ft^2-sec Environment. (Sample 1)

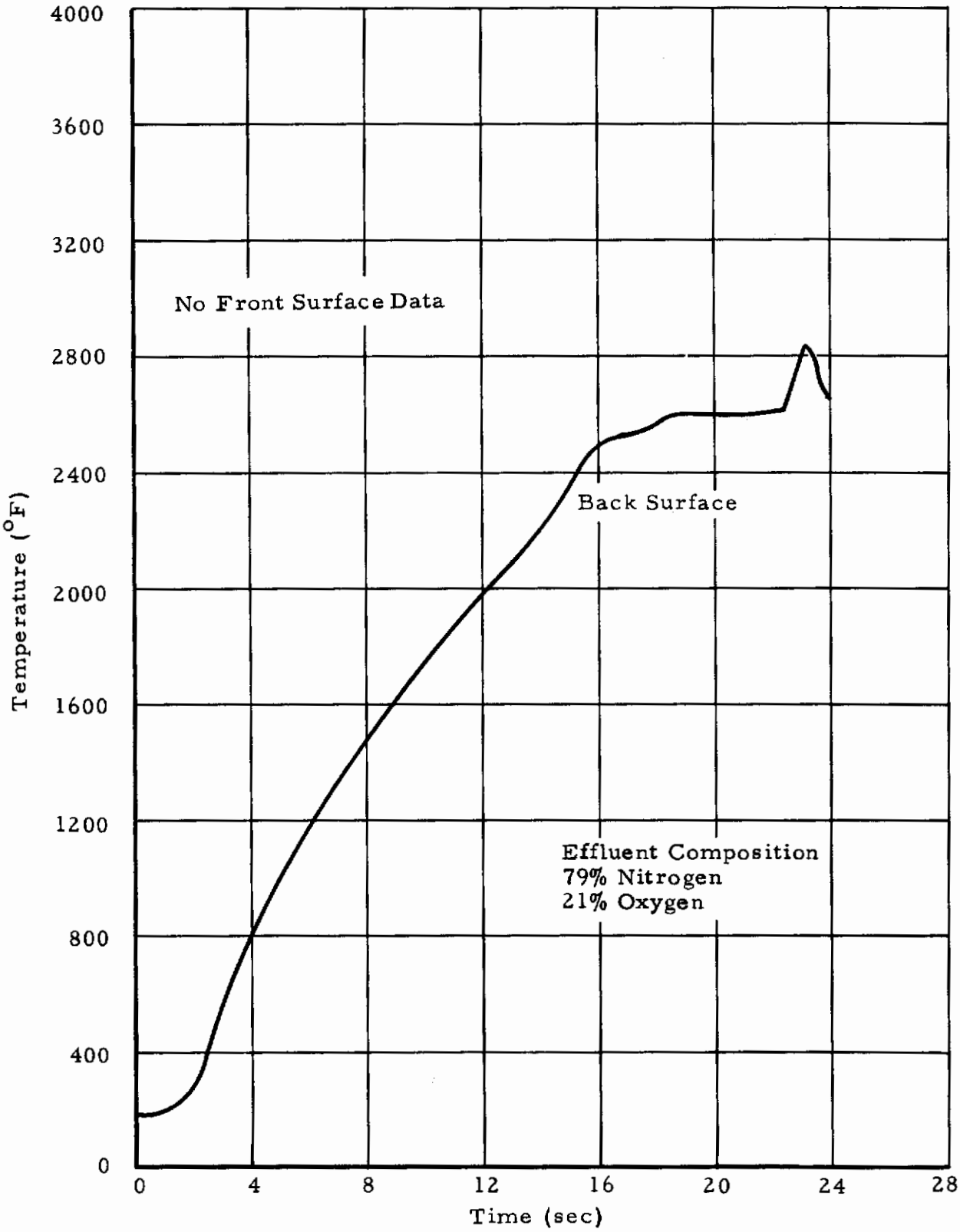

Figure 10. Temperature-Time History of Hot Pressed $ZrB_2 \cdot MoSi_2$ Exposed to a 500 Btu/ft^2-sec Environment. (Sample 2)

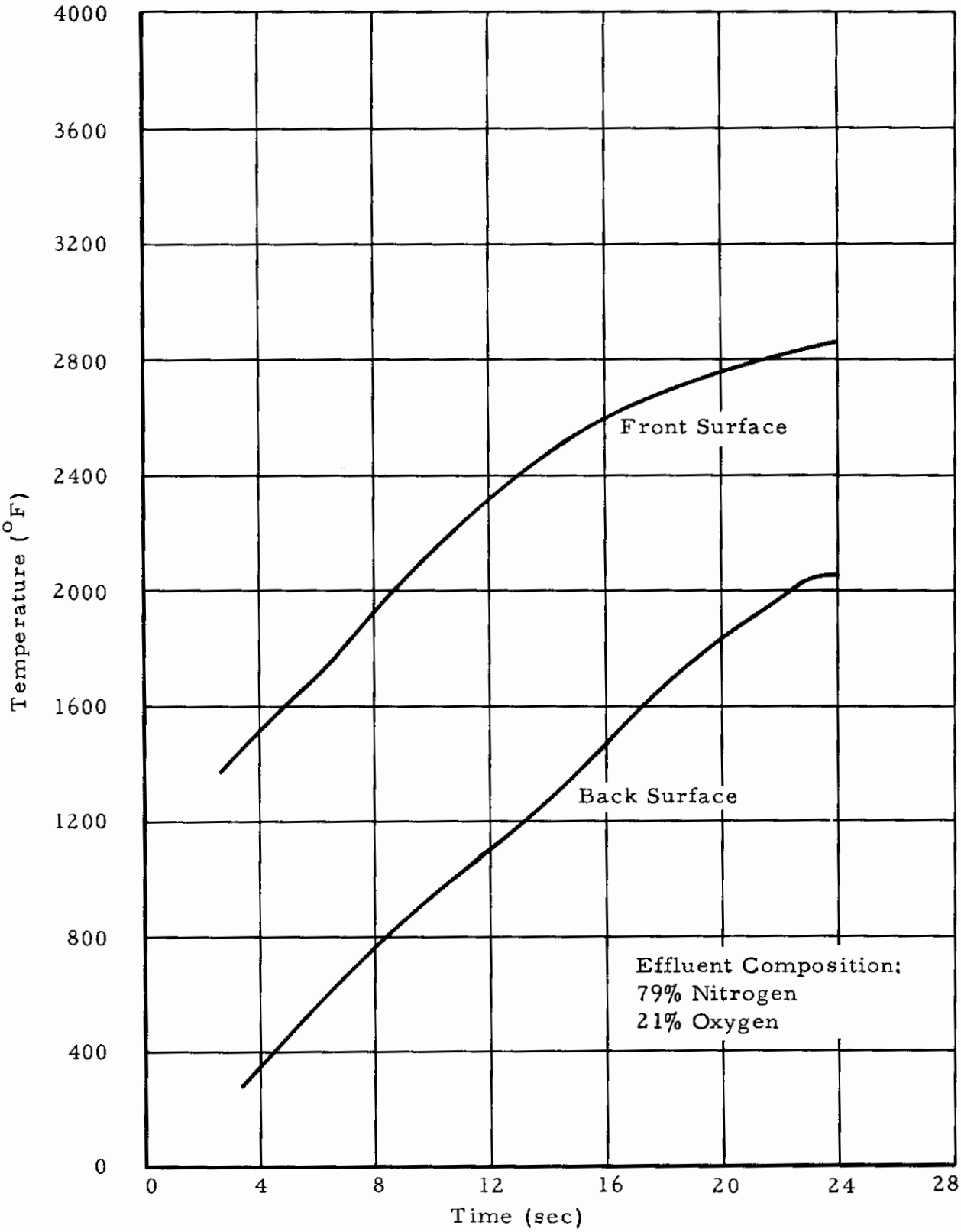

Figure 11. Temperature-Time History of Hot Pressed $ZrB_2 \cdot MoSi_2$ Exposed to a 470 Btu/ft^2-sec Environment (Sample 3.)

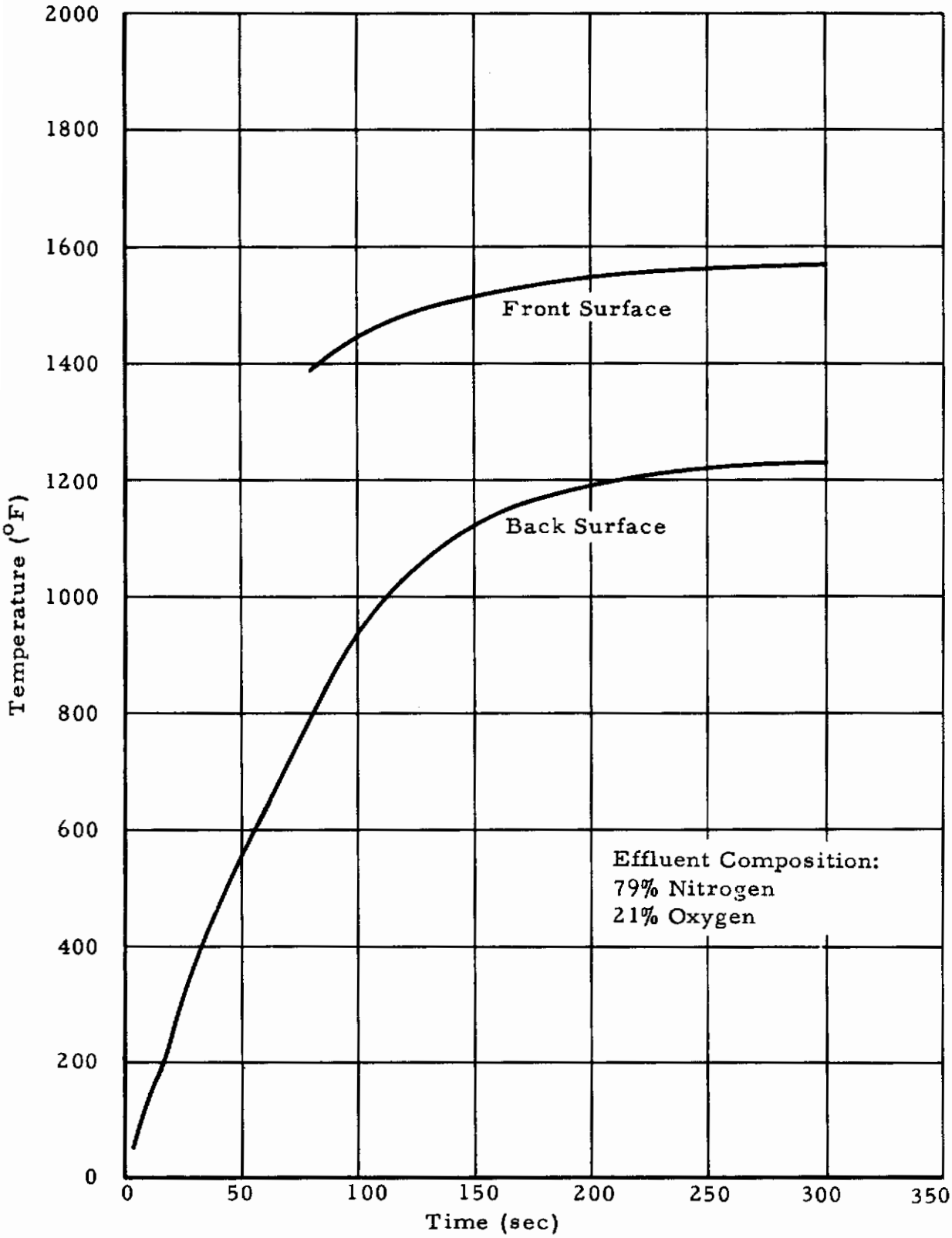

Figure 12 Temperature-Time History of Hot Pressed $ZrB_2 \cdot MoSi_2$ + 5% BN Exposed to a 102 Btu/ft^2-sec Environment (Sample 4.)

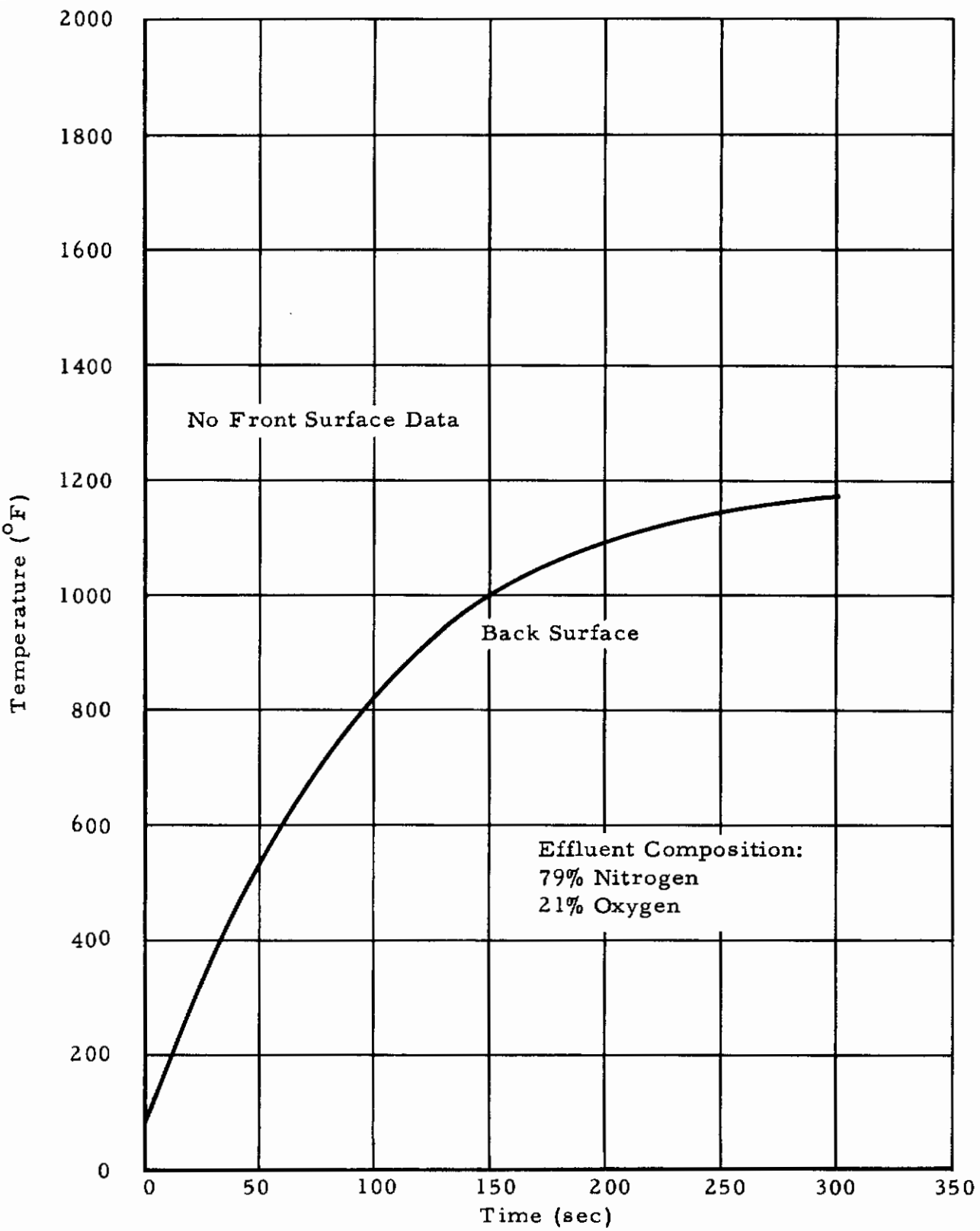

Figure 13. Temperature-Time History of Hot Pressed $ZrB_2 \cdot MoSi_2$ Exposed to a 108 Btu/ft^2-sec Environment (Sample 5.)

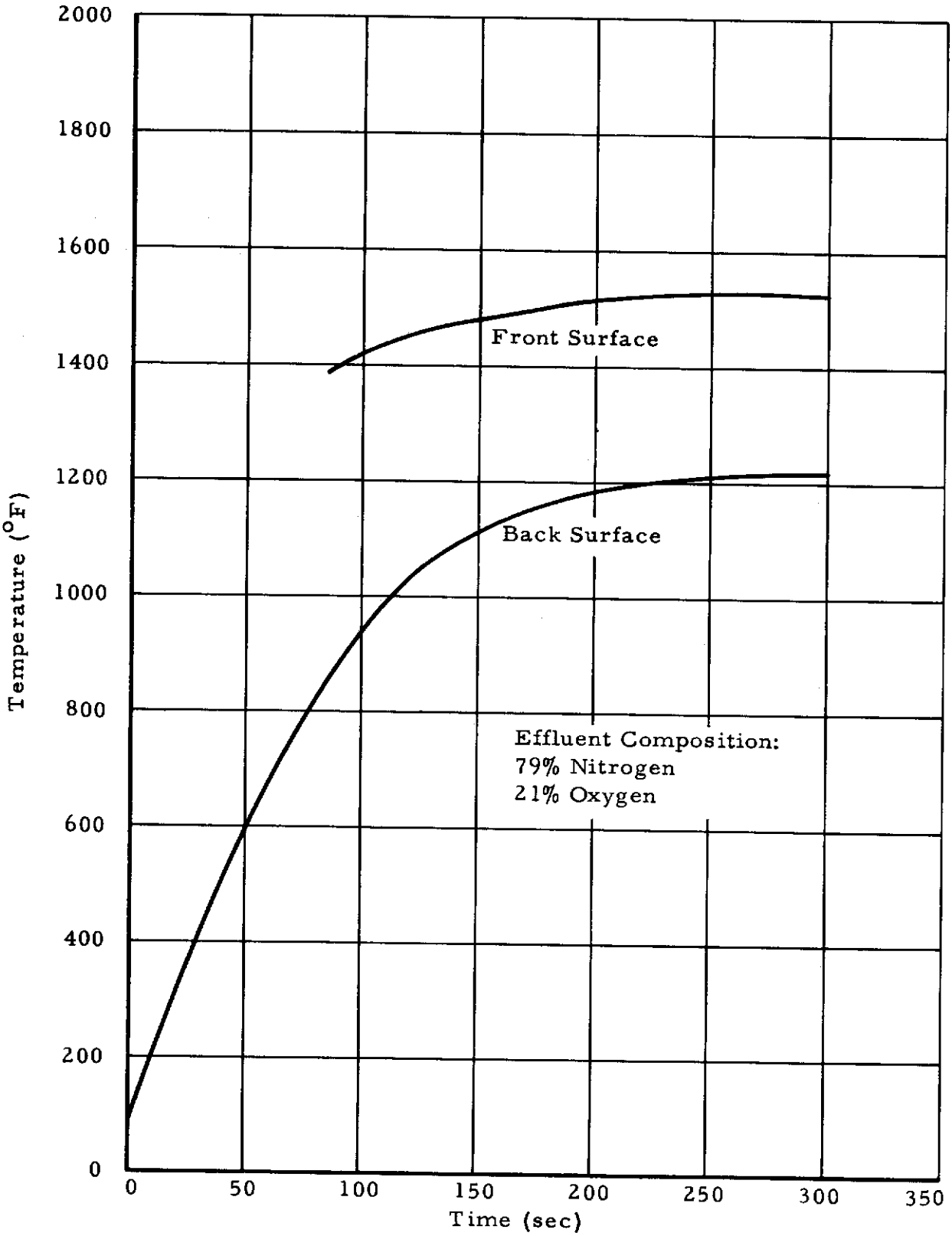

Figure 14. Temperature-Time History of Hot Pressed ZrB_2:$MoSi_2$ Exposed to a 102 Btu/ft^2-sec Environment (Sample 6.)

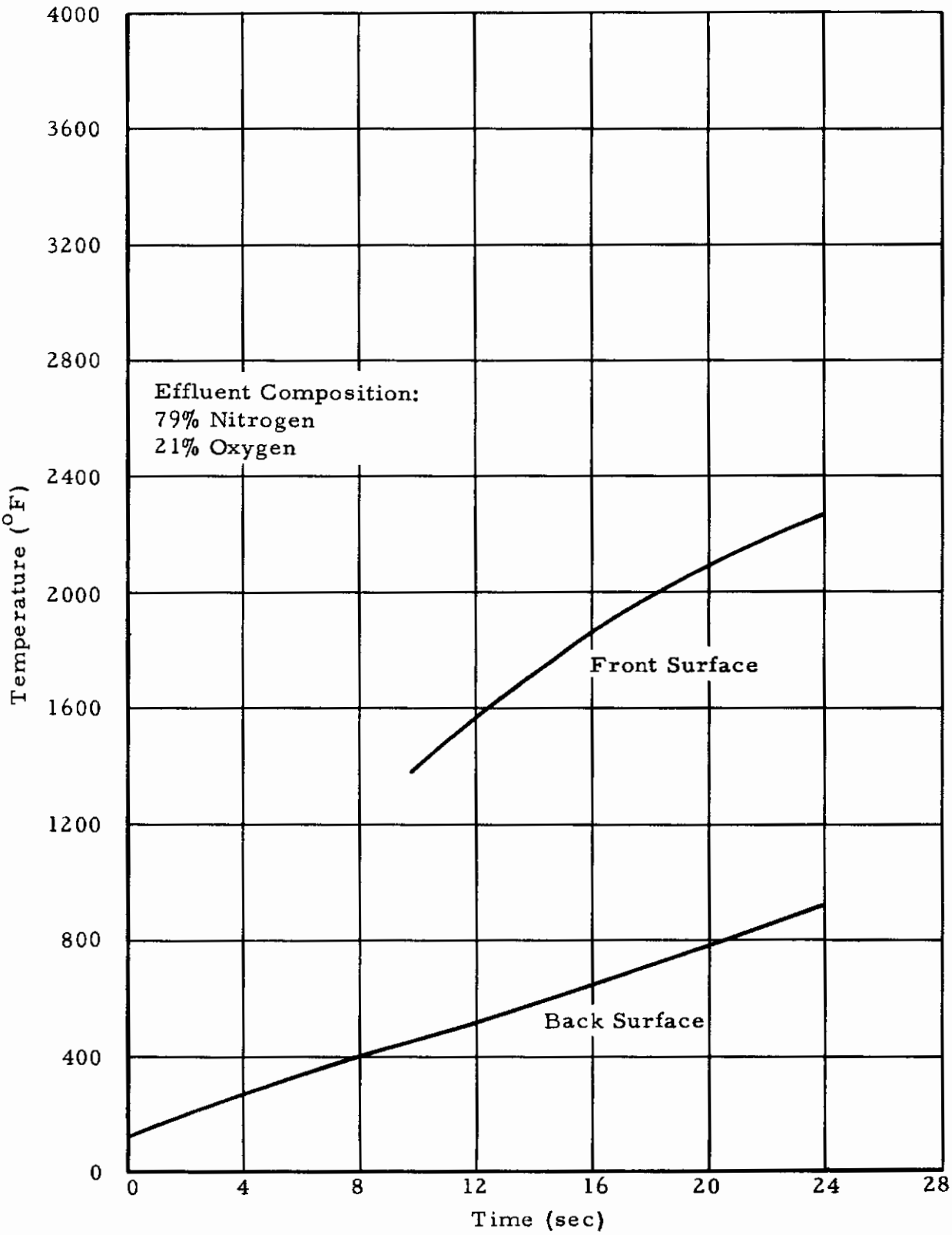

Figure 15. Temperature-Time History of KT Silicon Carbide Exposed to a 493 Btu/ft^2-sec Environment.

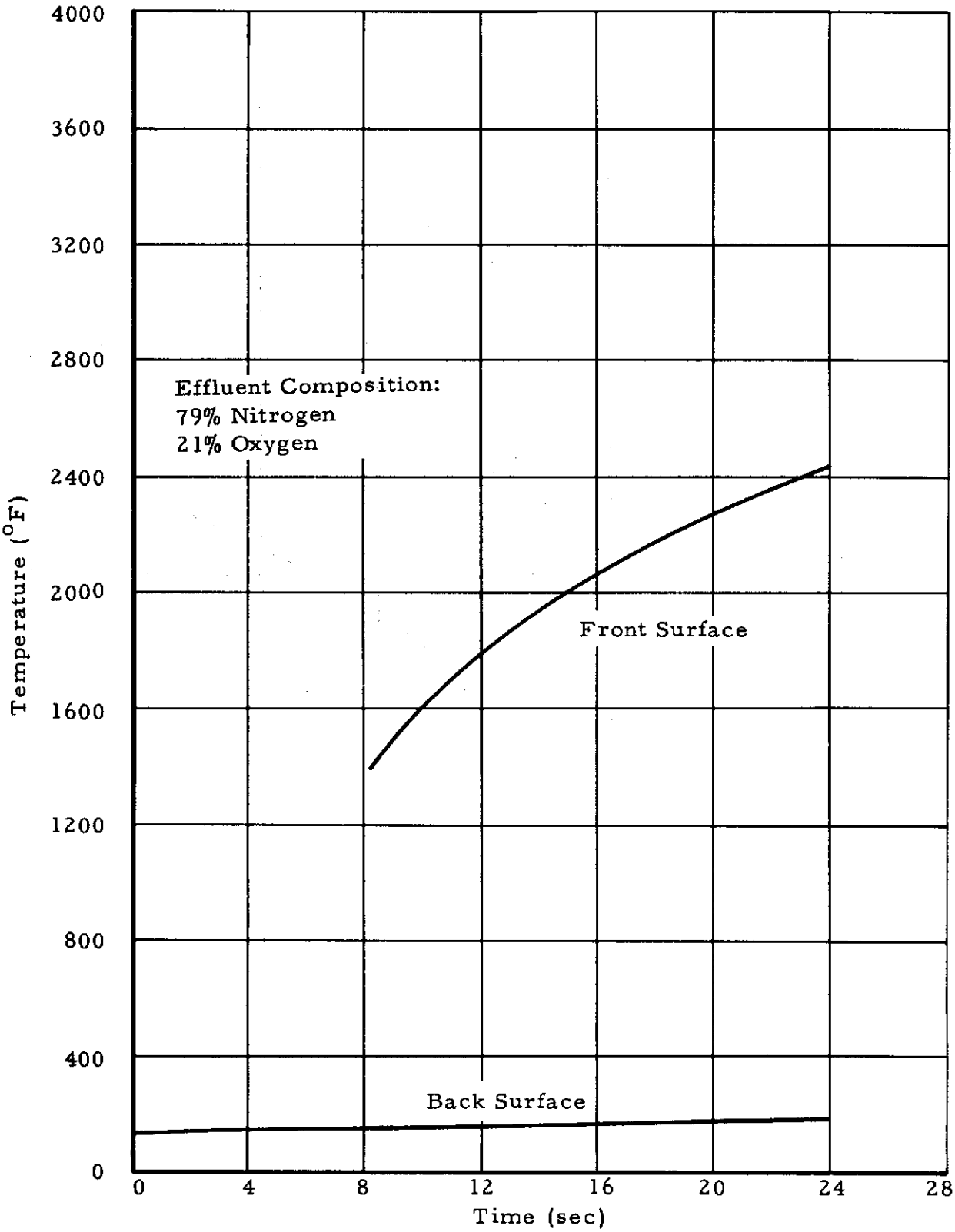

Figure 16. Temperature-Time History of GRB Silicon Carbide Exposed to a 493 Btu/ft^2-sec Environment.

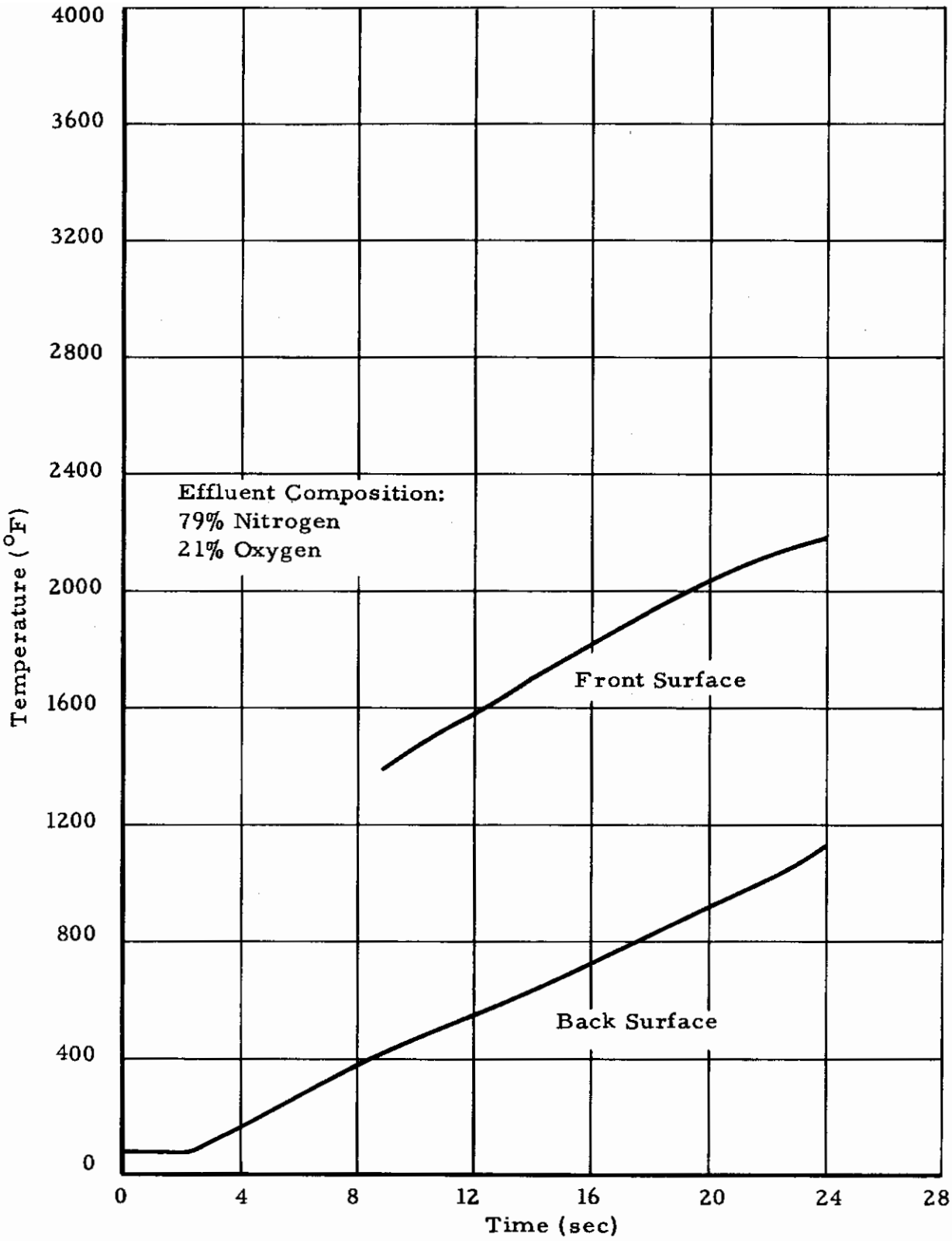

Figure 17. Temperature-Time History of Sintered $ZrB_2 \cdot MoSi_2$ Exposed to a 500 Btu/ft^2-sec Environment.

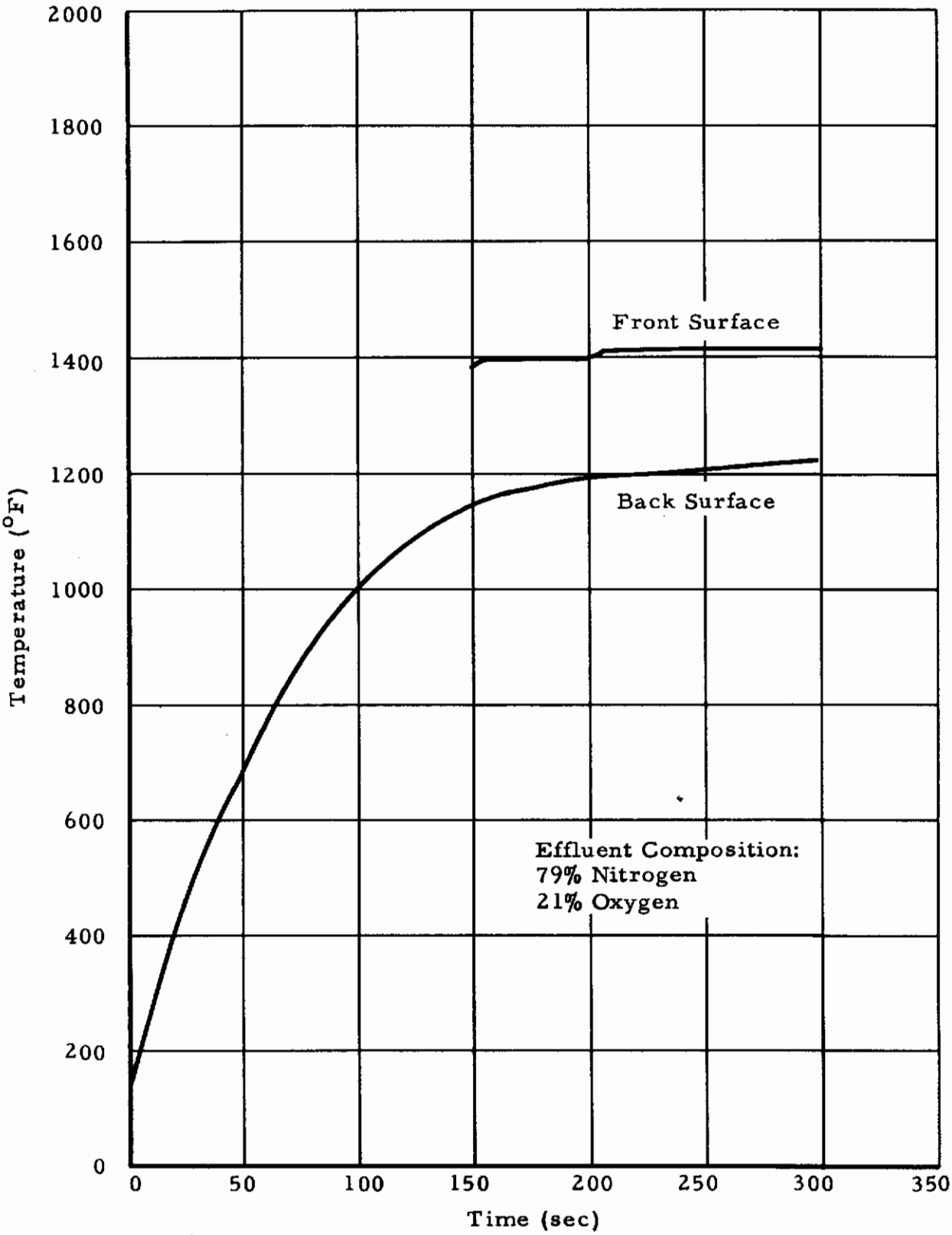

Figure 18. Temperature-Time History of KT Silicon Carbide Exposed to a 100 Btu/ft^2-sec Environment.

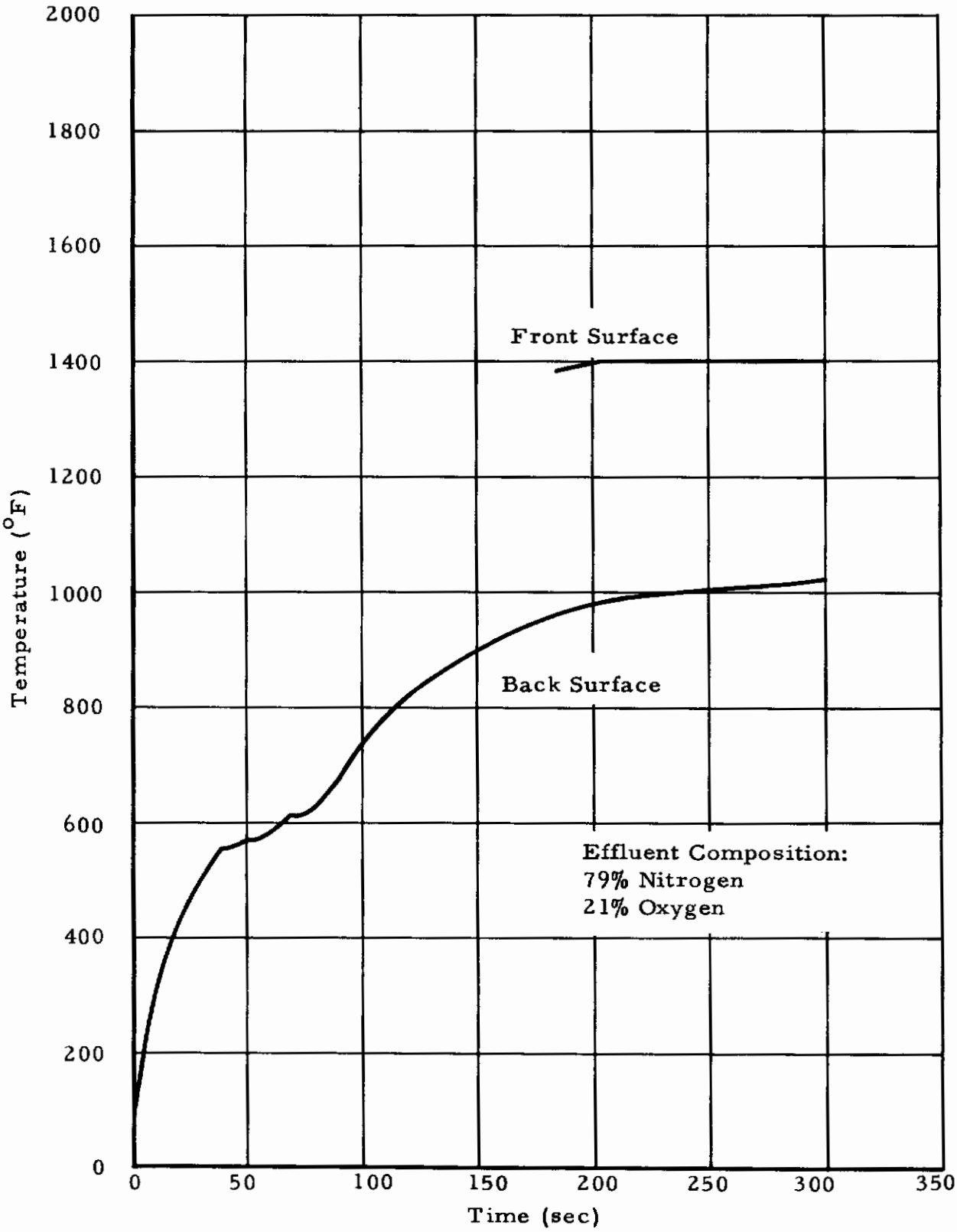

Figure 19. Temperature-Time History of GRB Silicon Carbide Exposed to a 100 Btu/ft^2-sec Environment.

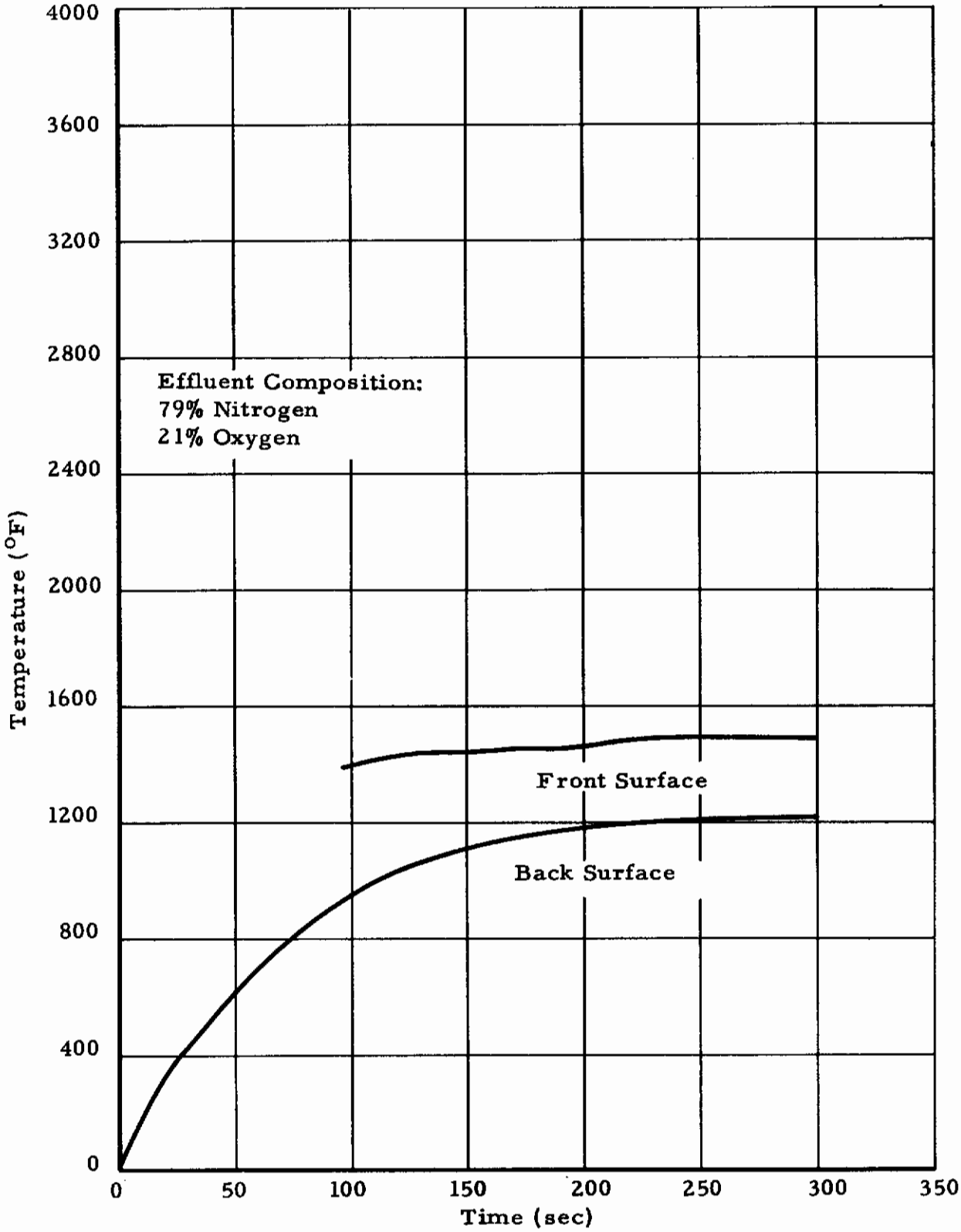

Figure 20. Temperature-Time History of Sintered $ZrB_2 \cdot MoSi_2$ Exposed to a 100 Btu/ft^2-sec Environment.

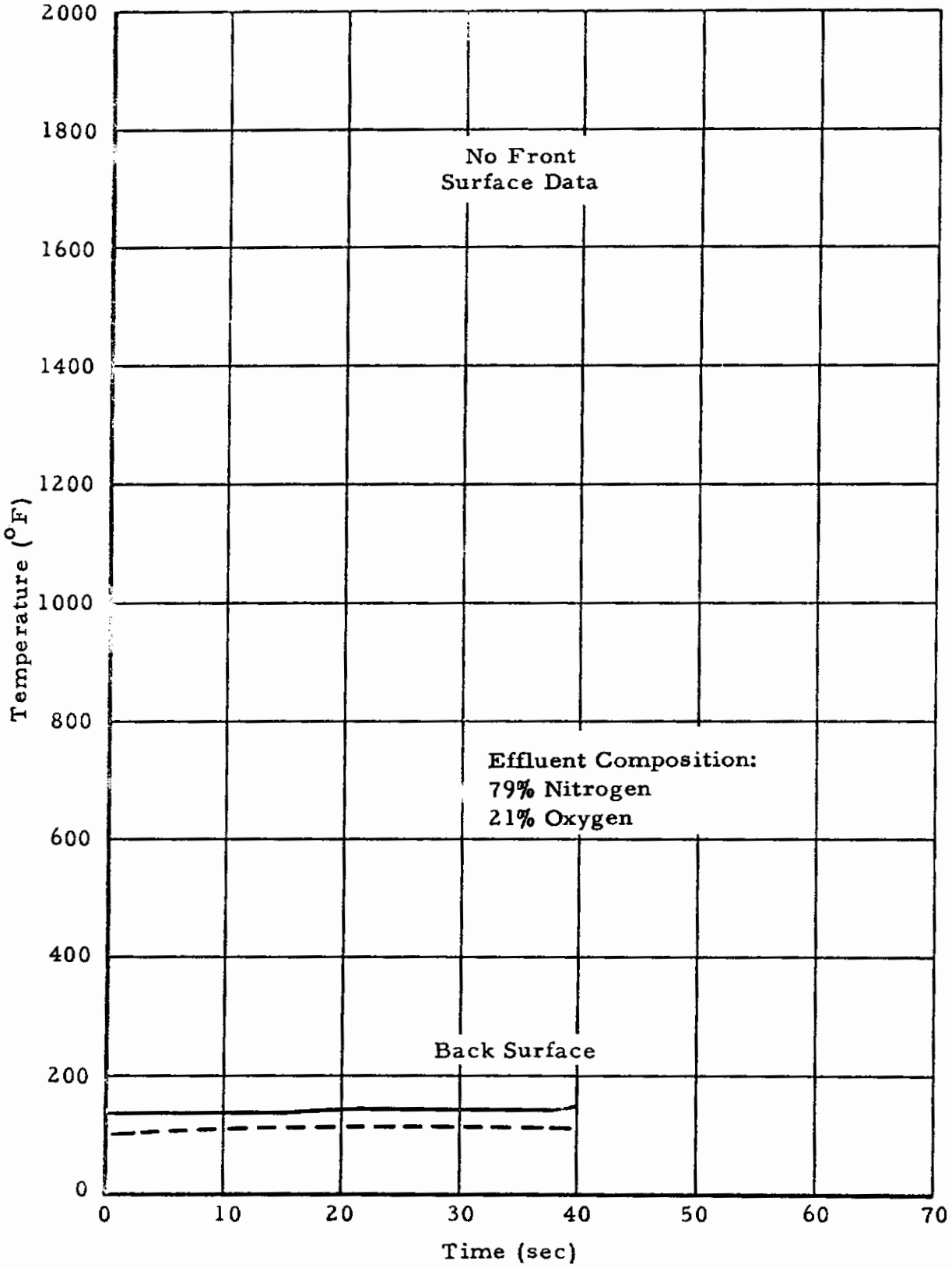

Figure 21. The Temperature-Time History of Filled Silicone Rubber Exposed to a 300 Btu/ft^2-sec Heat Flux Environment

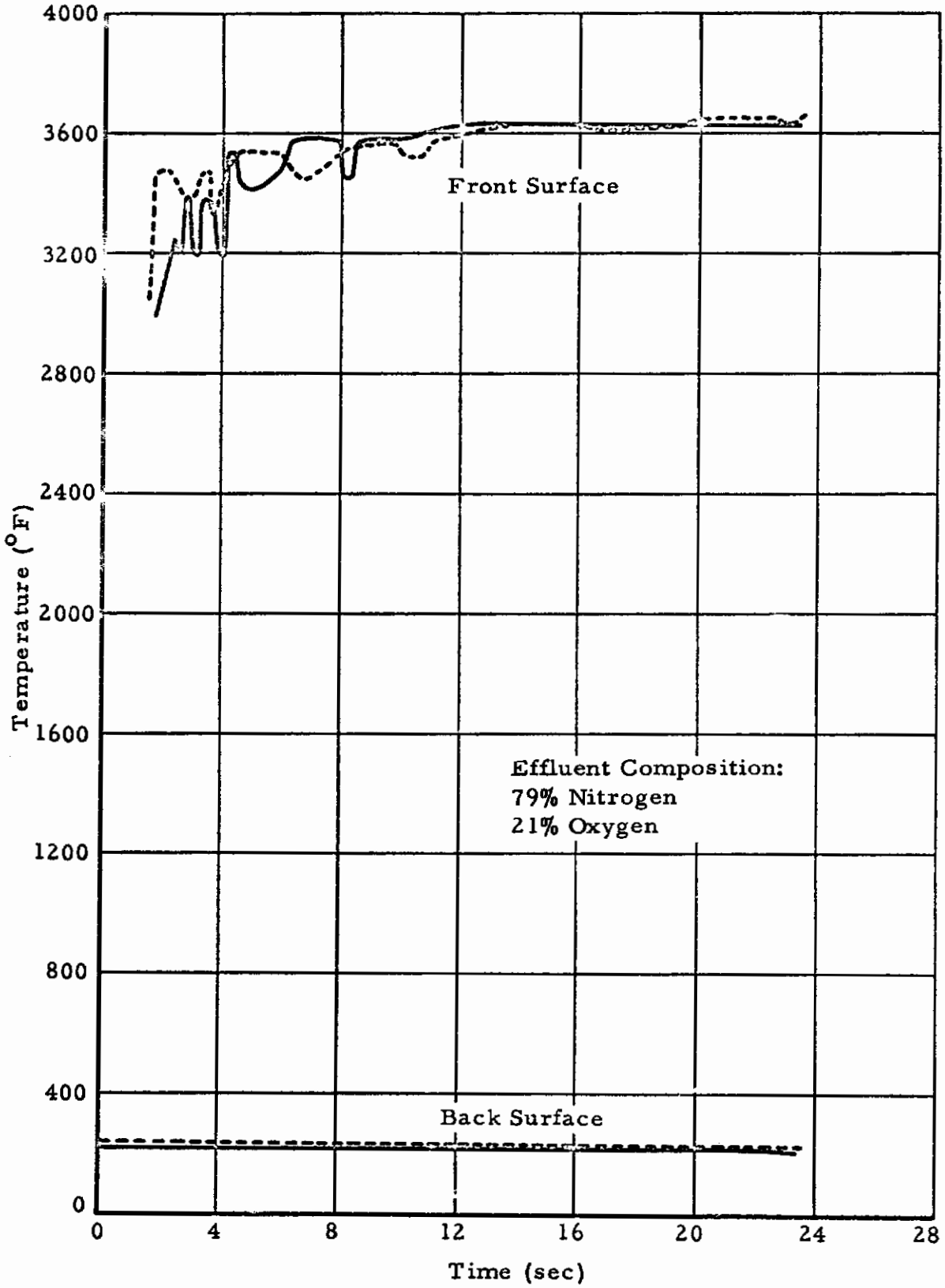

Figure 22. The Temperature-Time History of Filled Silicone Rubber Exposed to a 500 Btu/ft^2-sec Heat Flux Environment

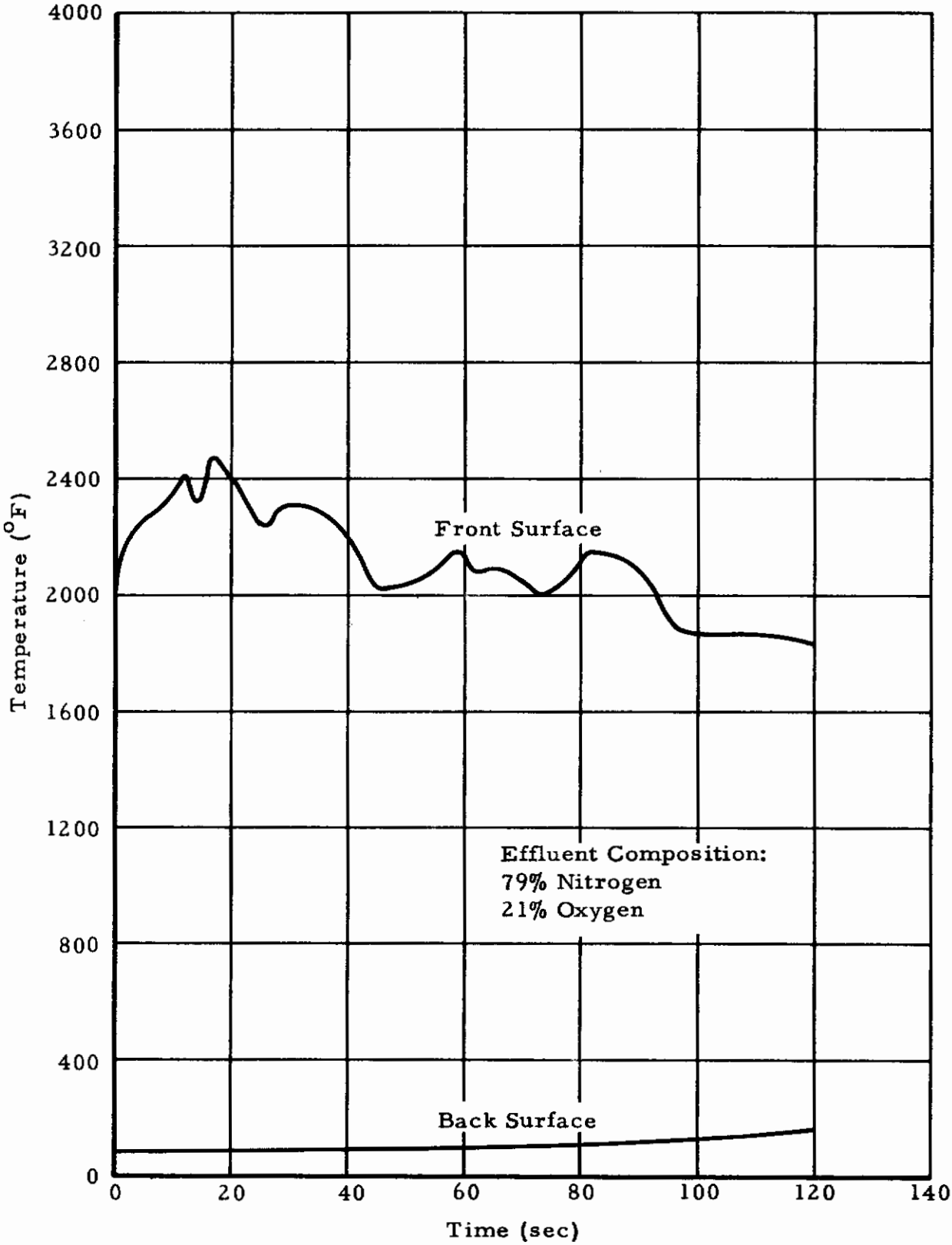

Figure 23. The Temperature-Time History of 015-V1 Molding Compound Exposed to a 100 Btu/ft^2-sec Environment.

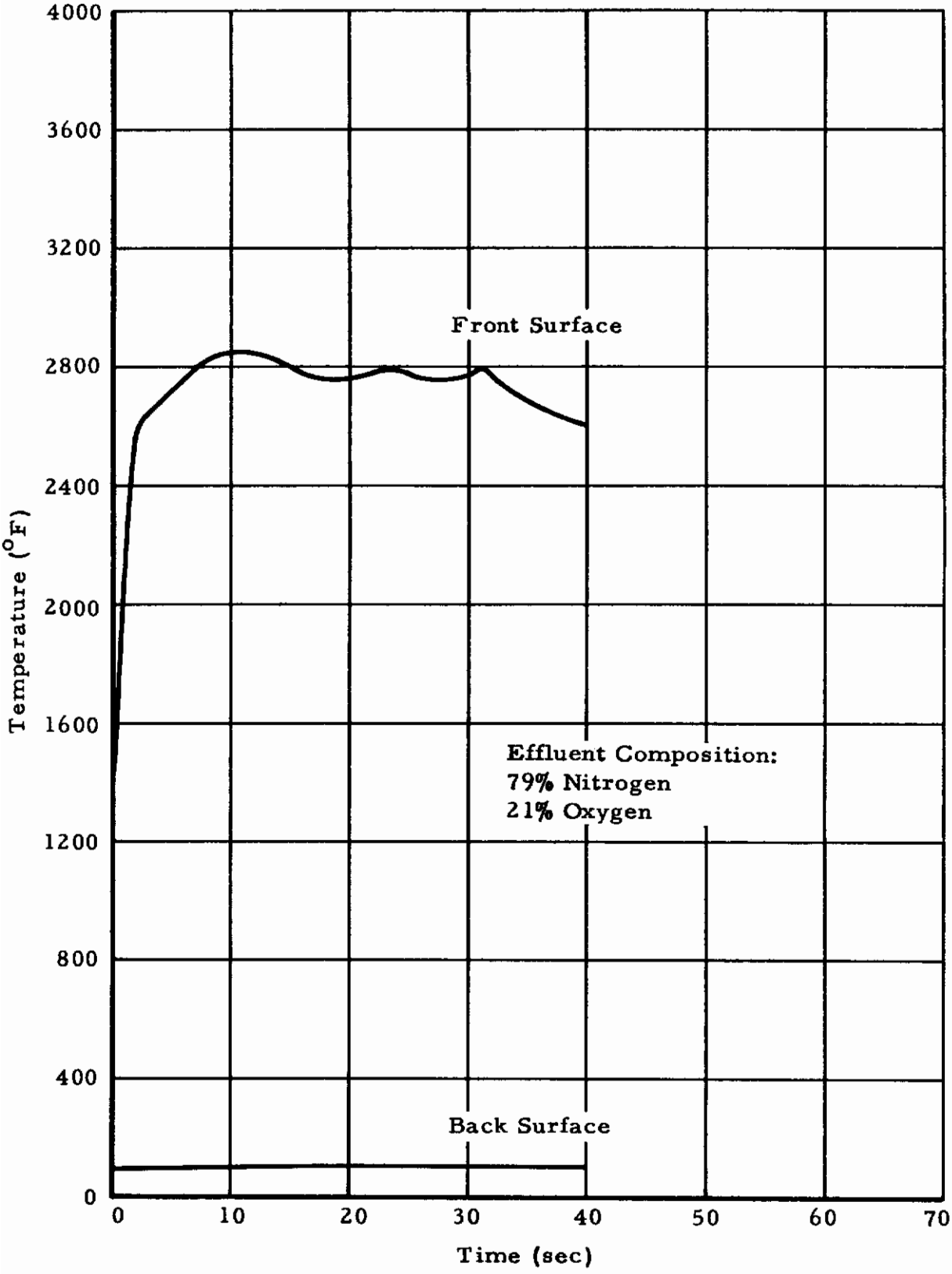

Figure 24. The Temperature-Time History of 015-V1 Molding Compound Exposed to a 300 Btu/ft^2-sec Environment.

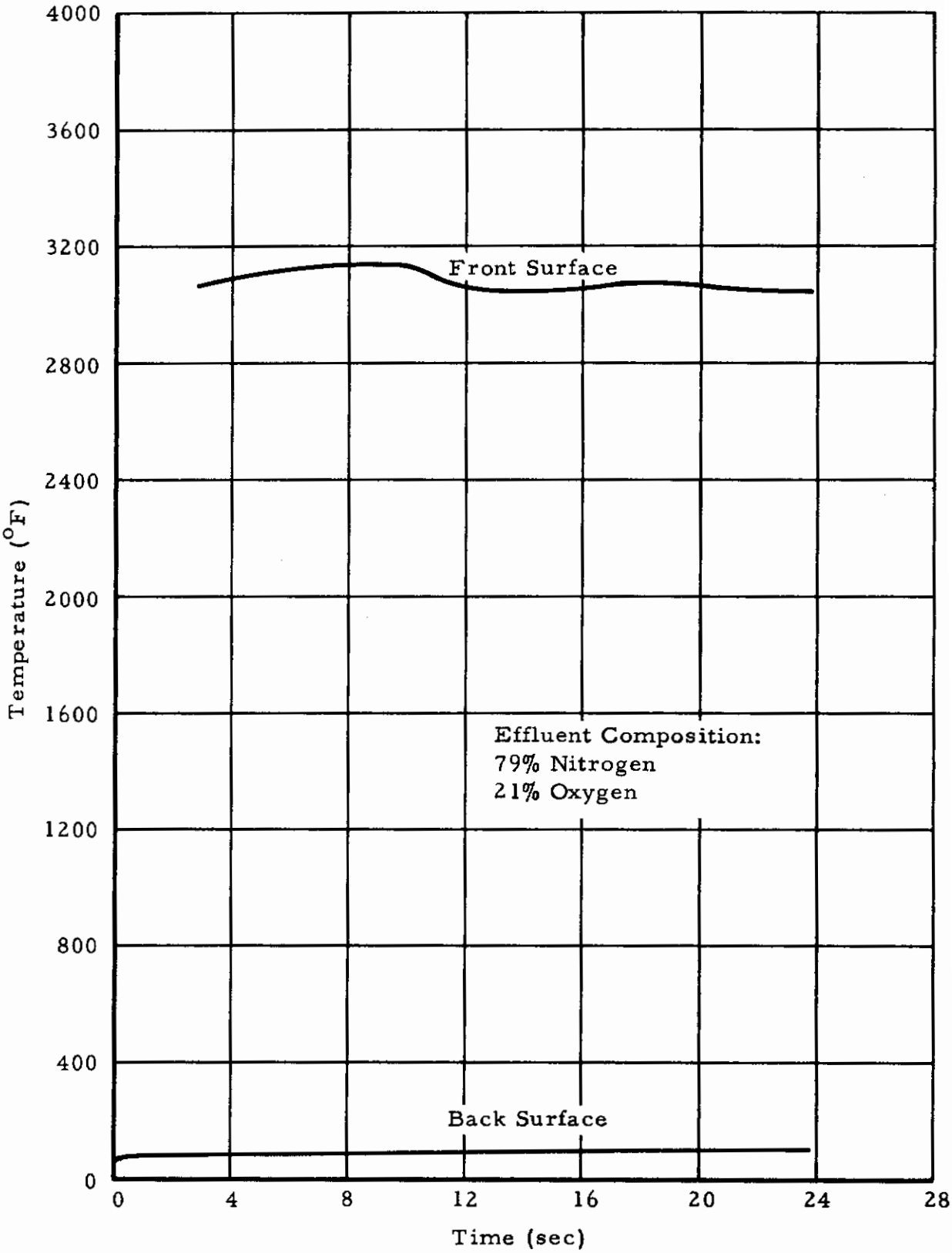

Figure 25. The Temperature-Time History of 015-V1 Molding Compound Exposed to a 500 Btu/ft^2-sec Environment.

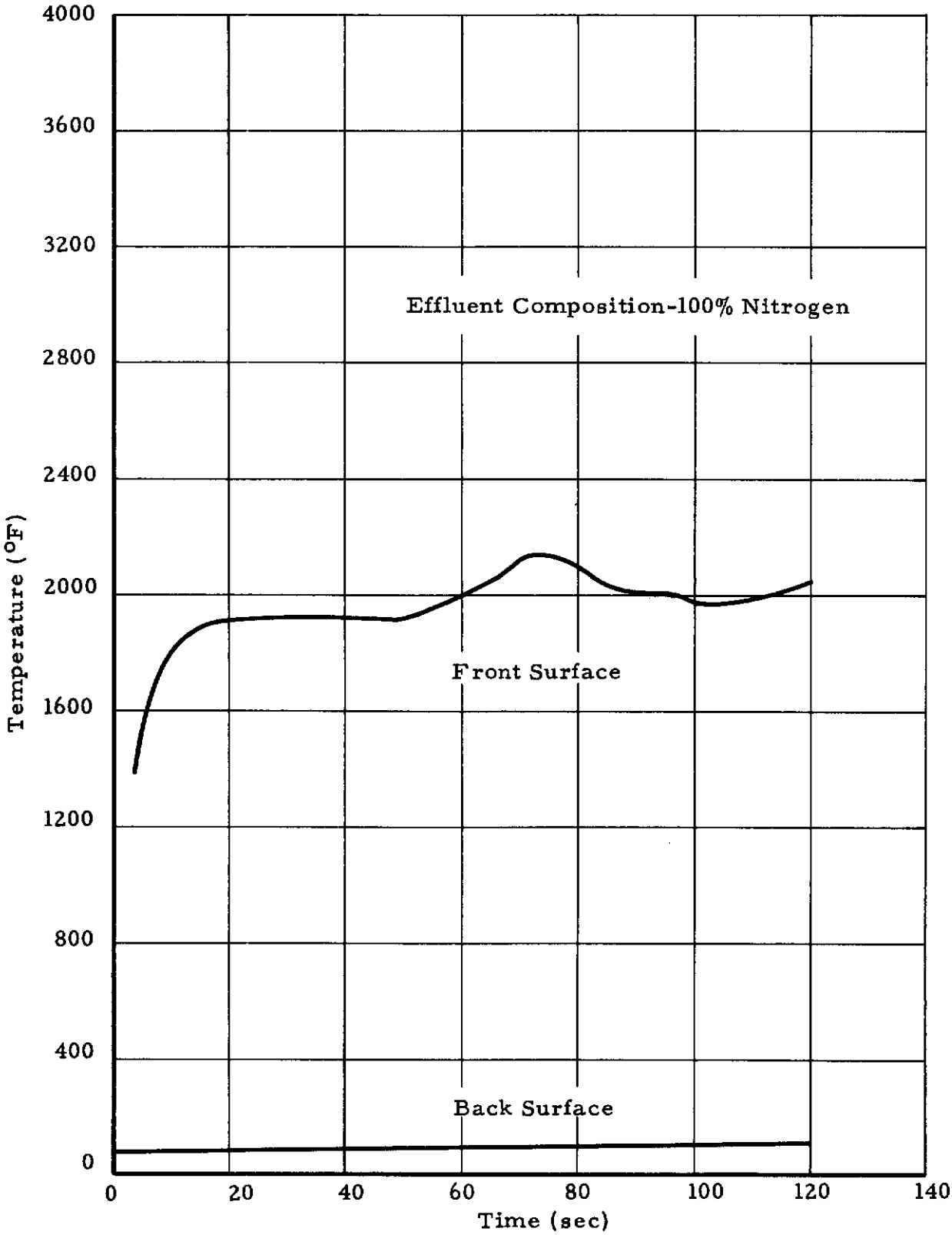

Figure 26. Temperature-Time History of 015-V1 Molding Compound Exposed to a 100 Btu/ft^2-sec Environment.

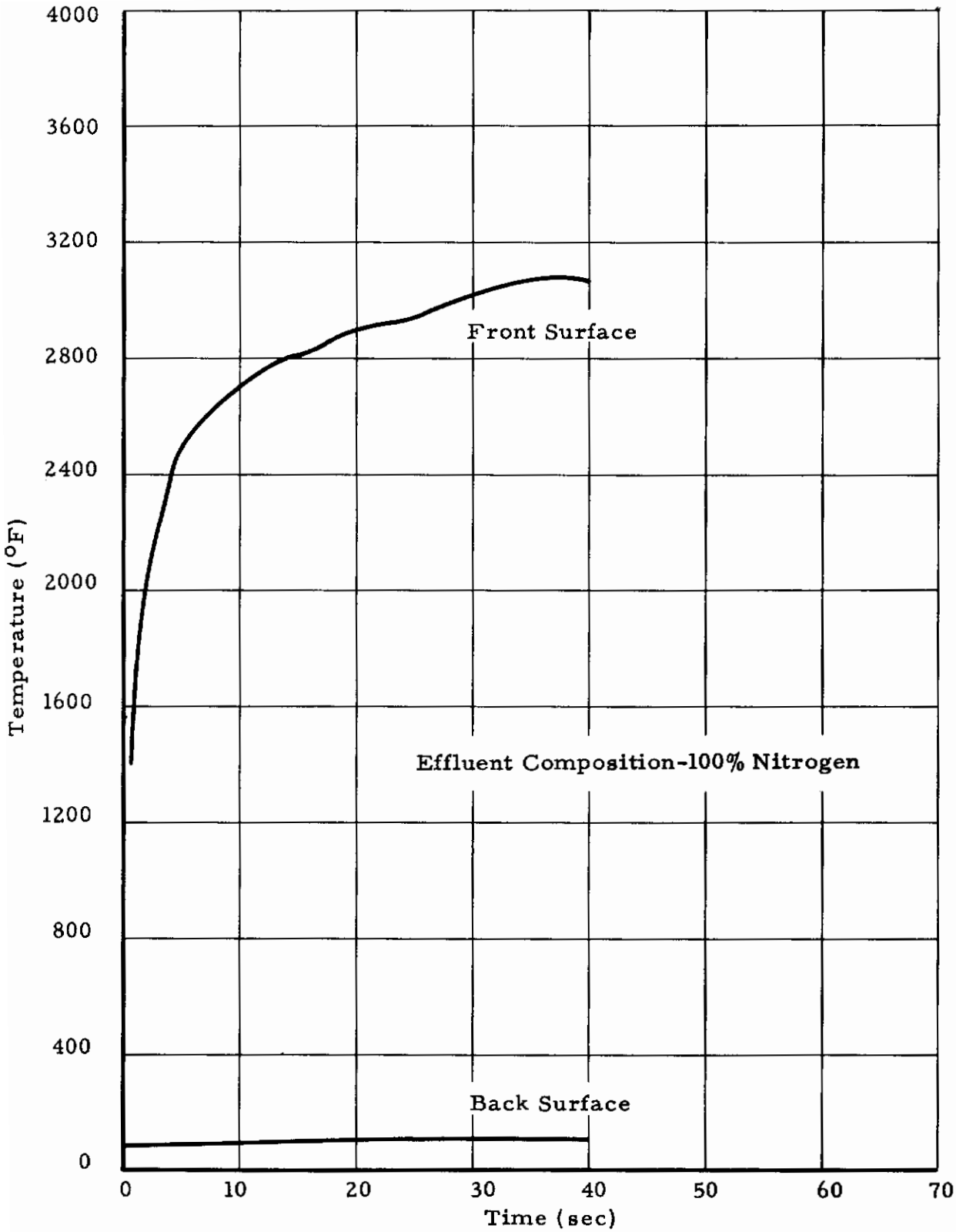

Figure 27. Temperature-Time History of 015-V1 Molding Compound Exposed to a 300 Btu/ft^2-sec Environment.

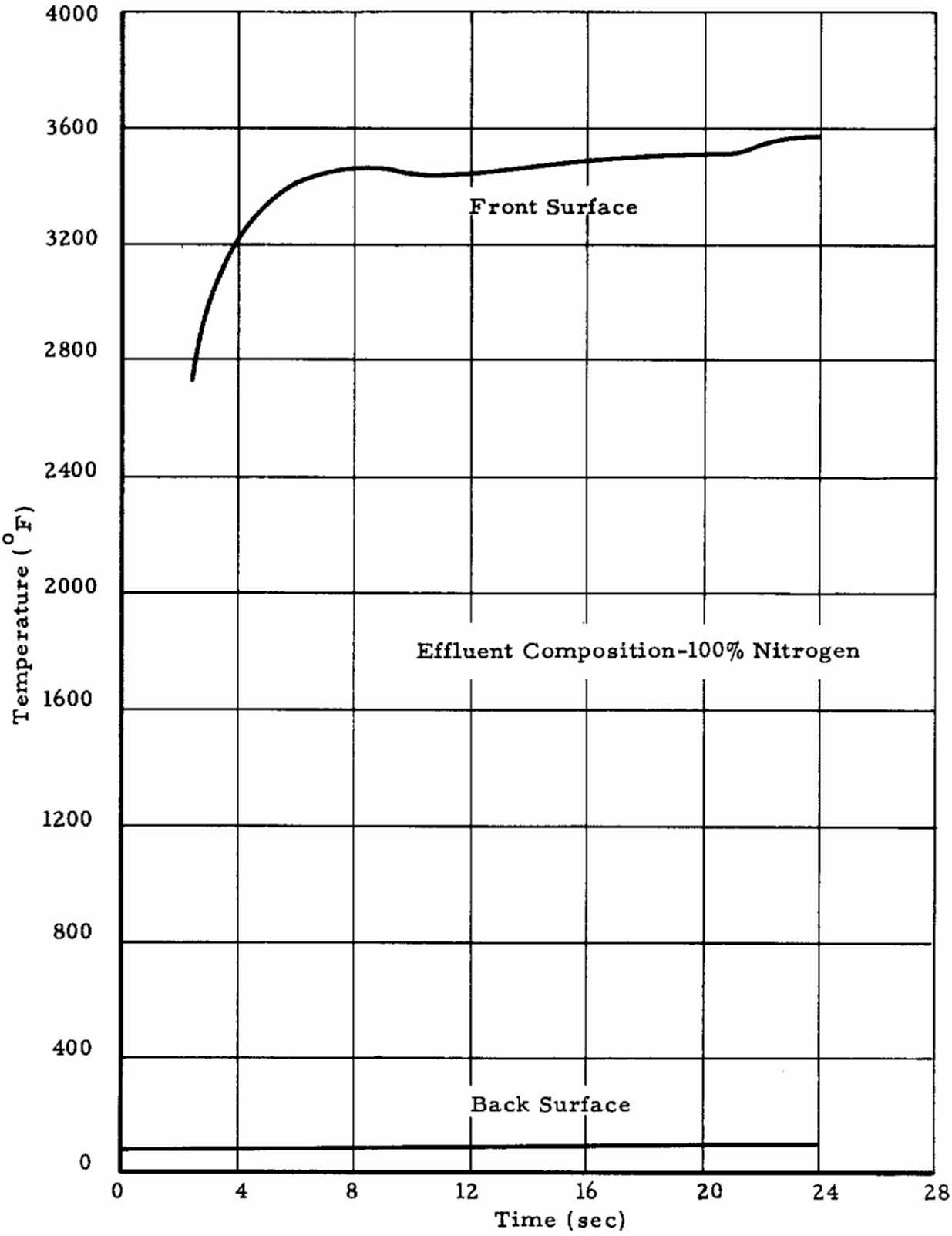

Figure 28. Temperature-Time History of 015-V1 Molding Compound Exposed to a 500 Btu/ft^2-sec Environment.

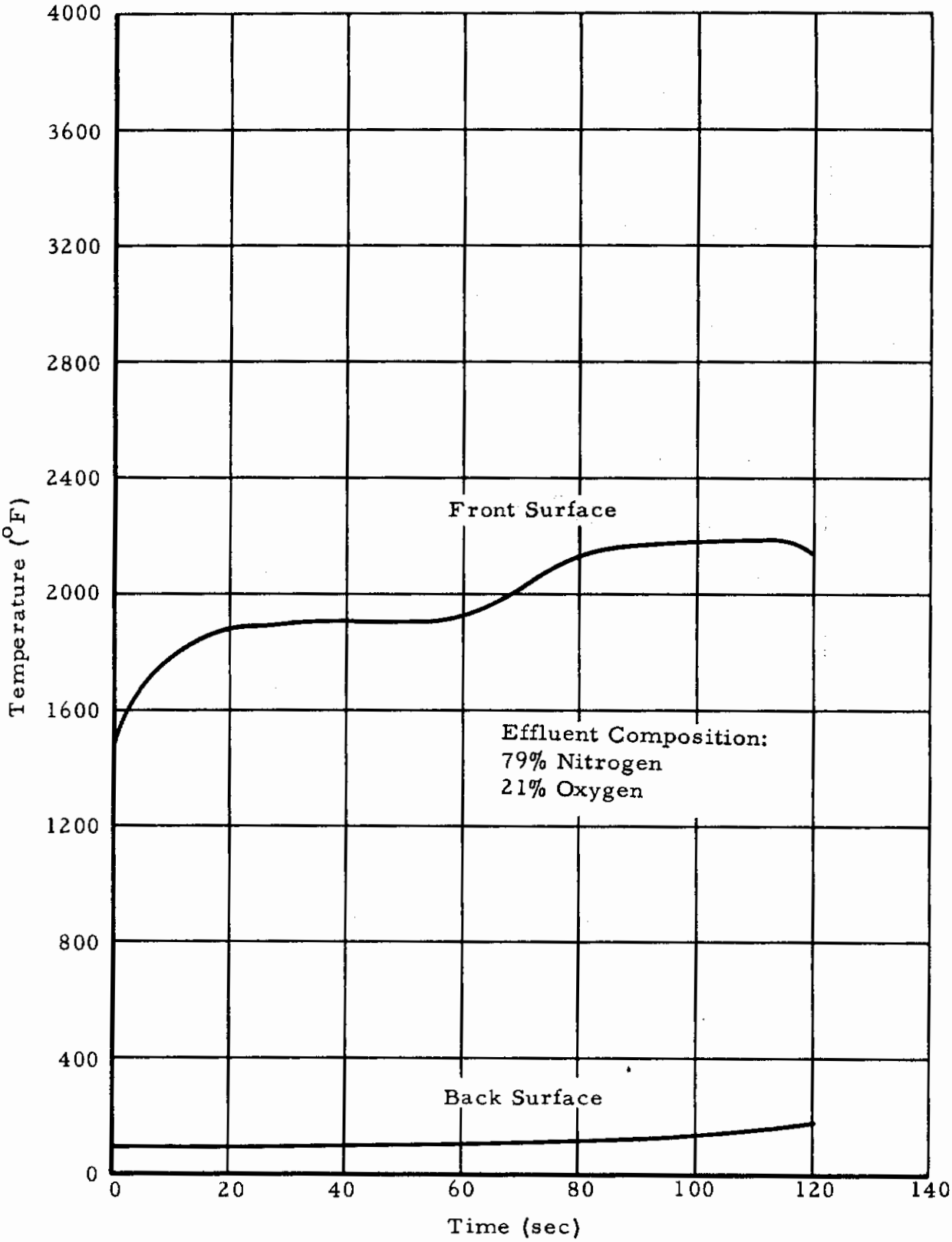

Figure 29. The Temperature-Time History of 015 Molding Compound Exposed to a 100 Btu/ft^2-sec Environment.

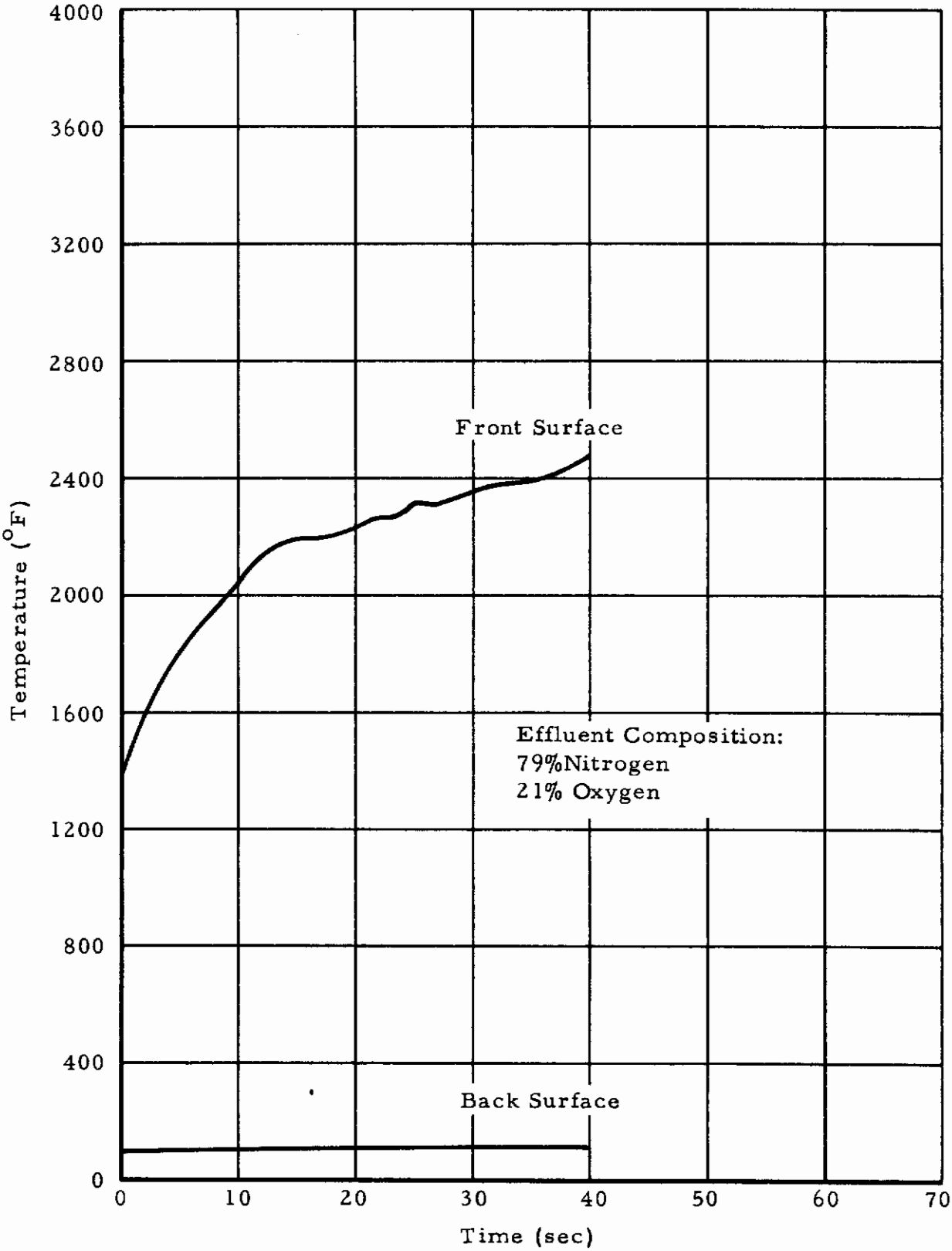

Figure 30. The Temperature-Time History of 015 Molding Compound Exposed to a 300 Btu/ft^2-sec Environment.

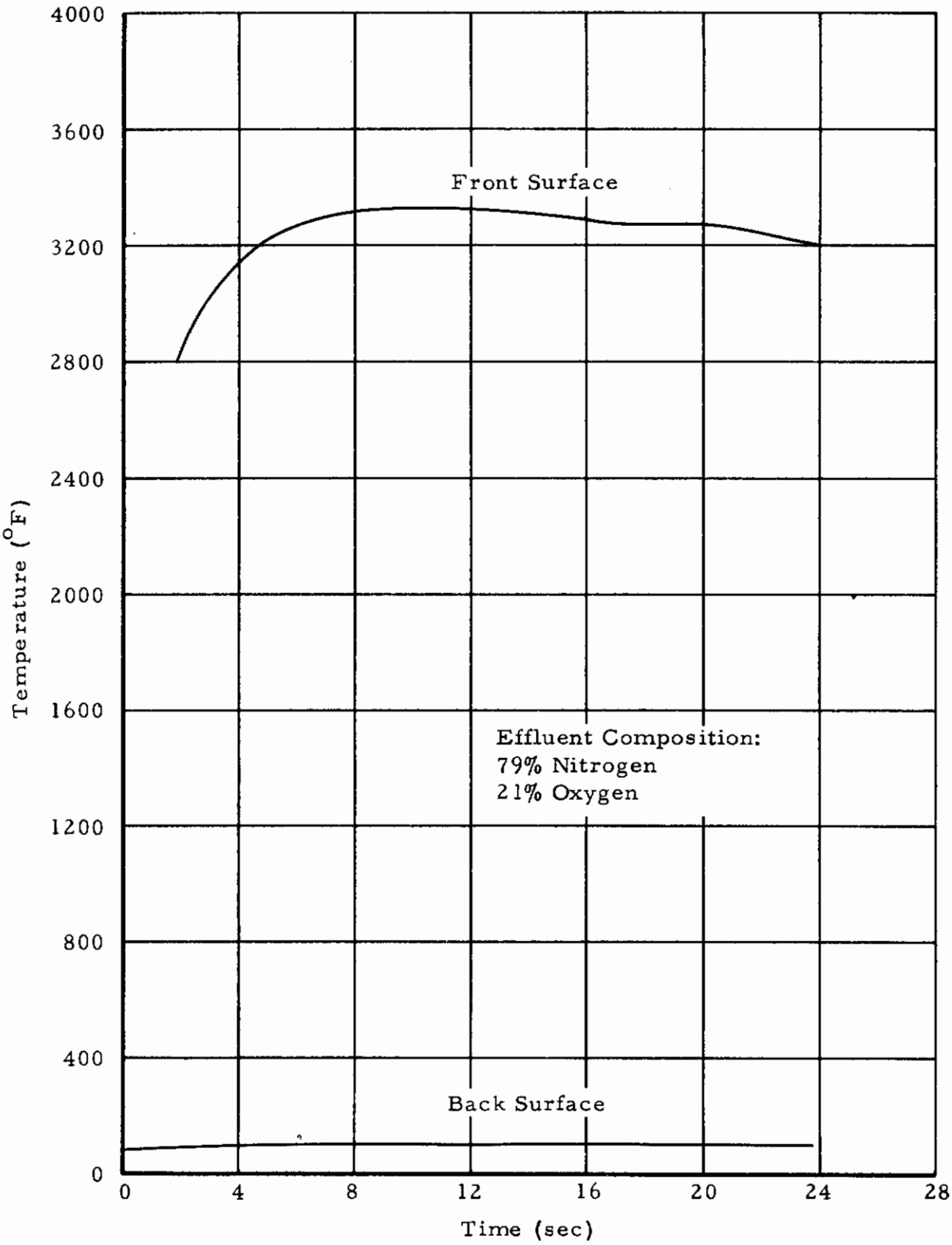

Figure 31. The Temperature-Time History of 015 Molding Compound Exposed to a 500 Btu/ft^2-sec Environment.

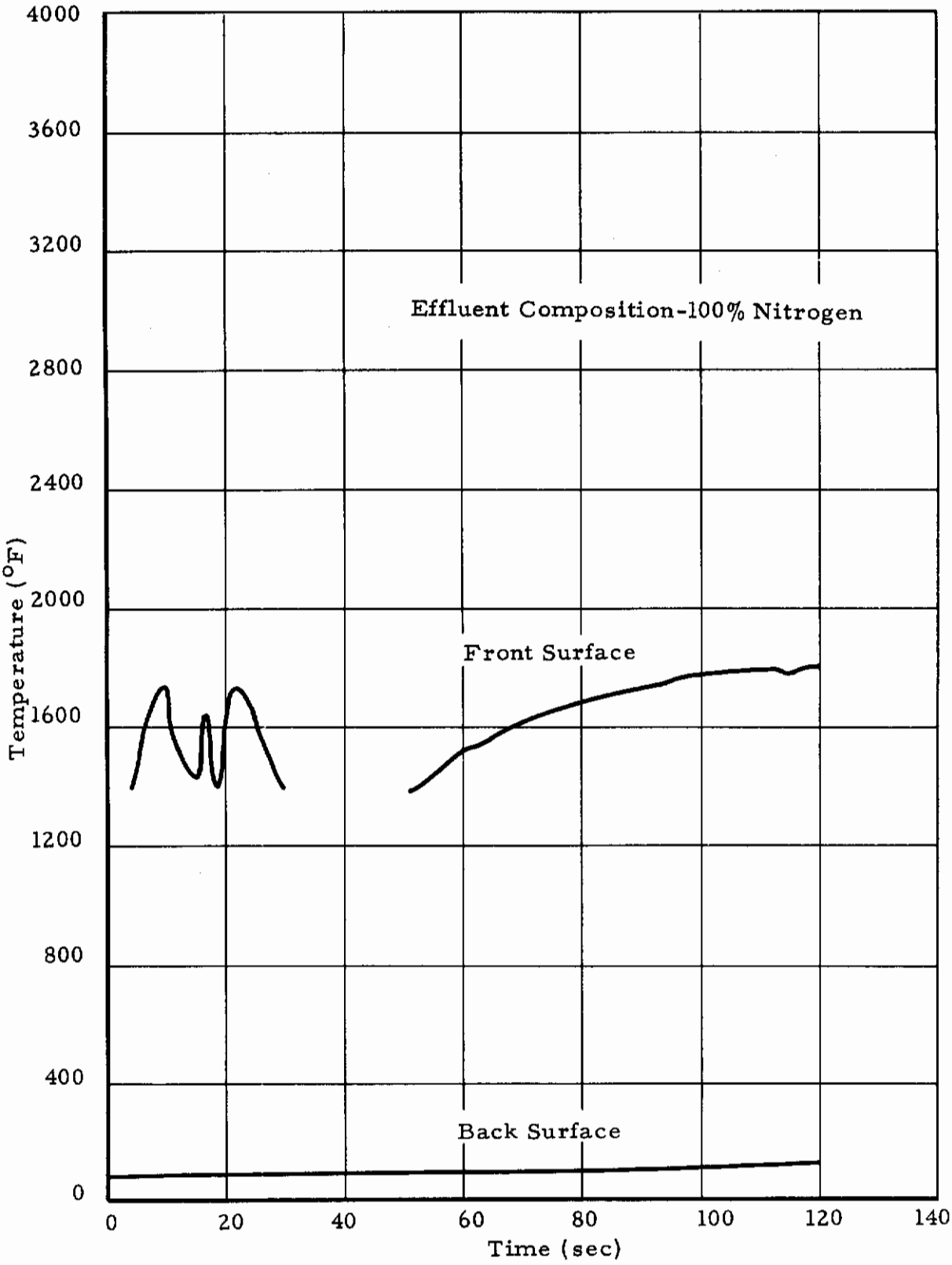

Figure 32. Temperature-Time History of 015 Molding Compound Exposed to a 100 Btu/ft^2-sec Environment.

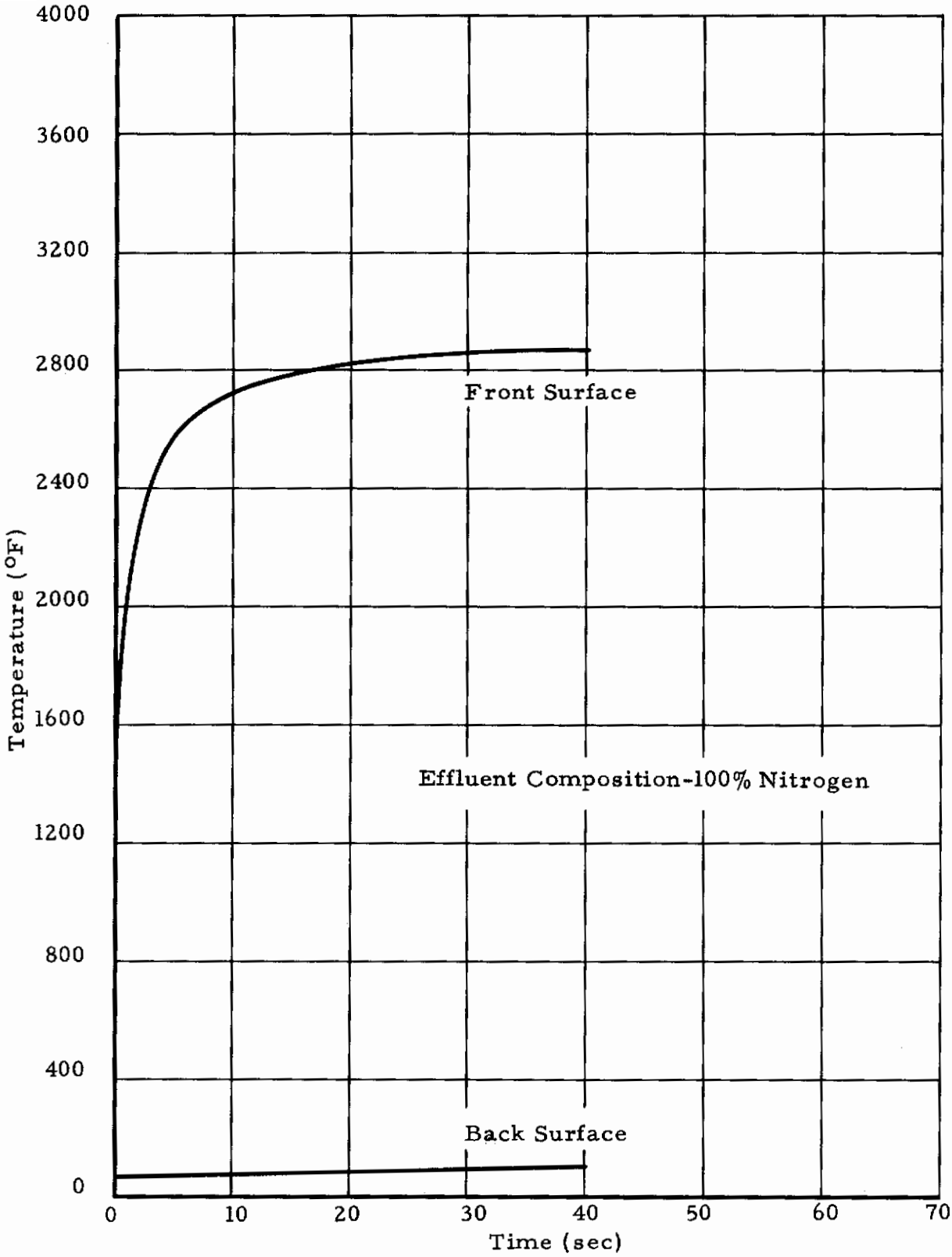

Figure 33. Temperature-Time History of 015 Molding Compound Exposed to a 300 Btu/ft^2-sec Environment.

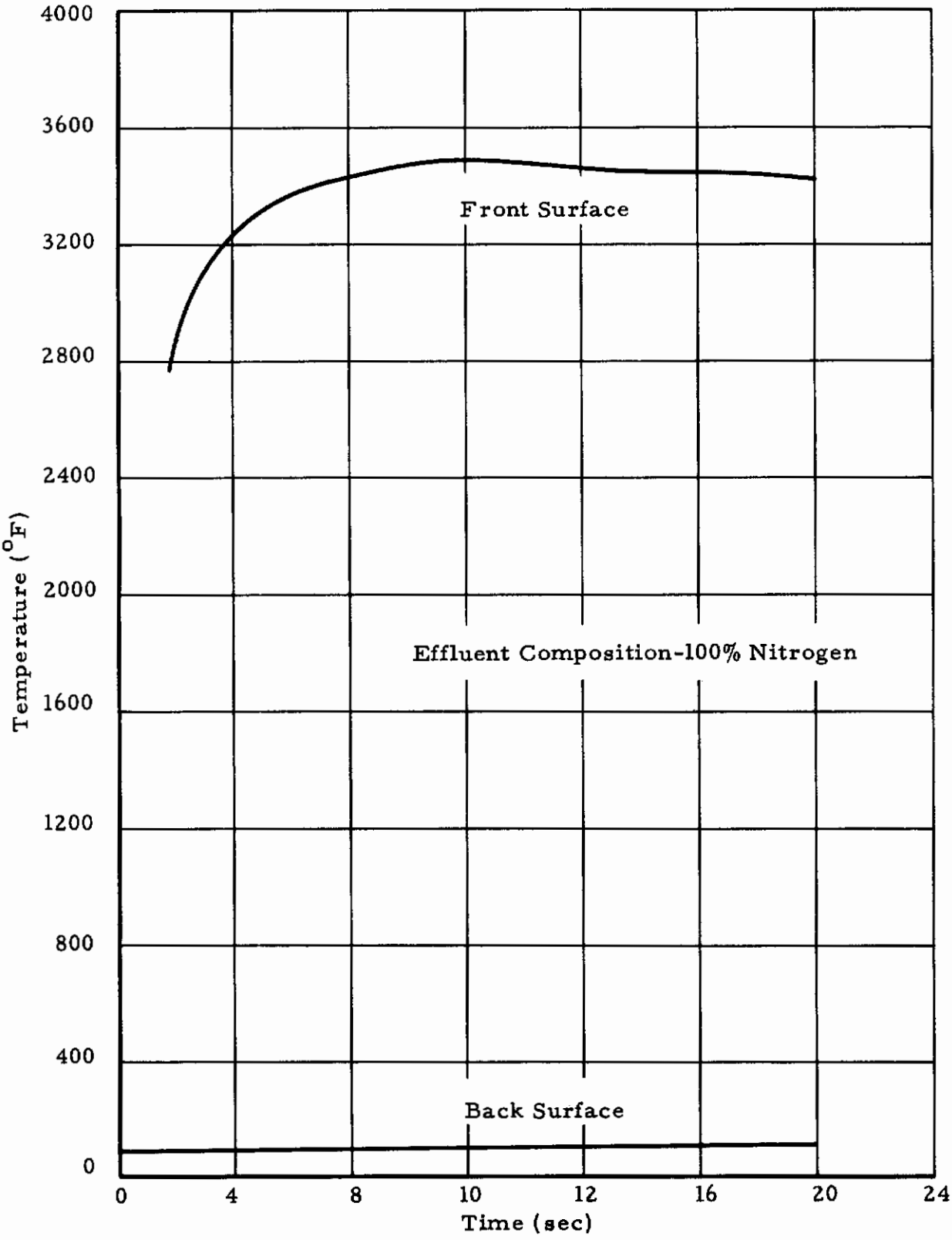

Figure 34. Temperature-Time History of 015 Molding Compound Exposed to a 500 Btu/ft^2-sec Environment.

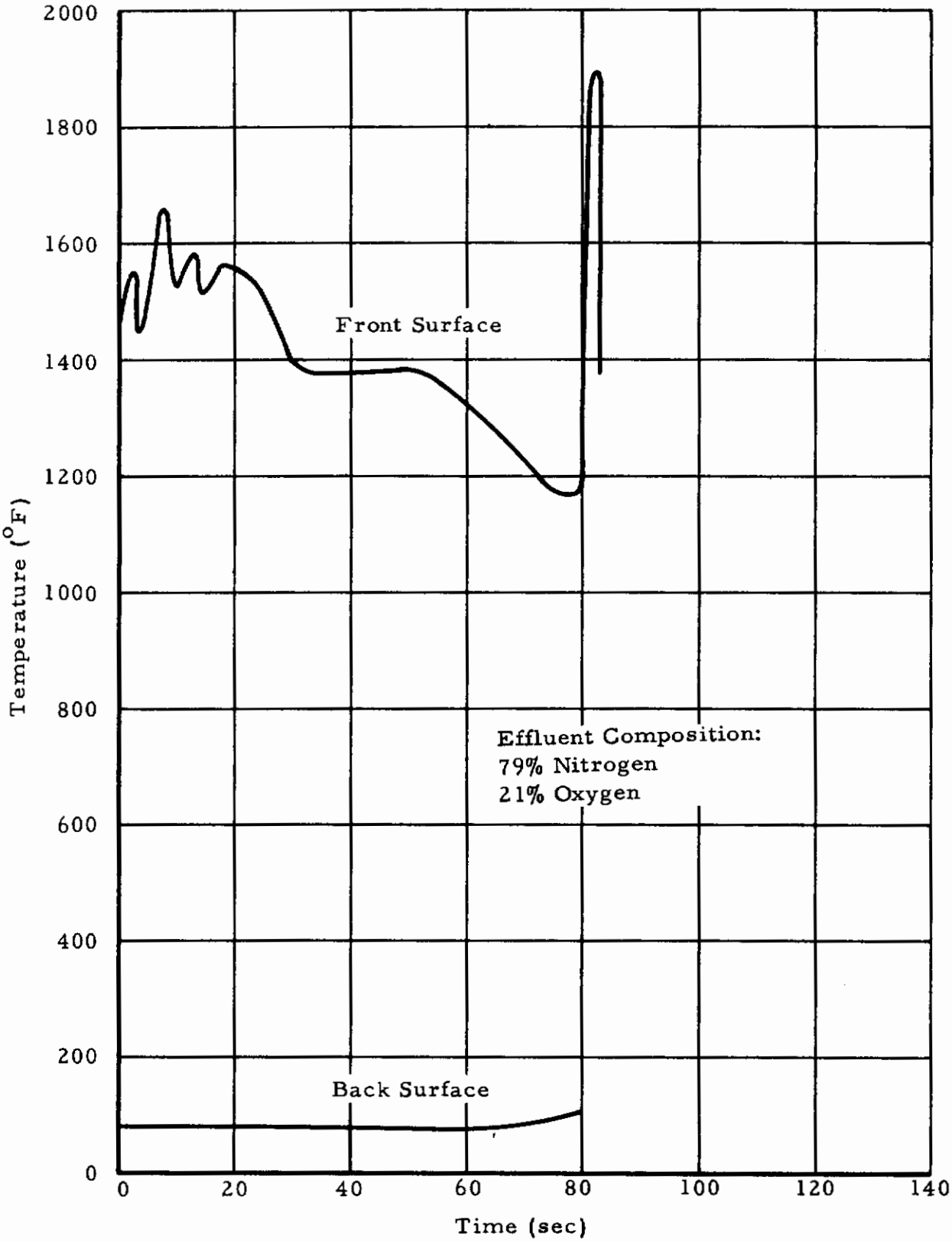

Figure 35. The Temperature-Time History of 010-V6 Molding Compound Exposed to a 100 Btu/ft^2-sec Environment.

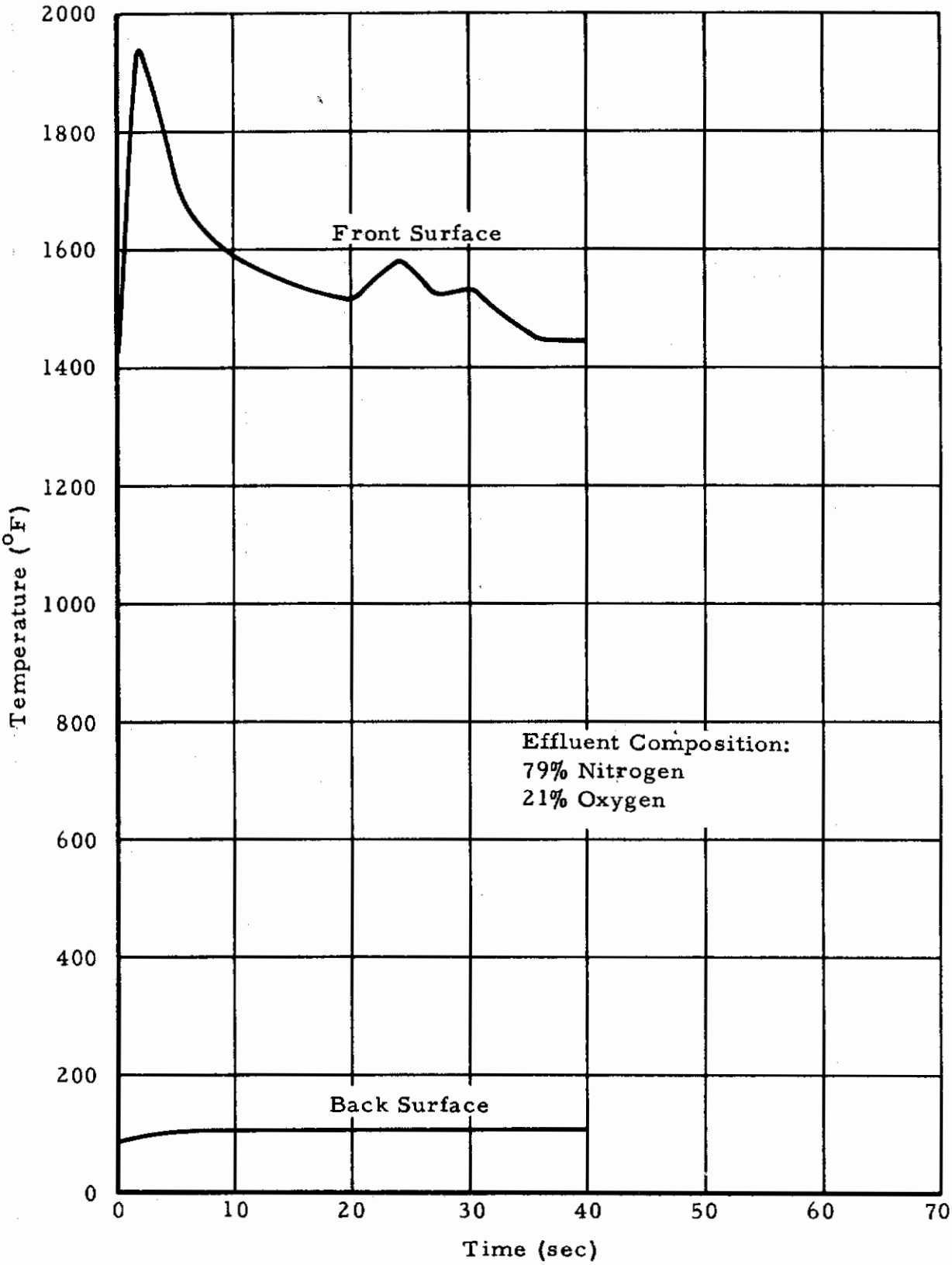

Figure 36. The Temperature-Time History of 010-V6 Molding Compound Exposed to a 300 Btu/ft^2-sec Environment.

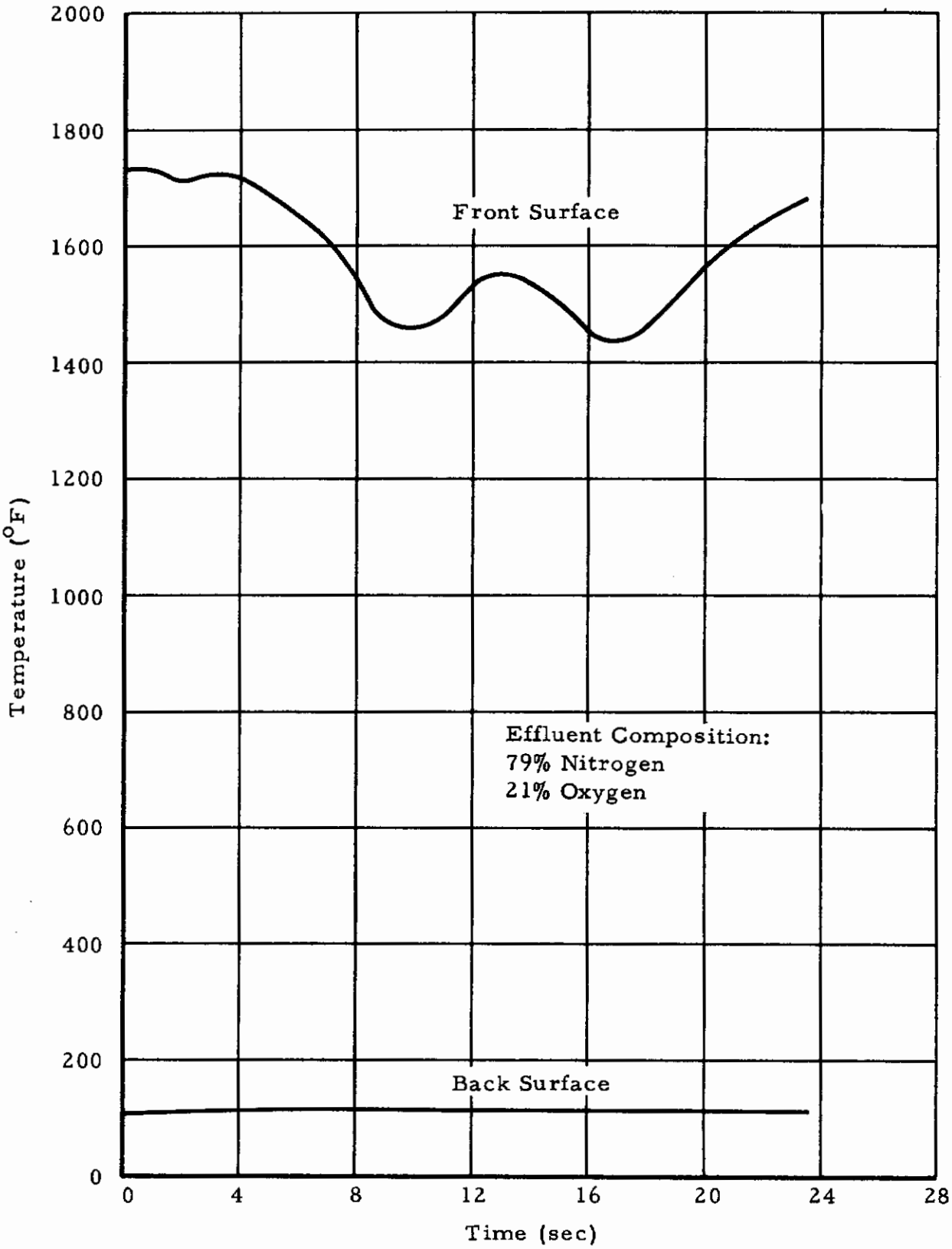

Figure 37. The Temperature-Time History of 010-V6 Molding Compound Exposed to a 500 Btu/ft^2-sec Environment.

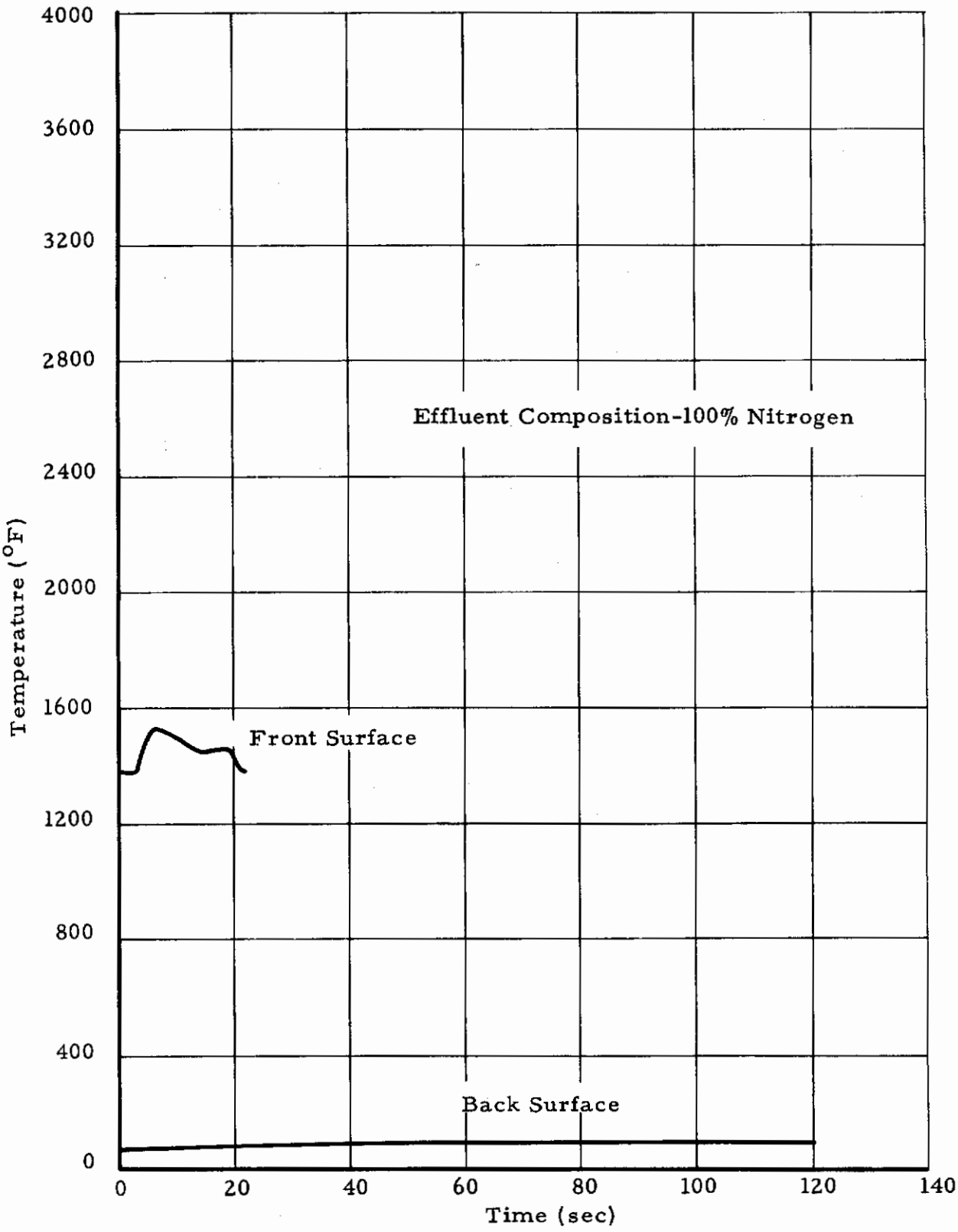

Figure 38. Temperature-Time History of 010-V6 Molding Compound Exposed to a 100 Btu/ft^2-sec Environment.

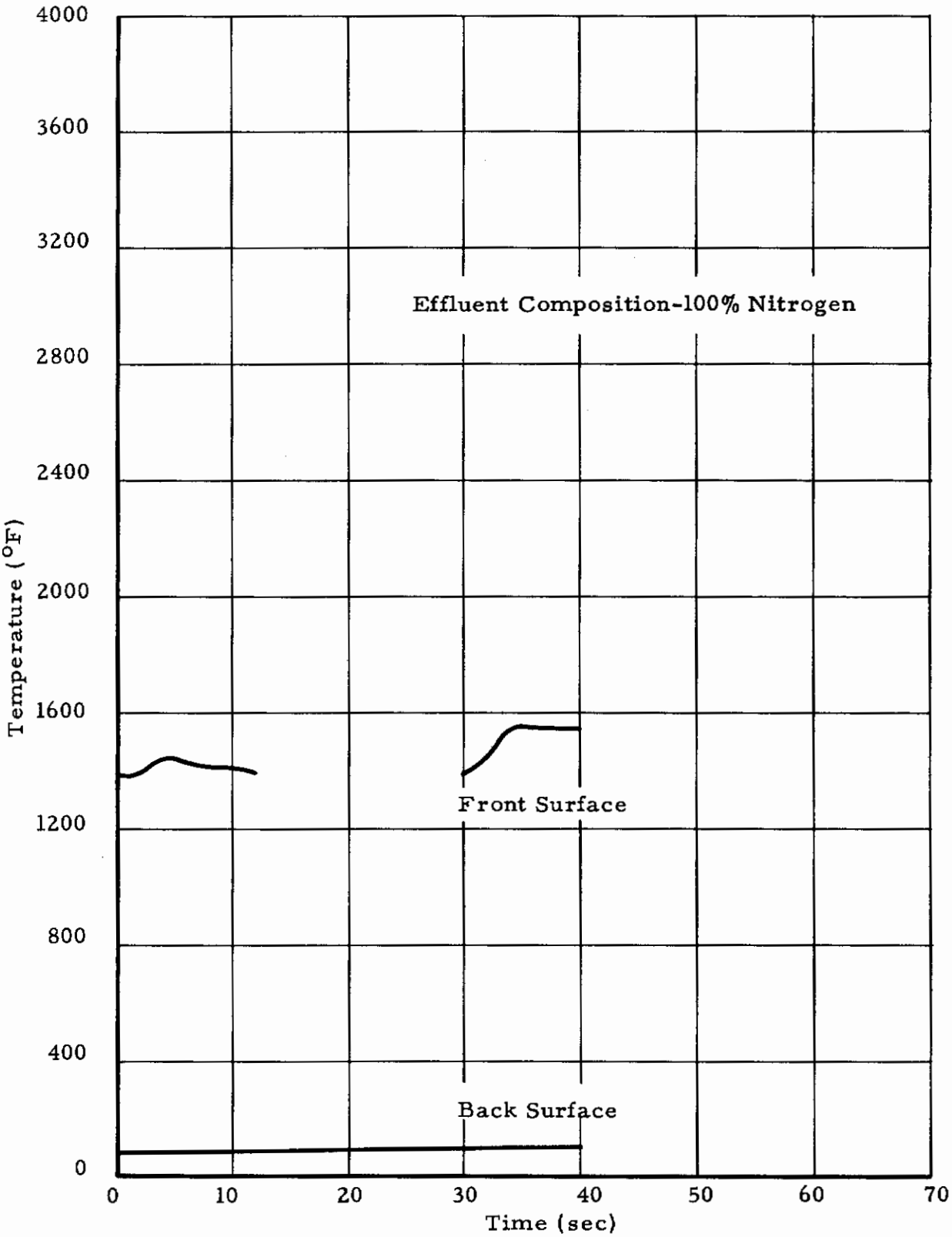

Figure 39. Temperature-Time History of 010-V6 Molding Compound Exposed to a 300 Btu/ft^2-sec Environment.

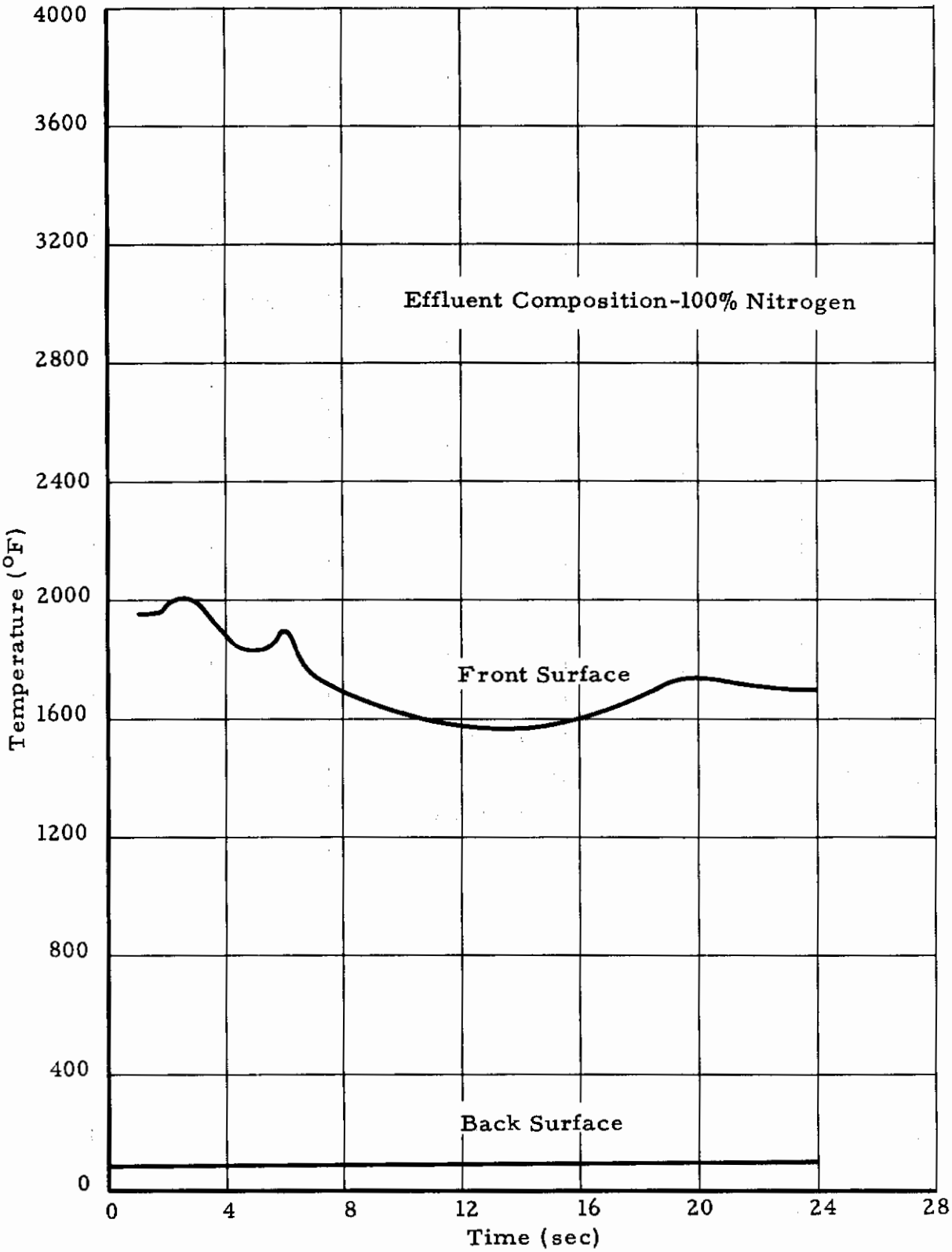

Figure 40. Temperature-Time History of 010-V6 Molding Compound Exposed to a 500 Btu/ft^2-sec Environment.

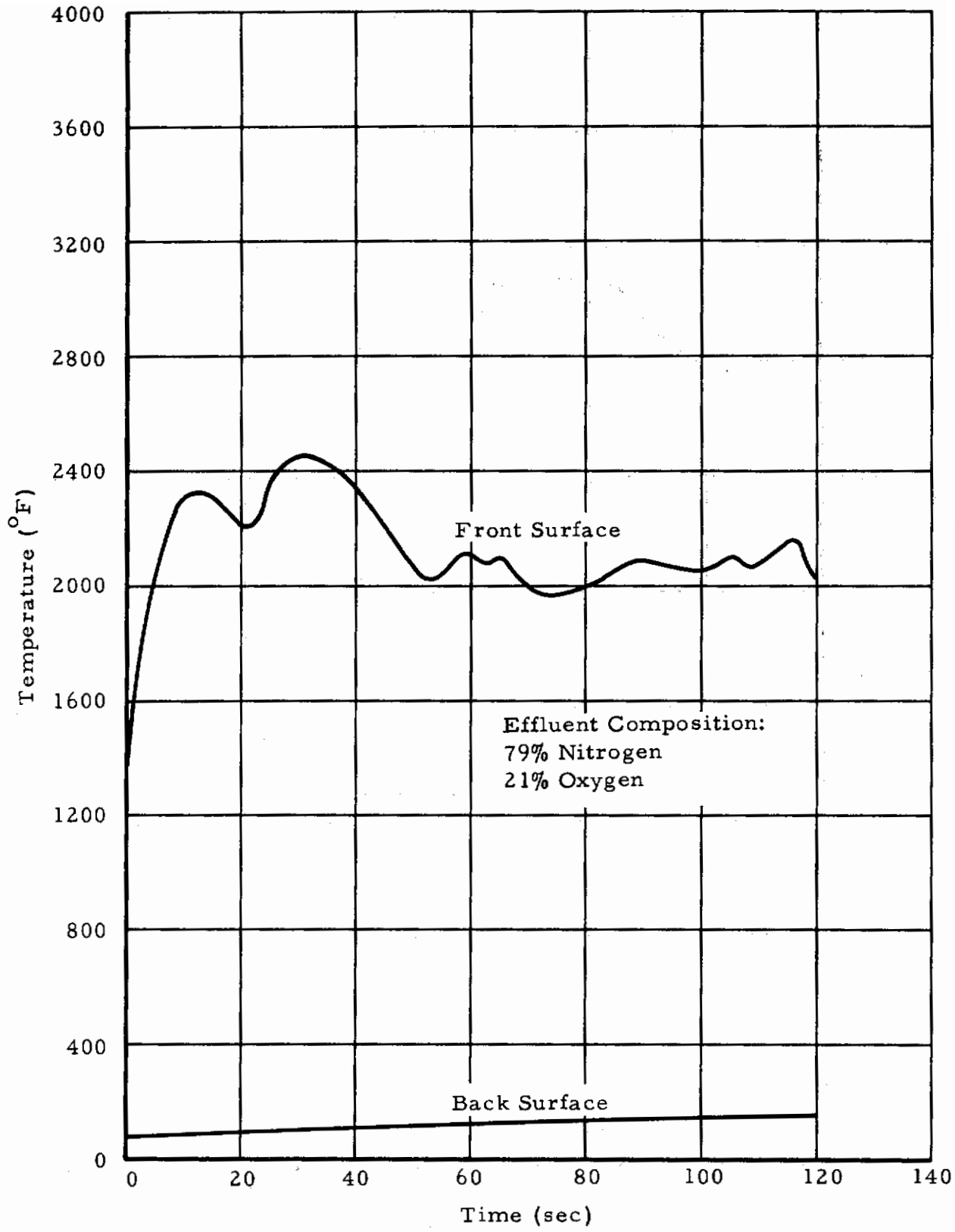

Figure 41. The Temperature-Time History of 015 End Grain Laminate of 181 Fiberglas Exposed to a 100 Btu/ft^2-sec Environment.

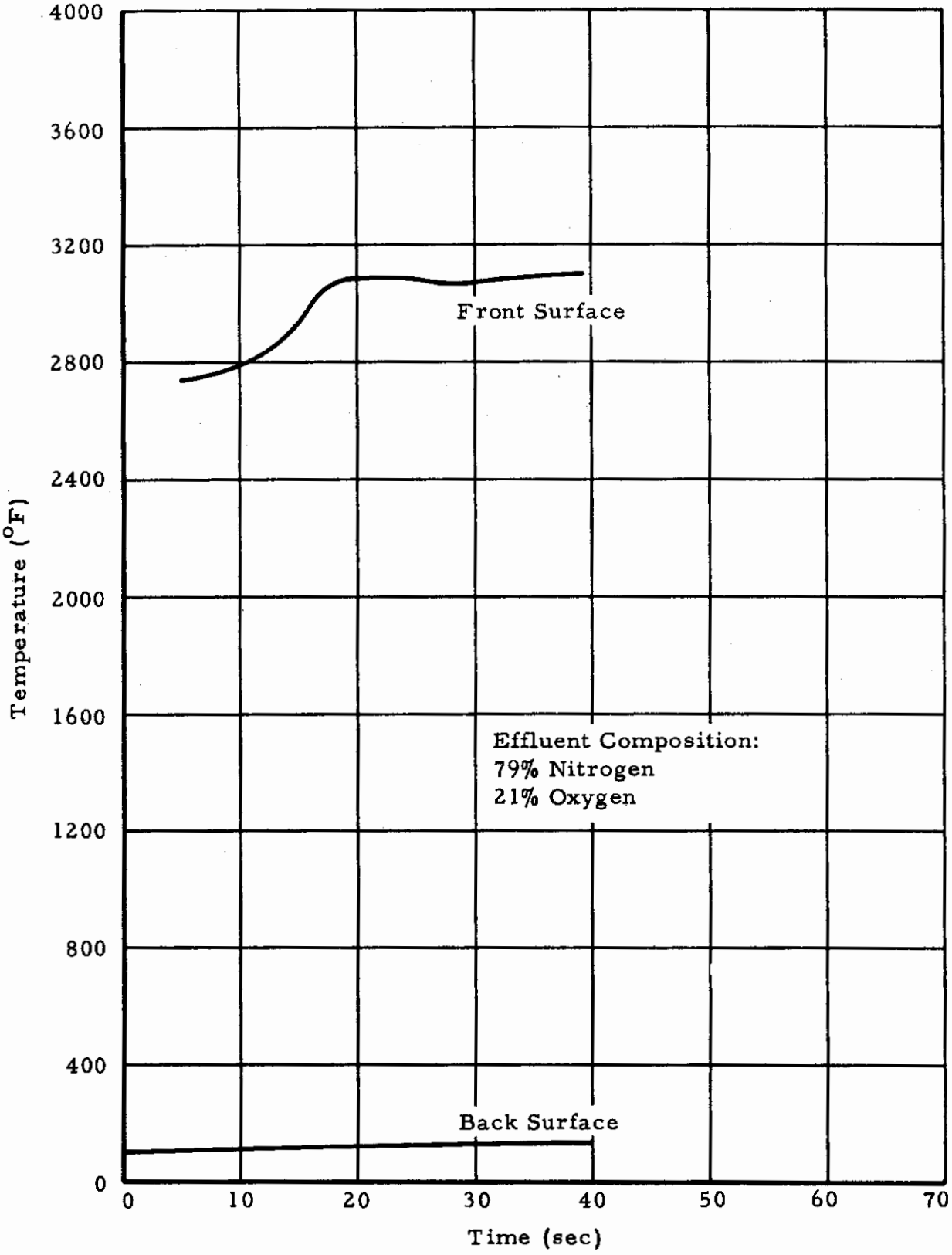

Figure 42. The Temperature-Time History of 015 End Grain Laminate of 181 Fiberglas Exposed to a 300 Btu/ft^2-sec Environment.

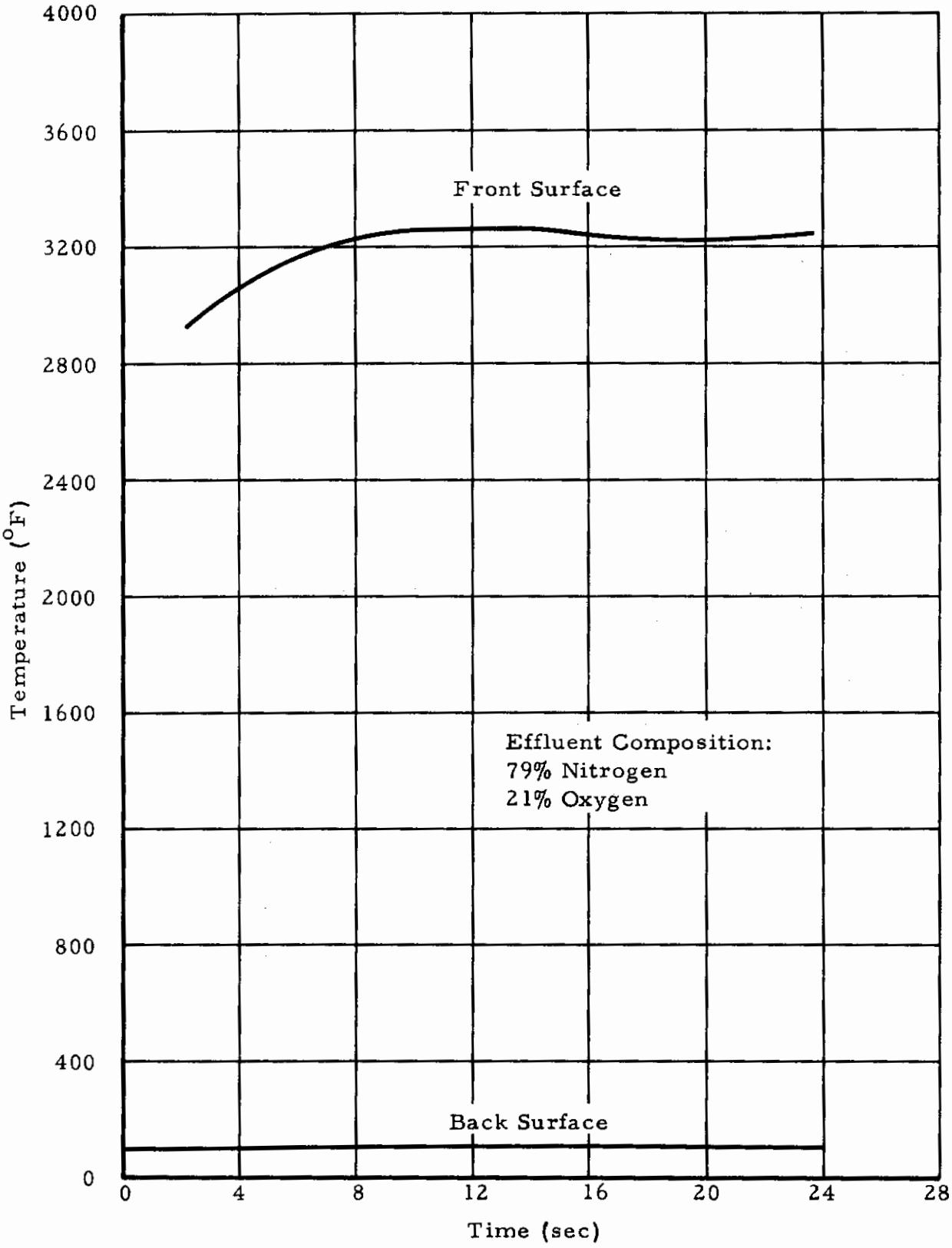

Figure 43. The Temperature-Time History of 015 End Grain Laminate of 181 Fiberglas Exposed to a 500 Btu/ft^2-sec Environment.

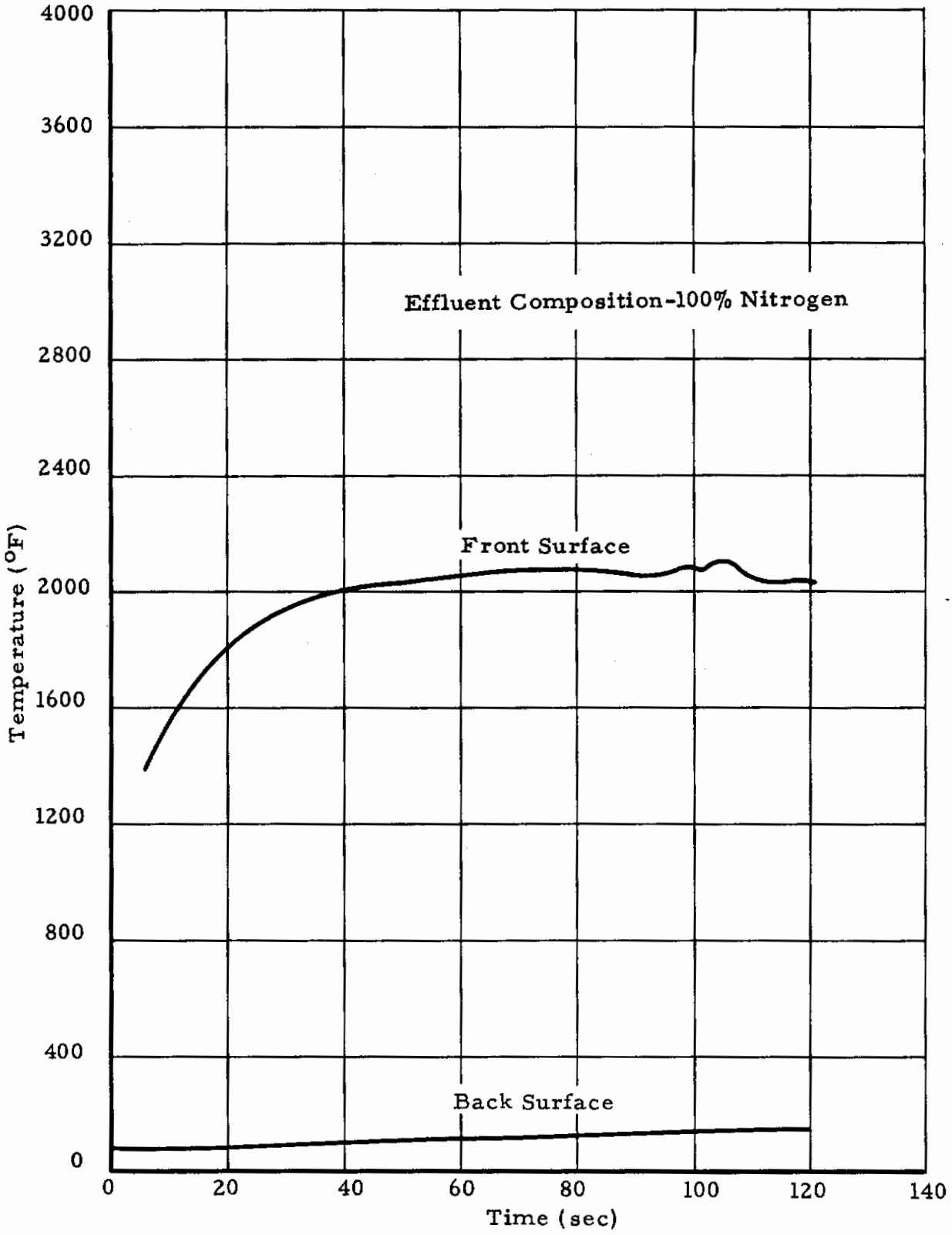

Figure 44. Temperature-Time History of 015 End Grain Laminate of 181 Fiberglas Exposed to a 100 Btu/ft^2-sec Environment.

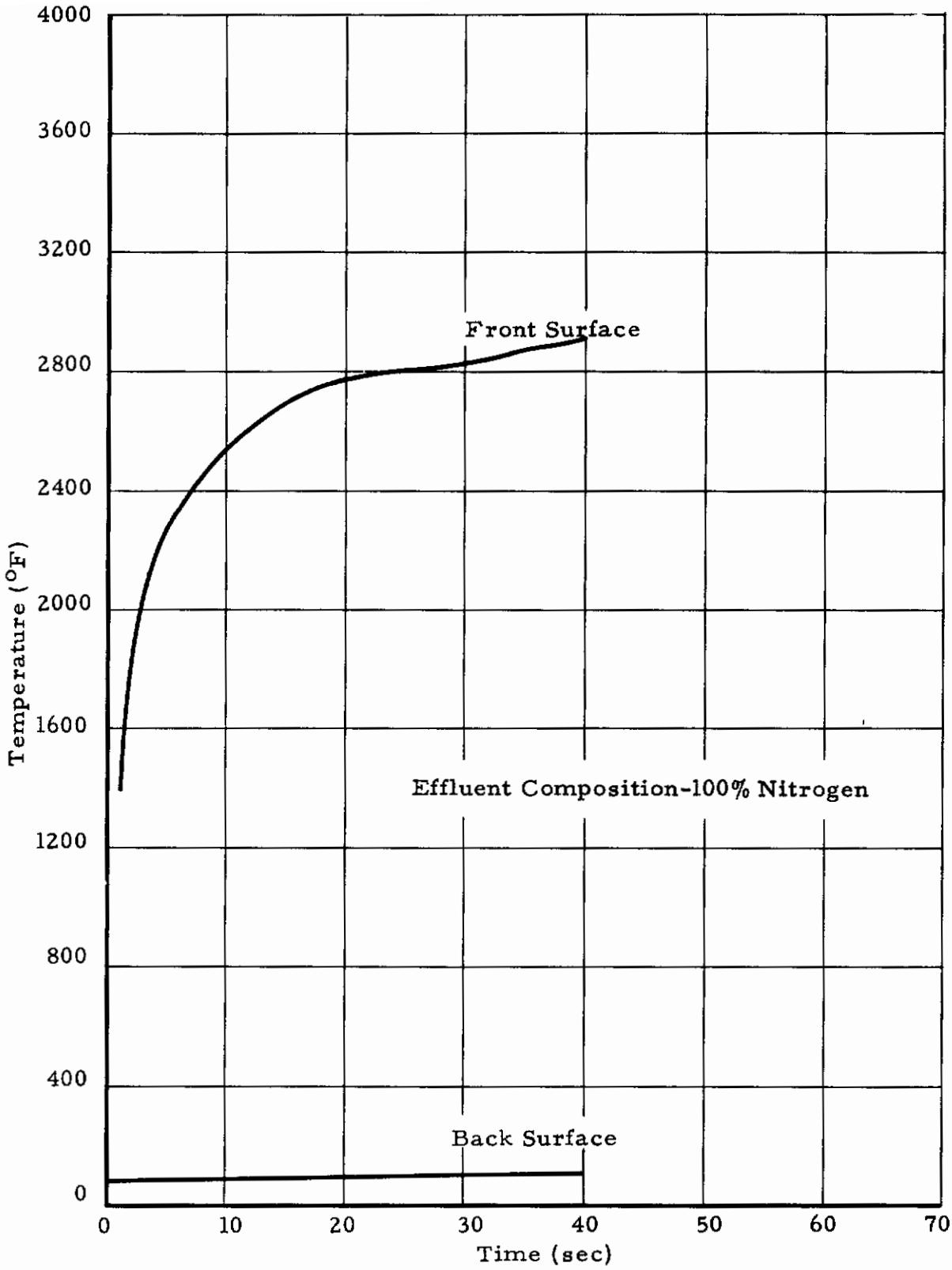

Figure 45. Temperature-Time History of 015 End Grain Laminate of 181 Fiberglas Exposed to a 300 Btu/ft^2-sec Environment

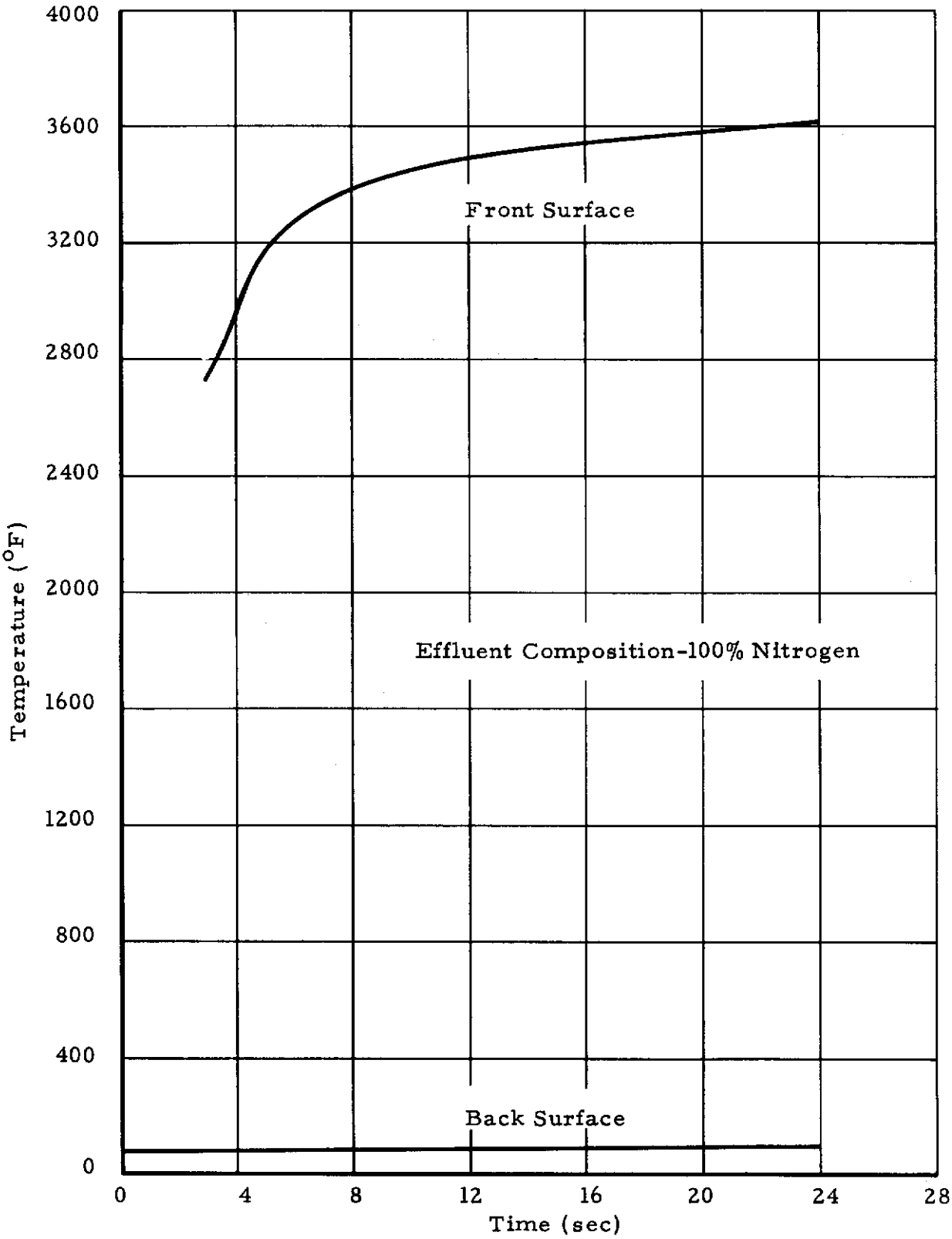

Figure 46. Temperature-Time History of 015 End Grain Laminate of 181 Fiberglas Exposed to a 500 Btu/ft^2-sec Environment.

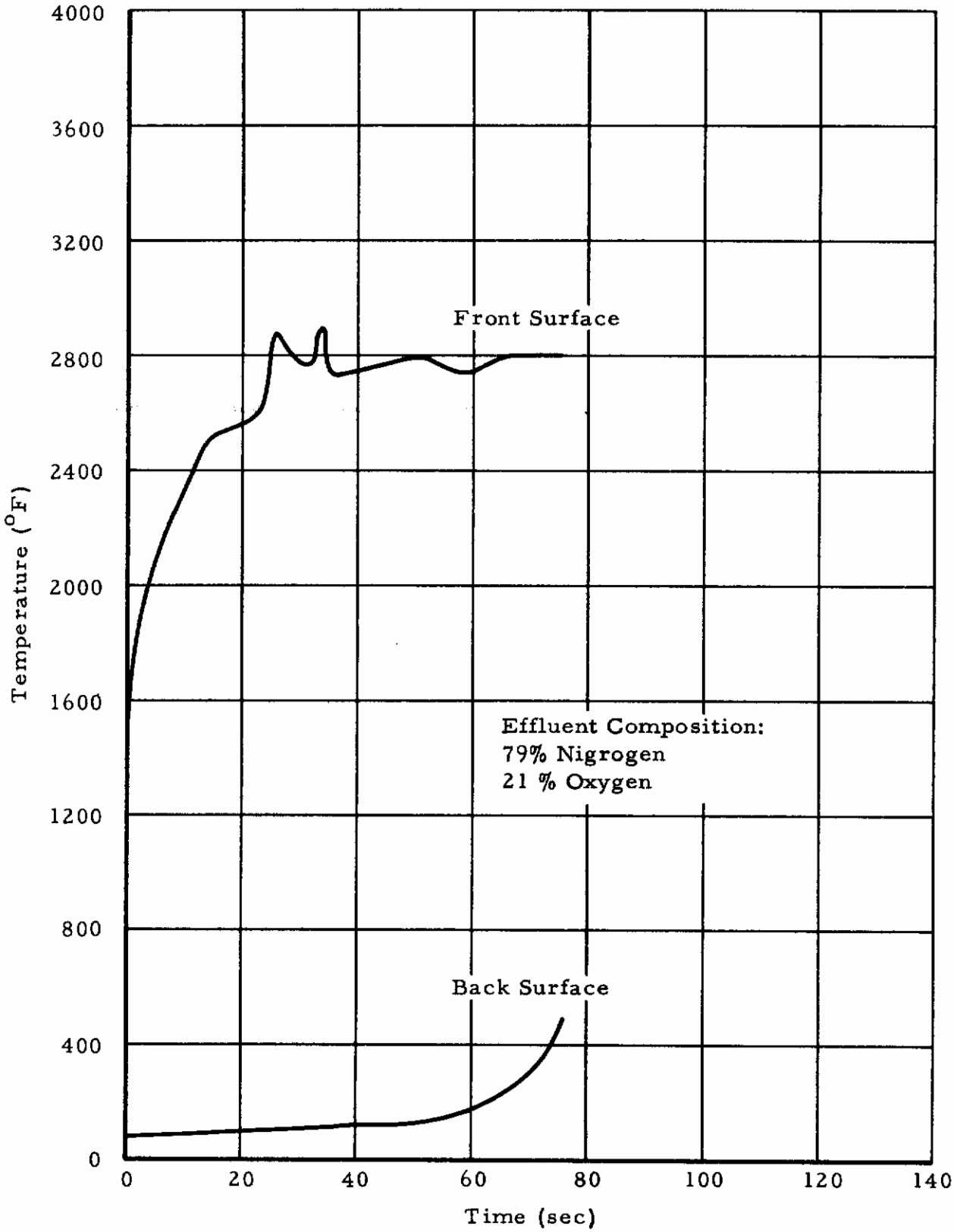

Figure 47. The Temperature-Time History of 010-V24 End Grain Laminate - Alternate Plies of 181 Fiberglas and Graphite Cloth Exposed to a 100 Btu/ft^2-sec Environment.

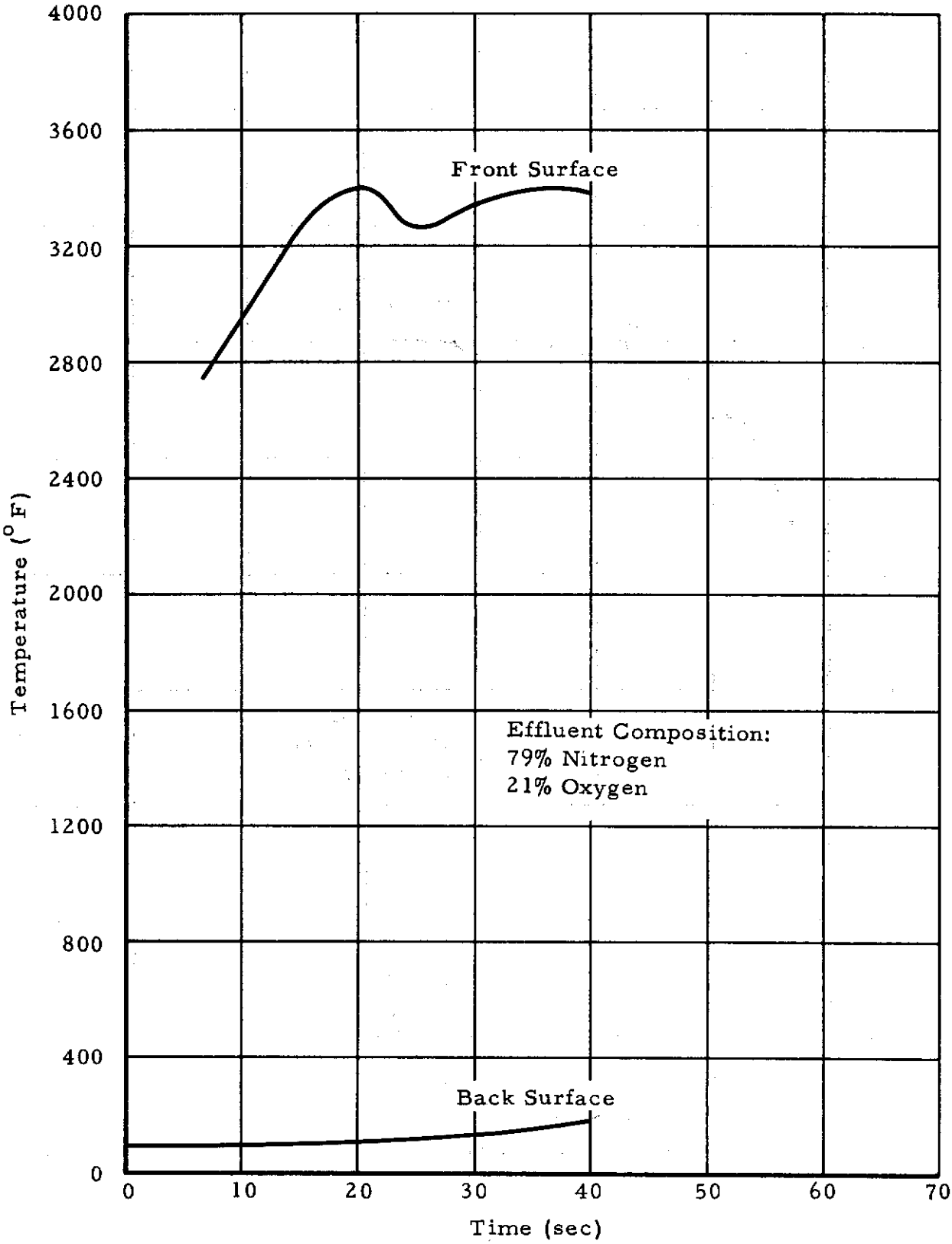

Figure 48. The Temperature-Time History of 010-V24 End Grain Laminate - Alternate Plies of 181 Fiberglas and Graphite Cloth Exposed to a 300 Btu/ft^2-sec Environment.

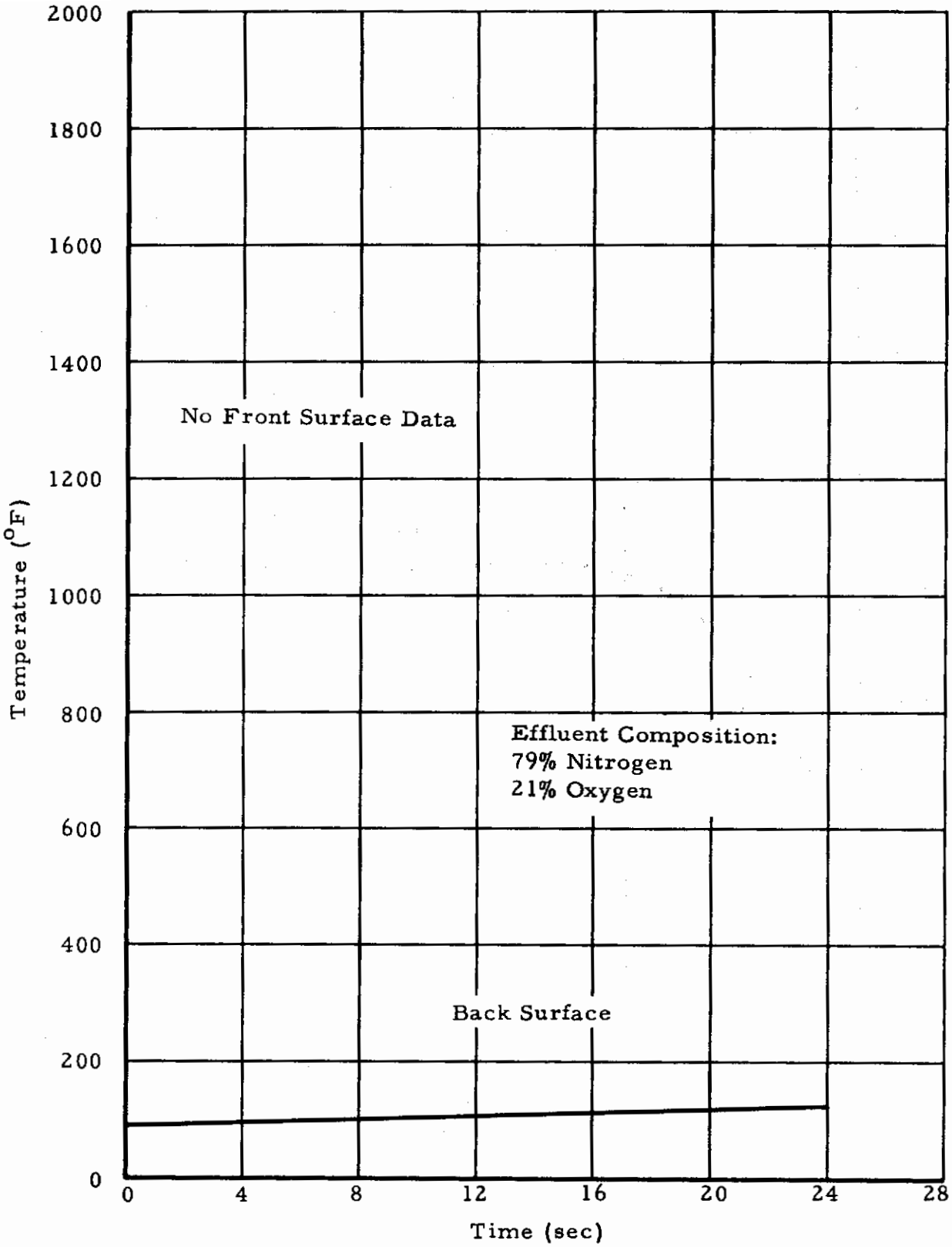

Figure 49. The Temperature-Time History of 010-V24 End Grain Laminate - Alternate Plies of 181 Fiberglas and Graphite Cloth Exposed to a 500 Btu/ft^2-sec Environment.

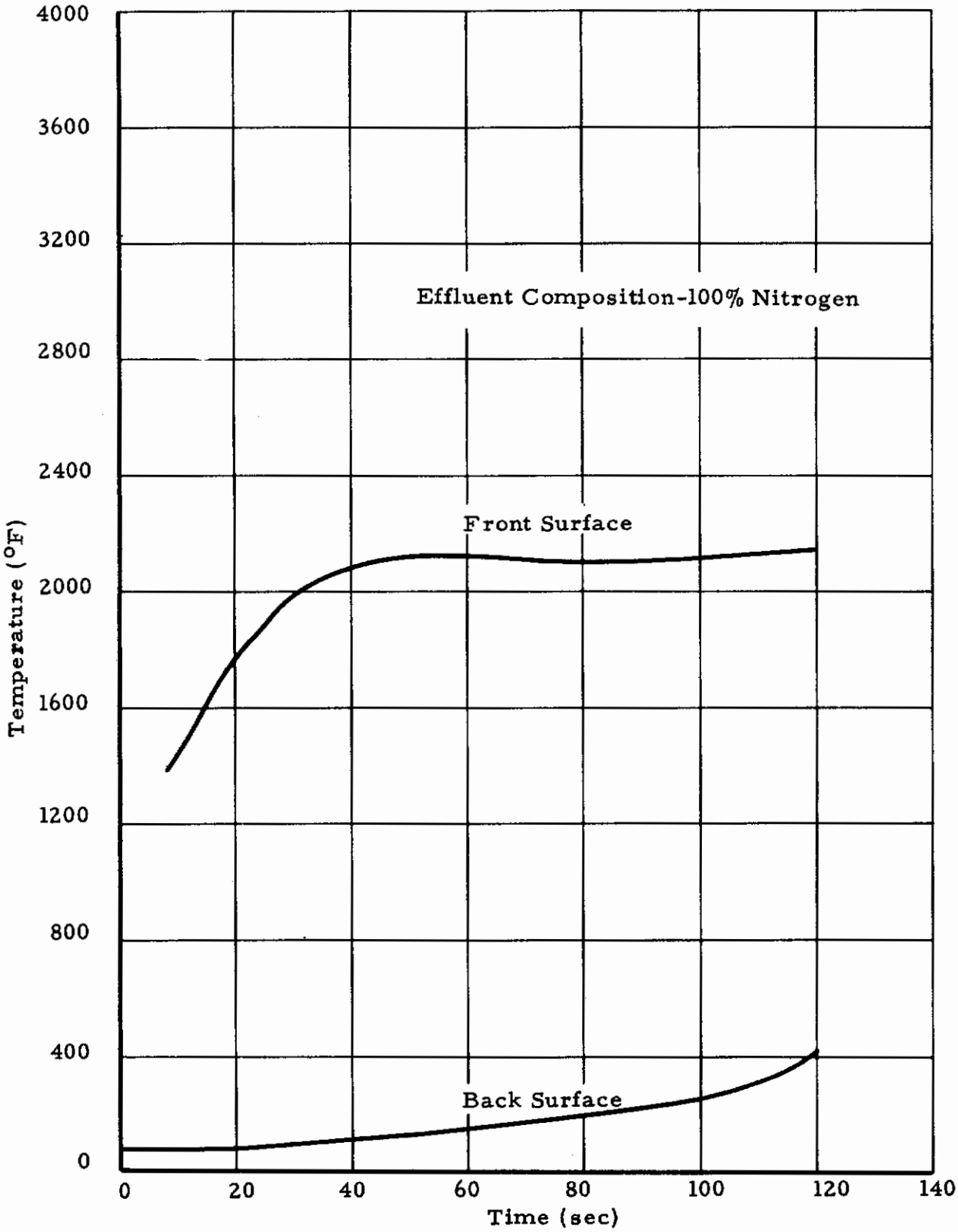

Figure 50: Temperature-Time History of 010-V24 End Grain Laminate-Alternate Plies of Fiberglas and Graphite Cloth Exposed to a 100 Btu/ft^2-sec Environment.

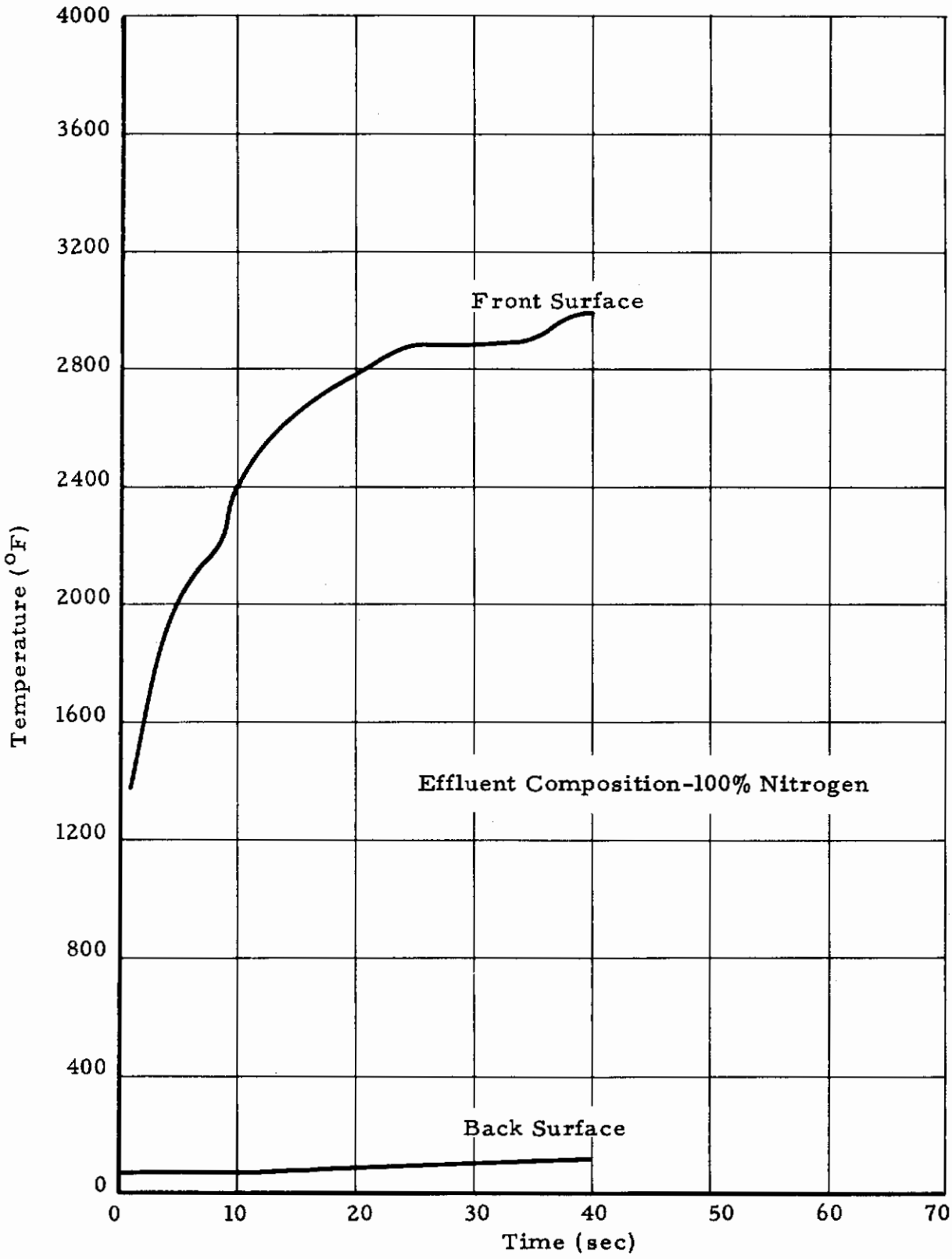

Figure 51: Temperature-Time History of 010-V24 End Grain Laminate-Alternate Plies of Fiberglas and Graphite Cloth Exposed to a 300 Btu/ft^2-sec Environment.

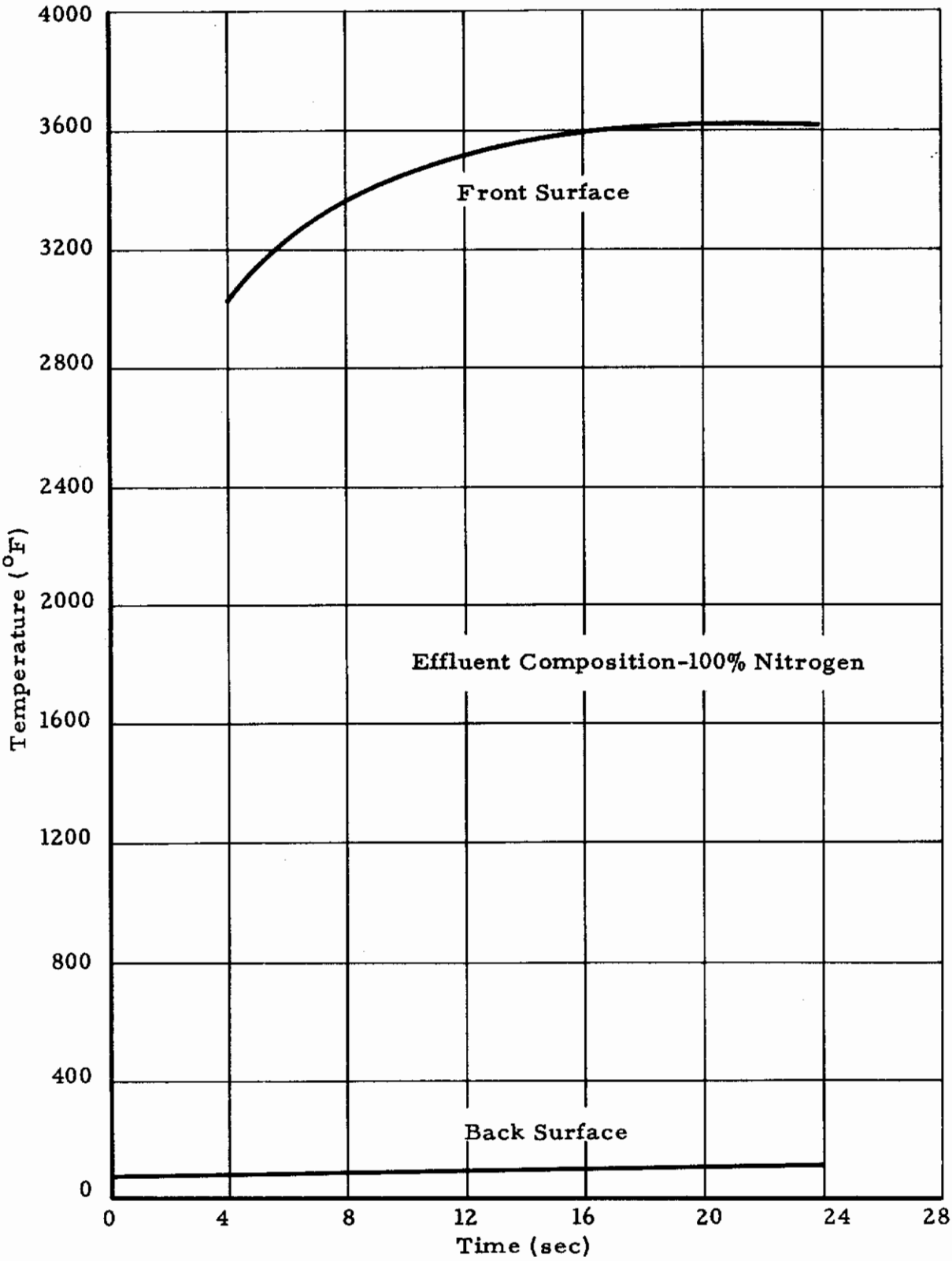

Figure 52. Temperature-Time History of 010-V24 End Grain Laminate-Alternate Plies of Fiberglas and Graphite Cloth Exposed to a 500 Btu/ft^2-sec Environment.

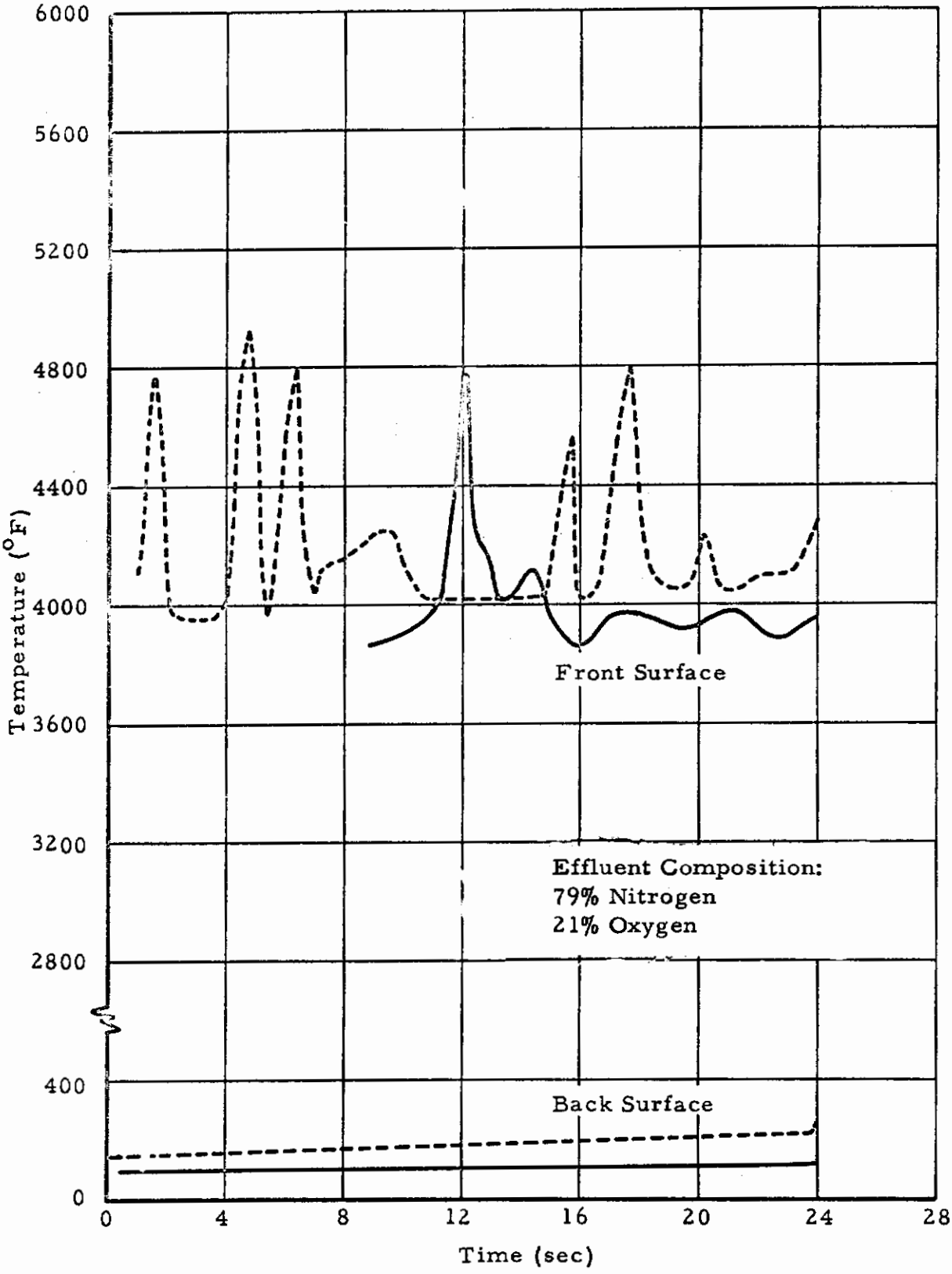

Figure 53. The Temperature-Time History of Co-polymerized Alkylated Phenyl Polyamide Resin with Graphite Cloth Exposed to a 500 Btu/ft^2-sec Heat Flux Environment

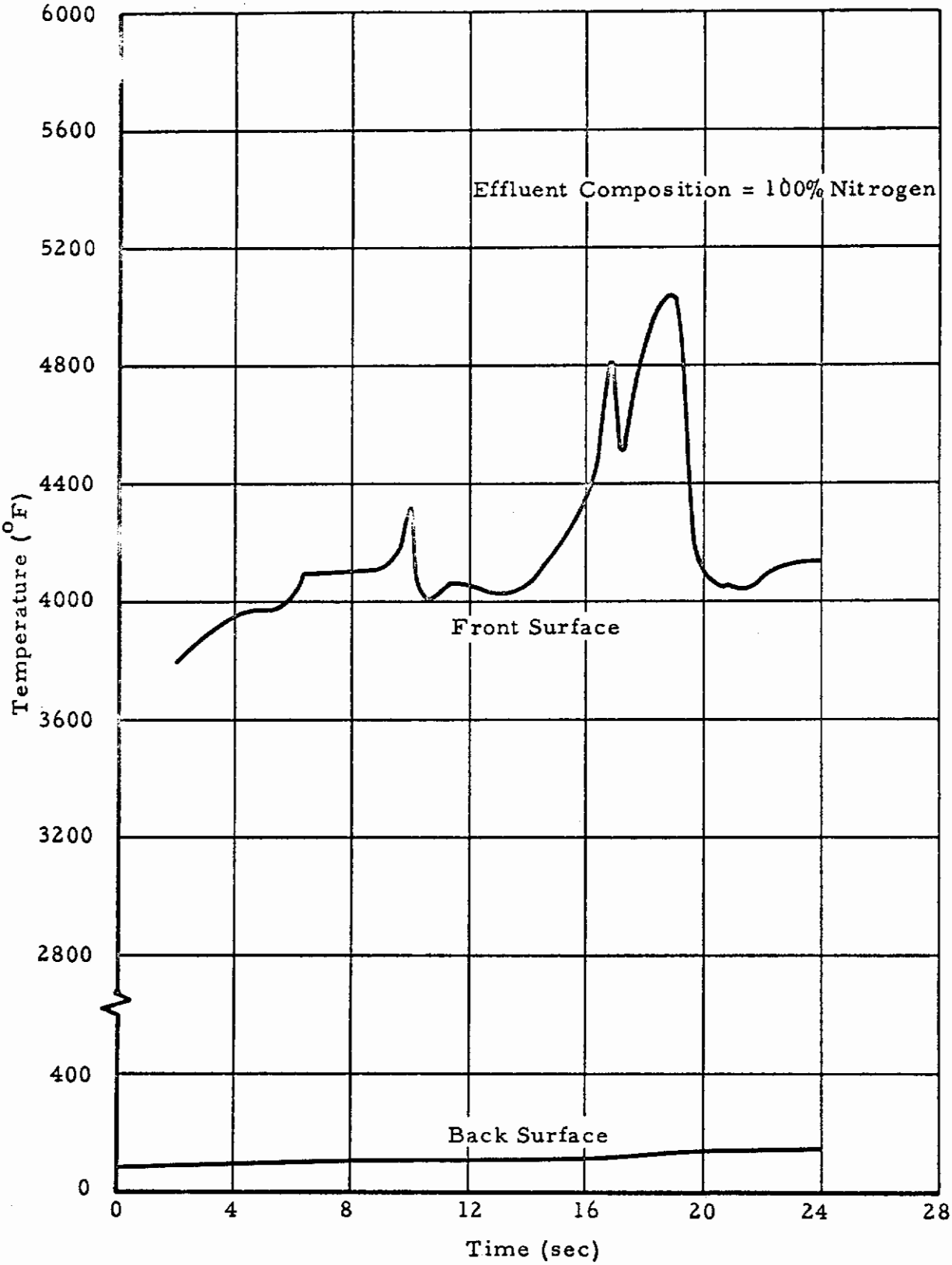

Figure 54. The Temperature-Time History of Co-polymerized Alkylated Phenyl Polyamide Resin with Graphite Cloth Exposed to a 500 Btu/ft^2-sec Heat Flux Environment

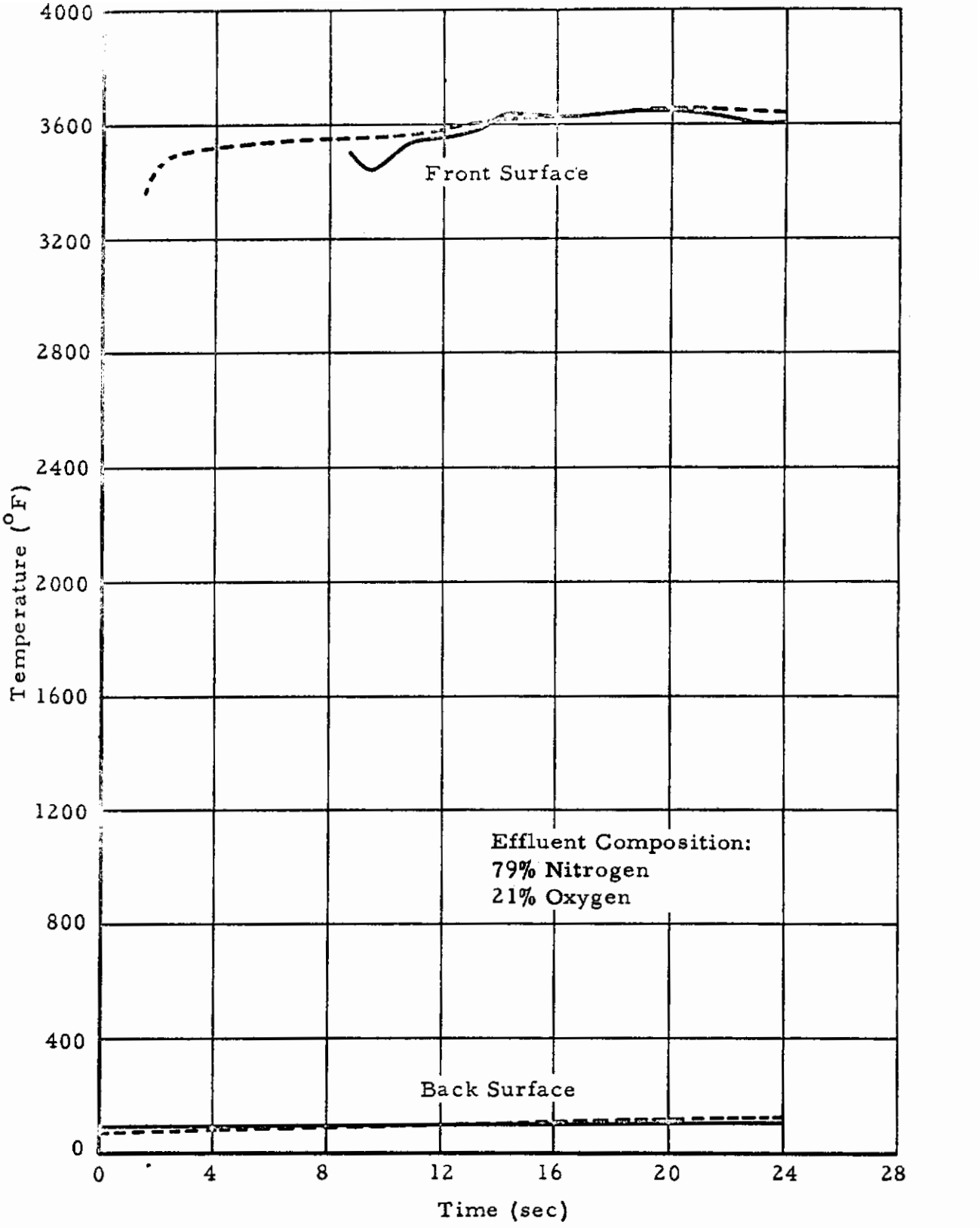

Figure 55. The Temperature-Time History of Co-polymerized Alkylated Phenyl Polyamide Resin with Linen Exposed to a 500 Btu/ft^2-sec Heat Flux Environment

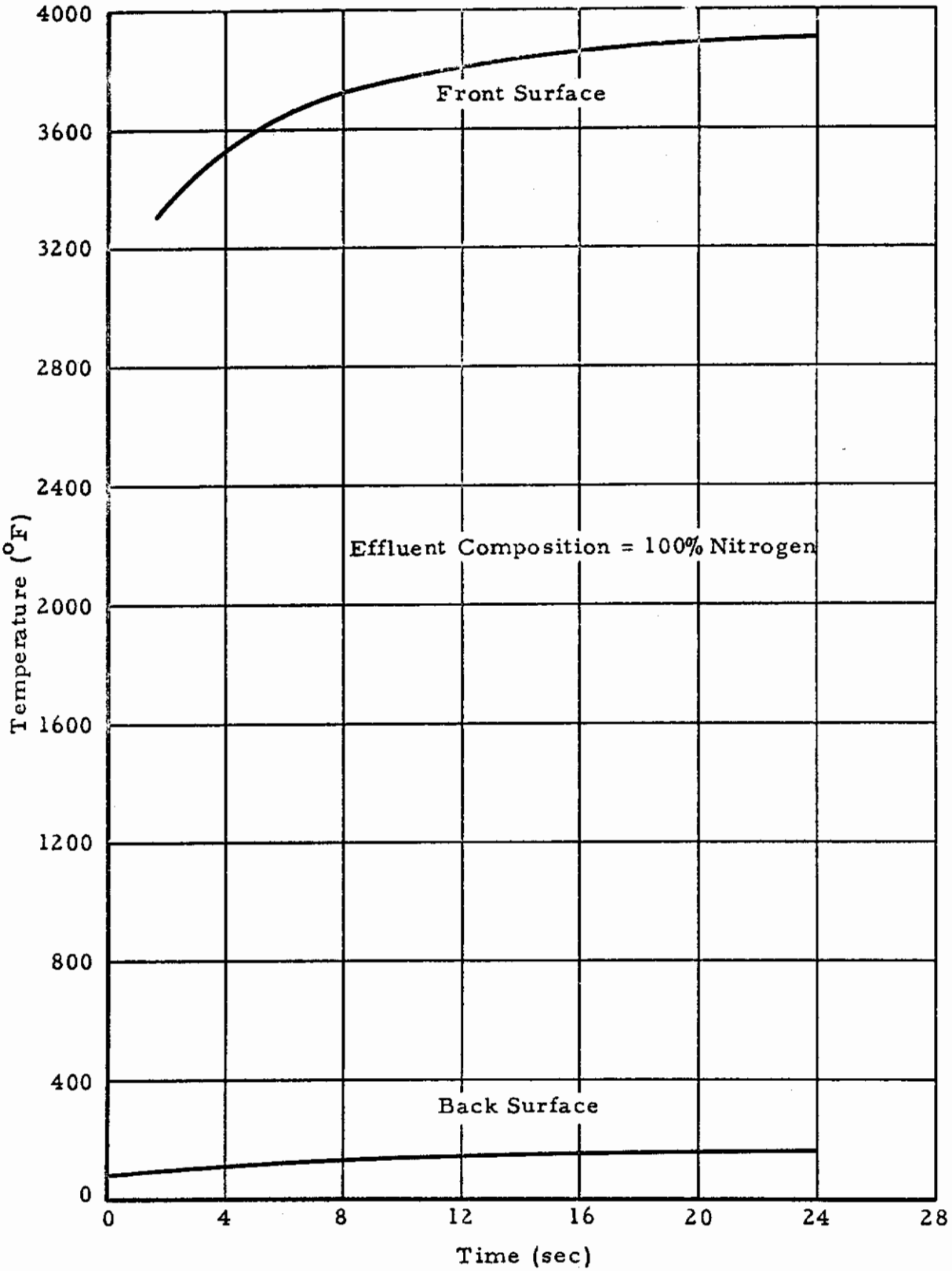

Figure 56. The Temperature-Time History of Co-polymerized Alkylated Phenyl Polyamide Resin with Linen Exposed to a 500 Btu/ft^2-sec Heat Flux Environment

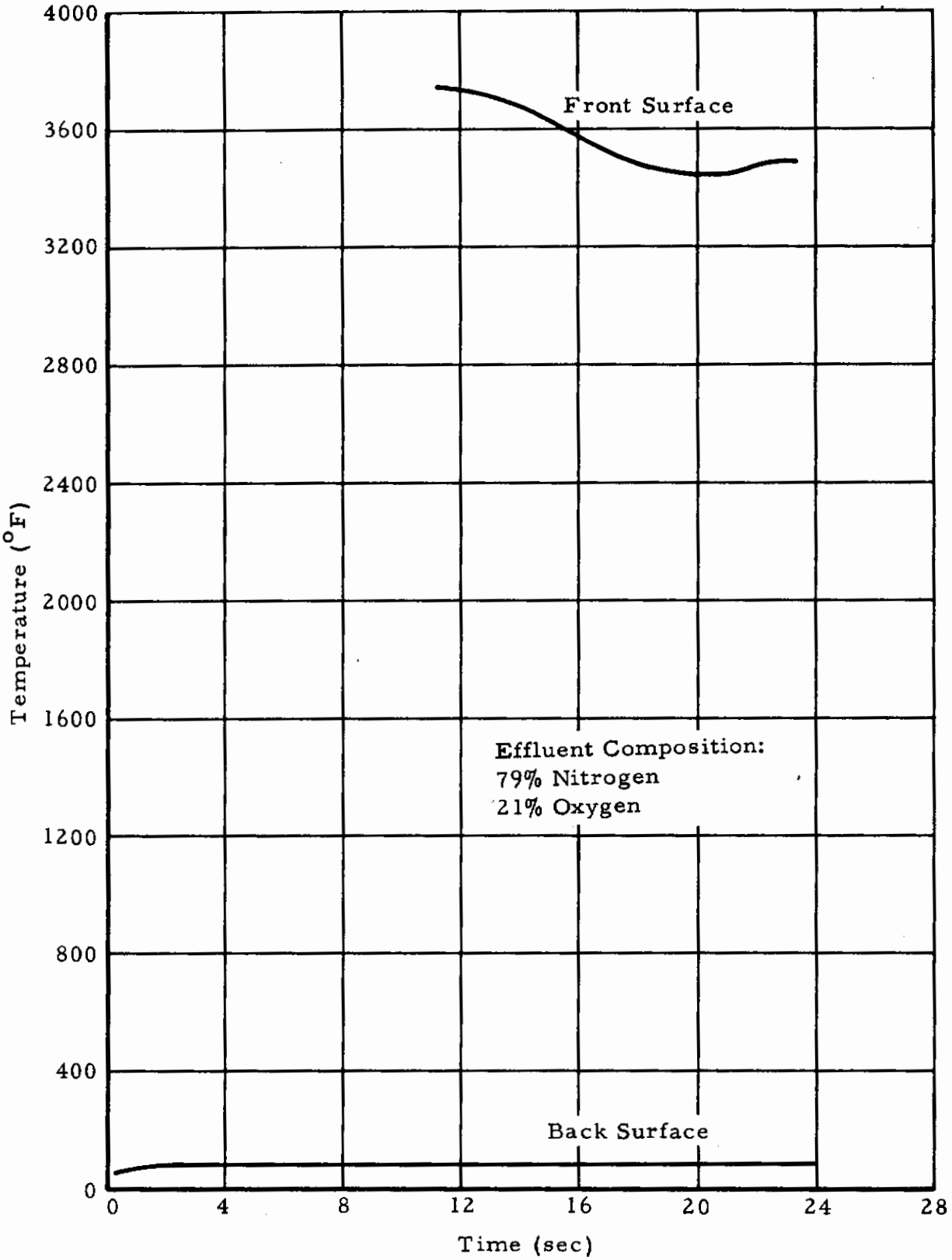

Figure 57. The Temperature-Time History of Co-polymerized Alkylated Phenyl Polyamide on Linen Exposed to a 480 Btu/ft^2-sec Heat Flux Environment.

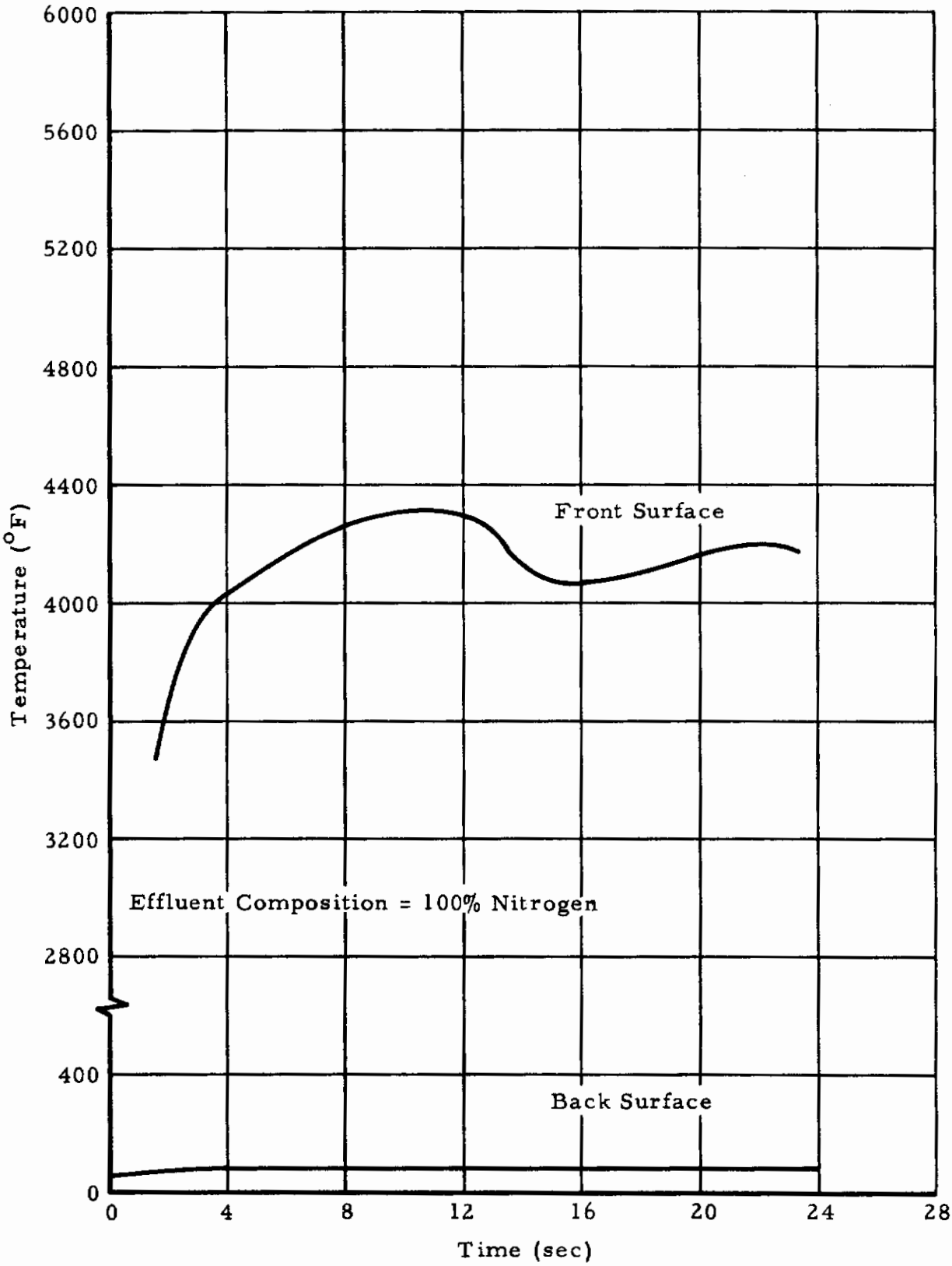

Figure 58. The Temperature-Time History of Co-polymerized Alkylated Phenyl Polyamide on Linen Exposed to a 500 Btu/ft^2-sec Heat Flux Environment.

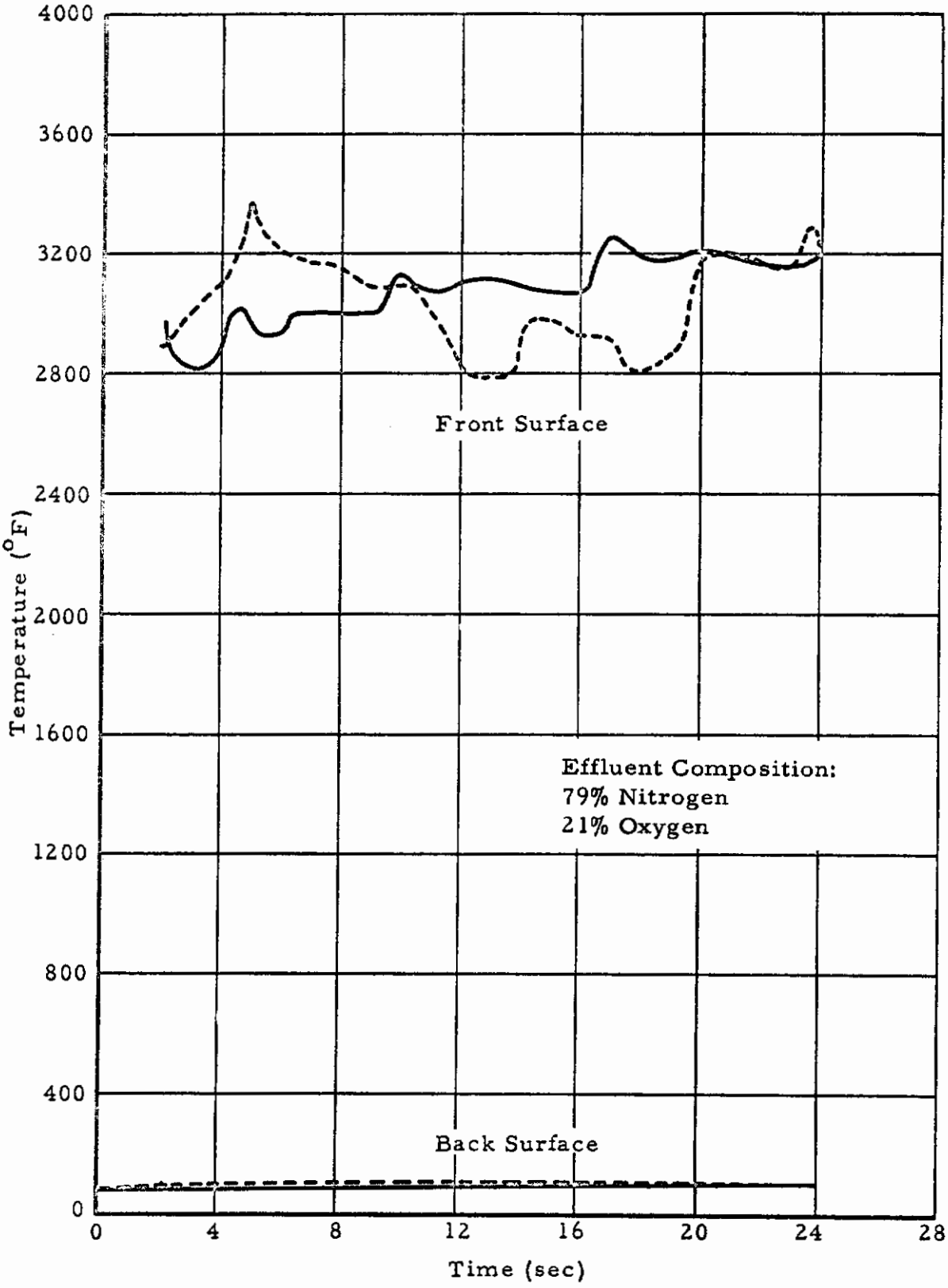

Figure 59. The Temperature-Time History of Co-polymerized Alkylated Phenyl Polyamide Resin with Refrasil Exposed to a 500 Btu/ft^2-sec Heat Flux Environment.

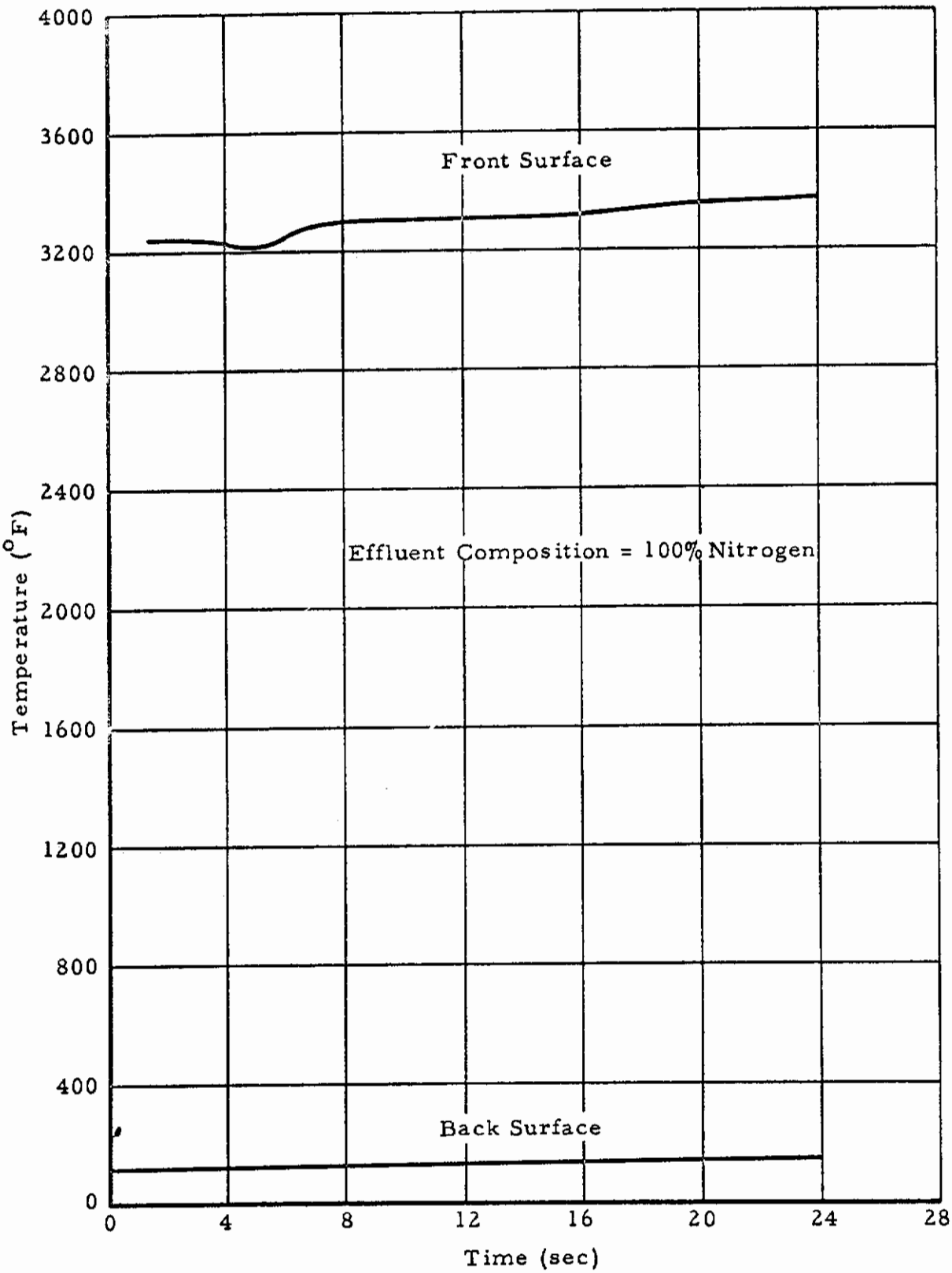

Figure 60. The Temperature-Time History of Co-polymerized Alkylated Phenyl Polyamide Resin with Refrasil Exposed to a 500 Btu/ft^2-sec Heat Flux Environment.

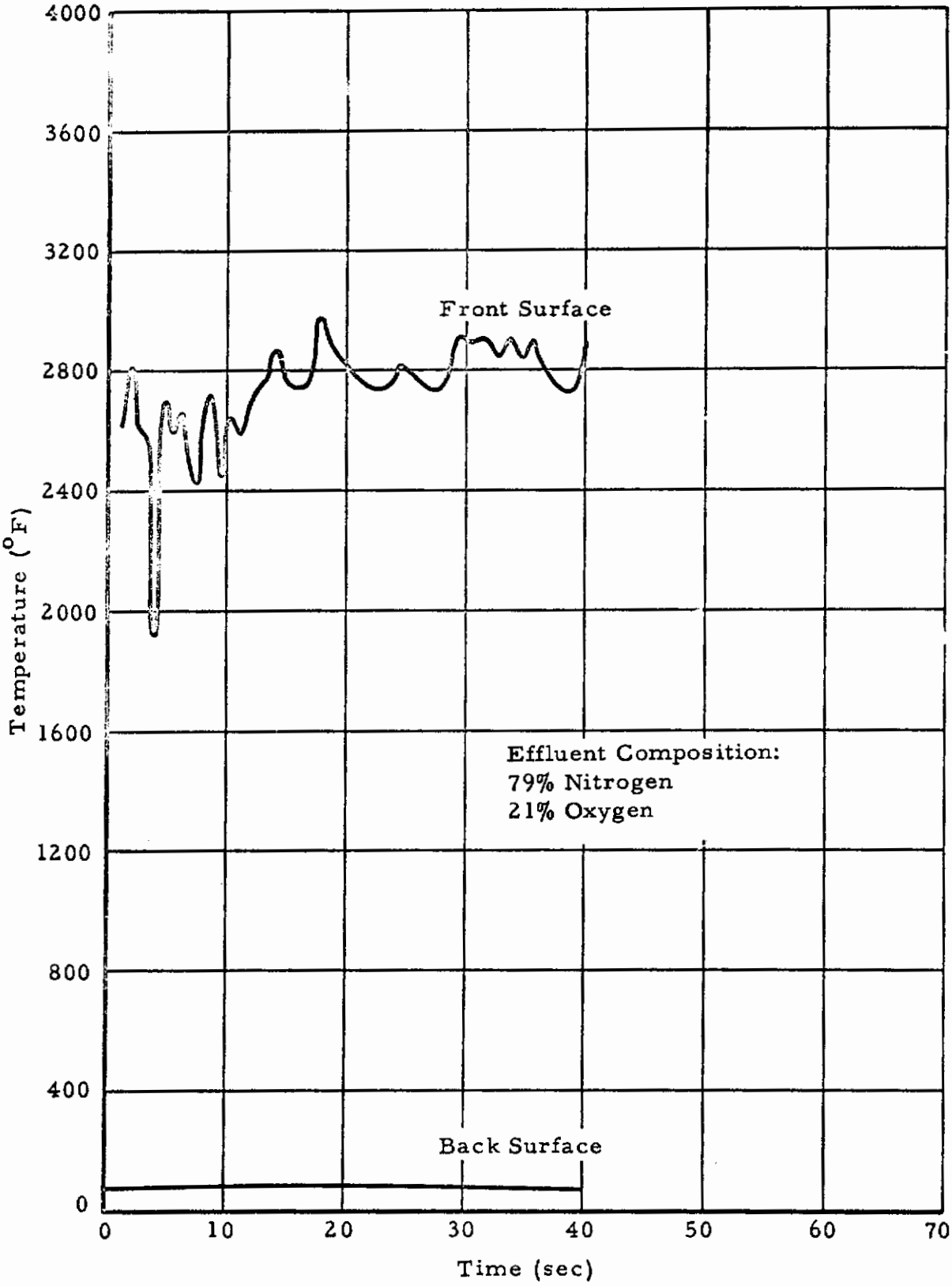

Figure 61. The Temperature-Time History of Co-polymerized Alkylated Phenyl Polyamide Resin with Asbestos Exposed to a 300 Btu/ft^2-sec Heat Flux Environment.

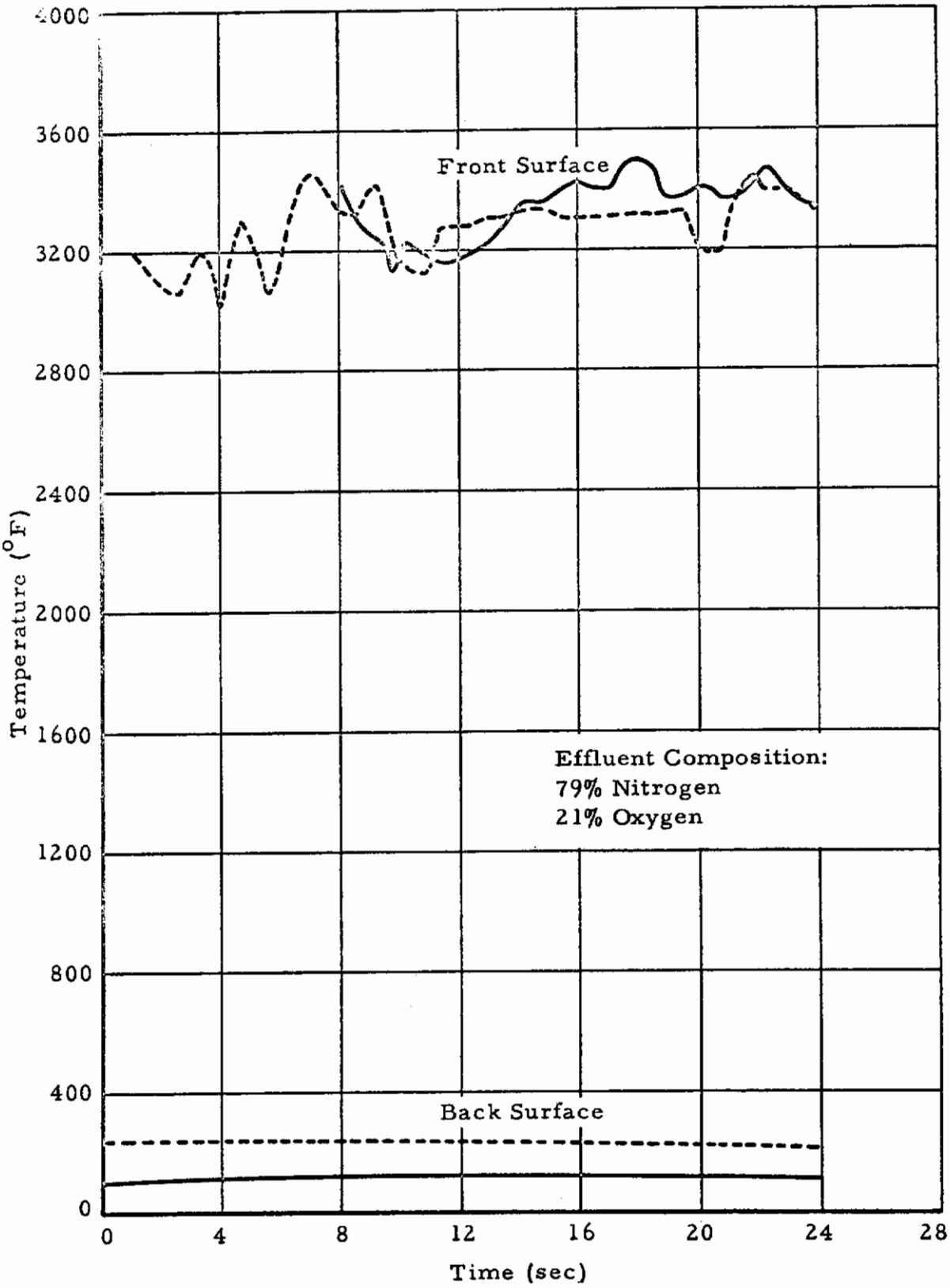

Figure 62. The Temperature-Time History of Co-polymerized Alkylated Phenyl Polyamide Resin with Asbestos Exposed to a 500 Btu/ft^2-sec Heat Flux Environment.

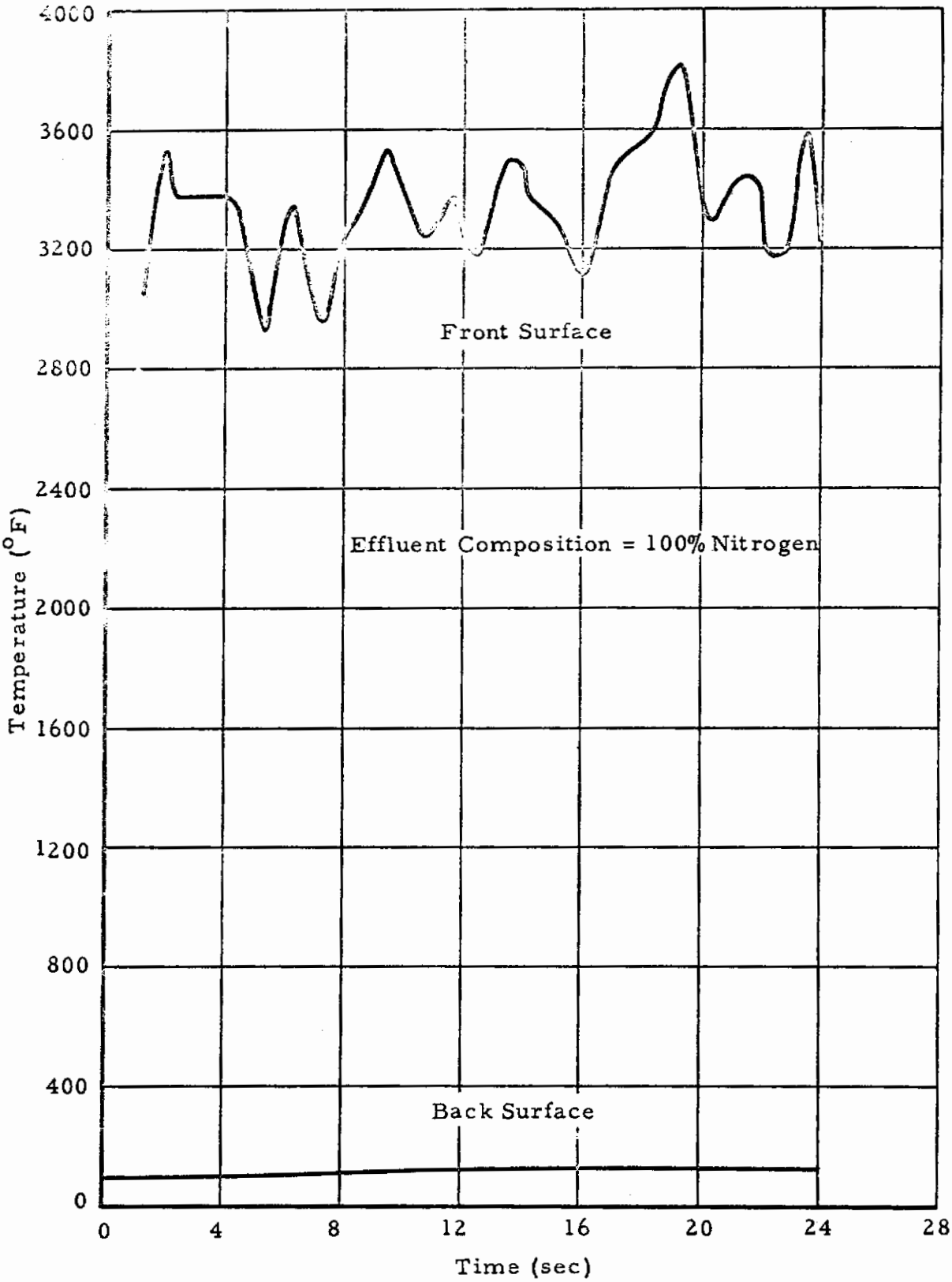

Figure 63. The Temperature-Time History of Co-polymerized Alkylated Phenyl Polyamide Resin with Asbestos Exposed to a 500 Btu/ft^2-sec Heat Flux Environment.

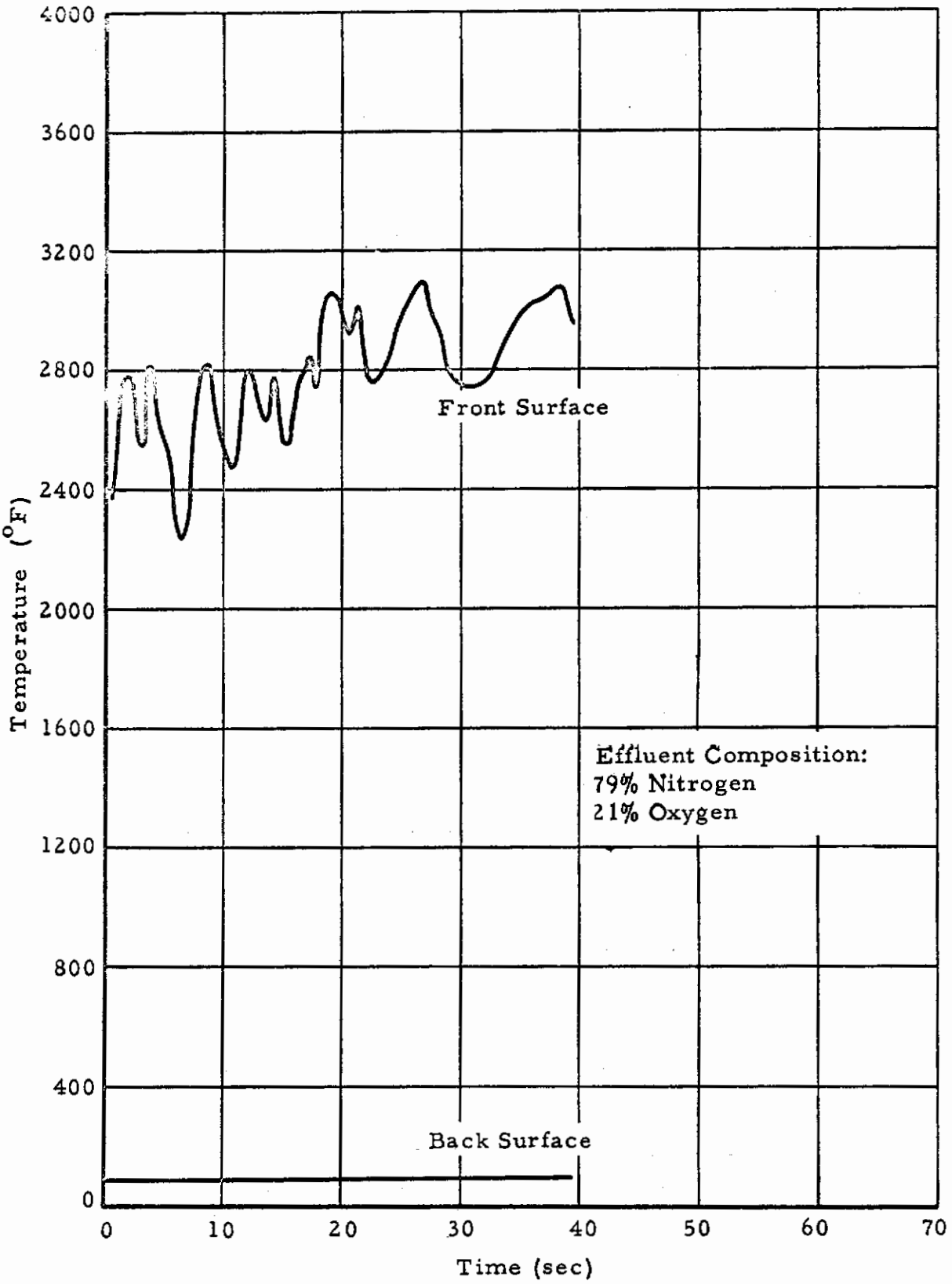

Figure 64. The Temperature-Time History of Co-polymerized Phenyl Polyamide Resin with Asbestos Exposed to a 300 Btu/ft^2-sec Heat Flux Environment.

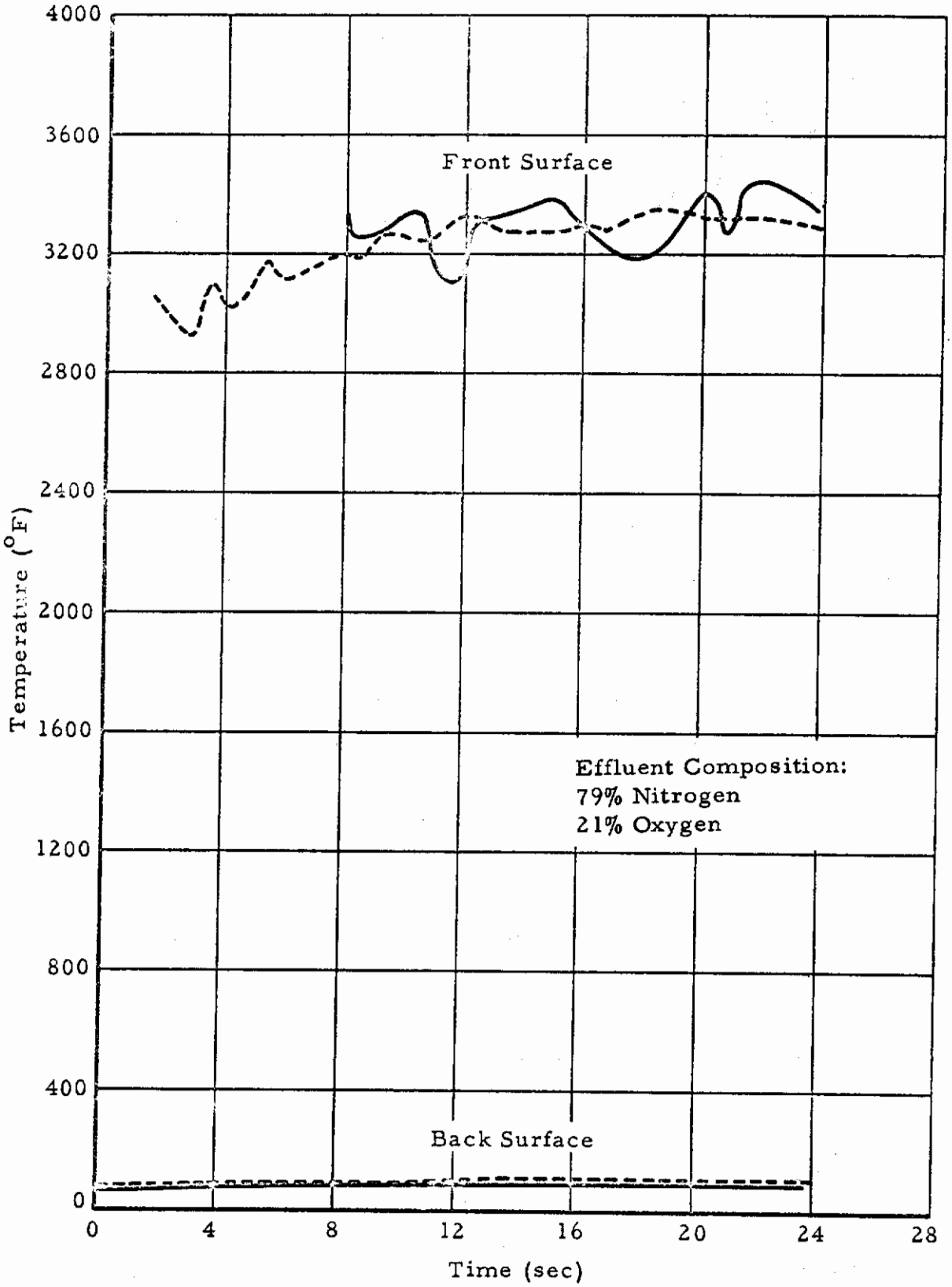

Figure 65. The Temperature-Time History of Co-polymerized Phenyl Polyamide Resin with Asbestos Exposed to a 500 Btu/ft^2-sec Heat Flux Environment.

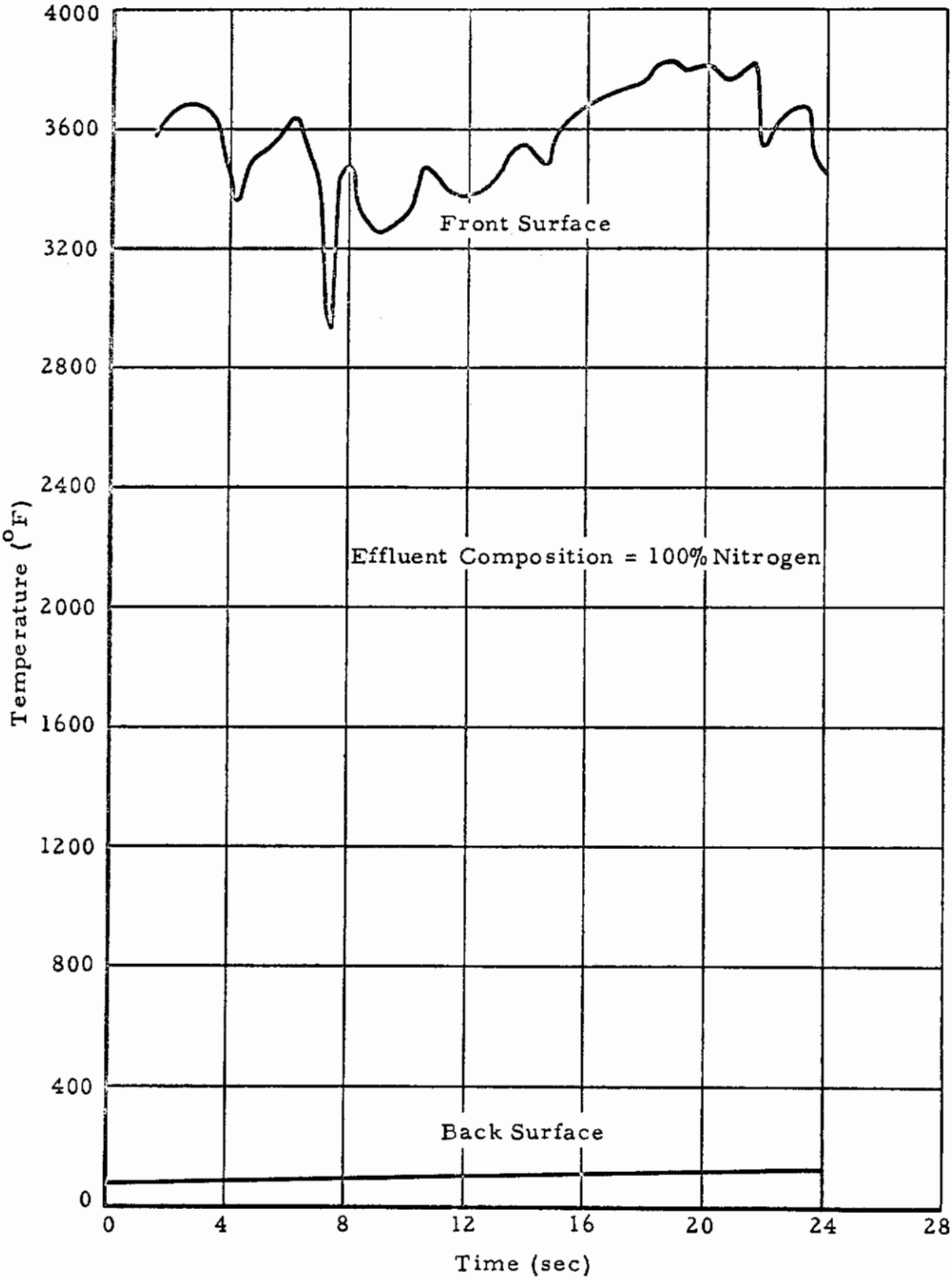

Figure 66. The Temperature-Time History of Co-polymerized Phenyl Polyamide Resin with Asbestos Exposed to a 500 Btu/ft^2-sec Heat Flux Environment.

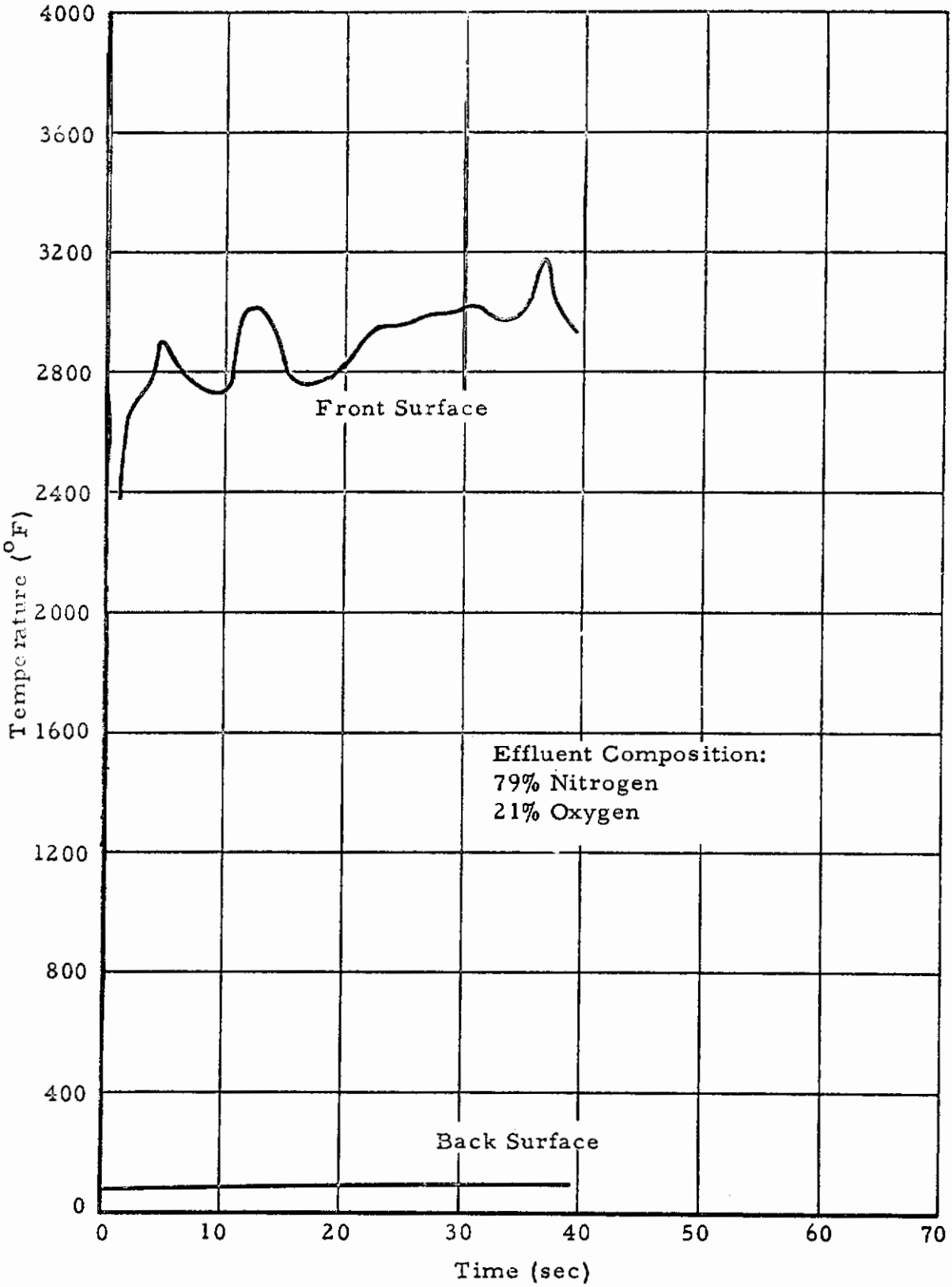

Figure 67. The Temperature-Time History of Nylon Phenolic Resin with Asbestos Exposed to a 300 Btu/ft^2-sec Heat Flux Environment

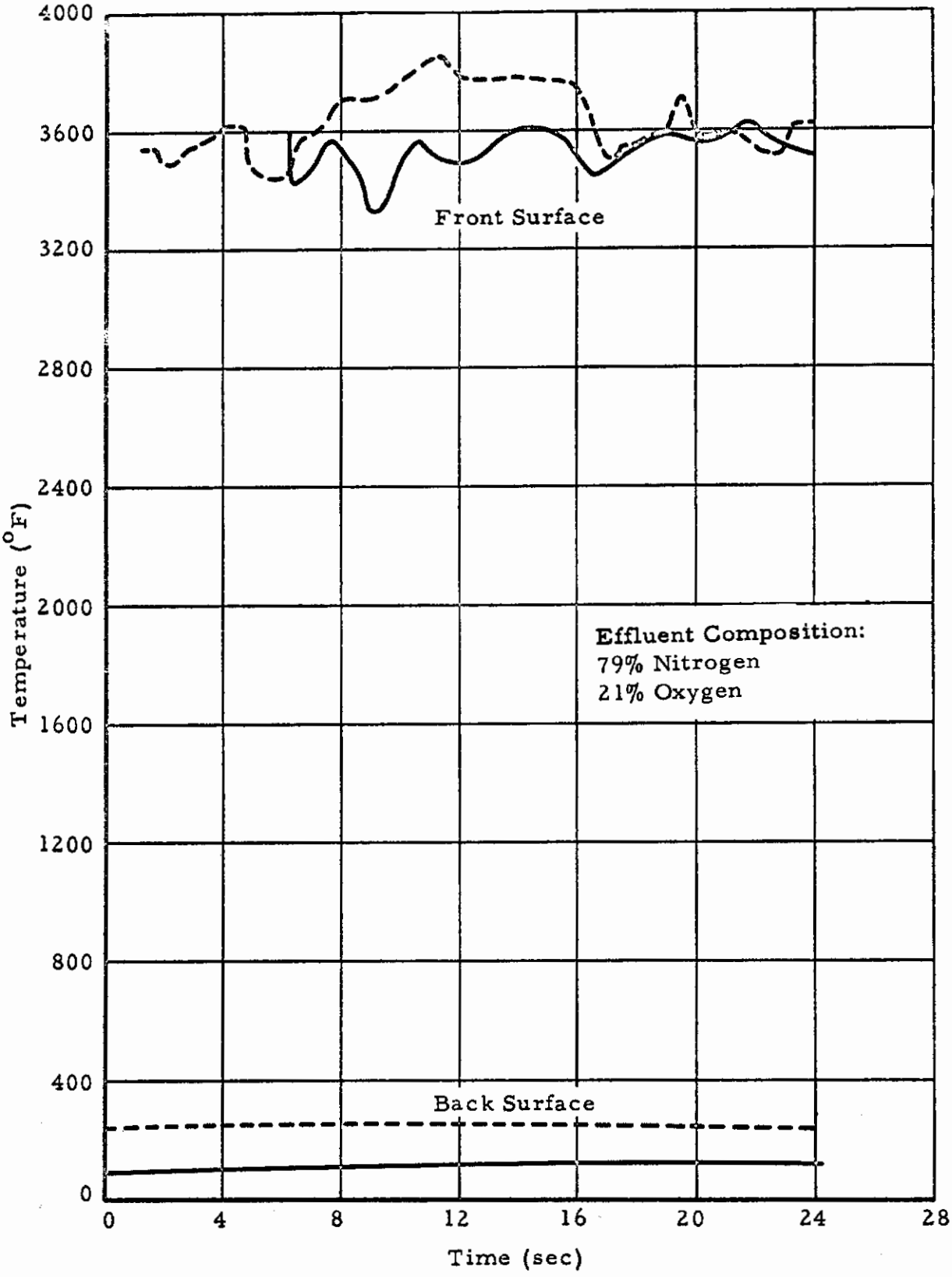

Figure 68. The Temperature-Time History of Nylon Phenolic Resin with Asbestos Exposed to a 500 Btu/ft^2-sec Heat Flux Environment

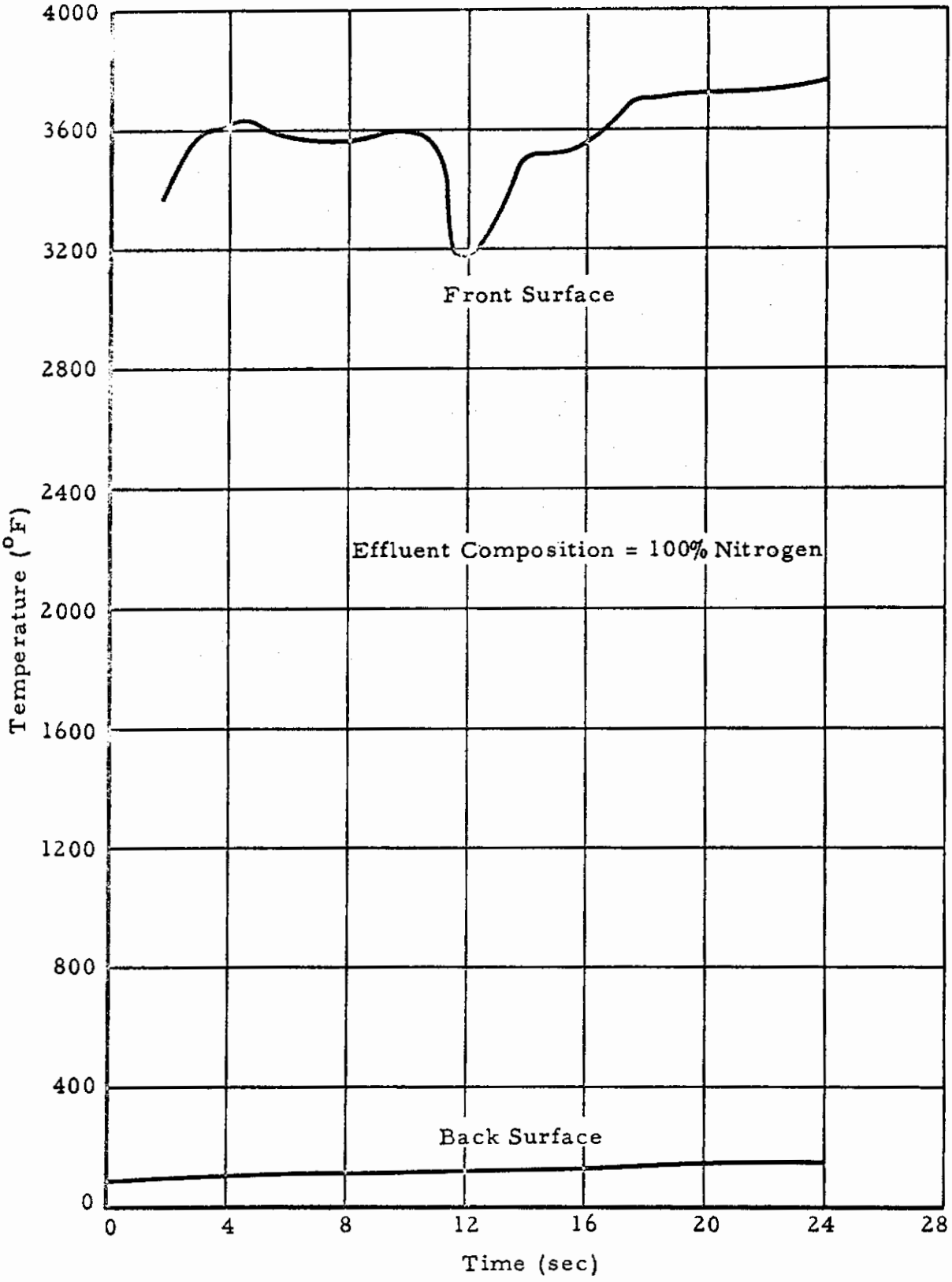

Figure 69. The Temperature-Time History of Nylon Phenolic Resin with Asbestos Exposed to a 500 Btu/ft^2-sec Heat Flux Environment

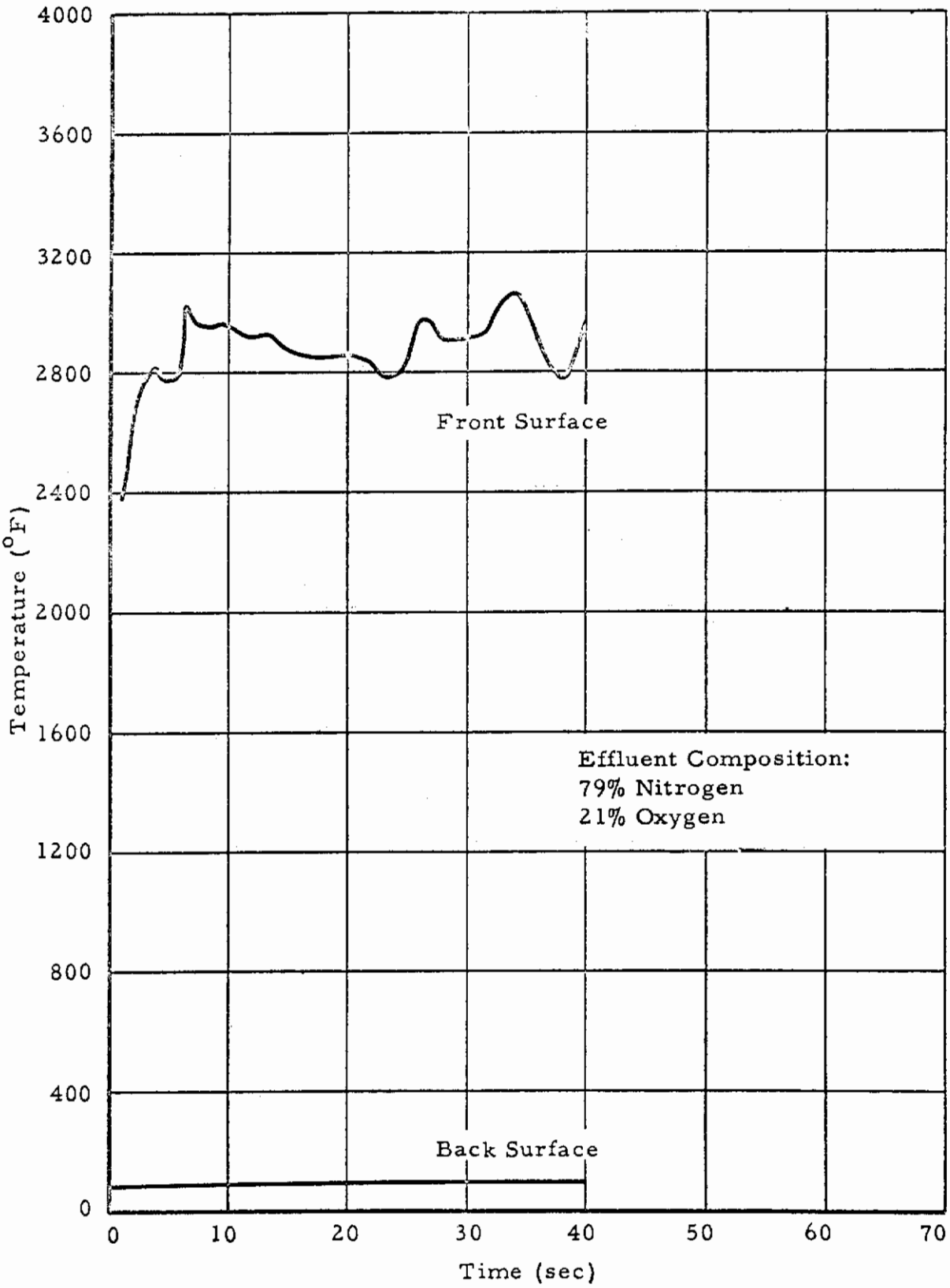

Figure 70. The Temperature-Time History of Phenolic with Asbestos Exposed to a 300 Btu/ft^2-sec Heat Flux Environment

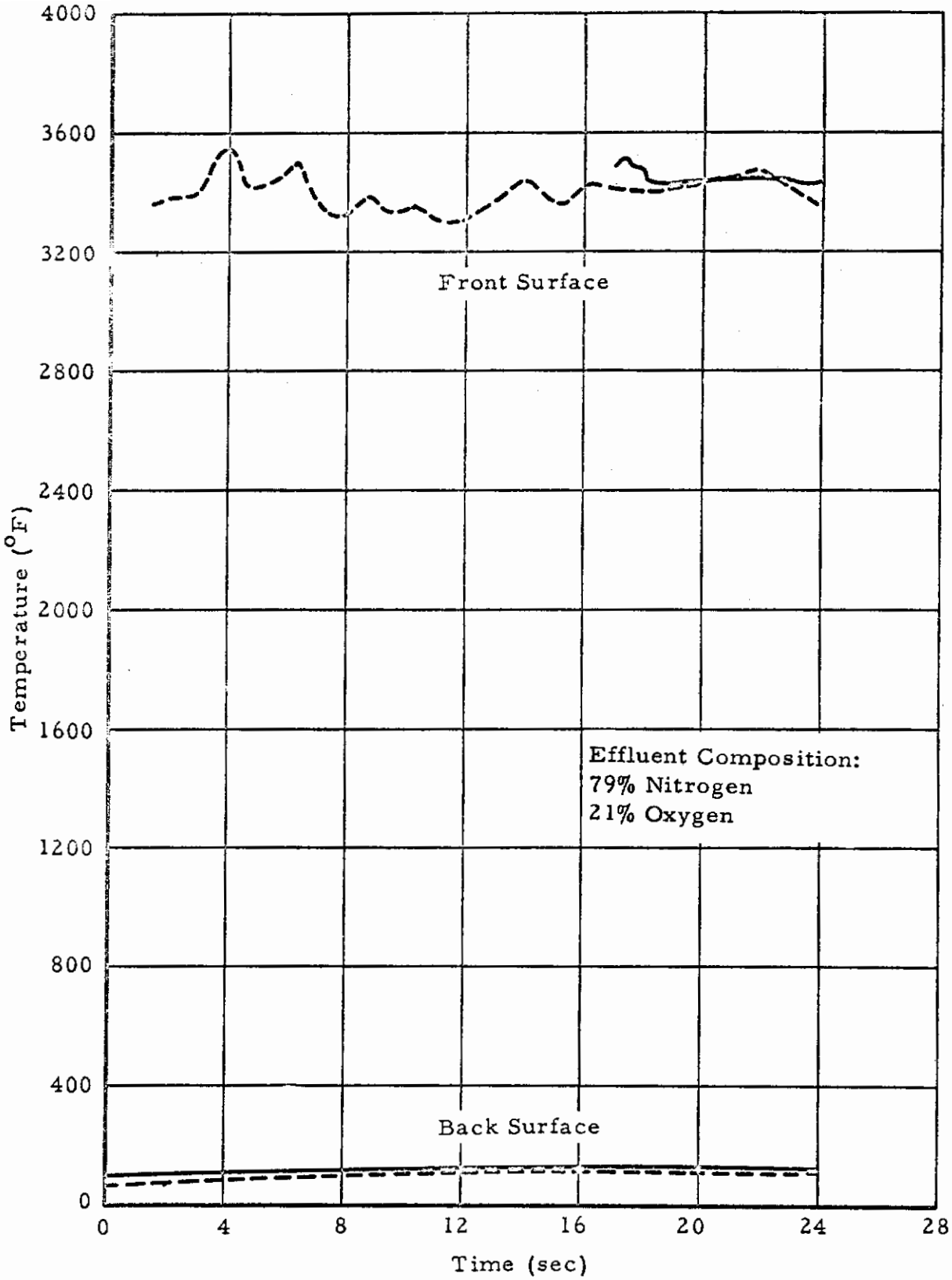

Figure 71. The Temperature-Time History of Phenolic with Asbestos Exposed to a 500 Btu/ft^2-sec Heat Flux Environment

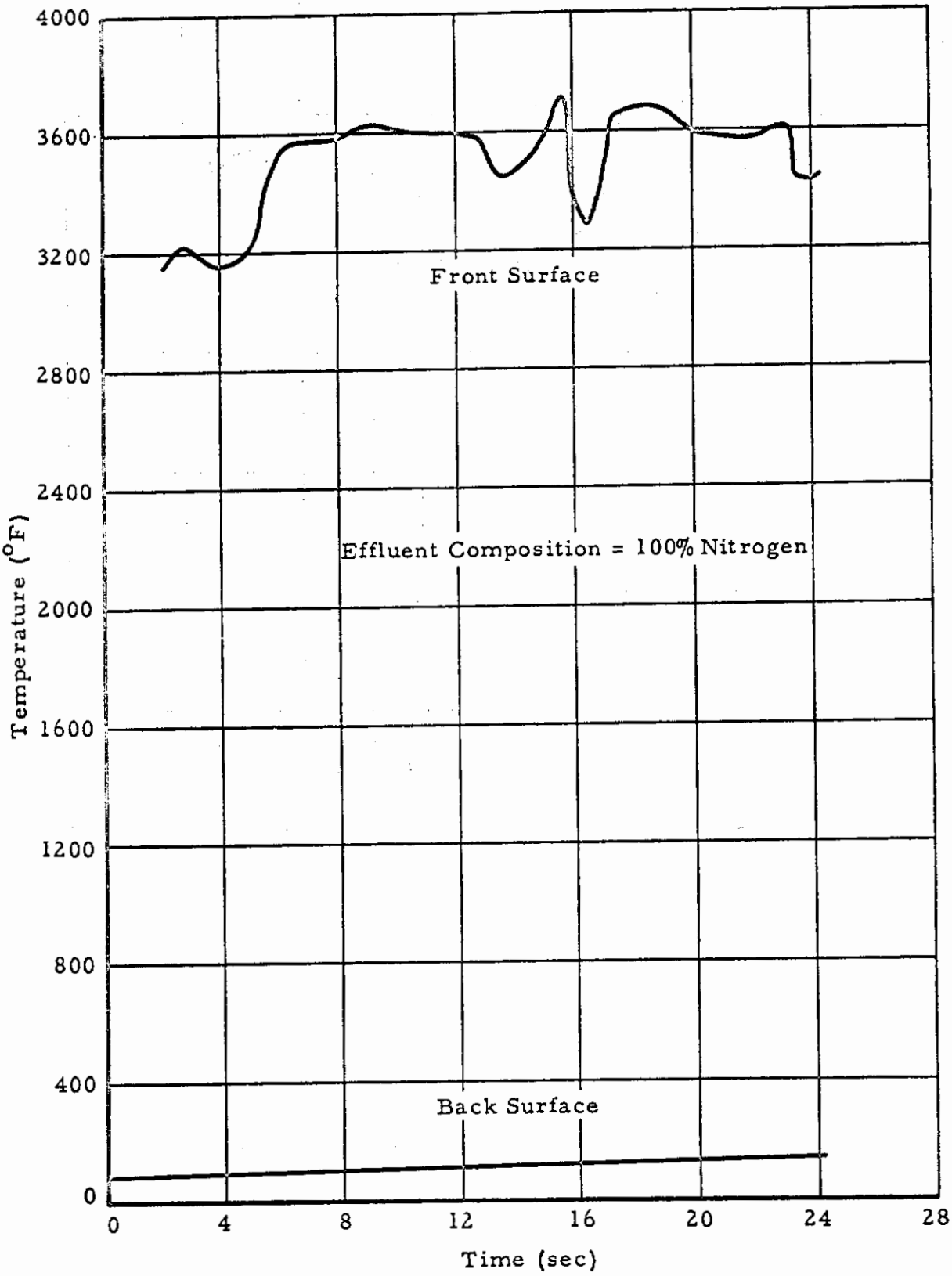

Figure 72. The Temperature-Time History of Phenolic with Asbestos Exposed to a 500 Btu/ft^2-sec Heat Flux Environment

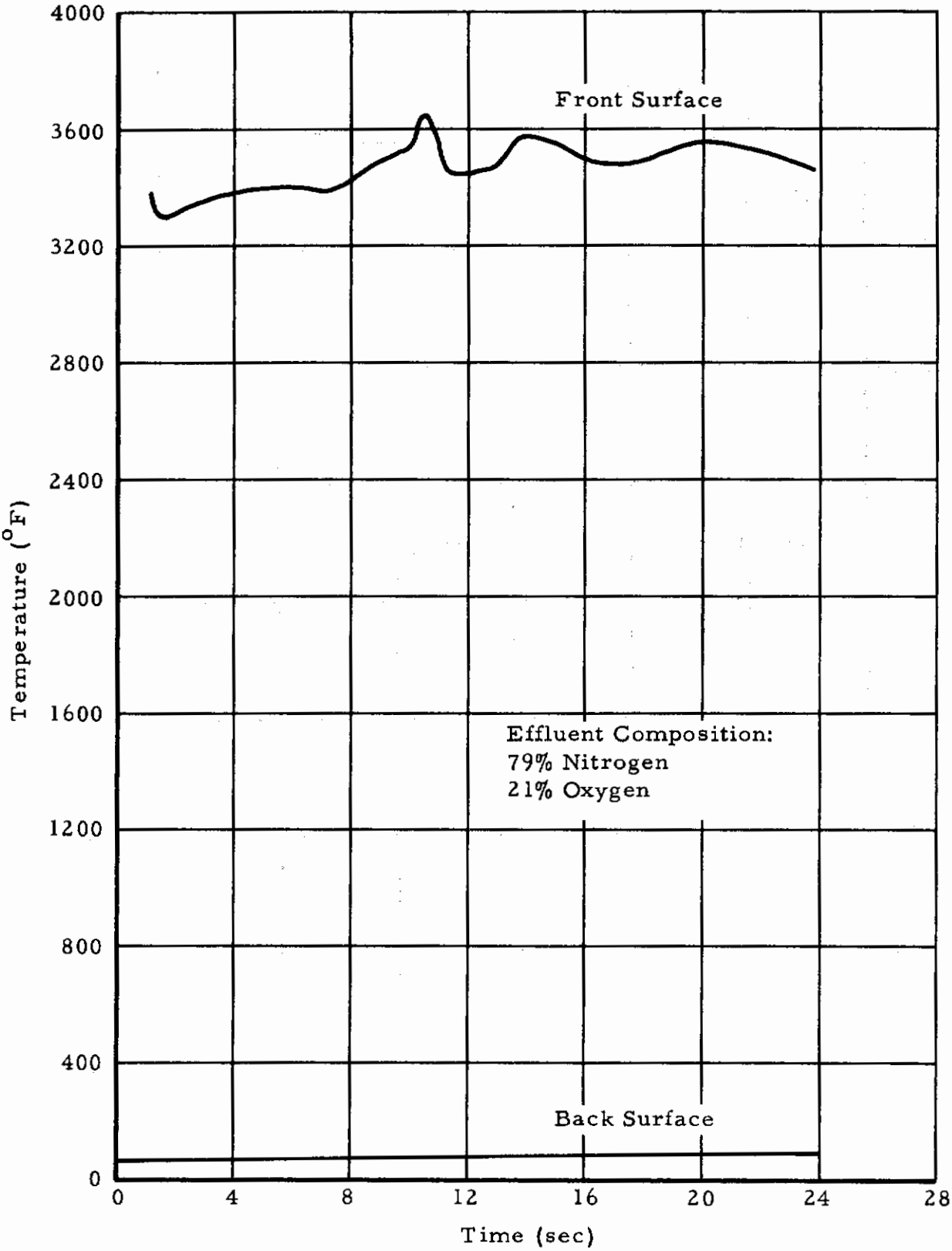

Figure 73. The Temperature-Time History of Halogenated Phenolic Resin on Refrasil Exposed to a 480 Btu/ft^2-sec. Heat Flux Environment.

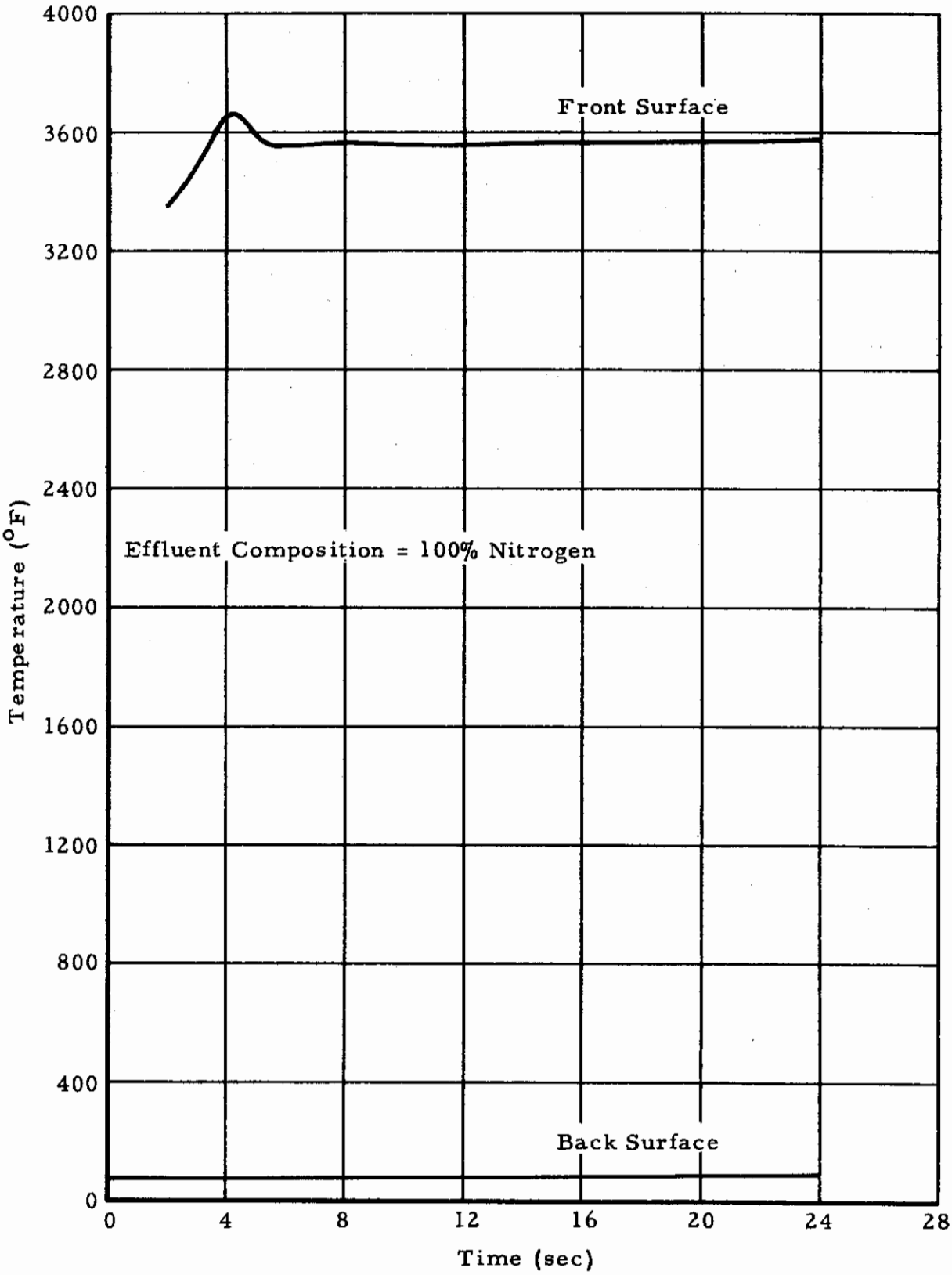

Figure 74. The Temperature-Time History of Halogenated Phenolic Resin on Refrasil Exposed to a 500 Btu/ft^2-sec Heat Flux Environment.

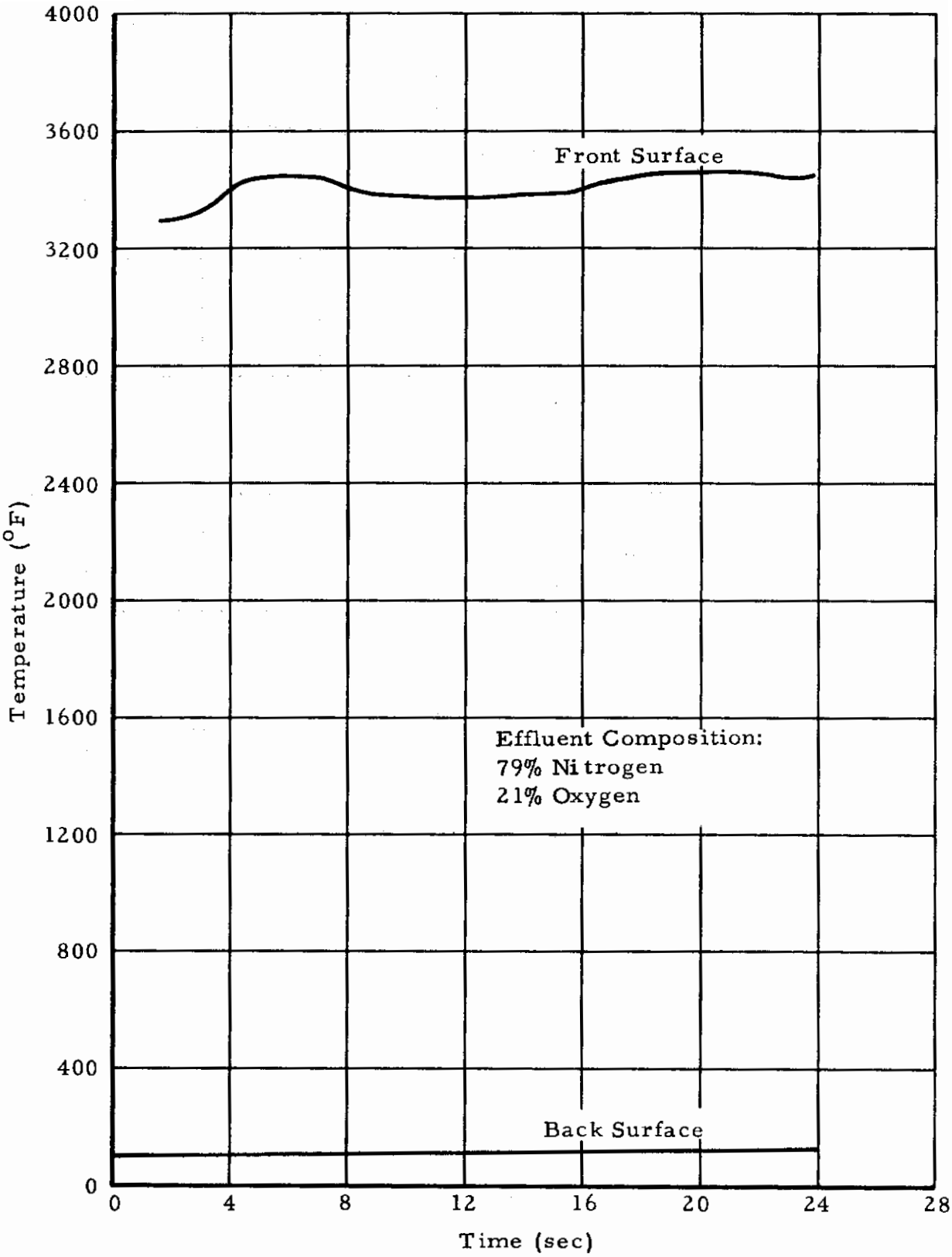

Figure 75. The Temperature-Time History of Modified Halogenated Phenyl Co-polymerized Silane Resin on Refrasil Exposed to a 480 Btu/ft^2-sec Heat Flux Environment.

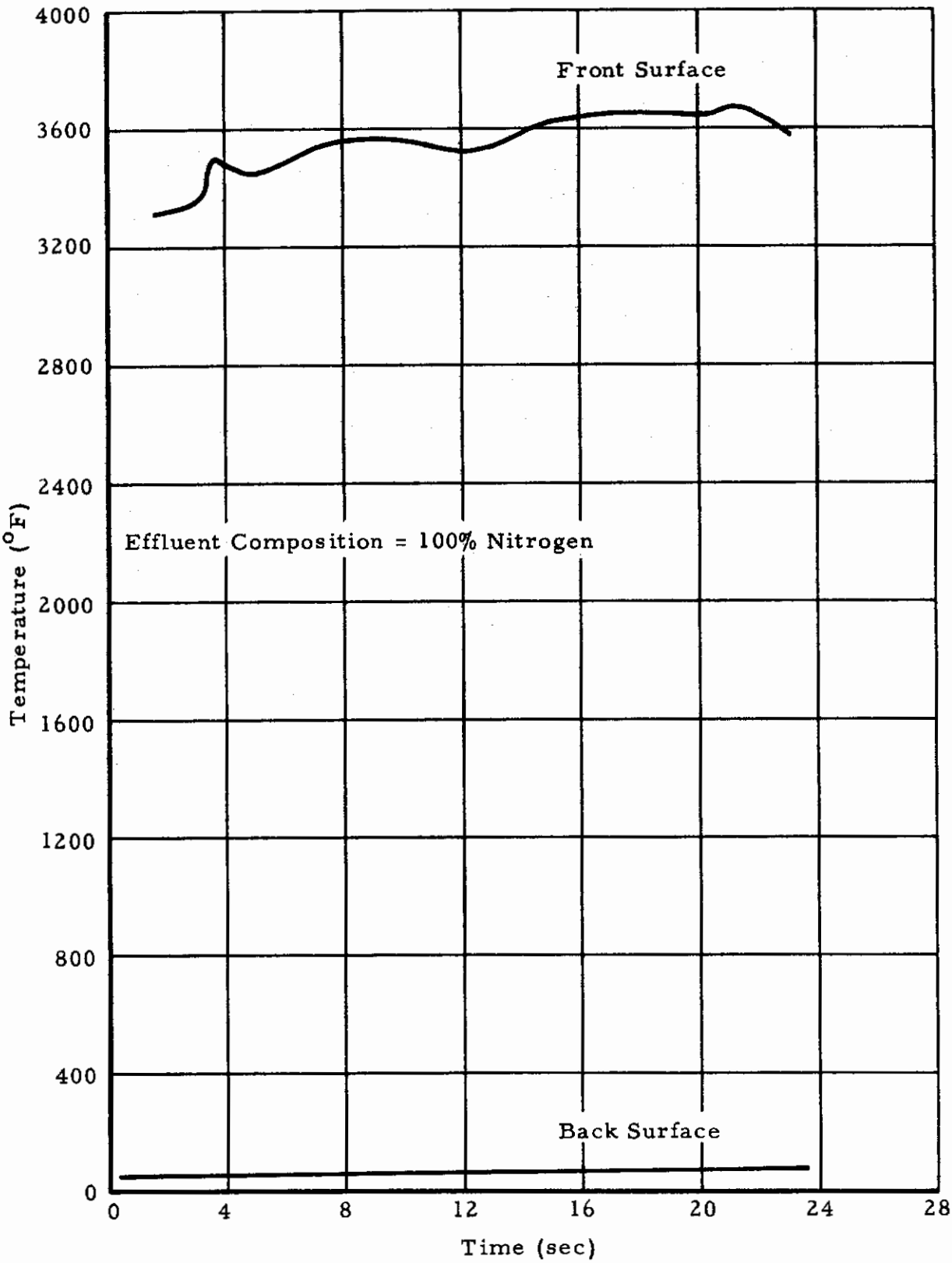

Figure 76. The Temperature-Time History of Modified Halogenated Phenyl Co-polymerized Silane Resin on Refrasil Exposed to a 500 Btu/ft^2-sec Heat Flux Environment.

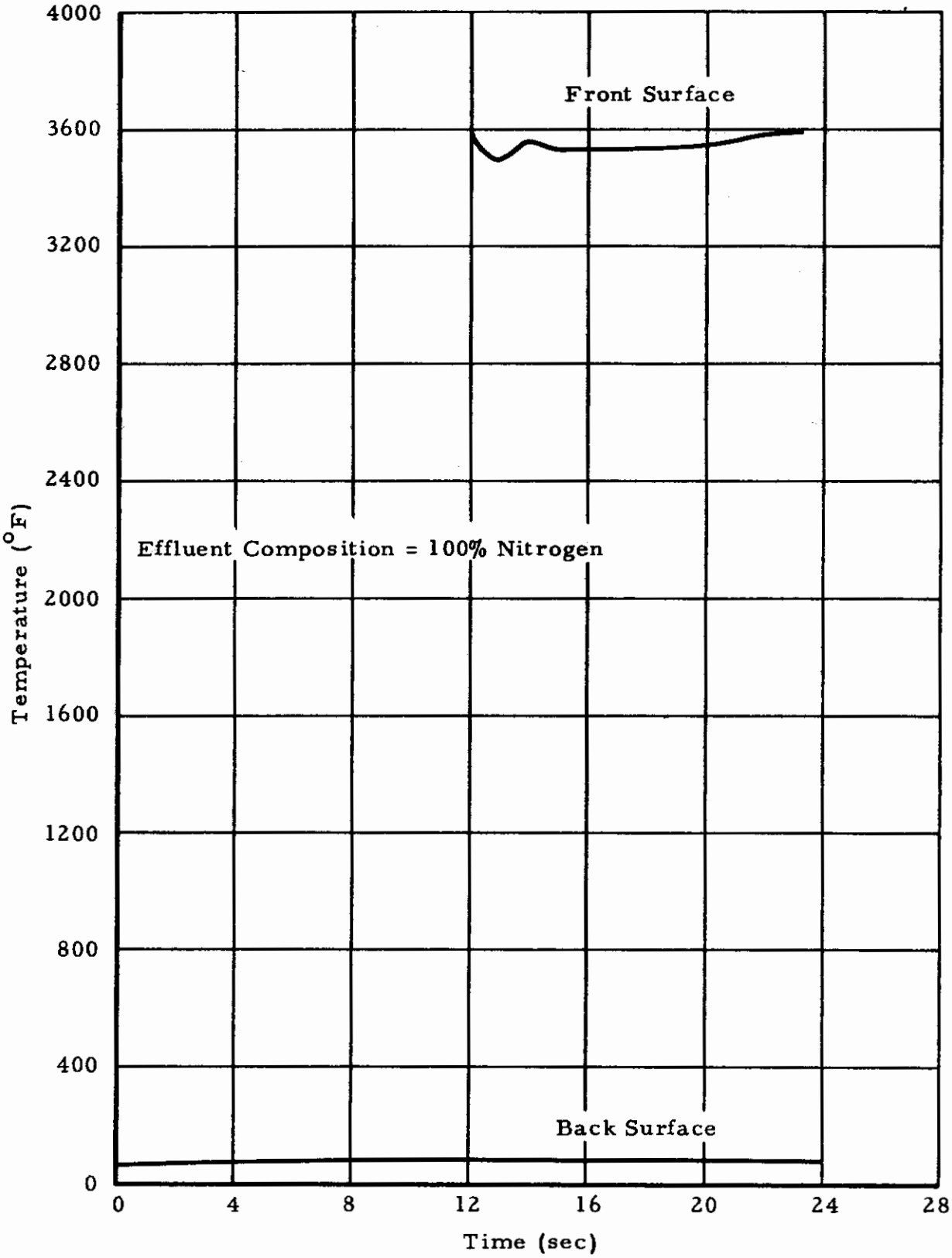

Figure 77. The Temperature-Time History of Halogenated Phenyl Co-polymerized Silane Resin on Refrasil Exposed to a 500 Btu/ft^2-sec Heat Flux Environment.

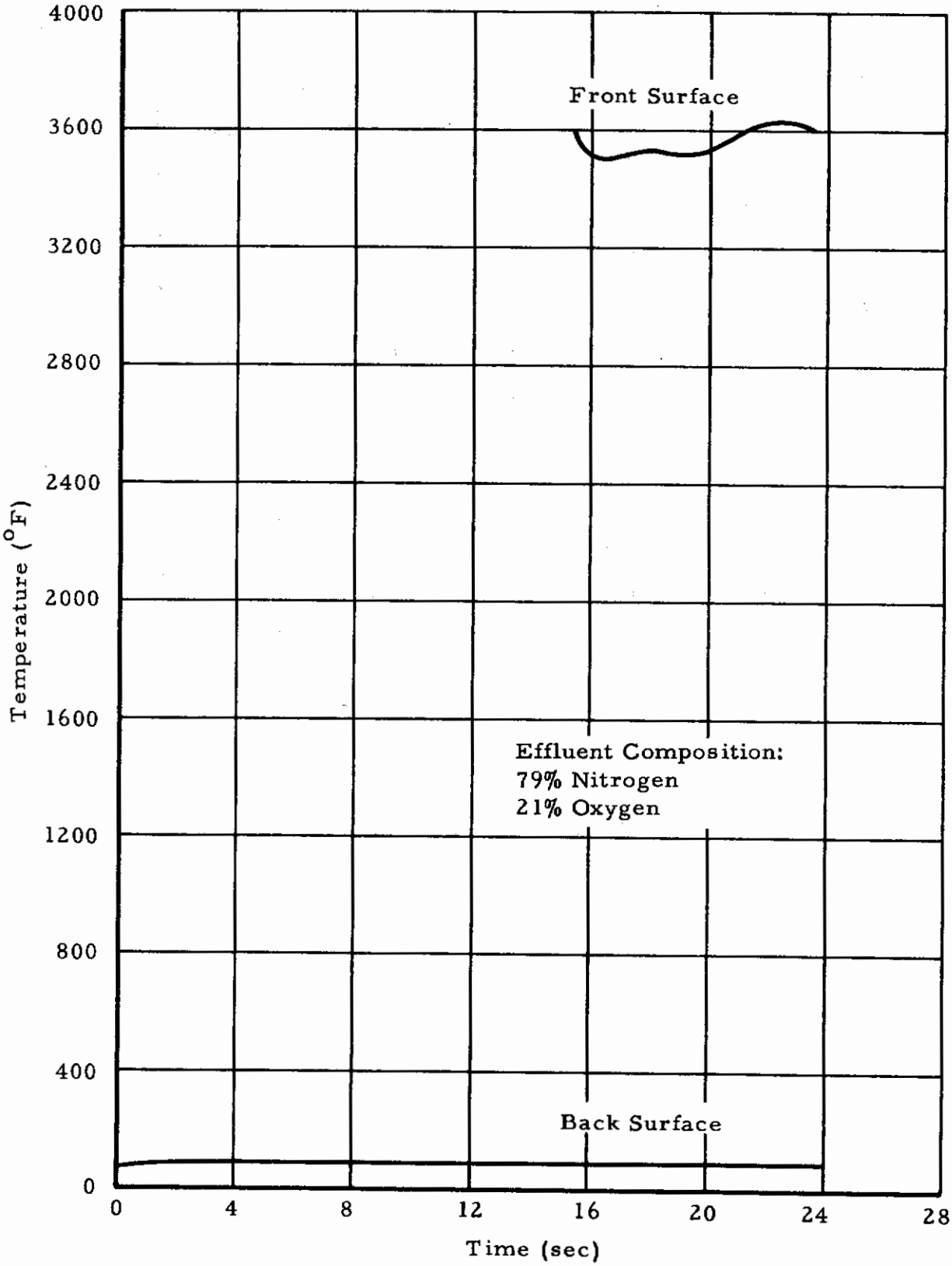

Figure 78. The Temperature-Time History of Halogenated Phenyl Co-polymerized Silane Resin on Refrasil Exposed to a 480 Btu/ft^2-sec Heat Flux Environment.

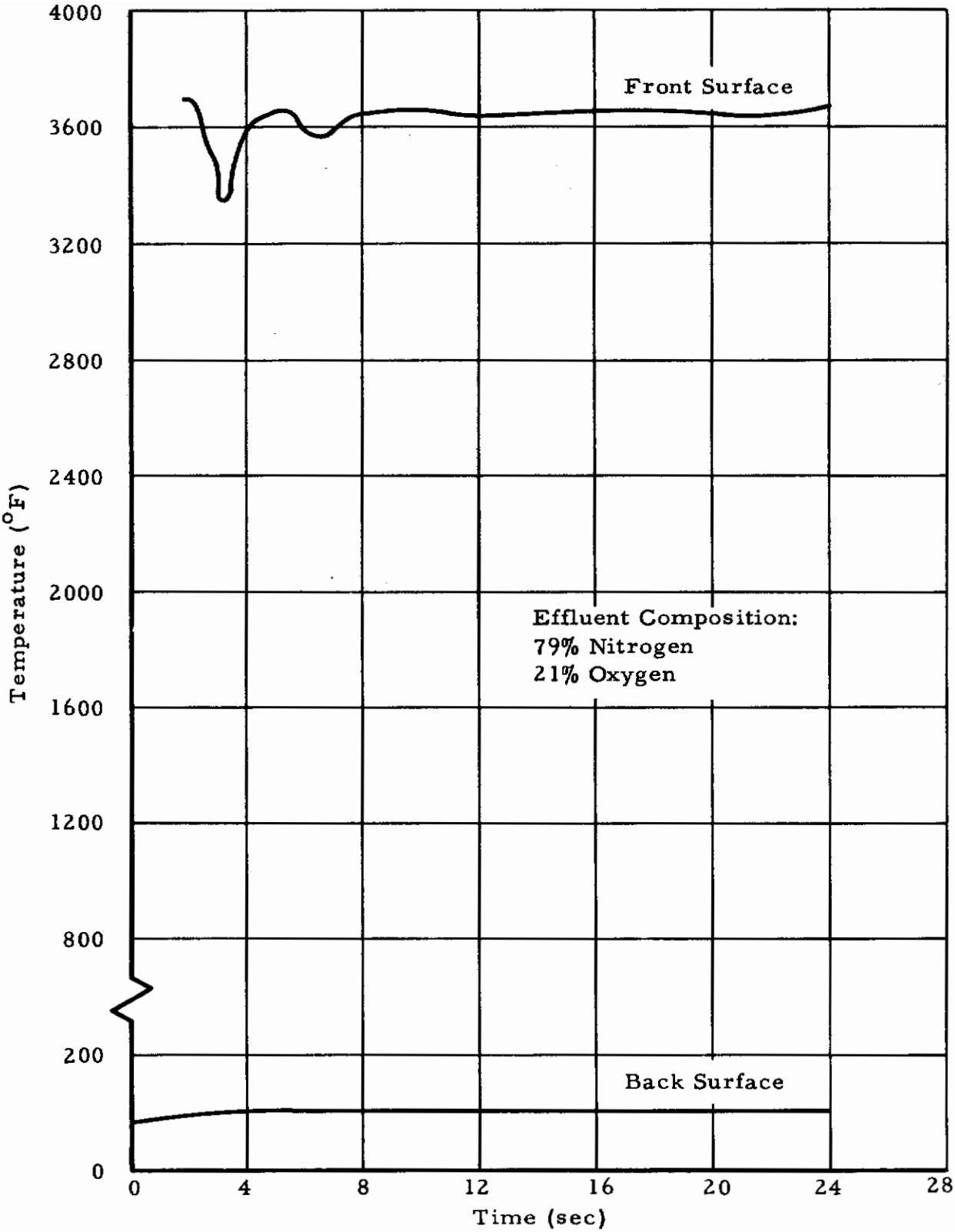

Figure 79. Temperature-Time History of Asbestos Felt with Phenolic and Titanium Dioxide Exposed to a 493 Btu/ft^2-sec Environment.

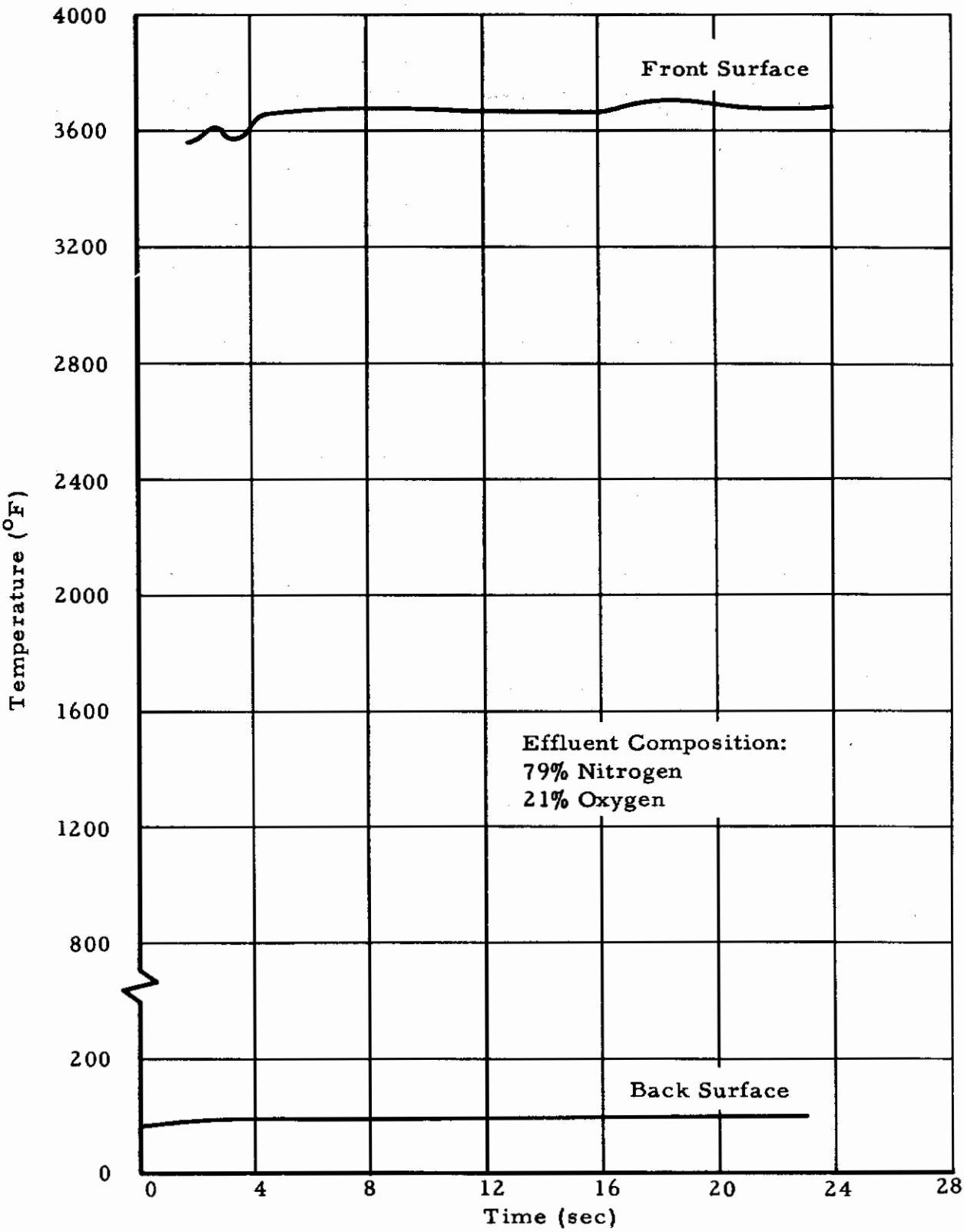

Figure 80. Temperature-Time History of Asbestos Felt with Phenolic and Potassium Titanate Exposed to a 493 Btu/ft^2-sec Environment.

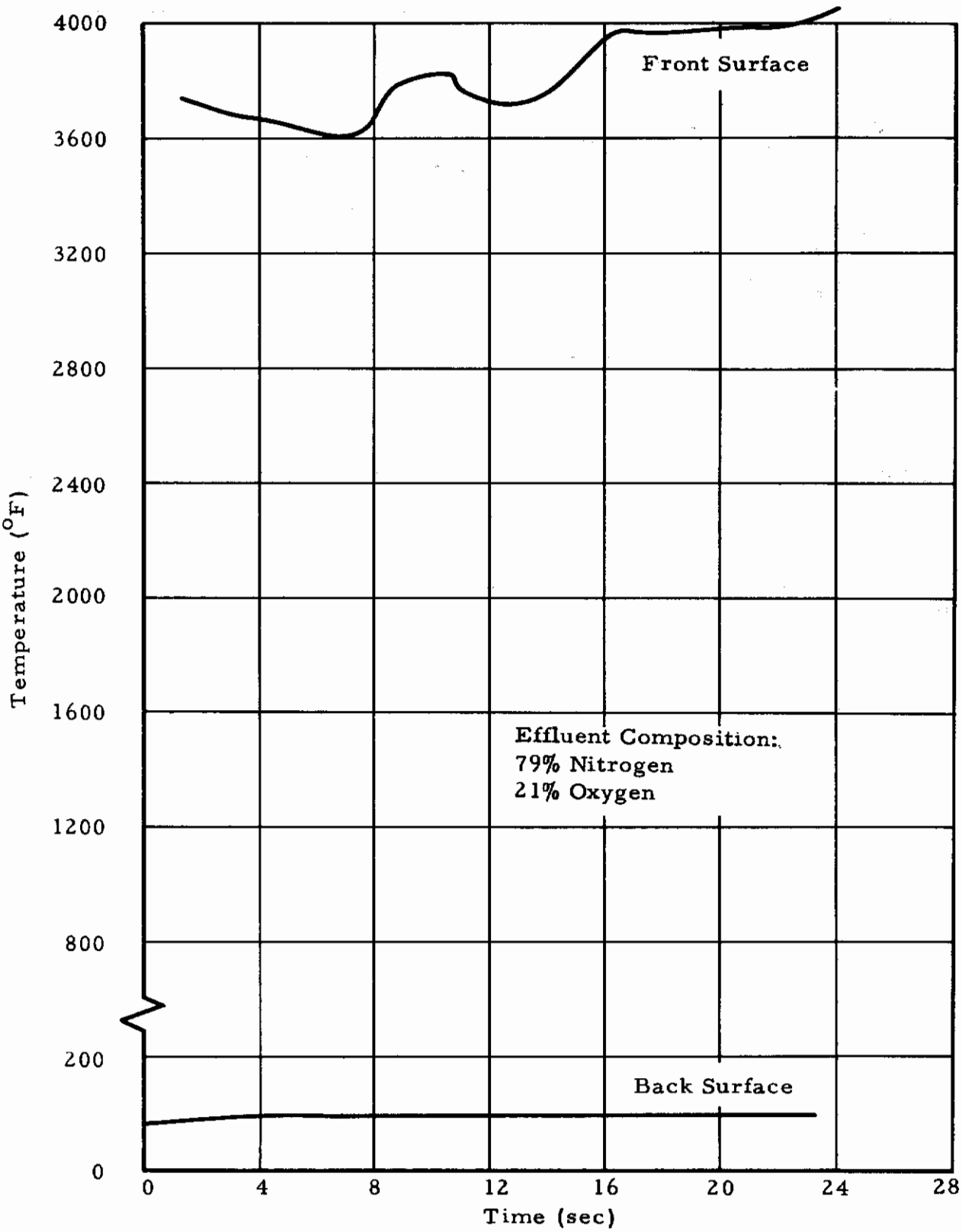

Figure 81. Temperature-Time History of Asbestos Felt with Phenolic and Tungsten Exposed to a 493 Btu/ft^2-sec Environment.

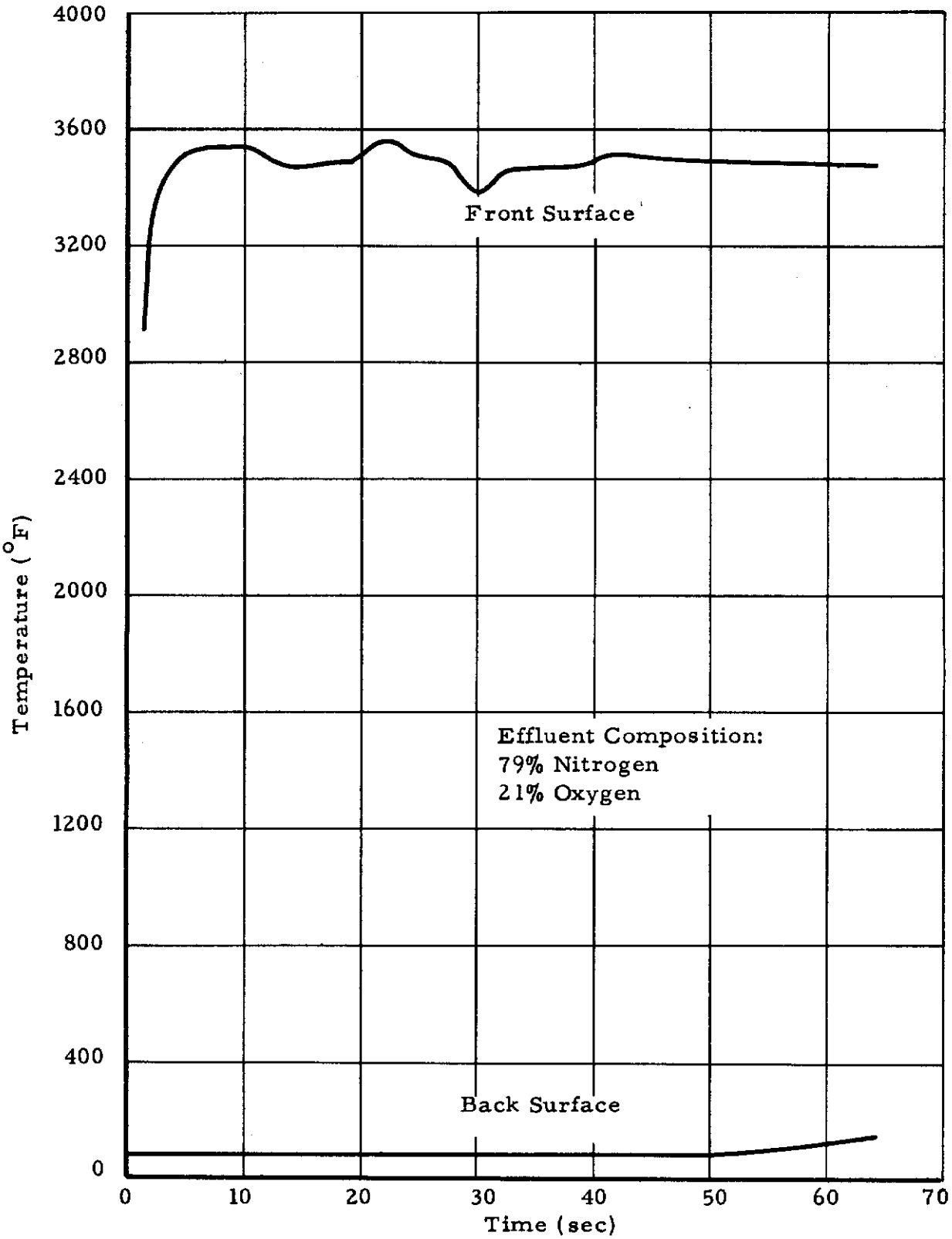

Figure 82. Temperature-Time History of Asbestos Felt With Phenolic and Titanium Dioxide Exposed to a 500 Btu/ft^2-sec Environment.

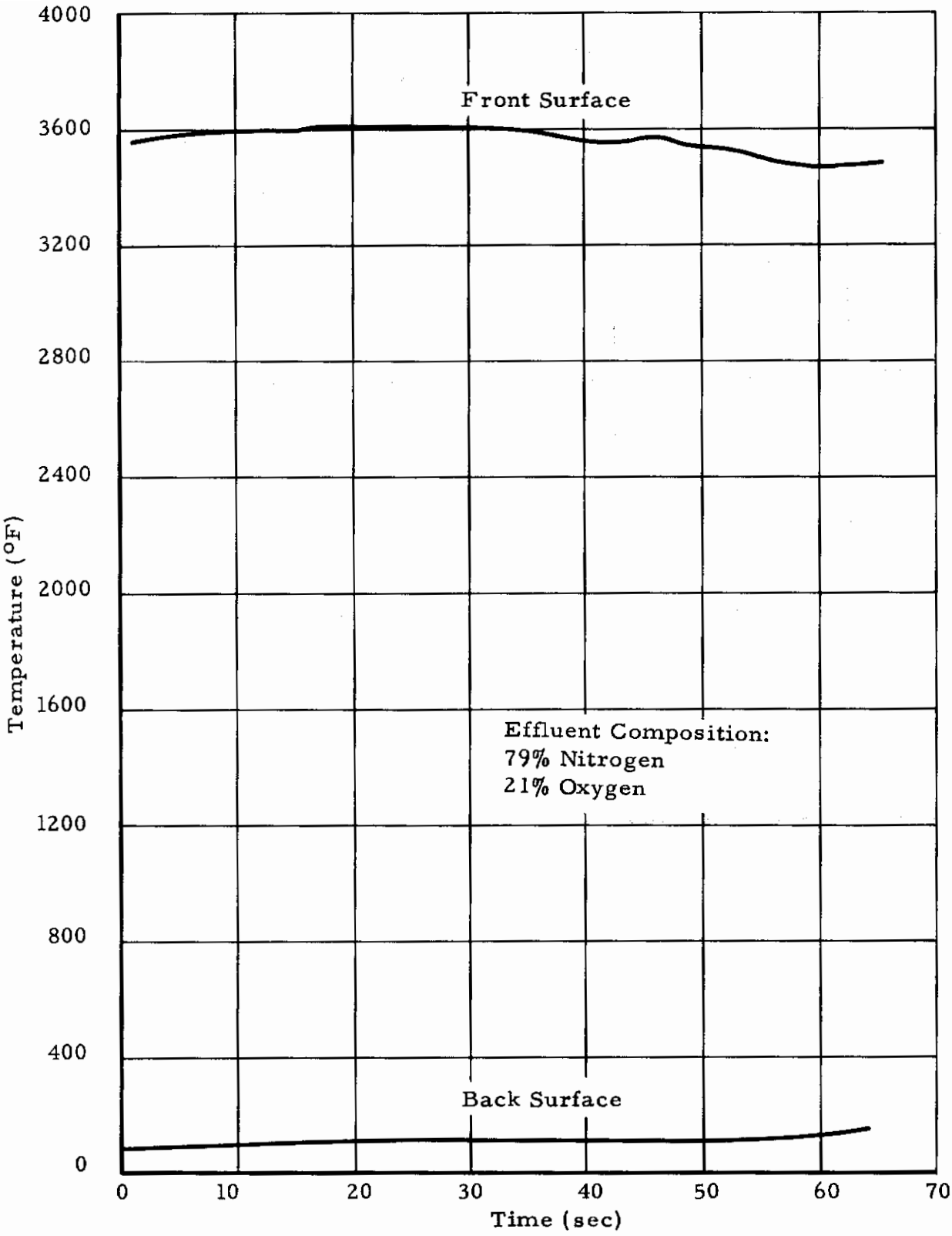

Figure 83. Temperature-Time History of Asbestos Felt With Phenolic and Potassium Titanate Exposed to a 500 Btu/ft^2-sec Environment.

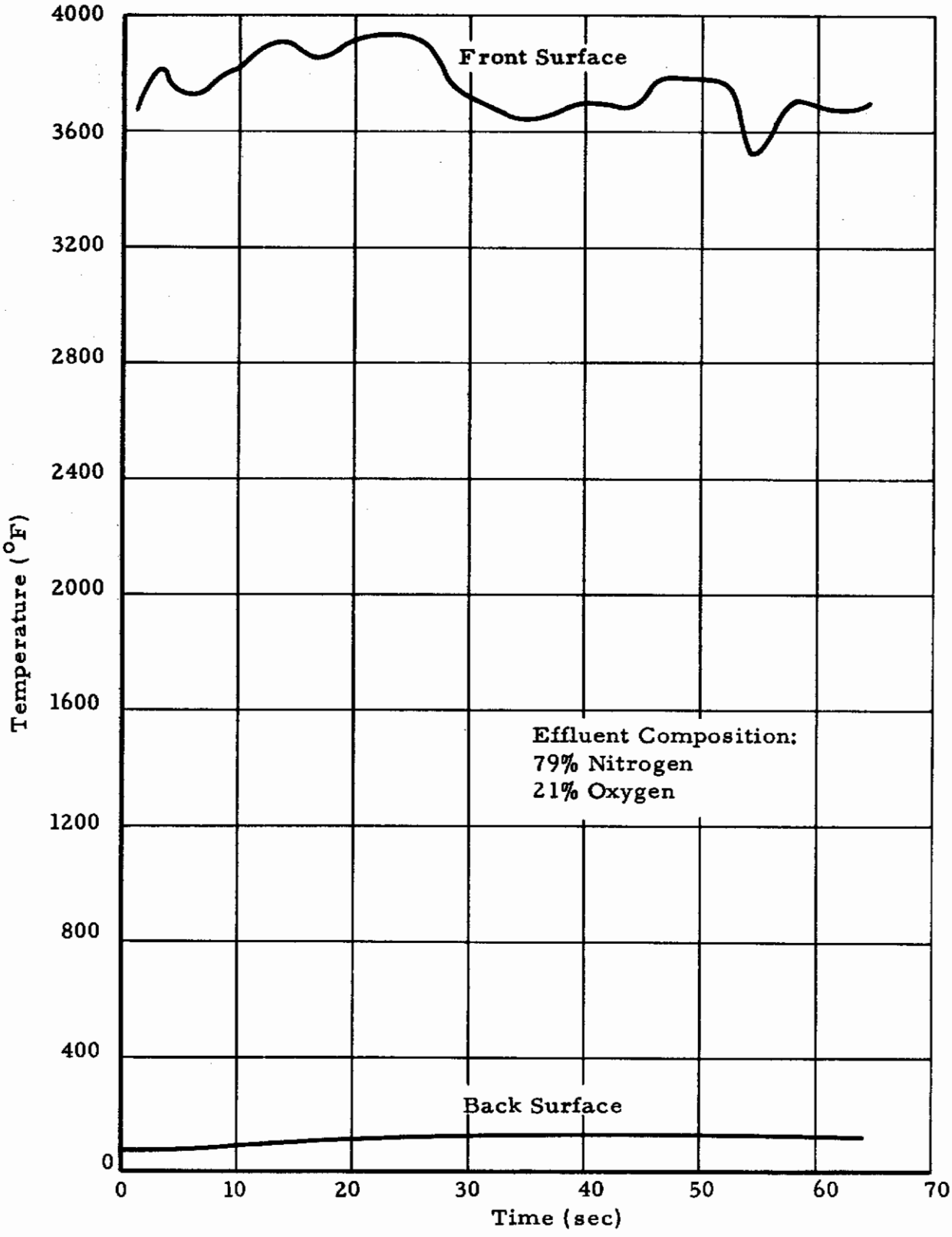

Figure 84. Temperature-Time History of Asbestos Felt With Phenolic and Tungsten Exposed to a 500 Btu/ft^2-sec Environment.

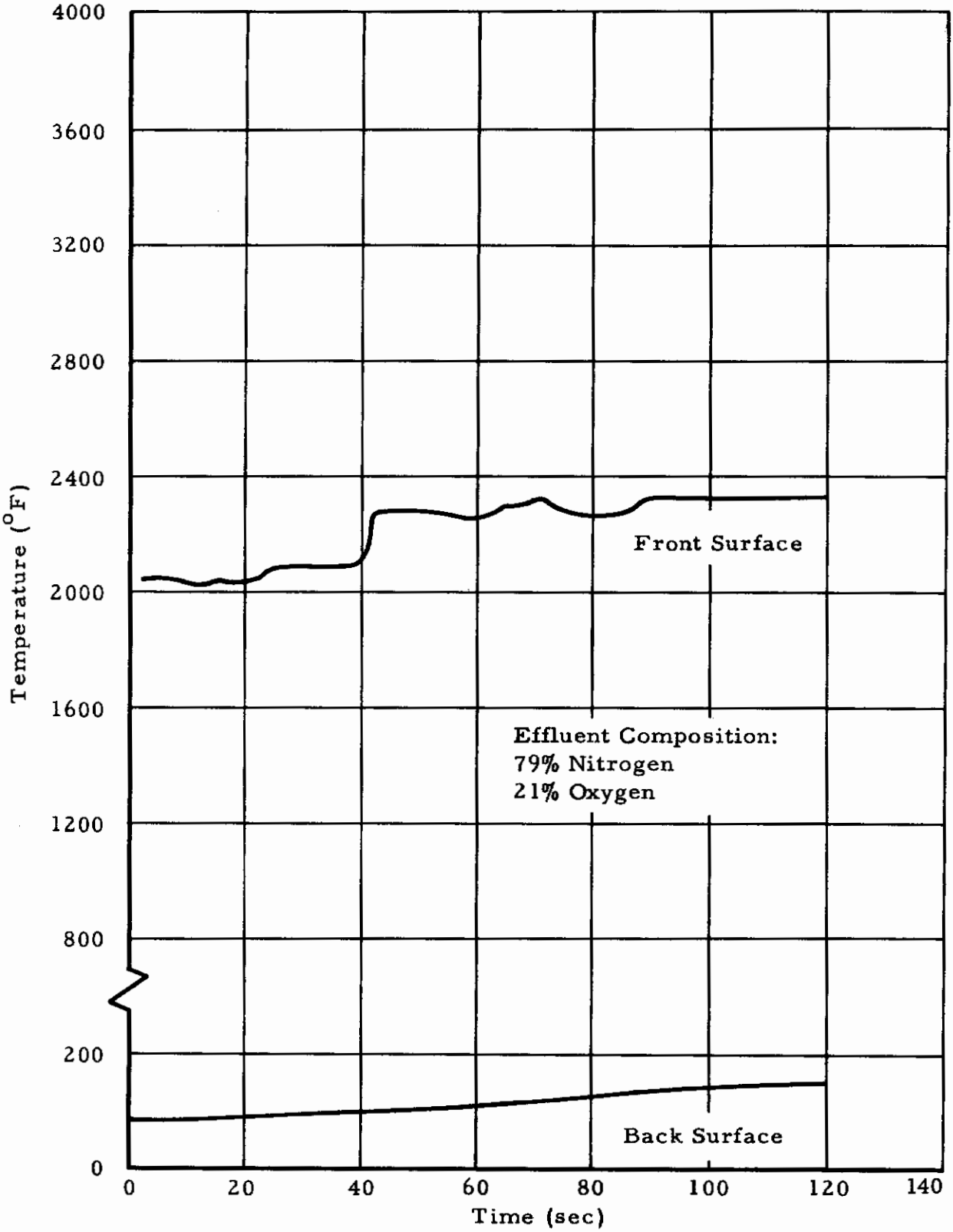

Figure 85. Temperature-Time History of Asbestos Felt with Phenolic and Titanium Dioxide Exposed to a 100 Btu/ft^2-sec Environment.

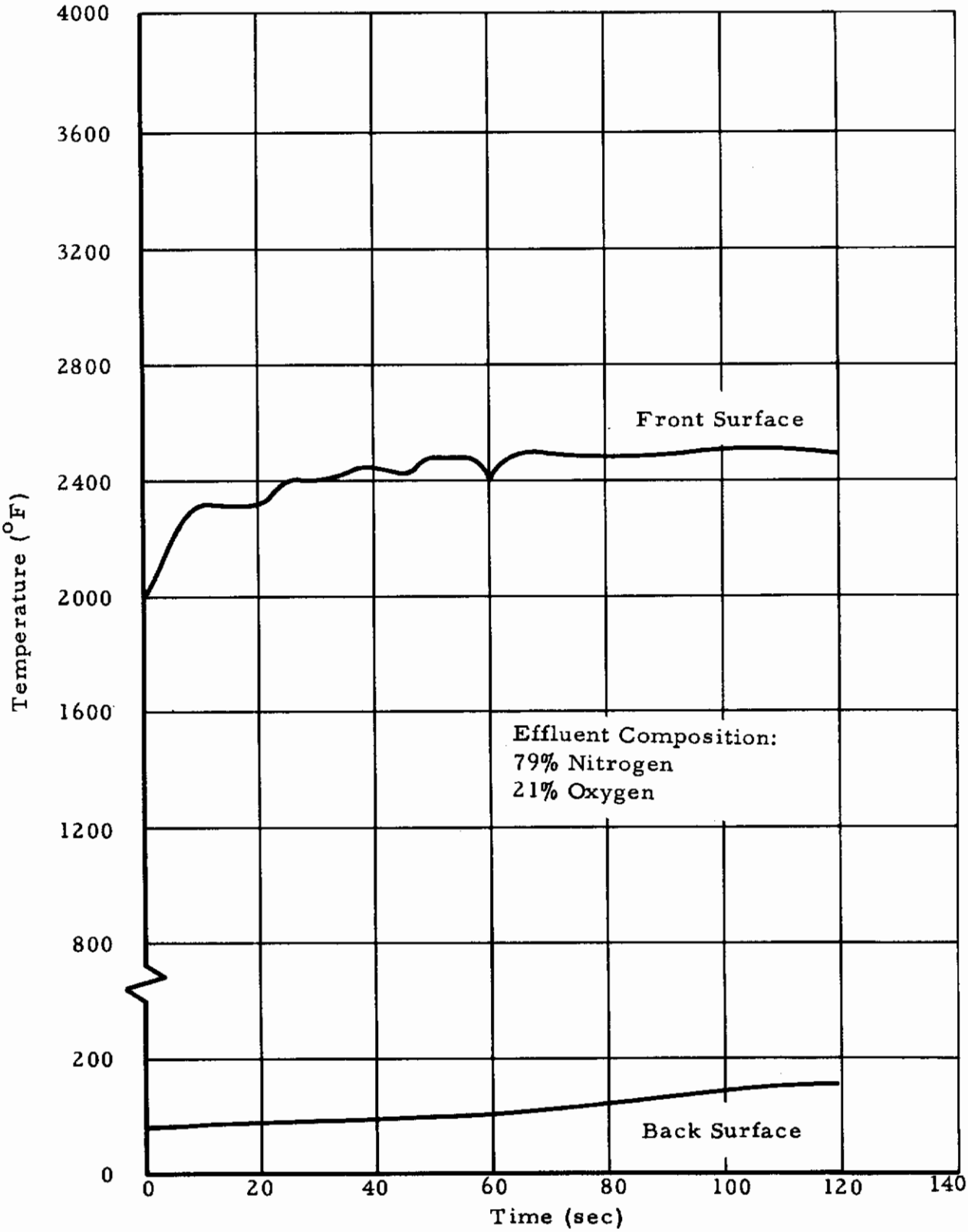

Figure 86. Temperature-Time History of Asbestos Felt with Phenolic and Potassium Titanate Exposed to a 100 Btu/ft^2-sec Environment.

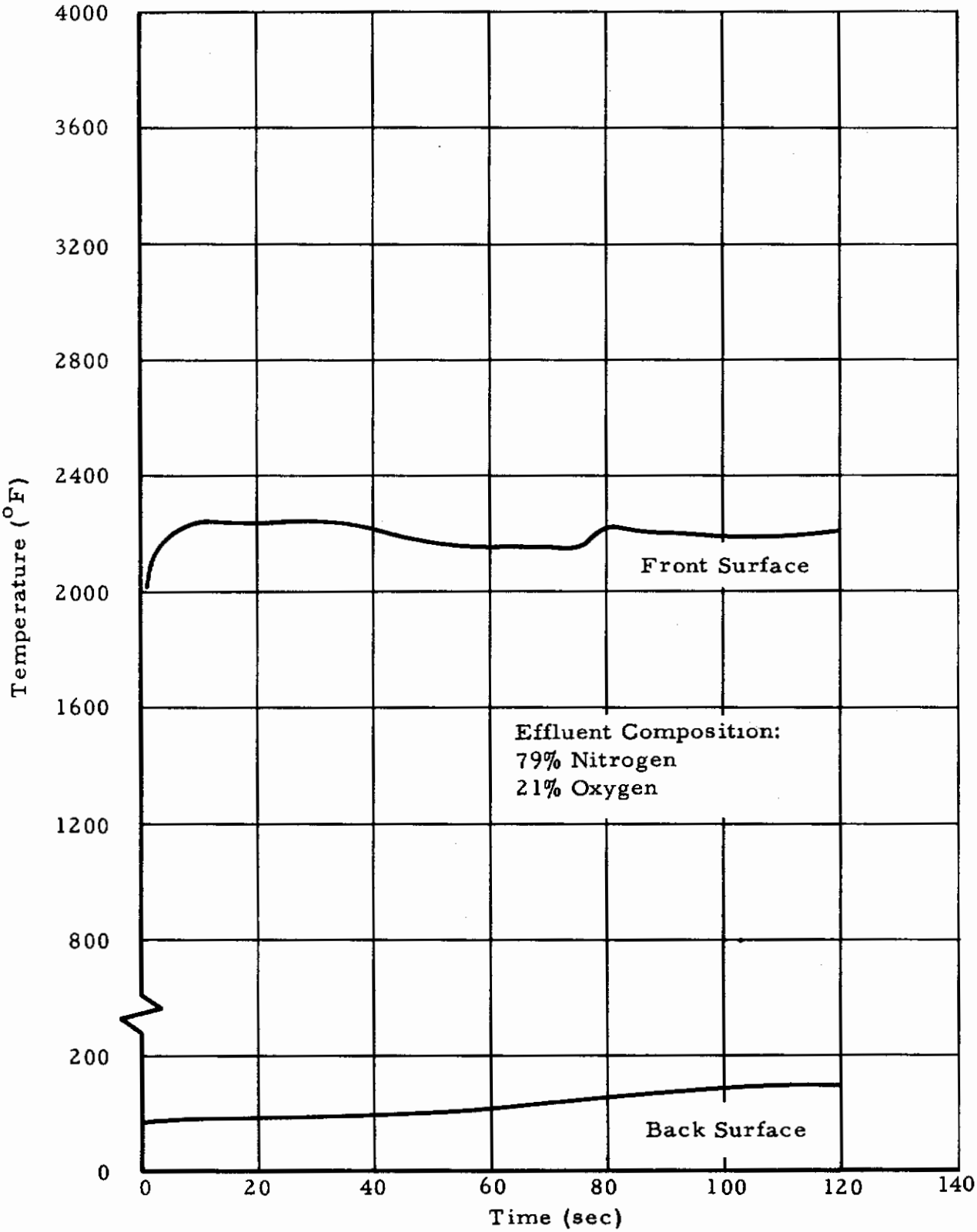

Figure 87. Temperature-Time History of Asbestos Felt with Phenolic and Tungsten Exposed to a 100 Btu/ft^2-sec Environment.

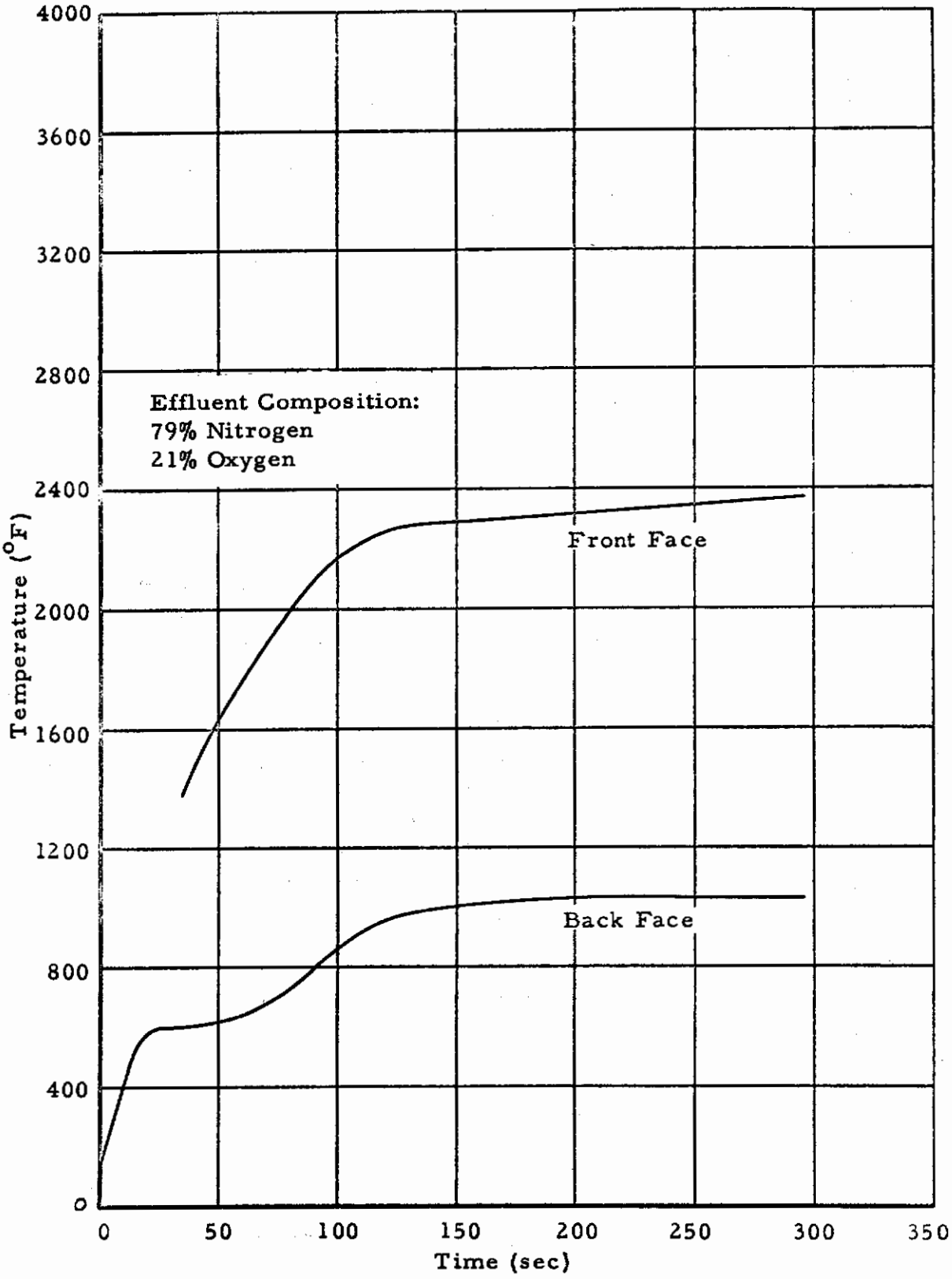

Figure 88. The Temperature-Time History of Cermet Plated Graphite Exposed to a 300 Btu/ft^2-sec Heat Flux Environment

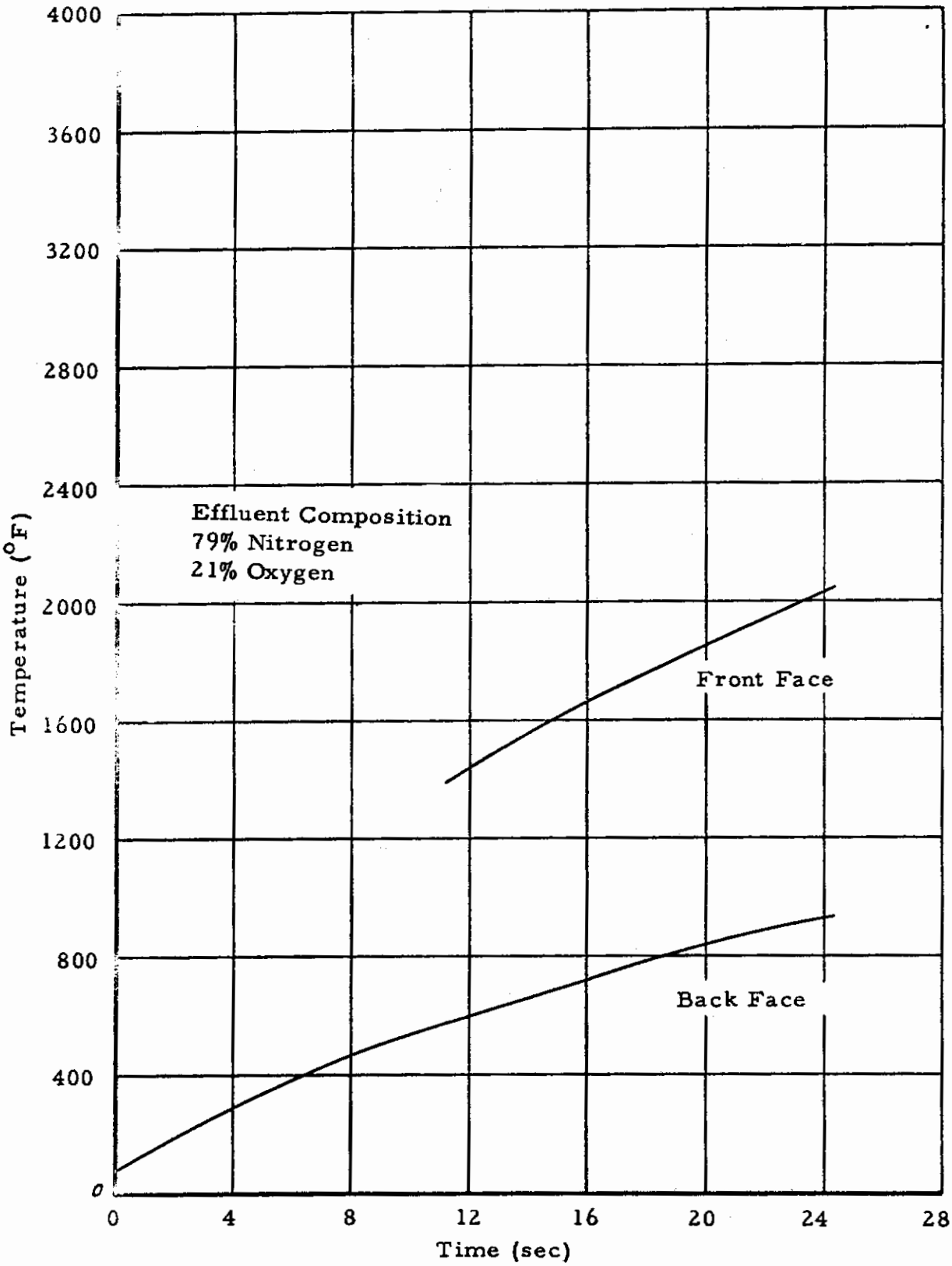

Figure 89. The Temperature-Time History of Cermet Plated Graphite Exposed to a 510 Btu/ft^2-Sec Heat Flux Environment

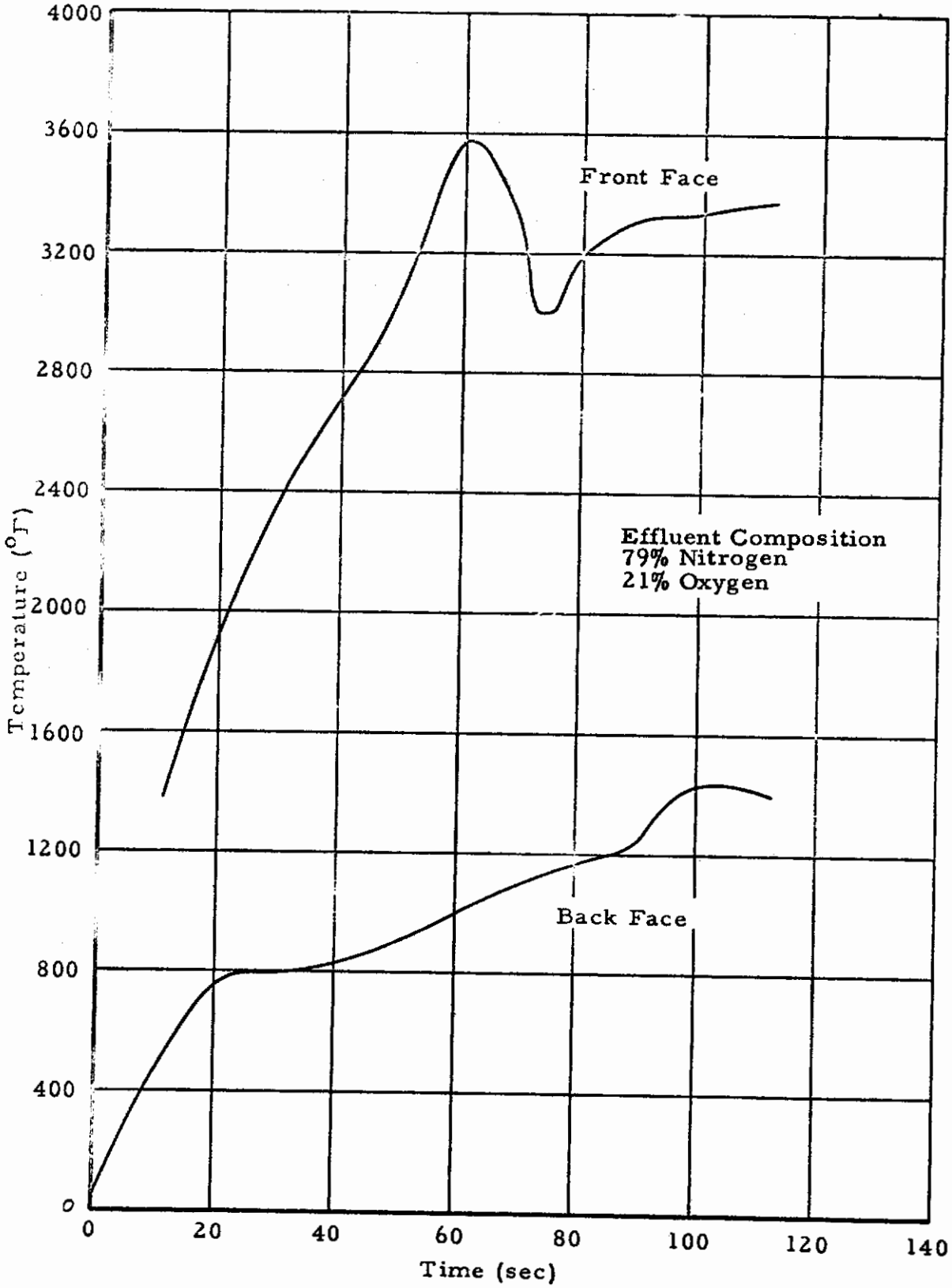

Figure 90. The Temperature-Time History of Cermet Plated Graphite Exposed to ≈ 510 Btu/ft^2-sec Heat Flux Environment

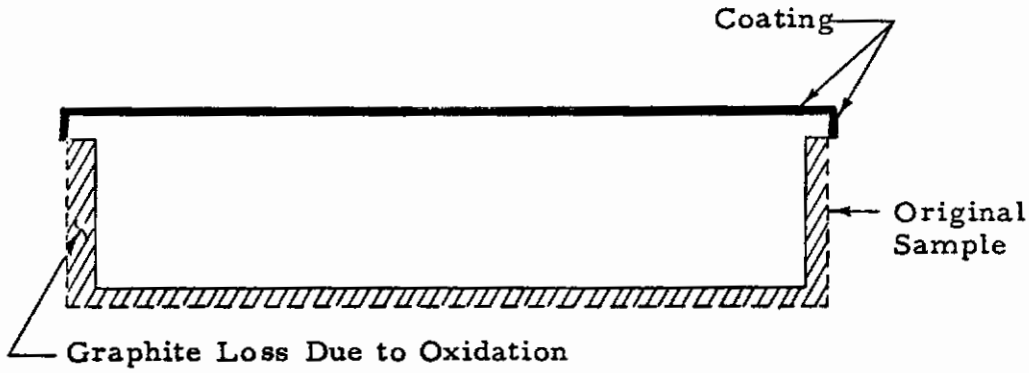

Figure 91. Schematic Cross-section of Cermet Plated Graphite Sample Showing Undercutting Due to Oxidation During Arc-Plasma Evaluation

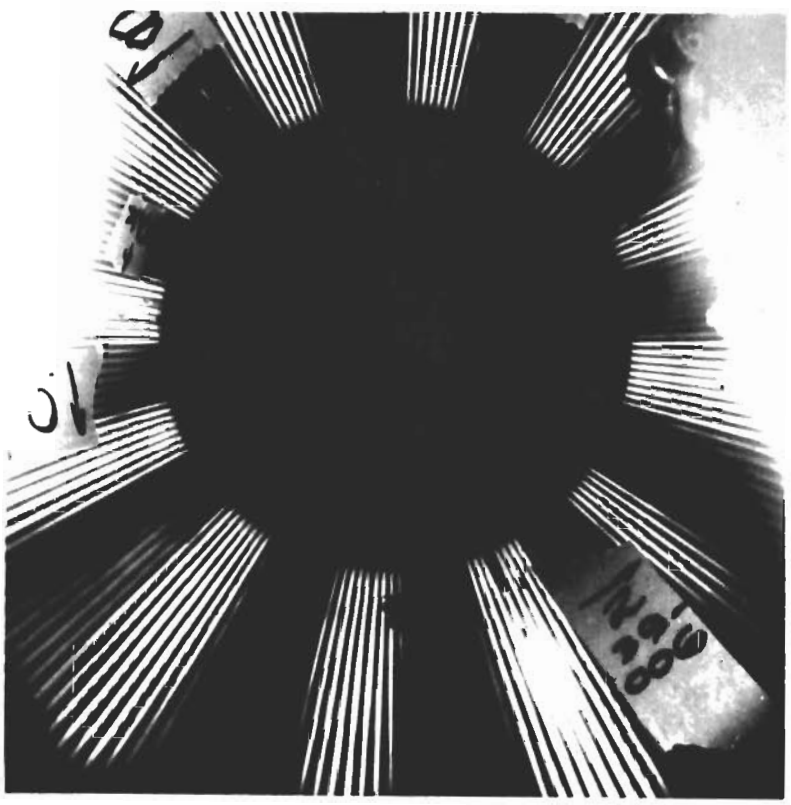

Figure 92. View of XLR-99 Thrust Chamber after Operation Showing the Pattern of White Streaks in the Rokide Z Coating.

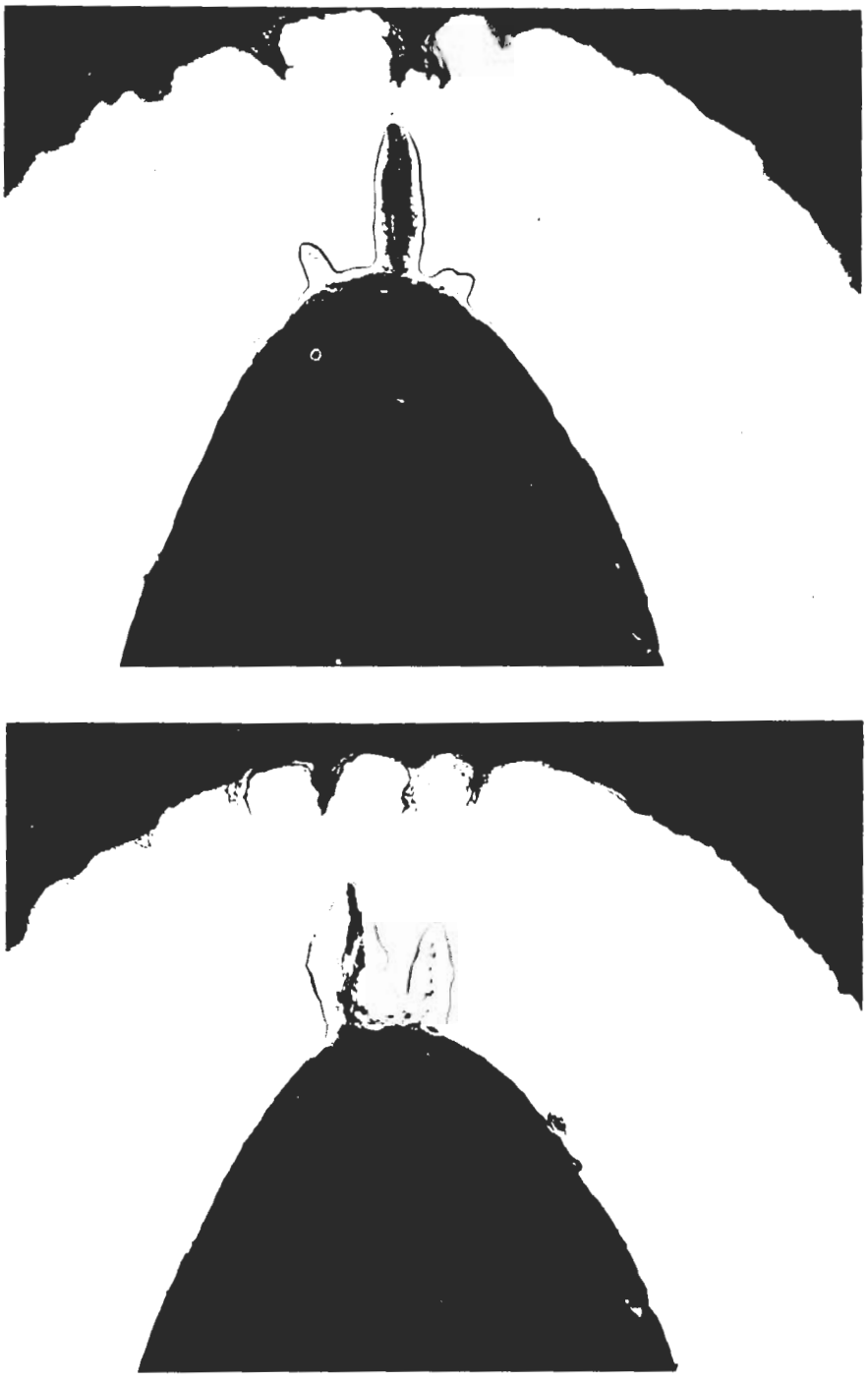

Unetched 50x

Figure 93. Microstructure of Failed Tube at Two Separate Locations Showing Surface Erosion and Diffusion Zone.

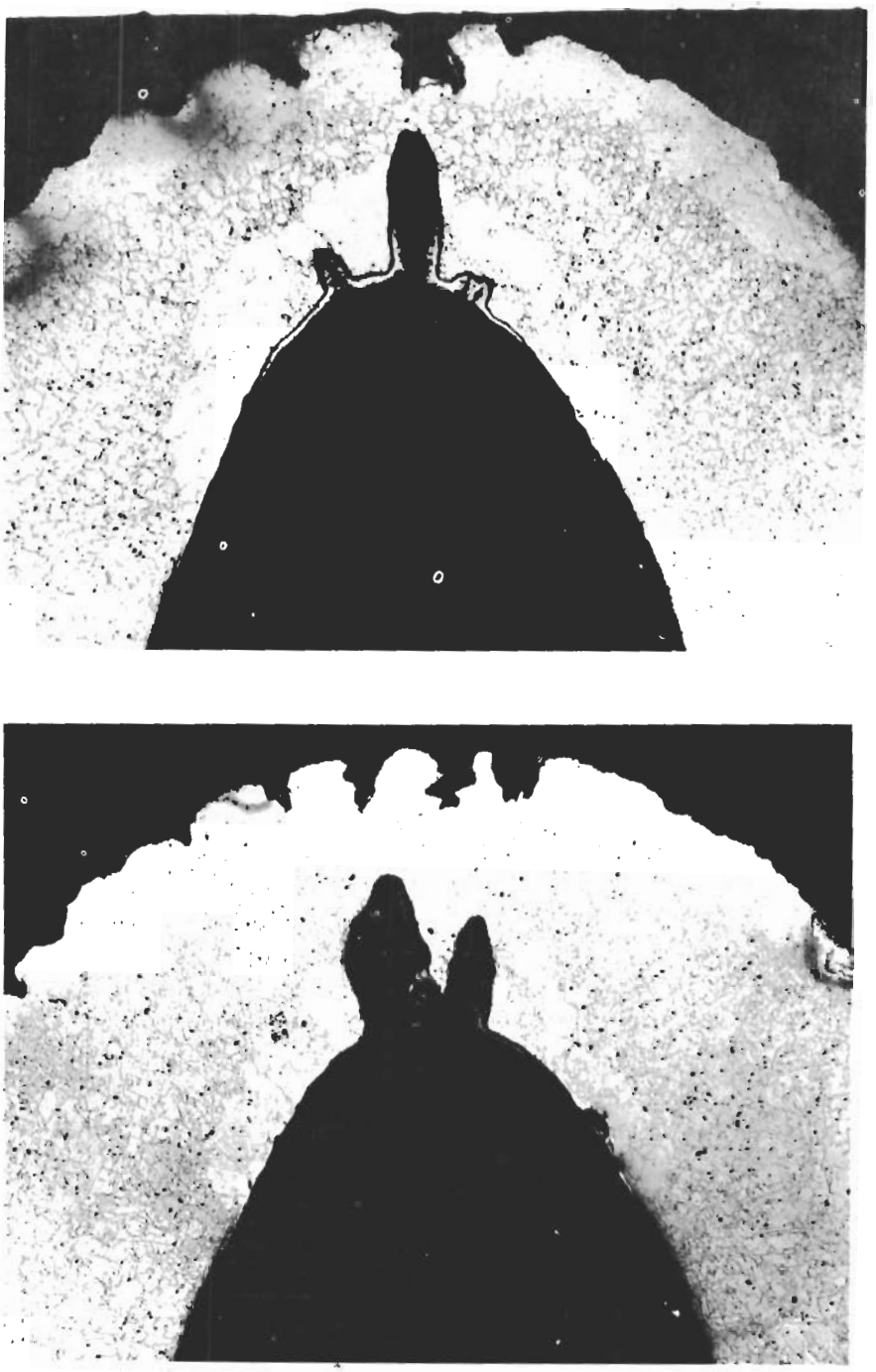

Etched 50x

Figure 94. Both Photomicrographs Are Duplicates of Figure 93 after Etching with 10% Oxalic Acid, Electrolytic 6 V.D.C.

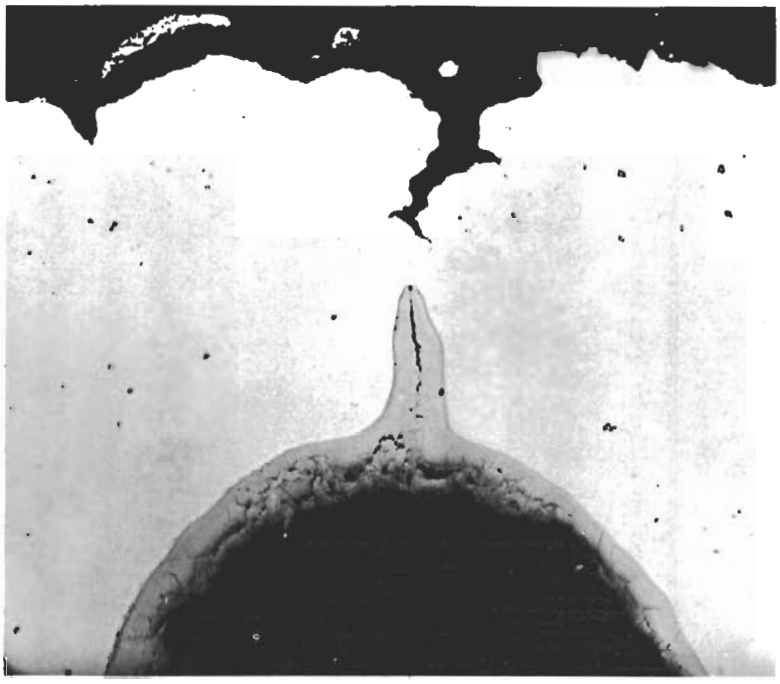

Figure 95. Microstructure of Failed Tube Showing Crack and Diffusion Zone.

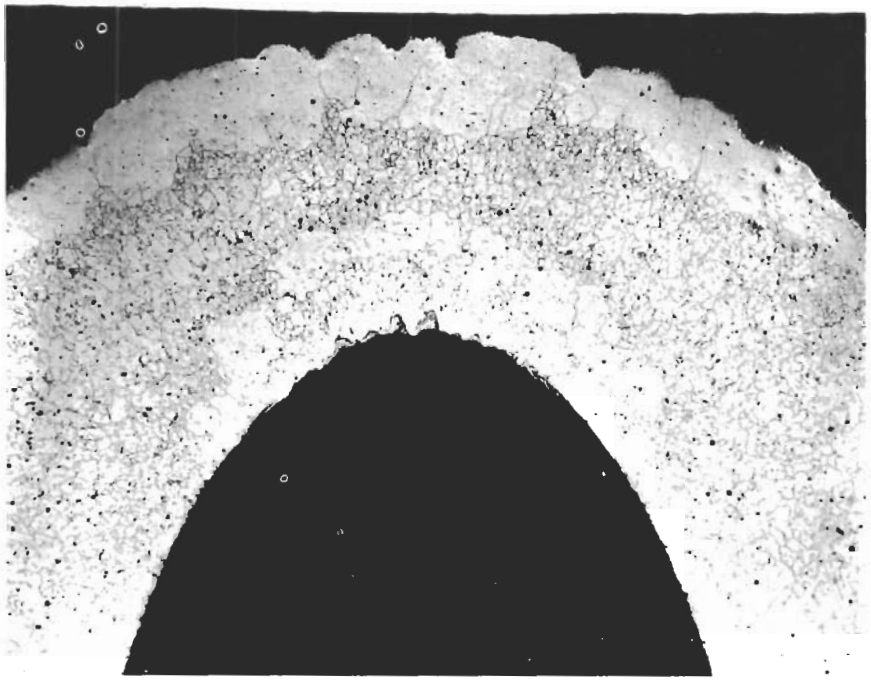

Etched 50x

Figure 96. Microstructural Condition of an Alternate Tube to That Which Contains the Crack.

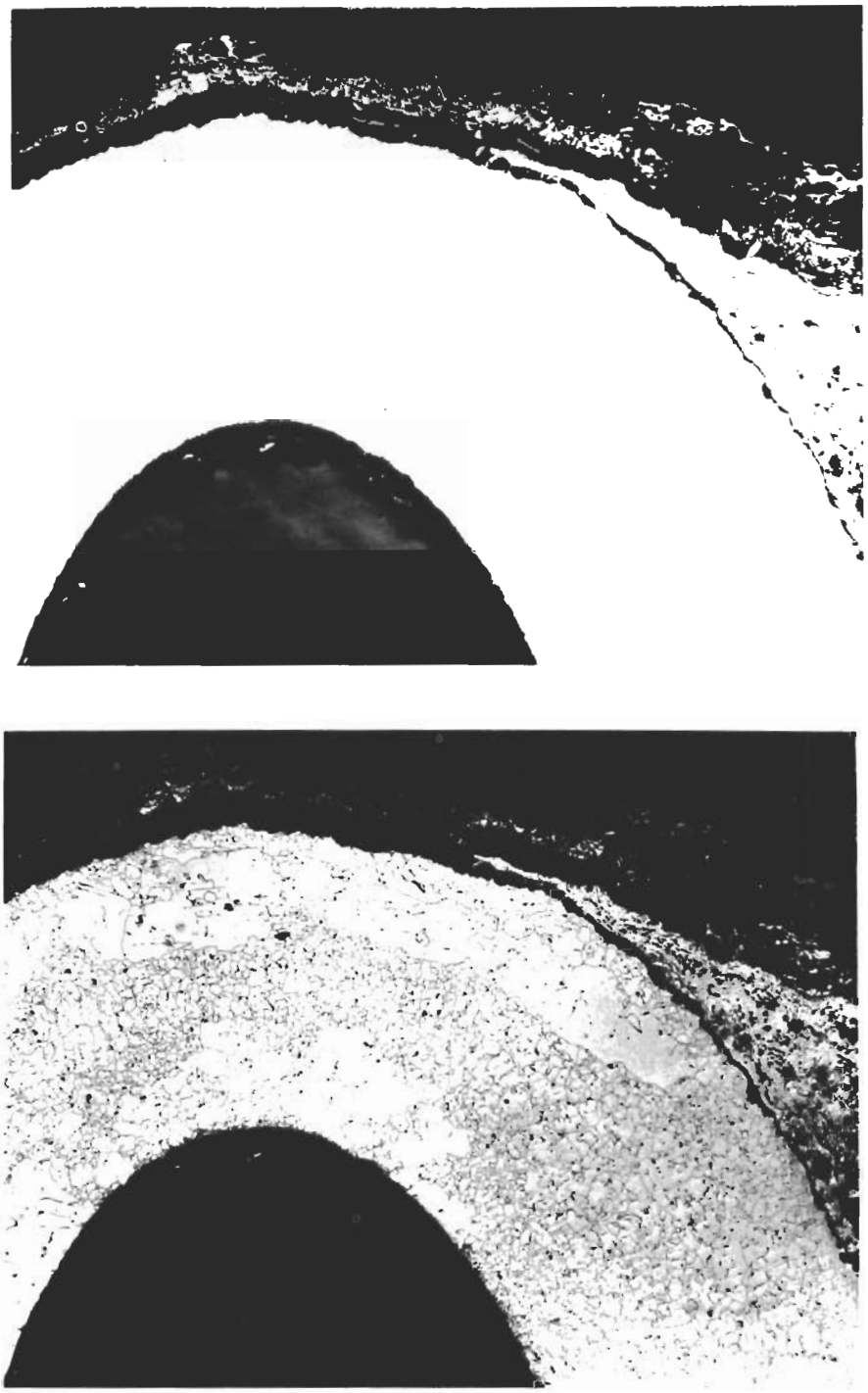

Etched 50x

Figure 97. Microstructural Condition of the Rokide Coating in an Area Where It Had Become White during Engine Operation.

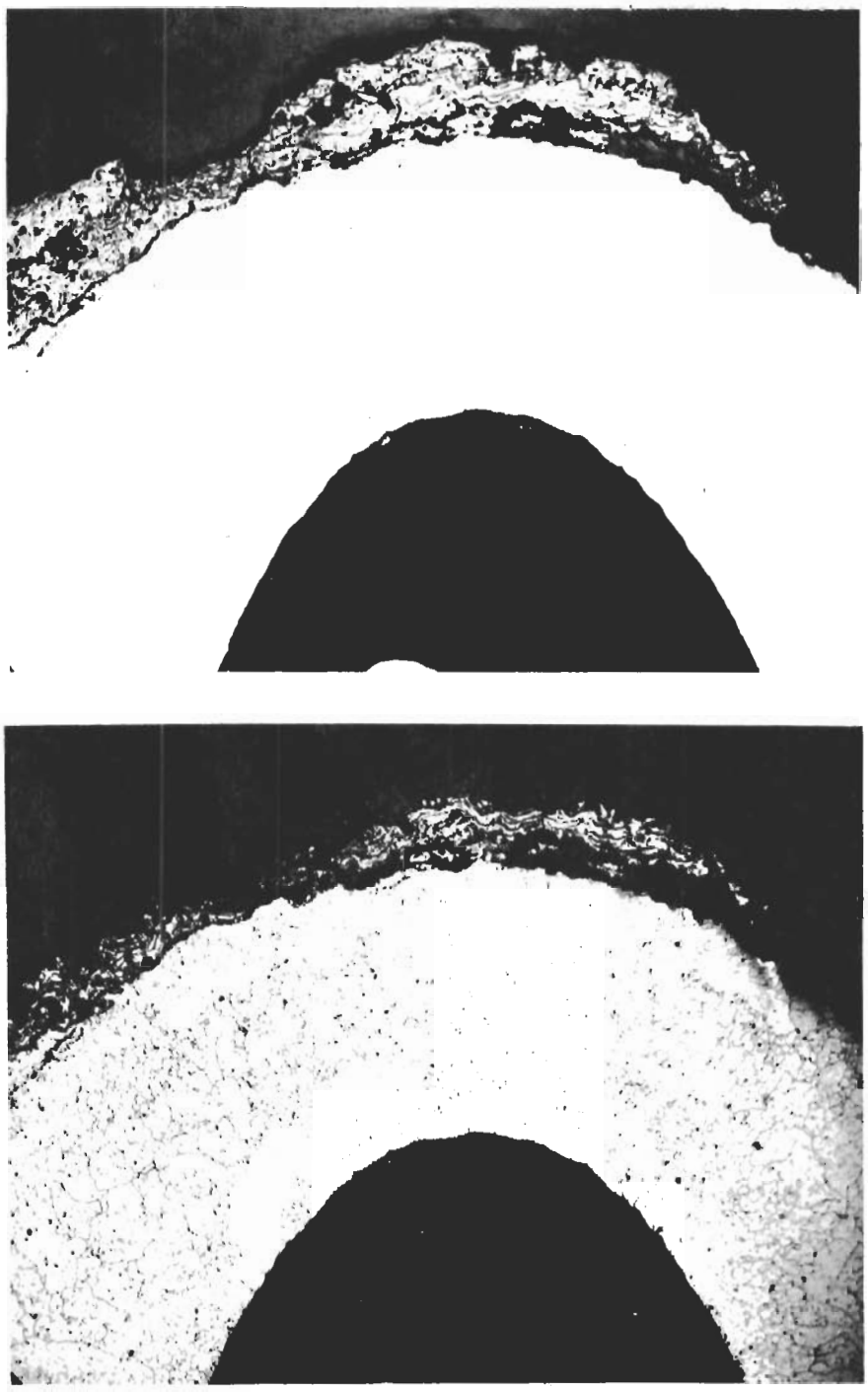

Etched 50x

Figure 98. Microstructure of a Stainless Steel Tube and Coating in a "White" Area Away from the Throat Section of the Nozzle.

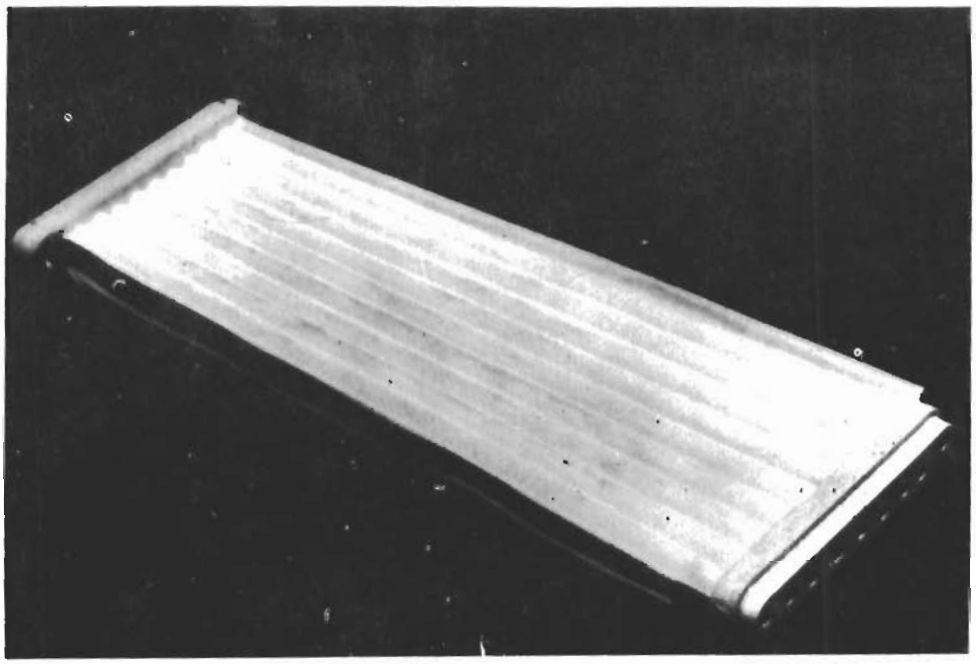

Figure 99. Typical Thermal Shock Test Panel.

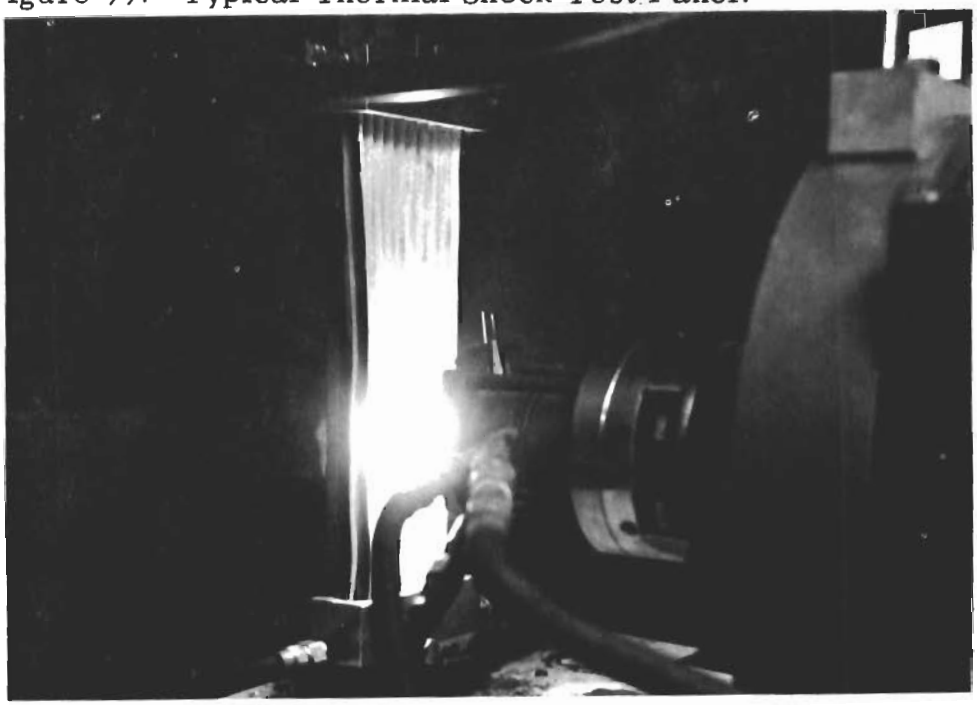

Figure 100. Plasma-Jet Test of Coated Panel.

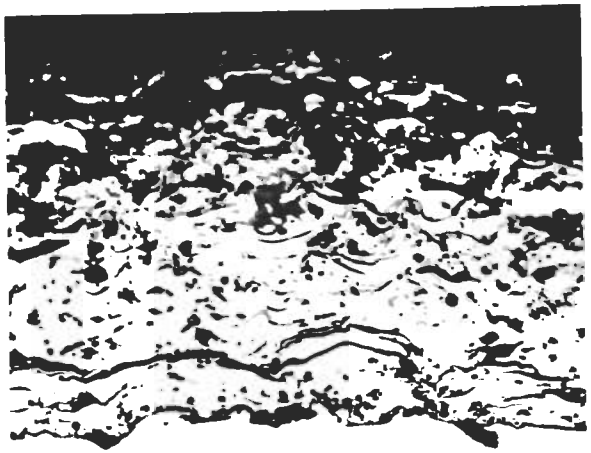

100x

Metal Graded ZrO_2

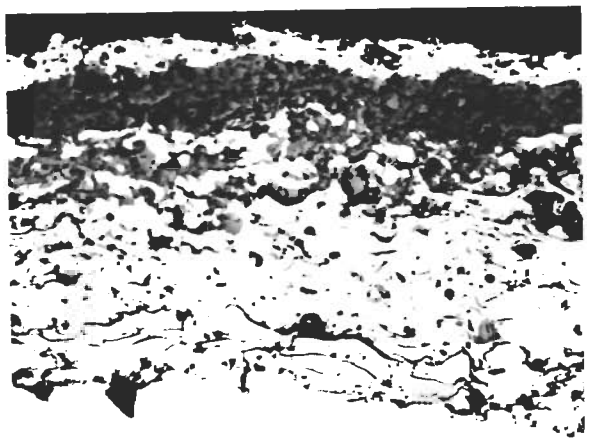

100x

Metal Graded ZrO_2 with a TiN Topcoat

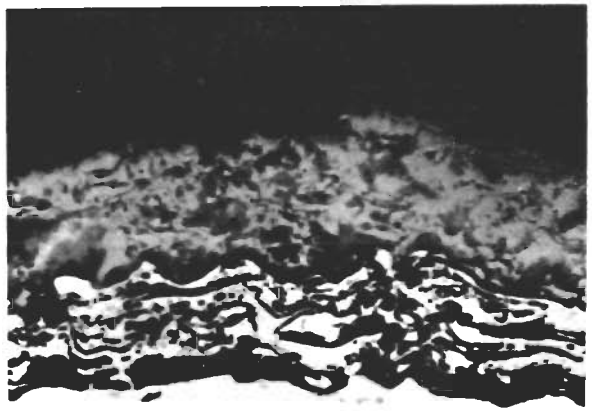

100x

Rokide Z with Nichrome Primer

Figure 101. Typical Sprayed Ceramic Coatings.

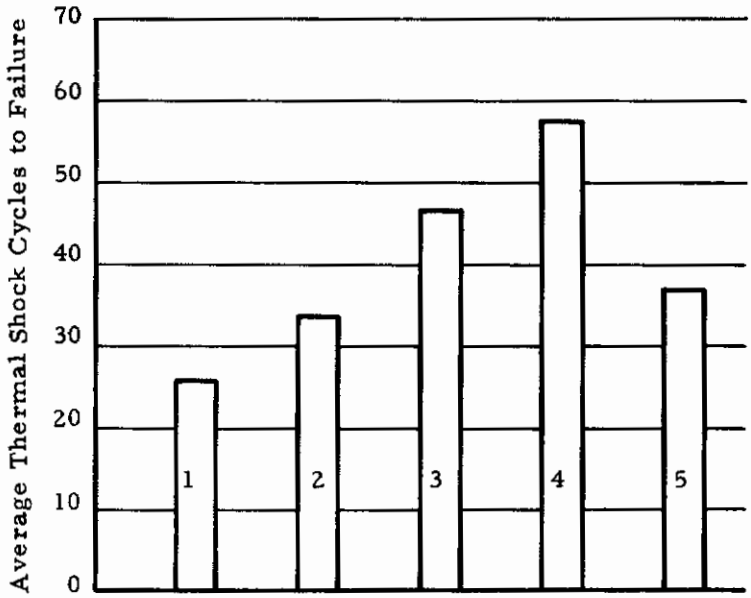

Coating Identification

1. Rokide Z (RMD)
2. Rokide Z with Nichrome Primer
3. Arc Sprayed ZrO_2 with Nichrome Primer
4. Rokide Z with Molybdenum Primer
5. Arc Sprayed ZrO_2 with Molybdenum Primer

Figure 102. A Comparison of the Thermal Shock Resistance of Several Monolithic ZrO_2 Coatings.

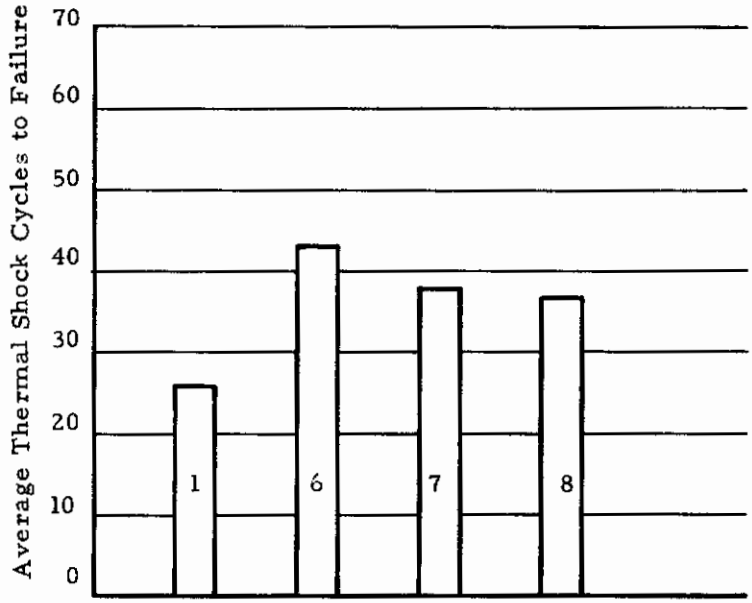

Coating Identification

1. Rokide Z (RMD)
6. Arc Sprayed ZrO_2 with Nichrome Primer and Two Graded Layers of Nichrome and ZrO_2
7. Arc Sprayed ZrO_2 with Nichrome Primer and Three Graded Layers of Nichrome and ZrO_2
8. Same as 7 but with Different Percentages of Metal and Ceramic in the Graded Layers.

Figure 103. A Comparison of the Thermal Shock Resistance of RMD Rokide Z and Nichrome Graded ZrO_2 with a Nichrome Primer.

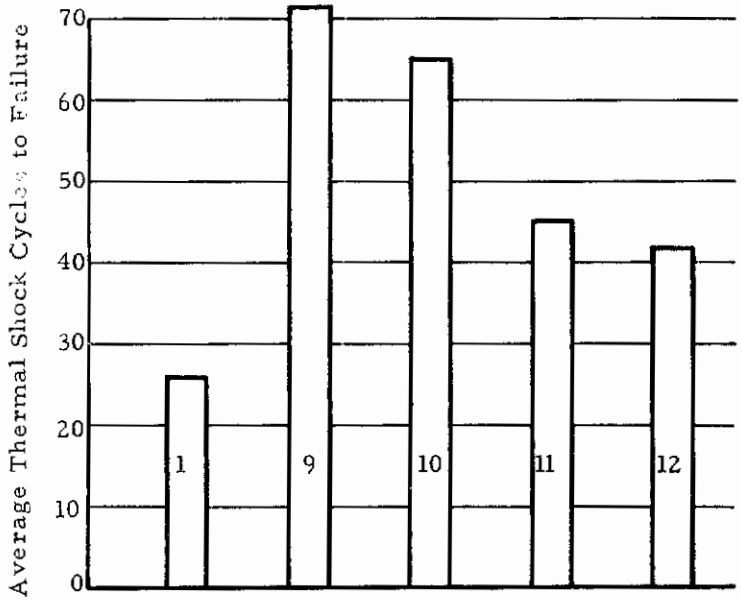

Coating Identification

1. Rokide Z (RMD)
9. Arc Sprayed ZrO_2 with Molybdenum Primer and Two Graded Layers of Nichrome and ZrO_2
10. Same as 9 but with Different Percentages of Metal and Ceramic in the Graded Layers
11. Arc Sprayed ZrO_2 with Molybdenum Primer and Two Graded Layers of Molybdenum and ZrO_2
12. Arc Sprayed ZrO_2 with Molybdenum Primer and Three Graded Layers of Molybdenum and ZrO_2

Figure 104. A Comparison of the Thermal Shock Resistance of RMD Rokide Z and Nichrome or Molybdenum Graded ZrO_2 with a Molybdenum Primer

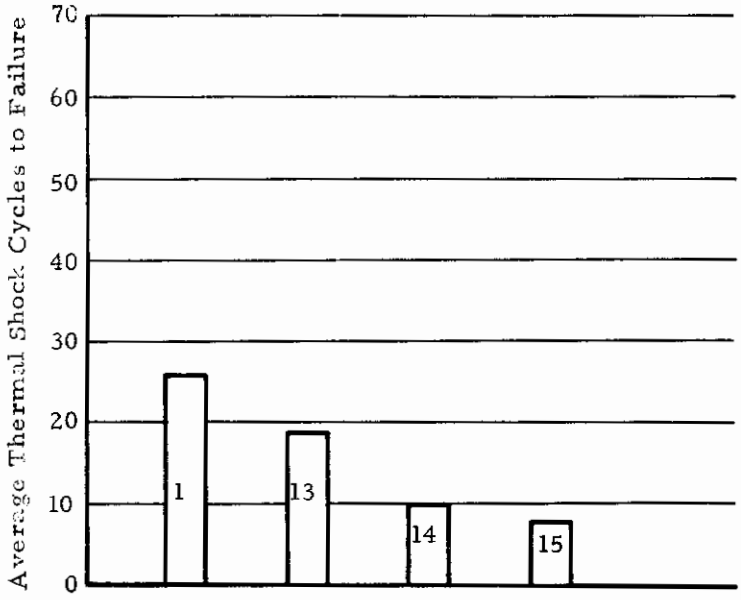

Coating Identification

1. Rokide Z (RMD)
13. Arc Sprayed ZrO_2 with Tungsten Primer and Three Graded Layers of Tungsten and ZrO_2
14. Same as 13 but with a 0.060 inch Tungsten Primer
15. Same as 13 but with a 0.030 inch Tungsten Primer

Figure 105. A Comparison of the Thermal Shock Resistance of RMD Rokide Z and Tungsten Graded ZrO_2 with a Tungsten Primer

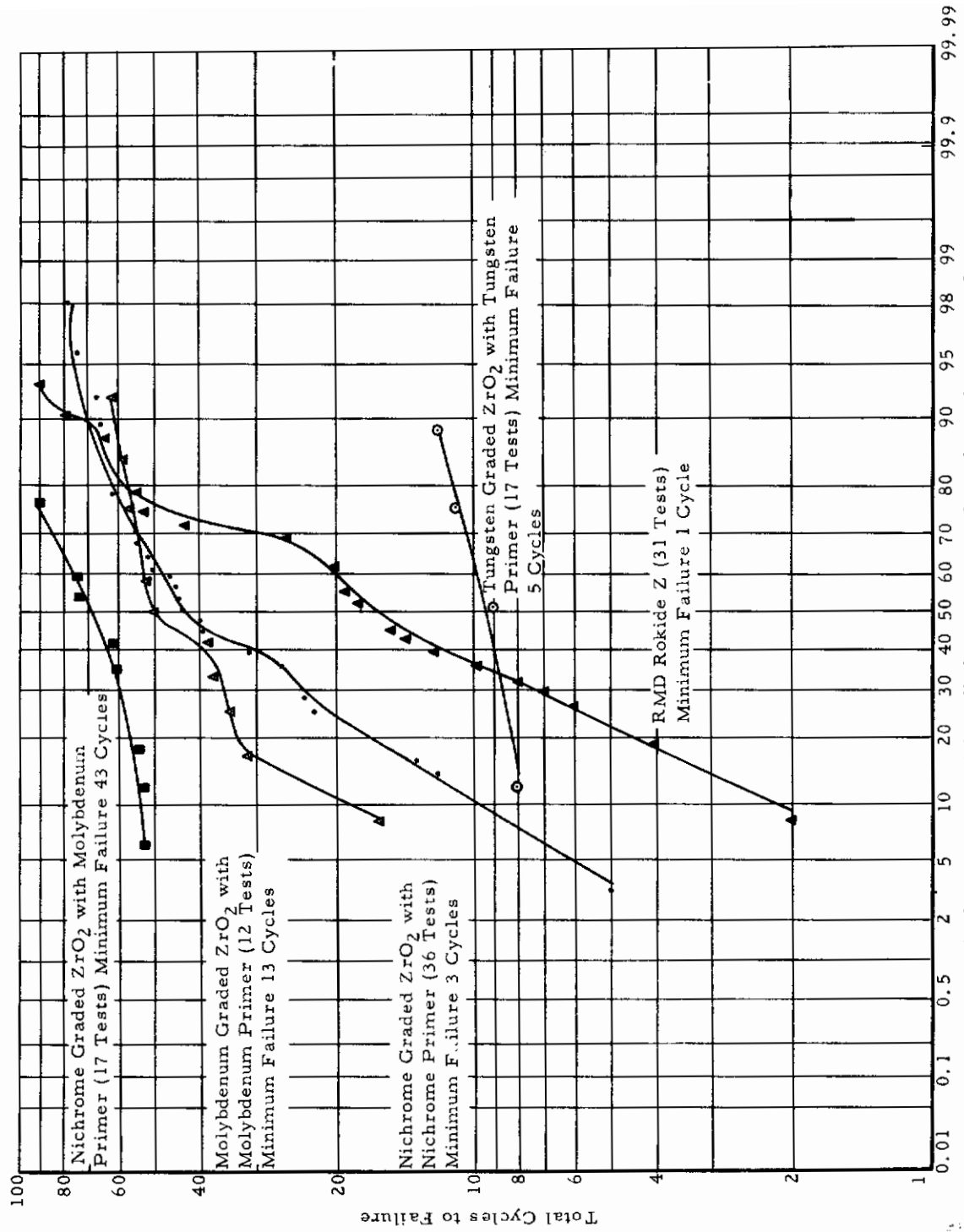

Figure 106. Probability Plot Comparing the Thermal Shock Resistance of Various Sprayed Coatings.

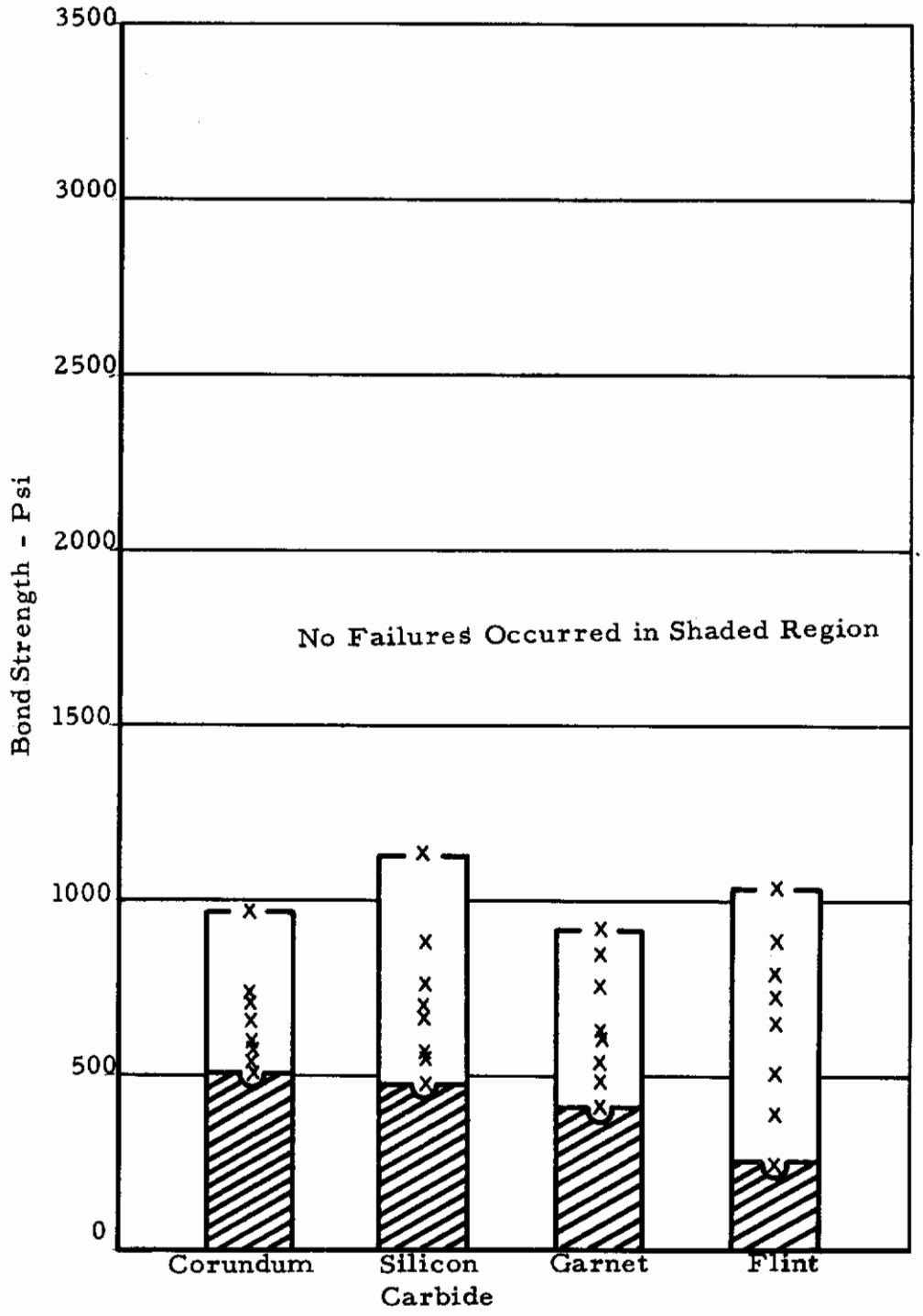

Figure 107. Bond Strength of 100% Alumina Coating on Inconel Substrate Grit Blasted with Various Media.

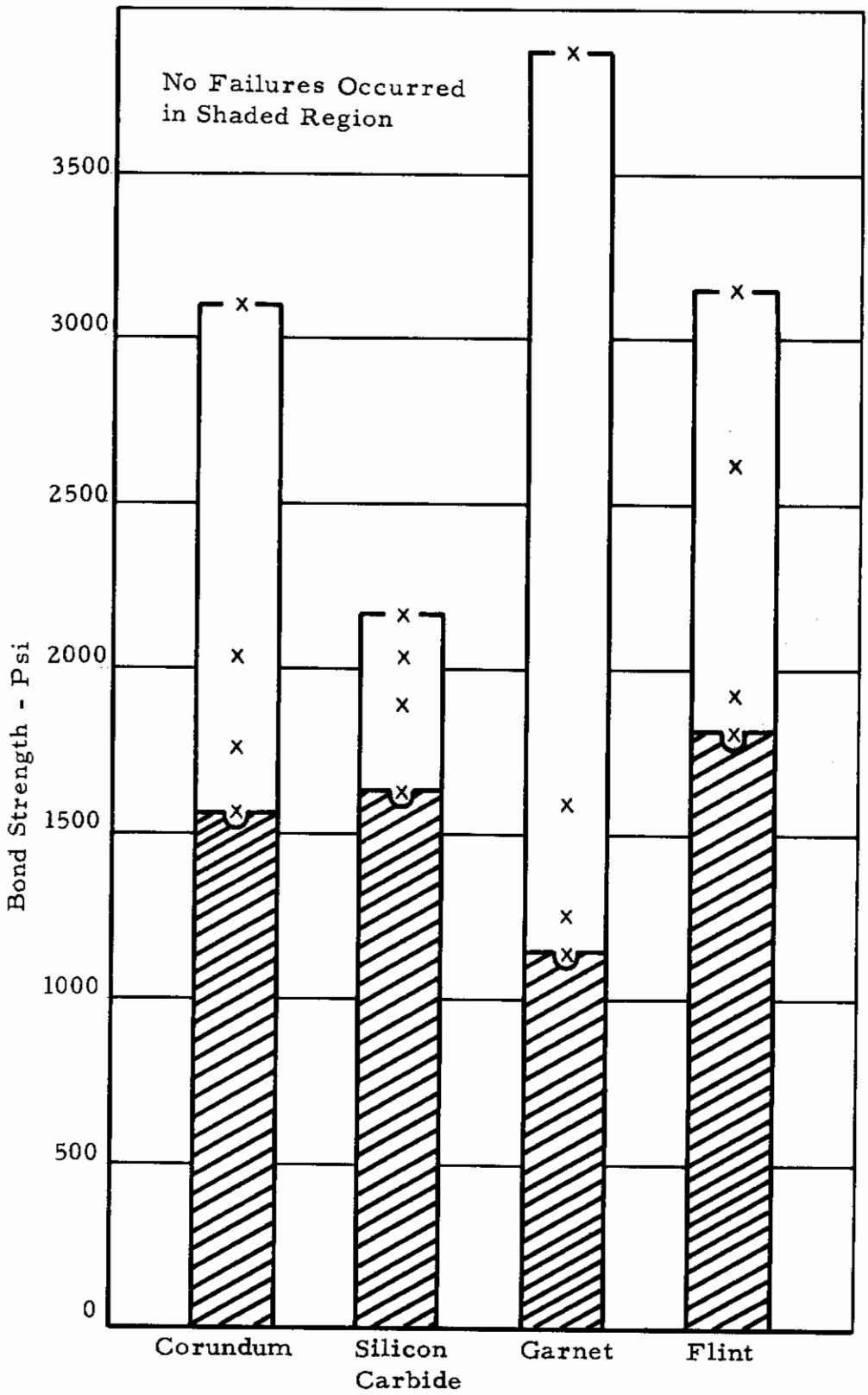

Figure 108. Bond Strength of 50% Alumina - 50 Nickel Coating on Inconel Substrate Grit Blasted with Various Media.

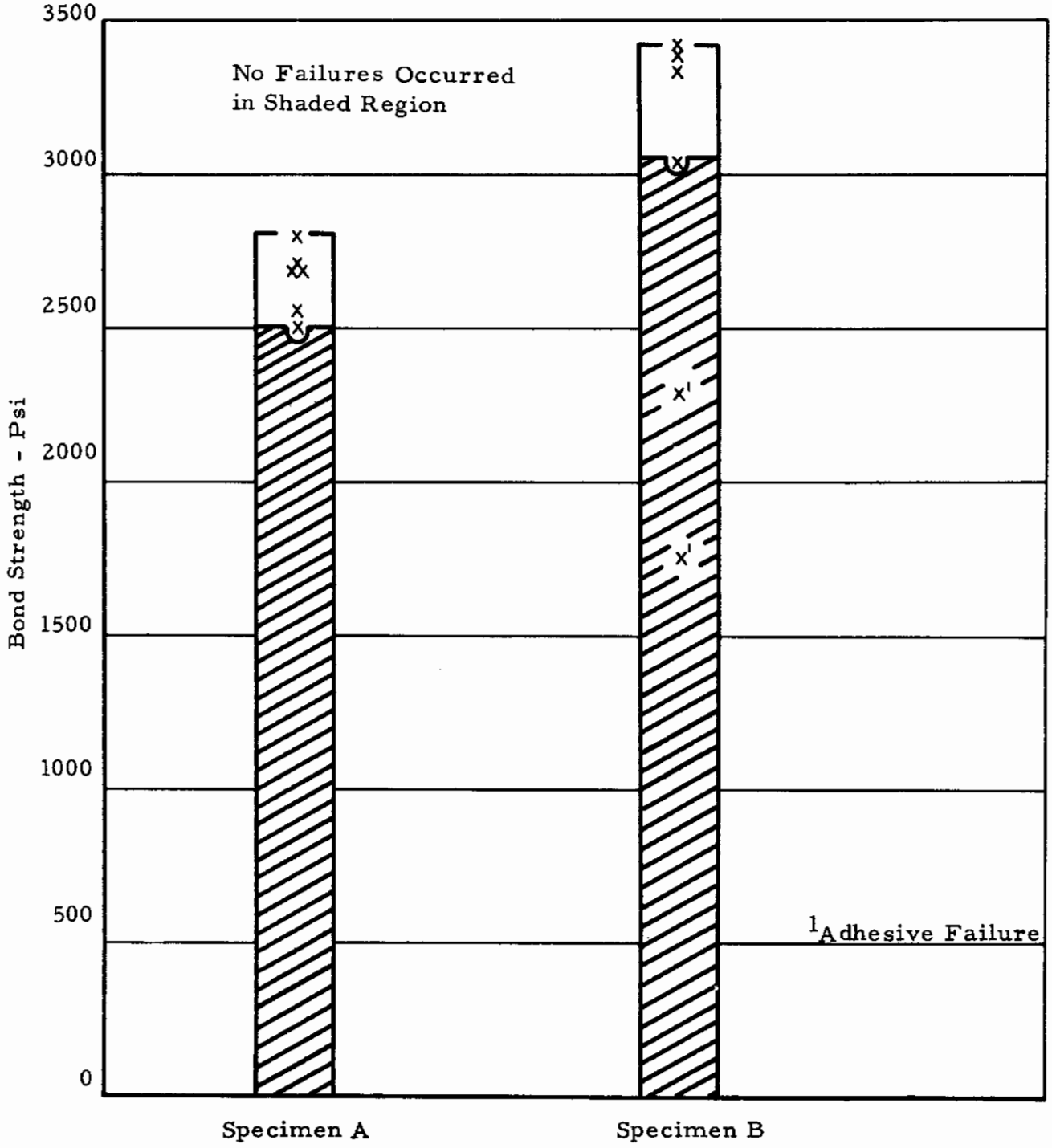

Figure 109. Bond Strength of Nichrome Graded ZrO_2 over Molybdenum Primed Stainless Steel for Two Methods of Sample Preparation.

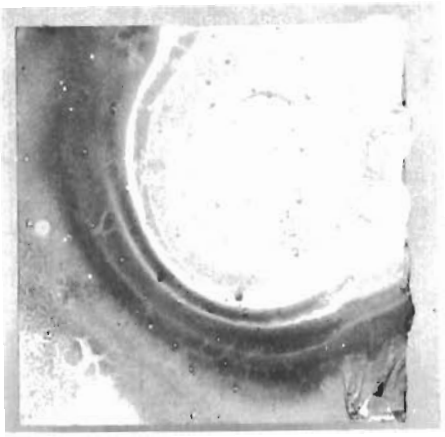

1 x

Tantalum

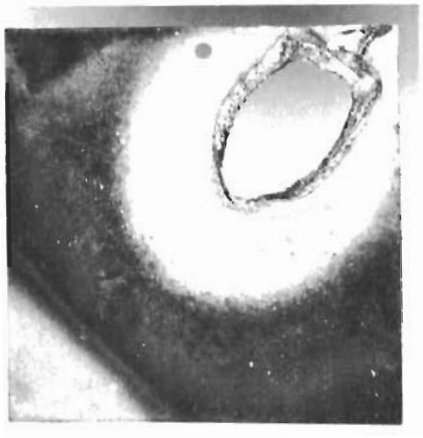

1 x

Columbium

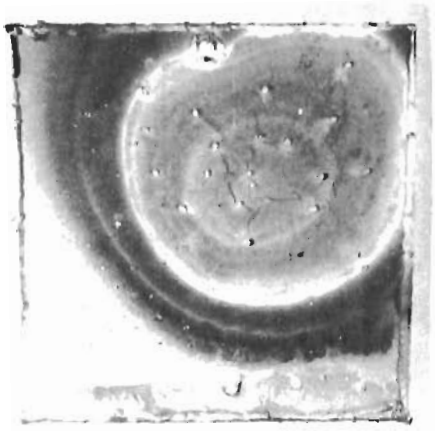

1 x

Molybdenum

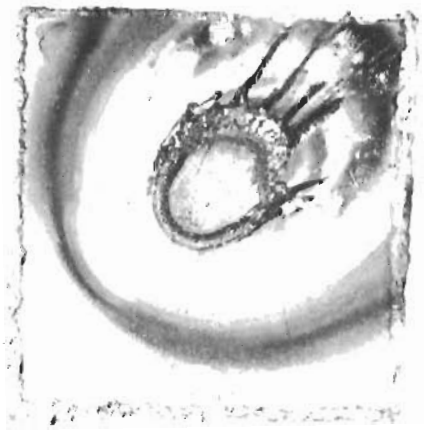

1 x

Tungsten

Figure 10. Photographs of Typical Manufacturer SY Specimens after Continuous Exposure Test in Arc-Plasma-Jet Effluent.

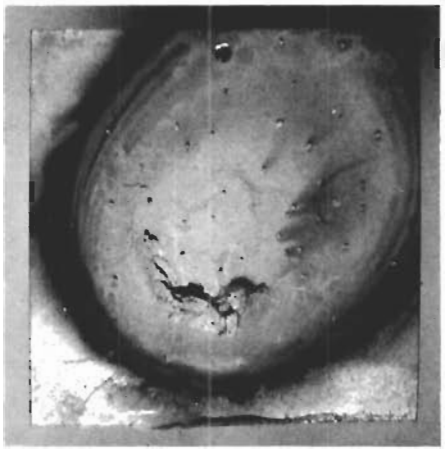

1 x

Tantalum

19 Thermal Cycles

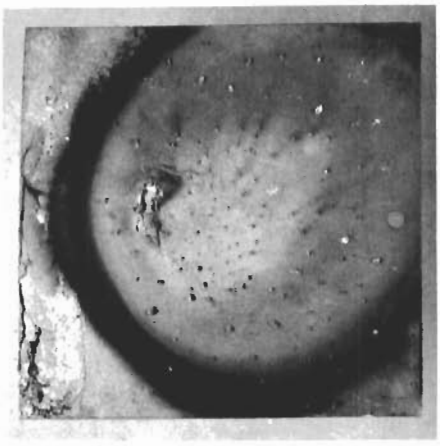

1 x

Tantalum

20 Thermal Cycles

1 x

Molybdenum

60 Thermal Cycles

Figure 111. Photographs of Typical Manufacturer SY Specimens after Thermal Cycling Test in an Arc-Plasma-Jet Effluent.

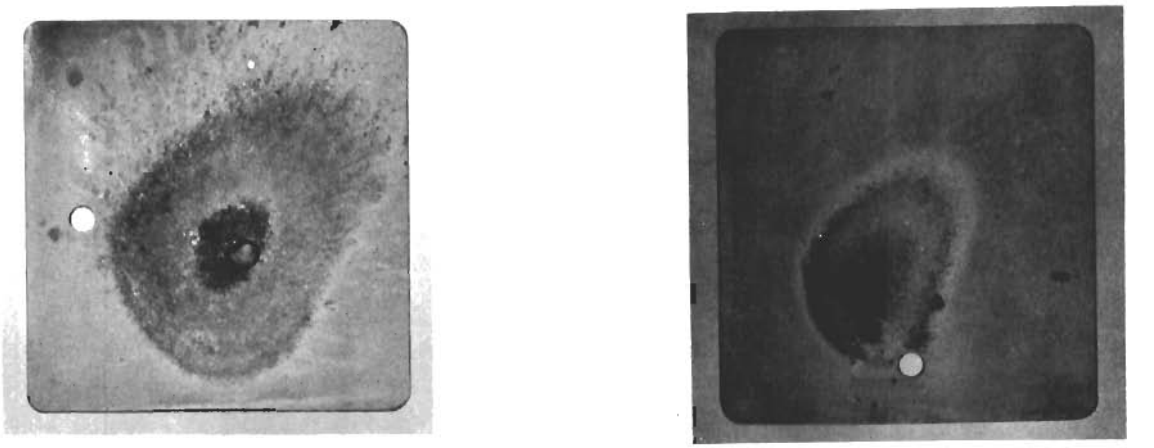

1x 1x

Boeing Fluidized Bed Silicide

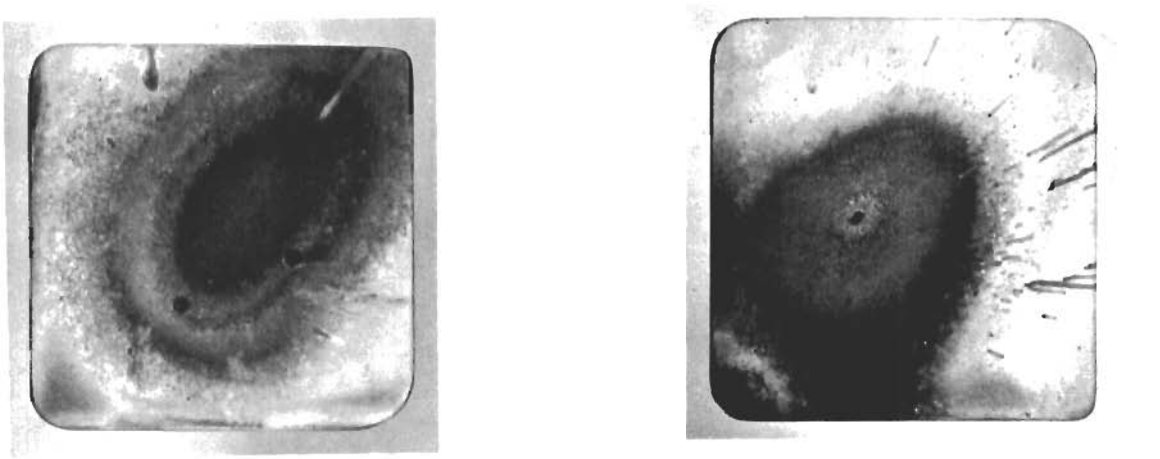

1x 1x

Boeing DiSil 1

Figure 112. Photographs of Coated Mo-1/2 Ti Samples after 3000°F Arc-Plasma-Jet Test.

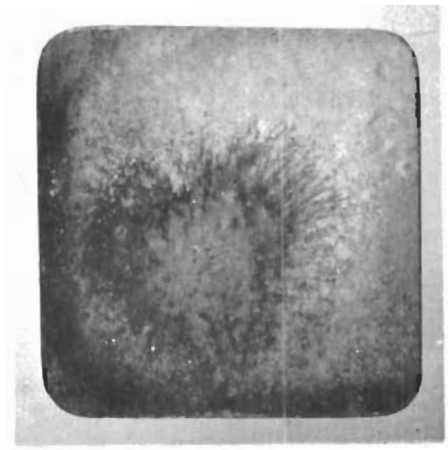

1x

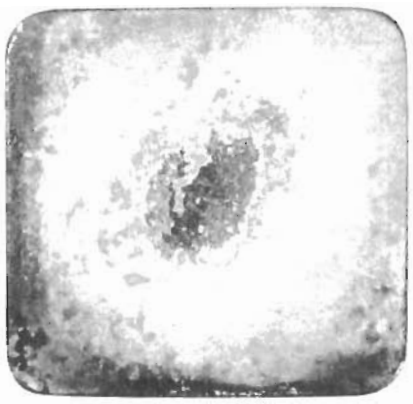

1x

Pfaudler PFR-6

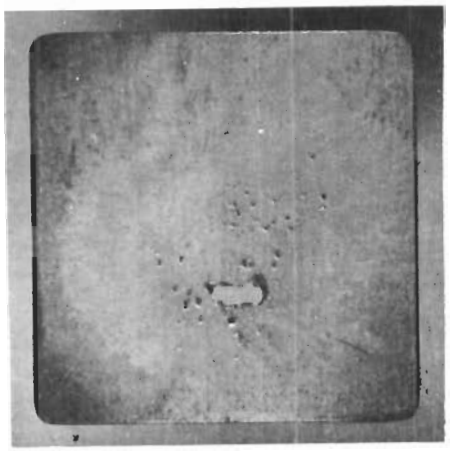

1x

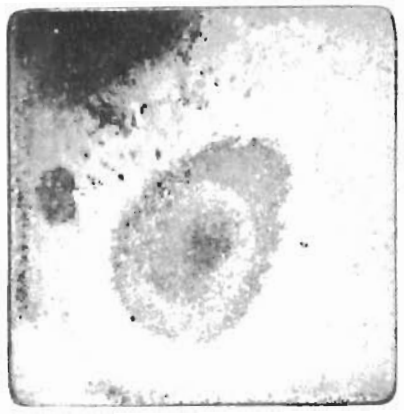

1x

Chromalloy W-2

Figure 113. Photographs of Coated Mo-1/2 Ti Samples after 3000°F Arc-Plasma-Jet Test.

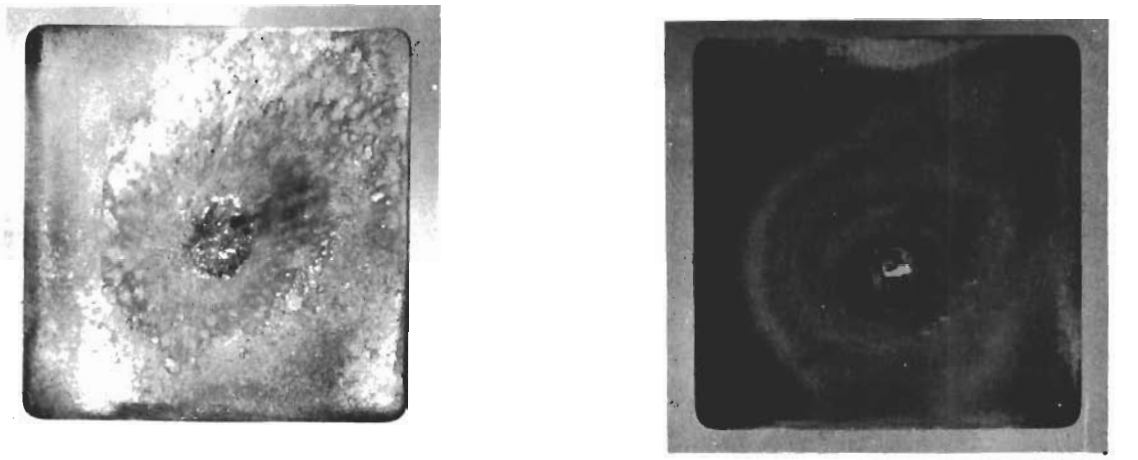

1x 1x

Change Vought-Vought II and IX

Figure 114. Photographs of Coated Mo-1/2 Ti Samples after 3000°F Arc-Plasma-Jet Test.

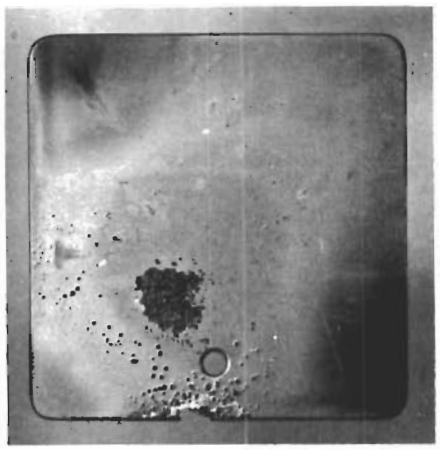

1x

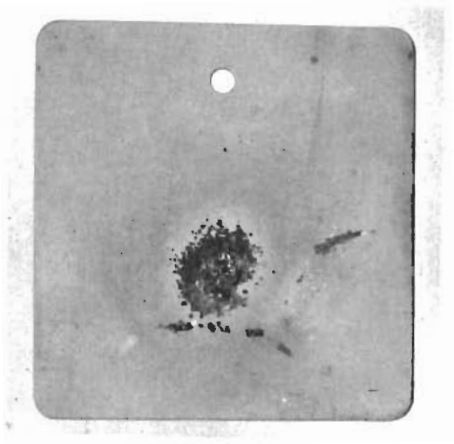

1x

Boeing Fluidized Bed Silicide

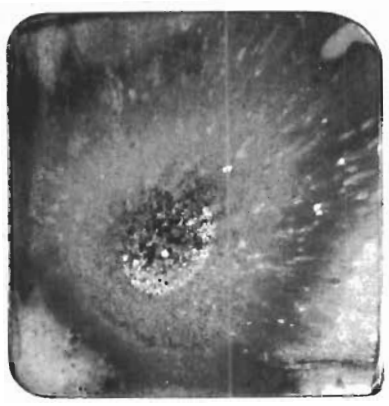

1x

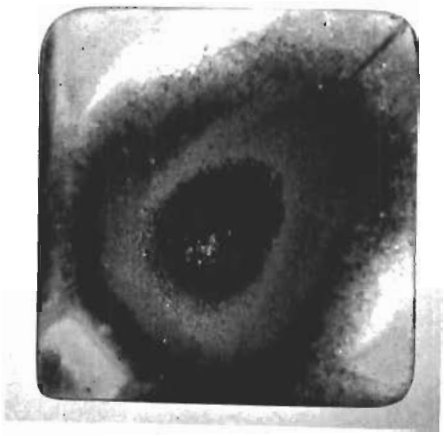

1x

Boeing DiSil 1

Figure 115. Photographs of Coated Mo-1/2 Ti Samples after Variable Temperature Arc-Plasma-Jet Test.

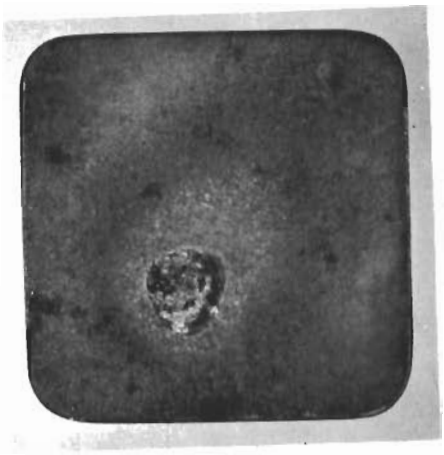

1x

1x

Pfaudler PFR-6

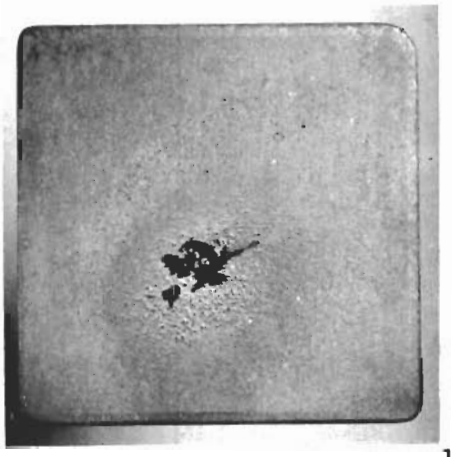

1x

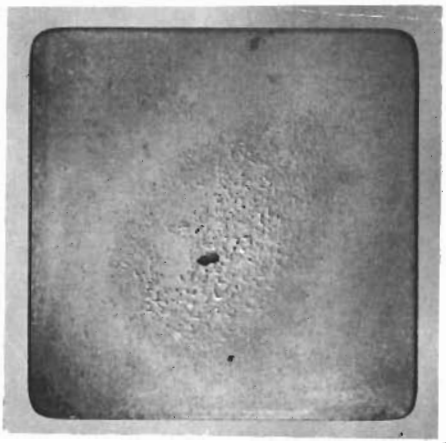

1x

Chromalloy W-2

Figure 116. Photographs of Coated Mo-1/2 Ti Samples after Variable Temperature Arc-Plasma-Jet Test.

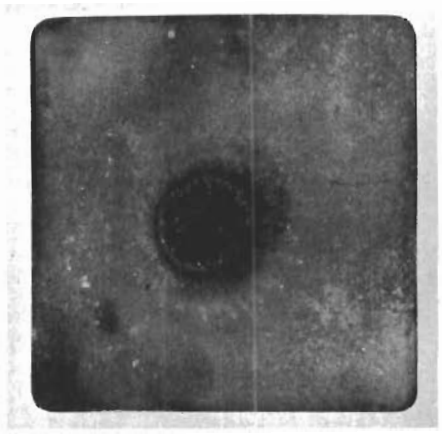

1x

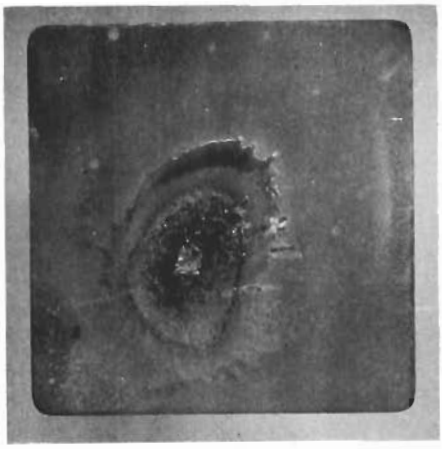

1x

Chance Vought - Vought II and IX

Figure 117. Photographs of Coated Mo-1/2 Ti Samples after Variable Temperature Arc-Plasma-Jet Test.

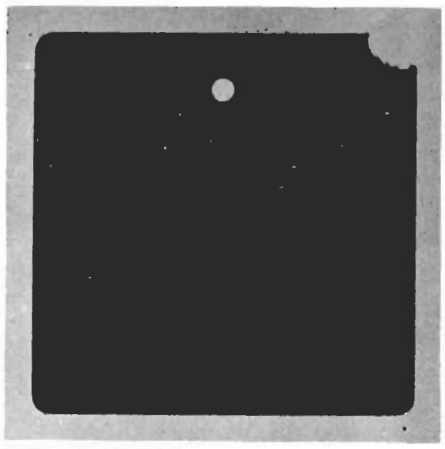

1x

Boeing Fluidized Bed Silicide

Figure 118. Photograph of a Coated Mo-1/2 Ti Sample after 50 Hour Still Air Test at 2000°F.

	Material		Cork Composition with Phenolic Resin Binder Bonded to Sheet Aluminum				
Test Conditions	Heat Flux (BTU/ft^2-sec)		10.8	10.8	10.8	10.8	
	Gas Enthalpy (BTU/lb)		990	1026	1150	1150	
	Test Duration (sec)		31	47	55	57	
	Stagnation Pressure (psig)		0.07	0.07	0.07	0.07	
	Gas Temperature ($^\circ$F)		3140	3230	3620	3620	
	Gas Velocity (ft/sec)		110	110	110	110	
Test Results	Decrease in Weight	Gms	2.0284	2.8101	6.5641	6.5333	
		%	18.1	24.8	37.4	36.5	
	Density (gm/cc)	Before	---	---	---	---	
		After	---	---	---	---	
	Depth of Erosion (in.)		---	---	---	---	
	Volume of Erosion (in^3)		---	---	---	---	
	Final Back Face Temp $^\circ$F		265	335	290	320	
	Final Front Face Temp $^\circ$F		<2000	<2000	<2000	<2000	
	Remarks		Specimen thickness 1/8 inch. Specimen to nozzle distance 5-7/8 inches.		Specimen thickness 1/4 inch. Specimen to nozzle distance 5-7/8 inches.		
	Sample Appearance		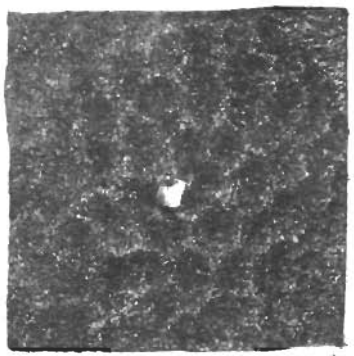		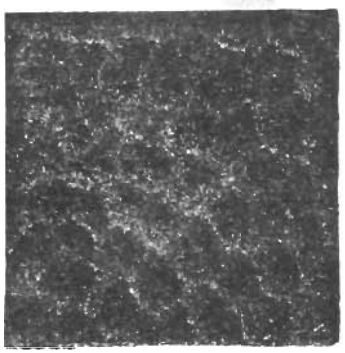		

Table 1

	Material		Foamed Plastic A	Foamed Plastic B	Foamed Plastic C
Test Conditions	Heat Flux (BTU/ft^2-sec)		100	100	100
	Gas Enthalpy (BTU/lb)		1560	1560	1730
	Test Duration (sec)		10	13	8
	Stagnation Pressure (psig)		0.375	0.375	0.397
	Gas Temperature ($^\circ$F)		4590	4590	4880
	Gas Velocity (ft/sec)		580	580	610
Test Results	Decrease in Weight	Gms	2.1243	2.6444	2.6896
		%	29.7	35.5	35.5
	Density (gm/cc)	Before	0.206	0.196	0.231
		After	0.209	0.204	0.223
	Depth of Erosion (in.)		0.338	0.457	See Remarks
	Volume of Erosion (in^3)		0.649	0.887	0.662
	Final Back Face Temp $^\circ$F		No Data	130	1790
	Final Front Face Temp $^\circ$F		2690	2690	2980
	Remarks				Extensive specimen degradation and complete burn-through in several areas.
	Sample Appearance		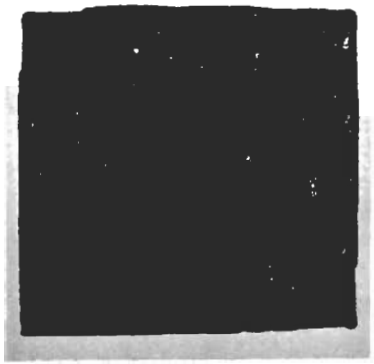	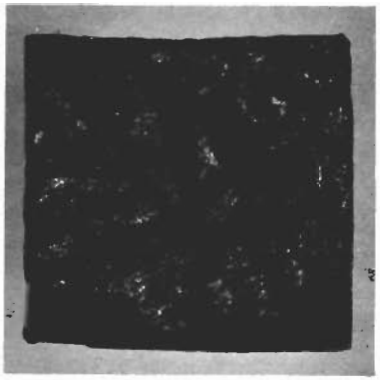	

Table 2

T36

	Material		ZrB_2:$MoSi_2$ + 5% BN	ZrB_2.$MoSi_2$	ZrB_2.$MoSi_2$
Test Conditions	Heat Flux (BTU/ft^2-sec)		493	500	470
	Gas Enthalpy (BTU/lb)		3790	3890	3790
	Test Duration (sec)		24	24	24
	Stagnation Pressure (psig)		0.765	0.794	0.765
	Gas Temperature (^oF)		7460	7625	7460
	Gas Velocity (ft/sec)		1180	1220	1180
Test Results	Decrease in Weight	Gms	(increase) -0.029	1.9256	(increase) -0.027
		%	-0.023	1.01	-0.027
	Density (gm/cc)	Before	5.530	5.6093	5.519
		After	5.527	---	5.518
	Depth of Erosion (in.)		0.009	---	0.003
	Volume of Erosion (in^3)		nil	---	nil
	Final Back Face Temp ^oF		1900	2660	2060
	Final Front Face Temp ^oF		3110	4550	3130
	Remarks		Sample thickness 0.343 inches. Surface cracks appeared after 2-3 seconds heating. (Sample 1)	Sample thickness 0.5 inches. Specimen failed in thermal shock after 2-3 seconds heating. (Sample 2)	Sample thickness 0.293 inches. Surface cracks appeared after 2-3 seconds heating. (Sample 3)
	Sample Appearance		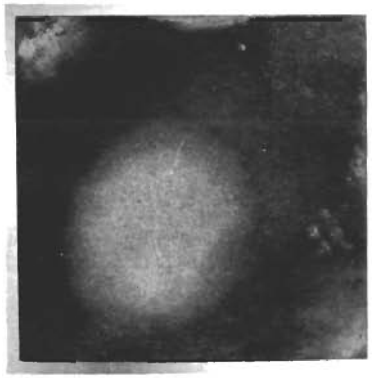	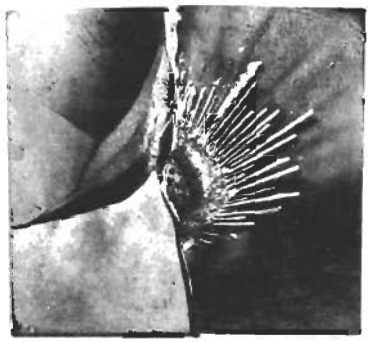	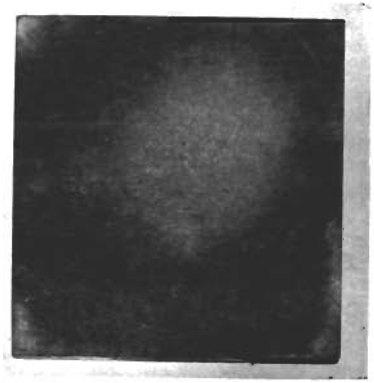

Table 3

137

			Material	$ZrB_2 . MoSi_2$ + 5% BN	$ZrB_2 . MoSi_2$	$ZrB_2 . MoSi_2$
Test Conditions	Heat Flux (BTU/ft^2-sec)			102	108	102
	Gas Enthalpy (BTU/lb)			1230	1260	1220
	Test Duration (sec)			300	300	300
	Stagnation Pressure (psig)			0.354	0.310	0.354
	Gas Temperature (^oF)			3860	3930	3820
	Gas Velocity (ft/sec)			540	480	540
Test Results	Decrease in Weight	Gms		(increase) -0.001	(increase) -0.010	(increase) -0.029
		%		(increase) -0.008	(increase) -0.006	(increase) -0.027
	Density (gm/cc)	Before		5.516	5.618	5.482
		After		5.515	---	5.485
	Depth of Erosion (in.)			0.004	---	(increase) -0.002
	Volume of Erosion (in^3)			nil	---	nil
	Final Back Face Temp ^oF			1220	1190	1220
	Final Front Face Temp ^oF			---	2010	---
	Remarks			Sample thickness 0.321 inches. Crack running completely through sample appeared after 15 seconds of test. (Sample 4)	Sample thickness 0.5 inches. Crack running completely through sample appeared after 240 seconds of test. (Sample 5)	Sample thickness 0.313 inches. Surface cracks appeared after 48 seconds of test. (Sample 6)
	Sample Appearance			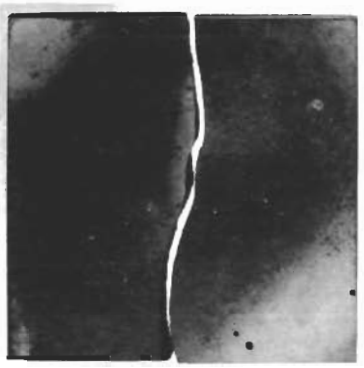		

TABLE 4

			Material	KT Silicon Carbide	GRB Silicon Carbide	Sintered ZrB_2. $MoSi_2$
Test Conditions	Heat Flux (BTU/ft^2-sec)			493	493	500
	Gas Enthalpy (BTU/lb)			3810	3790	3610
	Test Duration (sec)			24	24	24
	Stagnation Pressure (psig)			0.812	0.827	0.801
	Gas Temperature ($^\circ$F)			7460	7420	7120
	Gas Velocity (ft/sec)			1250	1270	1230
Test Results	Decrease in Weight	Gms		0.0105	0.082	(increase) -0.0516
		%		0.011	0.11	-0.043
	Density (gm/cc)	Before		3.081	2.766	5.0132
		After		3.087	2.772	5.0188
	Depth of Erosion (in.)			nil	nil	0.002
	Volume of Erosion (in^3)			nil	nil	nil
	Final Back Face Temp $^\circ$F			935	190	1140
	Final Front Face Temp $^\circ$F			2590	2490	2370
	Remarks			Sample thickness 0.537 inches. Sample cracked upon cooling at termination of test.	Sample thickness 0.417 inches. Sample cracked upon cooling at termination of test.	Sample thickness 0.374 inches. Sample cracked upon cooling at termination of test.
	Sample Appearance				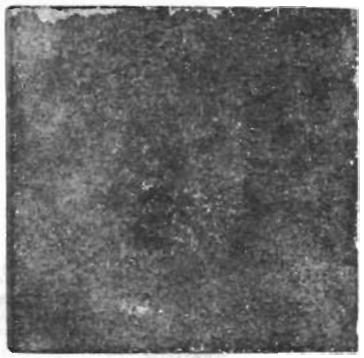	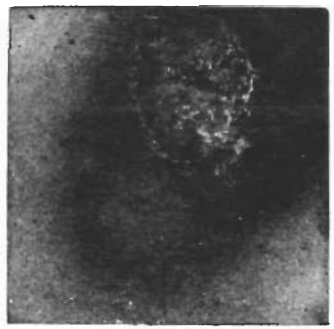

Table 5

139

			KT Silicon Carbide	GRB Silicon Carbide	Sintered ZrB_2. $MoSi_2$
Test Conditions	Heat Flux (BTU/ft^2-sec)		100	100	100
	Gas Enthalpy (BTU/lb)		1160	1190	1170
	Test Duration (sec)		300	300	300
	Stagnation Pressure (psig)		0.343	0.343	0.321
	Gas Temperature ($^\circ$F)		3660	3780	3680
	Gas Velocity (ft/sec)		530	530	495
Test Results	Decrease in Weight	Gms	0.0167	0.218	(increase) -0.0676
		%	0.021	0.29	-0.063
	Density (gm/cc)	Before	3.067	2.740	4.9079
		After	3.088	2.748	4.9060
	Depth of Erosion (in.)		nil	nil	0.003
	Volume of Erosion (in^3)		nil	nil	nil
	Final Back Face Temp $^\circ$F		1210	1020	1220
	Final Front Face Temp $^\circ$F		1980	1920	1890
	Remarks		Sample thickness 0.413 inches.	Sample thickness 0.420 inches.	Sample thickness 0.371 inches.
	Sample Appearance		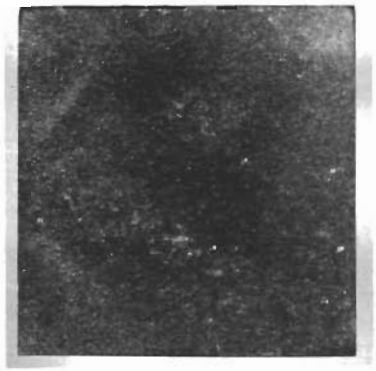	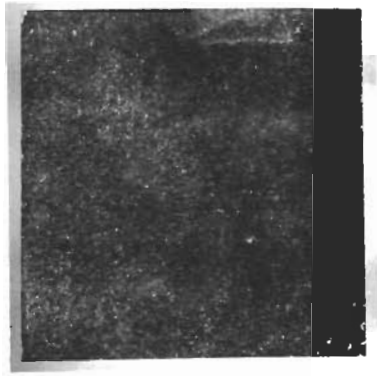	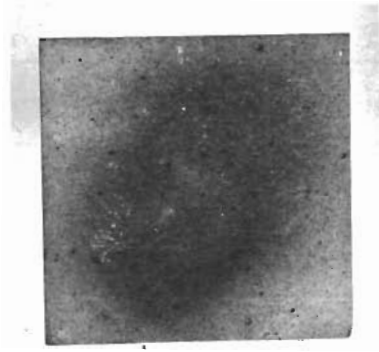

Table 6

	Material		Filled Silicone Rubber	Filled Silicone Rubber	
Test Conditions	Heat Flux (BTU/ft^2-sec)		300	300	
	Gas Enthalpy (BTU/lb)		2090	2030	
	Test Duration (sec)		40	40	
	Stagnation Pressure (psig)		0.516	0.516	
	Gas Temperature ($^\circ$F)		5380	5300	
	Gas Velocity (ft/sec)		794	794	
Test Results	Decrease in Weight	Gms	11.1782	8.0331	
		%	24.0	16.8	
	Density (gm/cc)	Before	1.480	1.482	
		After	1.457	1.457	
	Depth of Erosion (in.)		0.238	0.208	
	Volume of Erosion (in^3)		0.438	0.303	
	Final Back Face Temp $^\circ$F		150	109	
	Final Front Face Temp $^\circ$F		3450	3490	
	Remarks				
	Sample Appearance		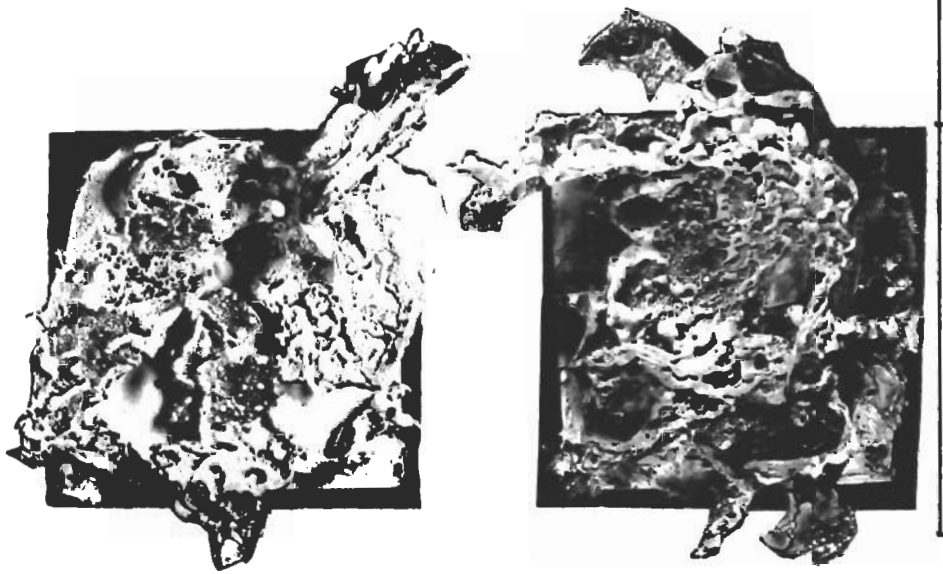		

Material			Filled Silicone Rubber	Filled Silicone Rubber	
Test Conditions	Heat Flux (BTU/ft^2-sec)		500	500	
	Gas Enthalpy (BTU/lb)		3510	3400	
	Test Duration (sec)		24	24	
	Stagnation Pressure (psig)		0.733	0.704	
	Gas Temperature ($^\circ$F)		7020	6840	
	Gas Velocity (ft/sec)		1130	1080	
Test Results	Decrease in Weight	Gms	15.8403	16.8594	
		%	31.5	33.1	
	Density (gm/cc)	Before	1.482	1.483	
		After	1.465	1.465	
	Depth of Erosion (in.)		0.360	0.349	
	Volume of Erosion (in^3)		0.635	0.676	
	Final Back Face Temp $^\circ$F		205	208	
	Final Front Face Temp $^\circ$F		3650	3690	
	Remarks				
	Sample Appearance		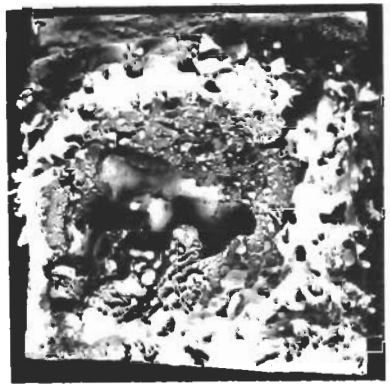	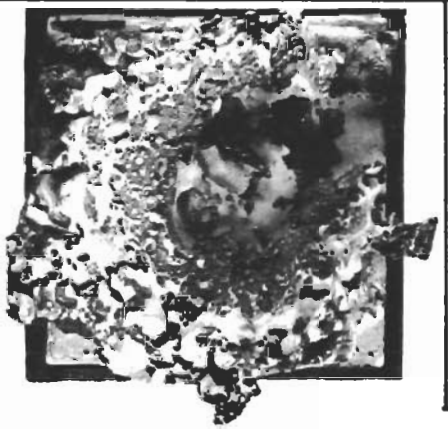	

Table 8

Material			015-V1 Molding Compound		
Test Conditions	Heat Flux (BTU/ft^2-sec)		100	300	500
	Gas Enthalpy (BTU/lb)		1550	2810	4110
	Test Duration (sec)		120	40	24
	Stagnation Pressure (psig)		0.354	0.560	0.747
	Gas Temperature ($^\circ$F)		4580	6150	8000
	Gas Velocity (ft/sec)		545	863	1150
Test Results	Decrease in Weight	Gms	17.6578	11.2827	9.58
		%	41.7	25.8	22.4
	Density (gm/cc)	Before	1.2298	1.2704	1.2517
		After	1.1223	1.2352	1.2196
	Depth of Erosion (in.)		0.426	0.269	0.209
	Volume of Erosion (in^3)		0.759	0.498	0.424
	Final Back Face Temp $^\circ$F		168	96	95
	Final Front Face Temp $^\circ$F		2590	2870	3220
	Remarks				
	Sample Appearance		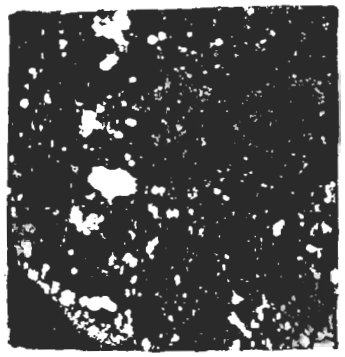	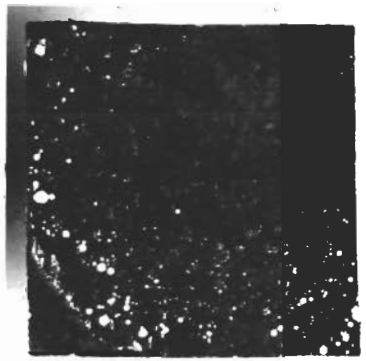	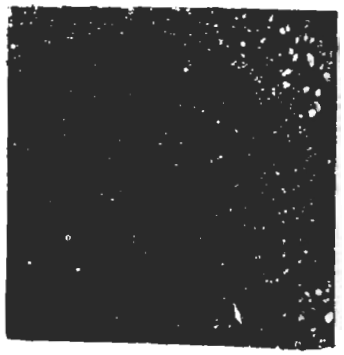

Table 9

Material			015-V1 Molding Compound		
Test Conditions	Heat Flux (BTU/ft^2-sec)		100	300	500
	Gas Enthalpy (BTU/lb)		1180	2370	3900
	Test Duration (sec)		120	40	24
	Stagnation Pressure (psig)		0.307	0.534	0.809
	Gas Temperature ($^\circ$F)		3680	5670	7640
	Gas Velocity (ft/sec)		472	823	1245
Test Results	Decrease in Weight	Gms	9.2943	7.4187	8.6804
		%	20.9	17.3	19.8
	Density (gm/cc)	Before	1.2772	1.2412	1.2551
		After	1.1675	1.1681	1.1976
	Depth of Erosion (in.)		0.178	0.146	0.213
	Volume of Erosion (in^3)		0.286	0.255	0.339
	Final Back Face Temp $^\circ$F		114	106	103
	Final Front Face Temp $^\circ$F		2400	3200	3990
	Remarks		Effluent Composition-100% Nitrogen	Effluent Composition-100% Nitrogen	Effluent Composition-100% Nitrogen
	Sample Appearance		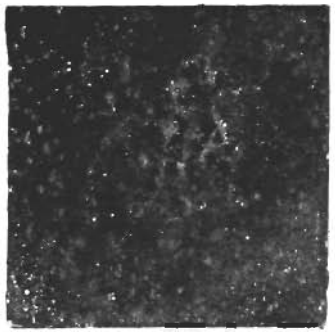	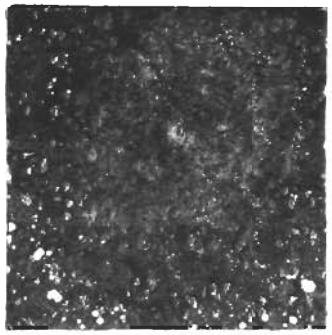	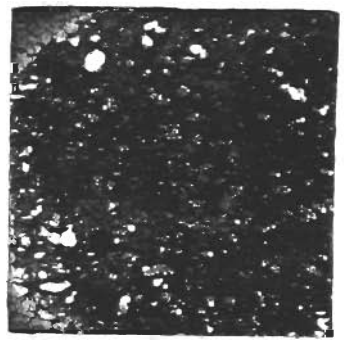

Material			015 Molding Compound		
Test Conditions	Heat Flux (BTU/ft^2-sec)		100	300	500
	Gas Enthalpy (BTU/lb)		1550	2810	4110
	Test Duration (sec)		120	40	24
	Stagnation Pressure (psig)		0.354	0.560	0.747
	Gas Temperature ($^\circ$F)		4580	6150	8000
	Gas Velocity (ft/sec)		545	863	1150
Test Results	Decrease in Weight	Gms	17.5141	13.8104	8.7645
		%	41.0	35.3	21.8
	Density (gm/cc)	Before	1.1869	1.1731	1.2049
		After	1.1334	1.1160	1.1731
	Depth of Erosion (in.)		0.413	0.343	0.197
	Volume of Erosion (in^3)		0.839	0.651	0.401
	Final Back Face Temp $^\circ$F		166	108	99
	Final Front Face Temp $^\circ$F		2190	2500	3270
	Remarks				
	Sample Appearance		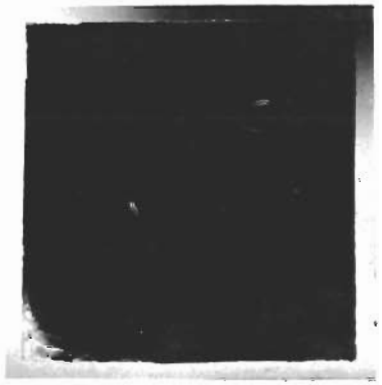	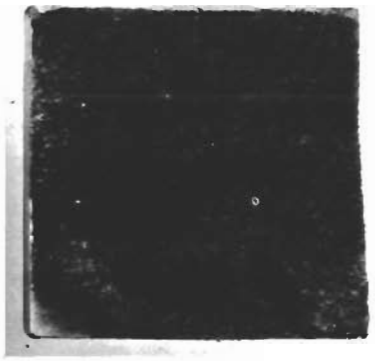	

Table II

145

Material			015 Molding Compound		
Test Conditions	Heat Flux (BTU/ft^2-sec)		100	300	500
	Gas Enthalpy (BTU/lb)		1170	2380	3760
	Test Duration (sec)		120	40	24
	Stagnation Pressure (psig)		0.307	0.534	0.805
	Gas Temperature ($^\circ$F)		3660	5690	7390
	Gas Velocity (ft/sec)		472	823	1240
Test Results	Decrease in Weight	Gms	13.1533	6.3657	8.7282
		%	36.7	16.2	21.5
	Density (gm/cc)	Before	1.1304	1.1796	1.1475
		After	1.0940	1.1133	1.0955
	Depth of Erosion (in.)		0.293	0.132	0.222
	Volume of Erosion (in^3)		0.669	0.227	0.383
	Final Back Face Temp $^\circ$F		123	117	114
	Final Front Face Temp $^\circ$F		2050	3120	3690
	Remarks		Effluent Composition-100% Nitrogen	Effluent Composition-100% Nitrogen	Effluent Composition-100% Nitrogen
	Sample Appearance		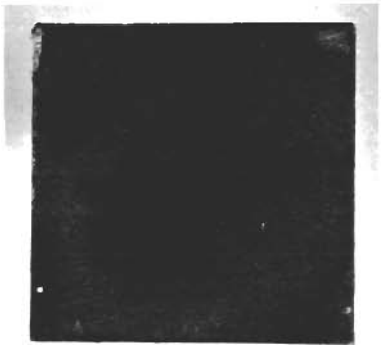		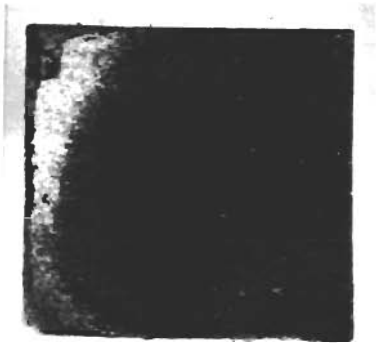

Table 12

Material			010-V6 Molding Compound		
Test Conditions	Heat Flux (BTU/ft^2-sec)		100	300	500
	Gas Enthalpy (BTU/lb)		1560	2770	3500
	Test Duration (sec)		83	40	24
	Stagnation Pressure (psig)		0.354	0.560	0.747
	Gas Temperature ($^\circ$F)		4580	6120	6980
	Gas Velocity (ft/sec)		545	863	1150
Test Results	Decrease in Weight	Gms	---	22.2651	19.0932
		%	---	46.1	39.1
	Density (gm/cc)	Before	1.3886	1.3940	1.3952
		After	---	1.2921	1.3177
	Depth of Erosion (in.)		---	0.411	0.322
	Volume of Erosion (in^3)		---	0.885	0.759
	Final Back Face Temp $^\circ$F		105	95	99
	Final Front Face Temp $^\circ$F		2200	2450	2470
	Remarks		Complete penetration of sample occurred during test.		
	Sample Appearance		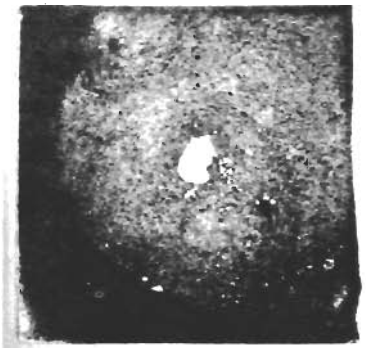	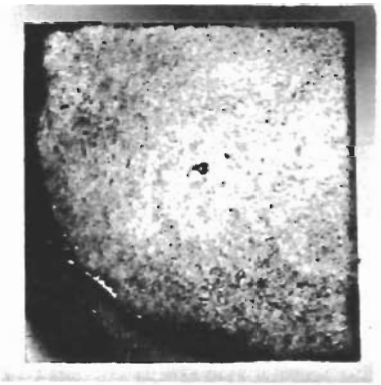	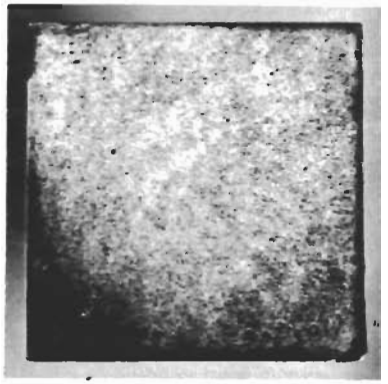

Table 13

Material			010-V6 Molding Compound		
Test Conditions	Heat Flux (BTU/ft^2-sec)		100	300	500
	Gas Enthalpy (BTU/lb)		1180	2380	3800
	Test Duration (sec)		120	40	24
	Stagnation Pressure (psig)		0.307	0.534	0.809
	Gas Temperature ($^\circ$F)		3680	5690	7460
	Gas Velocity (ft/sec)		472	823	1245
Test Results	Decrease in Weight	Gms	18.5902	20.8511	21.4180
		%	37.9	43.3	44.2
	Density (gm/cc)	Before	1.3969	1.3783	1.3912
		After	1.2282	1.2919	1.3045
	Depth of Erosion (in.)		0.359	0.328	0.371
	Volume of Erosion (in^3)		0.629	0.841	0.860
	Final Back Face Temp $^\circ$F		98	94	97
	Final Front Face Temp $^\circ$F		2090	2460	2670
	Remarks		Effluent Composition-100% Nitrogen	Effluent Composition-100% Nitrogen	Effluent Composition-100% Nitrogen
	Sample Appearance		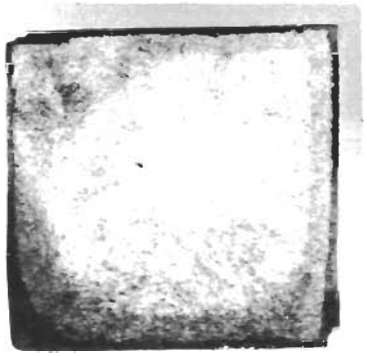	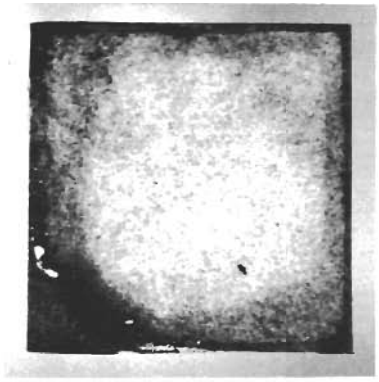	

Table 17

Material			015 End Grain Laminate of 181 Fiberglas		
Test Conditions	Heat Flux (BTU/ft^2-sec)		100	300	500
	Gas Enthalpy (BTU/lb)		1560	2770	3500
	Test Duration (sec)		120	40	24
	Stagnation Pressure (psig)		0.354	0.560	0.747
	Gas Temperature ($^\circ$F)		4580	6120	2980
	Gas Velocity (ft/sec)		545	863	1150
Test Results	Decrease in Weight	Gms	7.2930	8.2175	8.4445
		%	12.4	13.8	14.1
	Density (gm/cc)	Before	1.6964	1.6897	1.6940
		After	1.4167	1.5068	1.5743
	Depth of Erosion (in.)		0.056	0.166	0.133
	Volume of Erosion (in^3)		0.103	0.073	0.163
	Final Back Face Temp $^\circ$F		166	112	106
	Final Front Face Temp $^\circ$F		2440	3080	3290
	Remarks				
	Sample Appearance		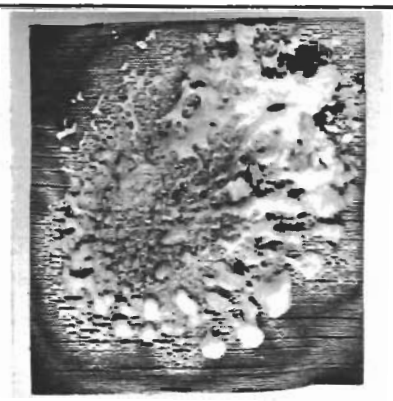	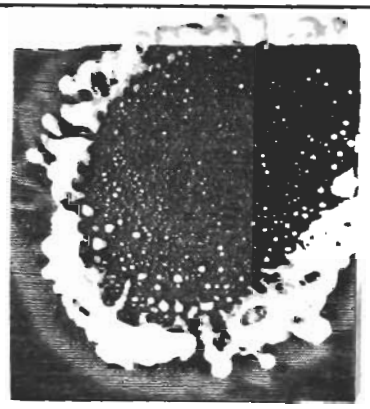	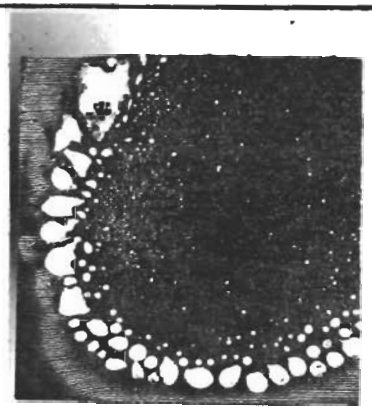

Table 15

149

	Material		015 End Grain Laminate of 181 Fiberglas		
Test Conditions	Heat Flux (BTU/ft^2-sec)		100	300	500
	Gas Enthalpy (BTU/lb)		1180	2380	3800
	Test Duration (sec)		120	40	24
	Stagnation Pressure (psig)		0.307	0.534	0.809
	Gas Temperature ($^\circ$F)		3680	5690	7460
	Gas Velocity (ft/sec)		472	823	1245
Test Results	Decrease in Weight	Gms	7.8169	6.9792	9.1417
		%	13.2	11.7	15.3
	Density (gm/cc)	Before	1.6702	1.6987	1.6926
		After	1.4636	1.5164	1.5404
	Depth of Erosion (in.)		0.009	0.053	0.137
	Volume of Erosion (in^3)		0.020	0.022	0.149
	Final Back Face Temp $^\circ$F		158	115	100
	Final Front Face Temp $^\circ$F		2510	3140	3860
	Remarks		Effluent Composition-100% Nitrogen	Effluent Composition-100% Nitrogen	Effluent Composition-100% Nitrogen
	Sample Appearance		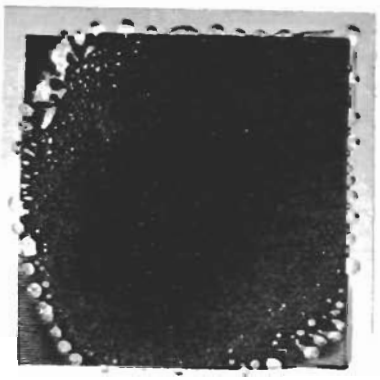	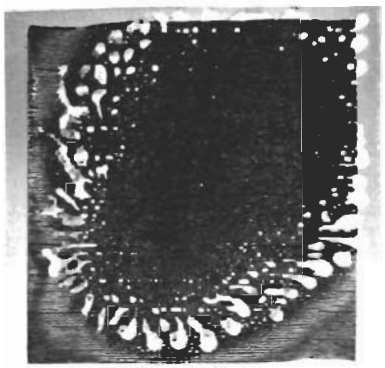	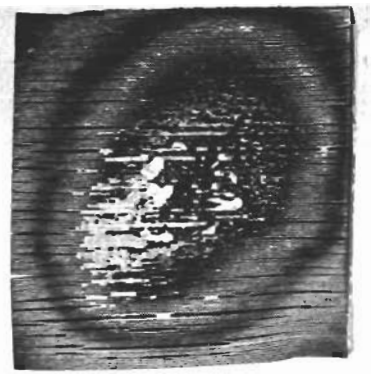

TABLE 16

150

Material			010-V24 End Grain Laminate-Alternate Plies of 181 Fiberglas and Graphite Cloth		
Test Conditions	Heat Flux (BTU/ft^2-sec)		100	300	500
	Gas Enthalpy (BTU/lb)		1560	2780	4130
	Test Duration (sec)		76	40	24
	Stagnation Pressure (psig)		0.354	0.560	0.747
	Gas Temperature ($^\circ$F)		4580	6120	8030
	Gas Velocity (ft/sec)		545	863	1150
Test Results	Decrease in Weight	Gms	21.6233	17.4153	14.2400
		%	45.6	37.4	30.6
	Density (gm/cc)	Before	1.3451	1.3524	1.3460
		After	0.9121	0.9914	1.0574
	Depth of Erosion (in.)		0.314	0.225	0.210
	Volume of Erosion (in^3)		0.427	0.307	0.246
	Final Back Face Temp $^\circ$F		498	176	123
	Final Front Face Temp $^\circ$F		2820	3430	3690
	Remarks		Test terminated because of severe delamination of sample.		
	Sample Appearance		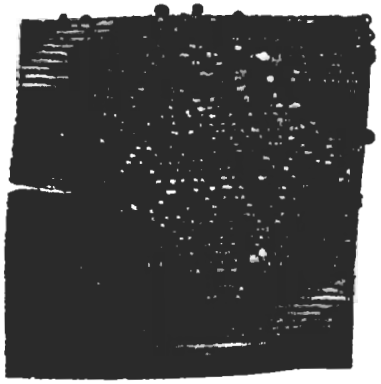	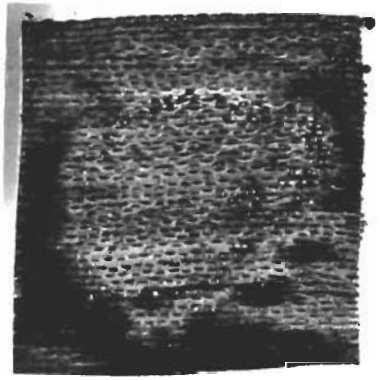	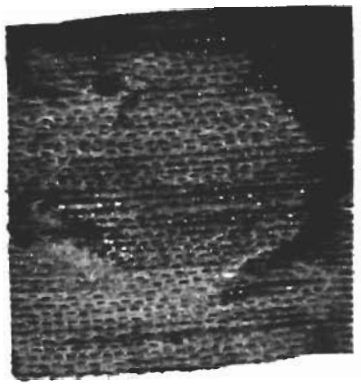

Table 17

151

Material			010-V24 End Grain Laminate - Alternate Plies of Fiberglas and Graphite Cloth		
Test Conditions	Heat Flux (BTU/ft^2-sec)		100	300	500
	Gas Enthalpy (BTU/lb)		1170	2380	3760
	Test Duration (sec)		120	40	24
	Stagnation Pressure (psig)		0.307	0.534	0.805
	Gas Temperature ($^\circ$F)		3660	5690	7390
	Gas Velocity (ft/sec)		472	820	1240
Test Results	Decrease in Weight	Gms	20.1684	14.9502	13.5291
		%	43.7	31.8	29.4
	Density (gm/cc)	Before	1.3243	1.3423	1.3511
		After	0.8272	1.0214	1.0247
	Depth of Erosion (in.)		0.188	0.177	0.151
	Volume of Erosion (in^3)		0.210	0.138	0.143
	Final Back Face Temp $^\circ$F		427	136	123
	Final Front Face Temp $^\circ$F		2610	3880	4150
	Remarks		Effluent Composition-100% Nitrogen	Effluent Composition-100% Nitrogen	Effluent Composition-100% Nitrogen
	Sample Appearance		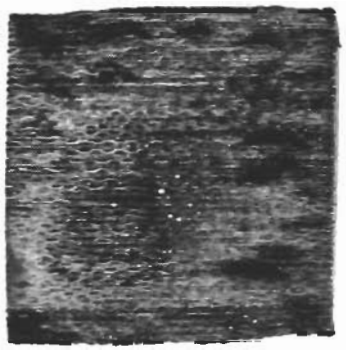	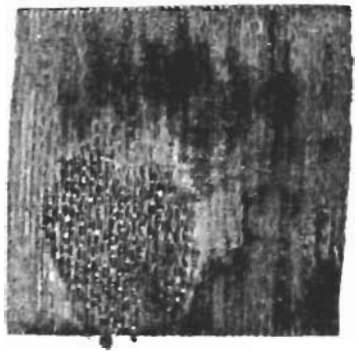	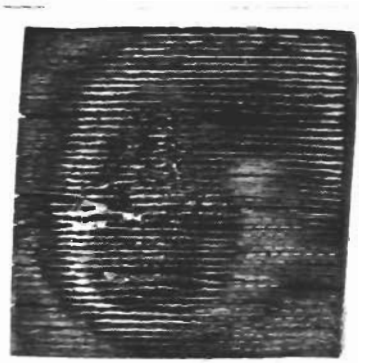

Table 18

Material			Co-polymerized Alkylated Phenyl Polyamide Resin with Graphite Cloth		
Test Conditions	Heat Flux (BTU/ft^2-sec)		500	500	500
	Gas Enthalpy (BTU/lb)		3490	3690	3120
	Test Duration (sec)		24	24	24
	Stagnation Pressure (psig)		0.707	0.745	0.563
	Gas Temperature ($^\circ$F)		6980	7280	6420
	Gas Velocity (ft/sec)		1090	1150	870
Test Results	Decrease in Weight	Gms	12.4645	15.3222	4.8578
		%	27.9	33.6	10.7
	Density (gm/cc)	Before	1.333	1.332	1.330
		After	1.190	1.214	1.241
	Depth of Erosion (in.)		0.116	0.152	0.013
	Volume of Erosion (in^3)		0.392	0.567	0.089
	Final Back Face Temp $^\circ$F		150	225	139
	Final Front Face Temp $^\circ$F		4170	4290	4170
	Remarks		Extensive delamination occurred during testing of all samples of this composition		Effluent composition = 100% nitrogen
	Sample Appearance		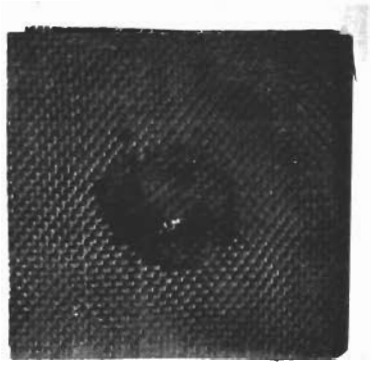		

Table 19

Material			Co-polymerized Alkylated Phenyl Polyamide with Linen		
Test Conditions	Heat Flux (BTU/ft^2-sec)		500	470	500
	Gas Enthalpy (BTU/lb)		3520	3480	3120
	Test Duration (sec)		24	24	24
	Stagnation Pressure (psig)		0.707	0.733	0.563
	Gas Temperature ($^\circ$F)		7020	6960	6420
	Gas Velocity (ft/sec)		1090	1130	870
Test Results	Decrease in Weight	Gms	11.6916	11.4262	7.2437
		%	28.6	28.0	18.0
	Density (gm/cc)	Before	1.334	1.330	1.335
		After	1.250	1.240	1.232
	Depth of Erosion (in.)		0.216	0.237	0.122
	Volume of Erosion (in^3)		0.445	0.426	0.205
	Final Back Face Temp $^\circ$F		125	123	163
	Final Front Face Temp $^\circ$F		4170	3675	3955
	Remarks				Effluent composition = 100% nitrogen
	Sample Appearance		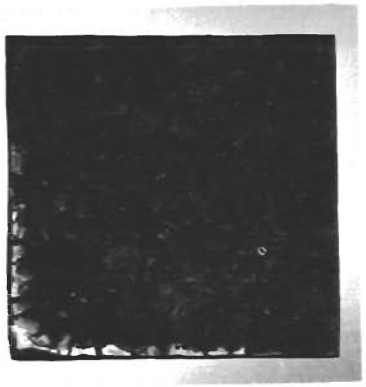	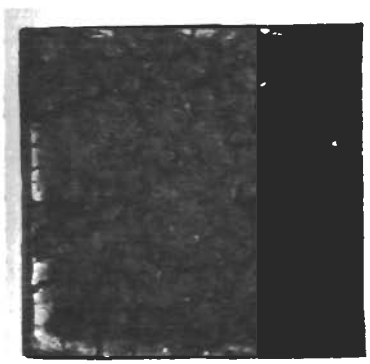	

Table 20

Material			Co-polymerized Alkylated Phenyl Polyamide with Linen (modified preparation)		
Test Conditions	Heat Flux (BTU/ft^2-sec)		480	500	
	Gas Enthalpy (BTU/lb)		4155	4290	
	Test Duration (sec)		24	24	
	Stagnation Pressure (psig)		0.751	0.686	
	Gas Temperature ($^{\circ}$F)		8060	8290	
	Gas Velocity (ft/sec)		1160	1060	
Test Results	Decrease in Weight	Gms	10.5727	8.5327	
		%	25.7	21.1	
	Density (gm/cc)	Before	1.312	1.310	
		After	1.261	1.240	
	Depth of Erosion (in.)		0.214	0.145	
	Volume of Erosion (in^3)		0.434	0.313	
	Final Back Face Temp $^{\circ}$F		80	80	
	Final Front Face Temp $^{\circ}$F		3900	4530	
	Remarks			Effluent composition = 100% nitrogen	
	Sample Appearance		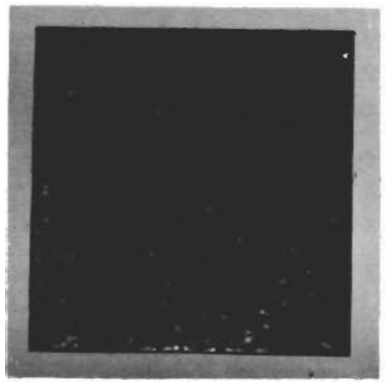	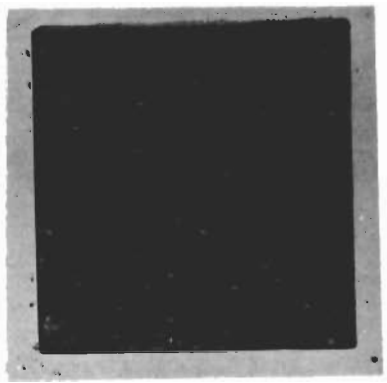	

Table 21

	Material		Co-polymerized Alkylated Phenyl Polyamide Resin with Refrasil		
Test Conditions	Heat Flux (BTU/ft^2-sec)		500	500	500
	Gas Enthalpy (BTU/lb)		3480	3650	3090
	Test Duration (sec)		24	24	24
	Stagnation Pressure (psig)		0.707	0.745	0.560
	Gas Temperature ($^\circ$F)		6960	7210	6460
	Gas Velocity (ft/sec)		1090	1150	862
Test Results	Decrease in Weight	Gms	4.4345	4.9181	3.4240
		%	8.5	9.2	6.5
	Density (gm/cc)	Before	1.633	1.634	1.634
		After	1.464	1.518	1.562
	Depth of Erosion (in.)		0.042	0.054	0.010
	Volume of Erosion (in^3)		0.143	0.045	0.043
	Final Back Face Temp $^\circ$F		111	94	145
	Final Front Face Temp $^\circ$F		3720	3730	3825
	Remarks				Effluent composition = 100% nitrogen
	Sample Appearance			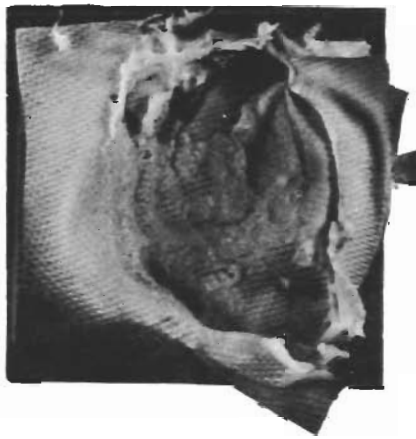	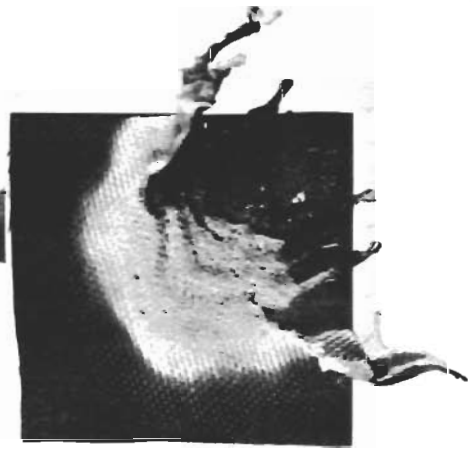

Table 22

	Material		Co-polymerized Alkylated Phenyl Polyamide Resin with Asbestos			
Test Conditions	Heat Flux (BTU/ft^2-sec)		300	470	500	500
	Gas Enthalpy (BTU/lb)		1790	3430	3530	3170
	Test Duration (sec)		40	24	24	24
	Stagnation Pressure (psig)		0.481	0.733	0.866	0.567
	Gas Temperature ($^\circ$F)		4980	6890	7020	6550
	Gas Velocity (ft/sec)		812	1130	1330	873
Test Results	Decrease in Weight	Gms	6.2891	12.5735	12.9016	6.4466
		%	11.5	22.3	23.7	11.5
	Density (gm/cc)	Before	1.700	1.692	1.704	1.699
		After	1.585	1.558	1.603	1.579
	Depth of Erosion (in.)		0.162	0.193	0.194	0.114
	Volume of Erosion (in^3)		0.099	0.317	0.368	0.096
	Final Back Face Temp $^\circ$F		100	208	128	120
	Final Front Face Temp $^\circ$F		2970	3470	3540	3775
	Remarks					Effluent composition = 100% nitrogen
	Sample Appearance		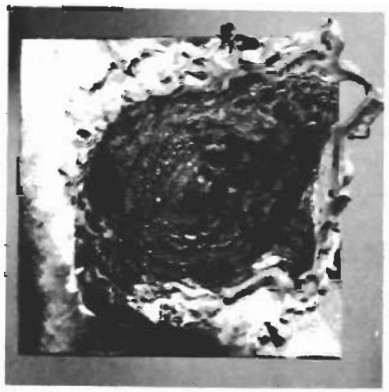	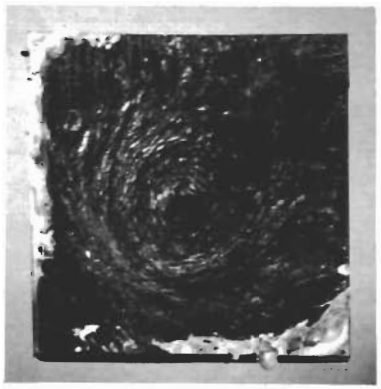		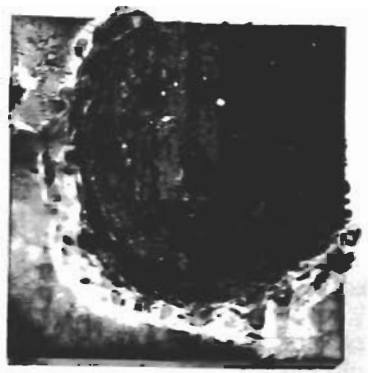

Table 23

	Material		Co-polymerized Phenyl Polyamide Resin with Asbestos		
Test Conditions	Heat Flux (BTU/ft^2-sec)		300	500 500	500
	Gas Enthalpy (BTU/lb)		1830	3600 3530	3170
	Test Duration (sec)		40	24 24	24
	Stagnation Pressure (psig)		0.481	0.758 0.866	0.567
	Gas Temperature ($^\circ$F)		5040	7120 7020	6550
	Gas Velocity (ft/sec)		810	1167 1330	870
Test Results	Decrease in Weight	Gms	6.9253	9.3339 11.7019	5.6460
		%	12.7	17.3 21.4	10.3
	Density (gm/cc)	Before	1.671	1.666 1.678	1.684
		After	1.576	1.578 1.588	1.515
	Depth of Erosion (in.)		0.164	0.250 0.140	0.072
	Volume of Erosion (in^3)		0.149	0.251 0.338	0.006
	Final Back Face Temp $^\circ$F		123	106 114	123
	Final Front Face Temp $^\circ$F		3070	3540 3580	3600
	Remarks				Effluent composition = 100% nitrogen
	Sample Appearance		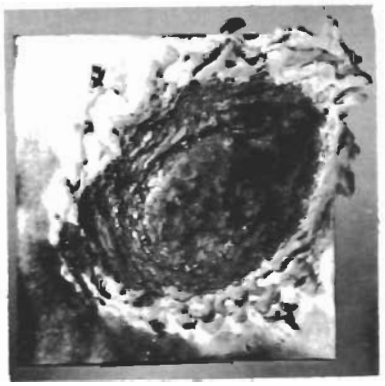	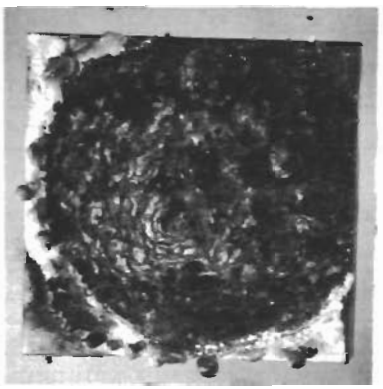	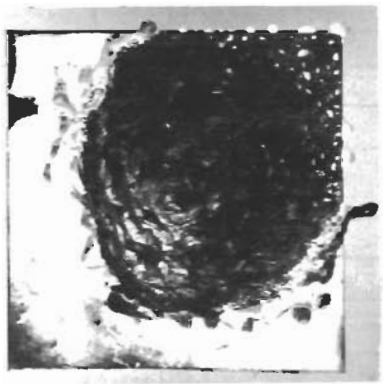

Table 24

	Material		Nylon-Phenolic Resin with Asbestos		
Test Conditions	Heat Flux (BTU/ft^2-sec)		300	470 500	500
	Gas Enthalpy (BTU/lb)		1770	3540 3570	3310
	Test Duration (sec)		40	24 24	24
	Stagnation Pressure (psig)		0.481	0.733 0.866	0.555
	Gas Temperature ($^\circ$F)		4940	7050 7090	6550
	Gas Velocity (ft/sec)		812	1130 1330	855
Test Results	Decrease in Weight	Gms	5.8756	11.5733 12.0100	5.0648
		%	11.0	21.4 22.7	9.4
	Density (gm/cc)	Before	1.638	1.633 1.635	1.636
		After	1.547	1.531 1.538	1.541
	Depth of Erosion (in.)		0.074	0.145 0.158	0.053
	Volume of Erosion (in^3)		0.114	0.327 0.351	0.077
	Final Back Face Temp $^\circ$F		117	223 147	134
	Final Front Face Temp $^\circ$F		3160	3630 3720	3790
	Remarks				Effluent composition = 100% nitrogen
	Sample Appearance		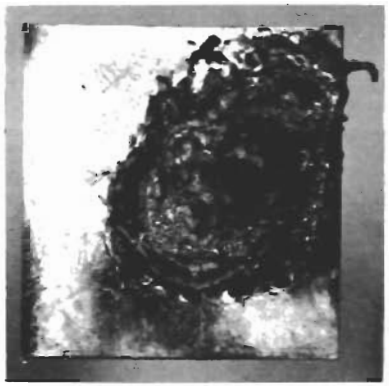	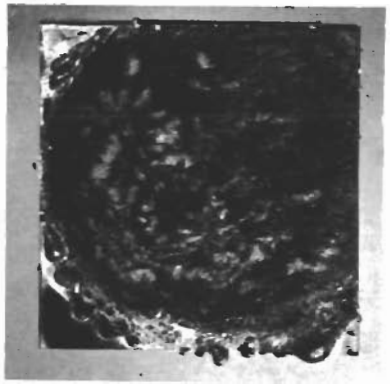	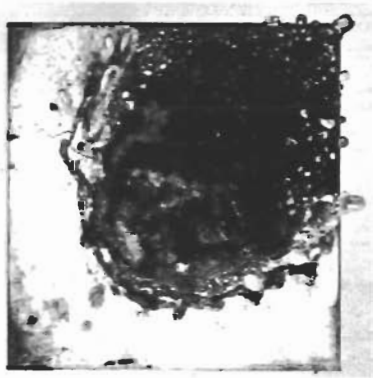

TABLE 27

Material			Phenolic Resin with Asbestos		
Test Conditions	Heat Flux (BTU/ft^2-sec)		300	500 500	500
	Gas Enthalpy (BTU/lb)		1770	3560 3460	3310
	Test Duration (sec)		40	24 24	24
	Stagnation Pressure (psig)		0.481	0.776 0.866	0.555
	Gas Temperature ($^\circ$F)		4940	7070 6930	6550
	Gas Velocity (ft/sec)		810	1195 1330	855
Test Results	Decrease in Weight	Gms	5.5804	8.5389 11.3345	4.5118
		%	9.5	15.1 19.5	7.8
	Density (gm/cc)	Before	1.773	1.752 1.766	1.765
		After	1.724	1.673 1.728	1.668
	Depth of Erosion (in.)		0.137	0.160 0.181	0.075
	Volume of Erosion (in^3)		0.140	0.218 0.356	0.048
	Final Back Face Temp $^\circ$F		111	108 139	128
	Final Front Face Temp $^\circ$F		3090	3530 3540	3580
	Remarks				Effluent composition = 100% nitrogen
	Sample Appearance		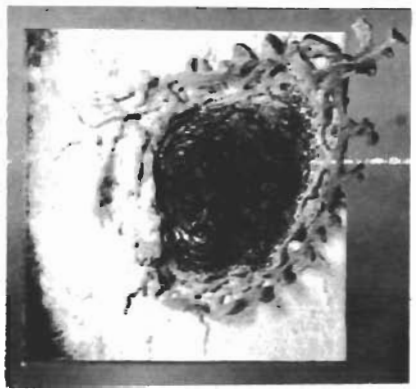	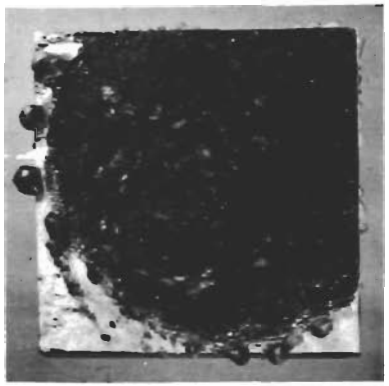	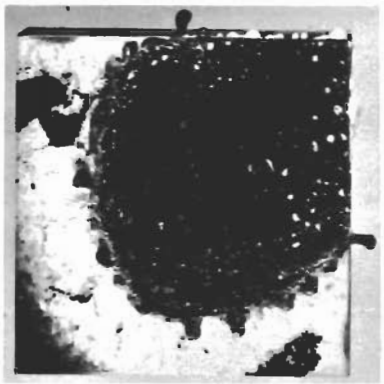

Table 26

Material			Halogenated Phenolic Resin on Refrasil		
Test Conditions	Heat Flux (BTU/ft^2-sec)		480	500	
	Gas Enthalpy (BTU/lb)		4160	4290	
	Test Duration (sec)		24	24	
	Stagnation Pressure (psig)		0.751	0.686	
	Gas Temperature ($^\circ$F)		8060	8290	
	Gas Velocity (ft/sec)		1160	1060	
Test Results	Decrease in Weight	Gms	4.0676	4.7124	
		%	6.7	7.8	
	Density (gm/cc)	Before	1.781	1.778	
		After	1.616	1.644	
	Depth of Erosion (in.)		0.019	0.014	
	Volume of Erosion (in^3)		+ 0.058	0.003	
	Final Back Face Temp $^\circ$F		80	90	
	Final Front Face Temp $^\circ$F		3630	3945	
	Remarks		Moderately severe delamination occurred.	Moderately severe delamination occurred. Effluent composition = 100% nitrogen	
	Sample Appearance			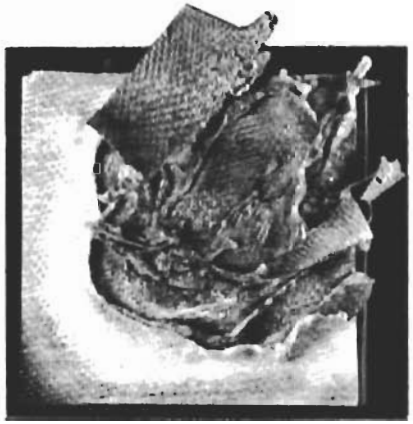	

Table 27

Material			Modified Halogenated Phenyl Co-polymerized Silane Resin on Refrasil		
Test Conditions	Heat Flux (BTU/ft^2-sec)		480	500	
	Gas Enthalpy (BTU/lb)		4220	4250	
	Test Duration (sec)		24	24	
	Stagnation Pressure (psig)		0.736	0.679	
	Gas Temperature ($^\circ$F)		8180	8230	
	Gas Velocity (ft/sec)		1130	1045	
Test Results	Decrease in Weight	Gms	2.8040	4.9462	
		%	5.52	9.7	
	Density (gm/cc)	Before	1.673	1.684	
		After	1.543	1.562	
	Depth of Erosion (in.)		0.010	0.030	
	Volume of Erosion (in^3)		0.045	0.049	
	Final Back Face Temp $^\circ$F		110	80	
	Final Front Face Temp $^\circ$F		3990	3770	
	Remarks		Moderately severe delamination occurred.	Moderately severe delamination occurred. Effluent composition = 100% nitrogen.	
	Sample Appearance		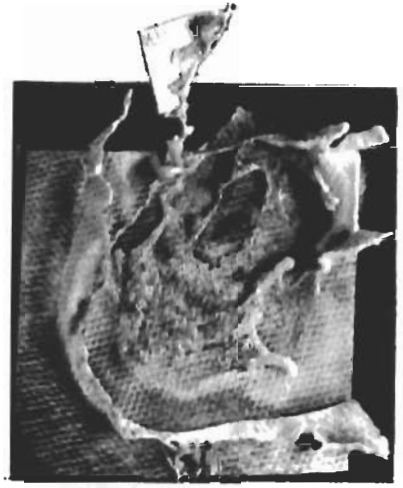	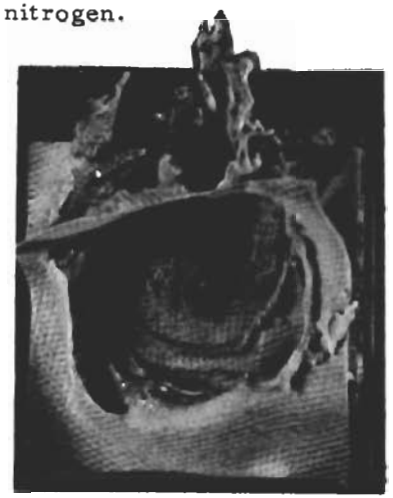	

Table 28

	Material		Halogenated Phenyl Co-polymerized Silane Resin on Refrasil		
Test Conditions	Heat Flux (BTU/ft^2-sec)		480	500	
	Gas Enthalpy (BTU/lb)		4220	4250	
	Test Duration (sec)		24	24	
	Stagnation Pressure (psig)		0.736	0.679	
	Gas Temperature ($^\circ$F)		8180	8230	
	Gas Velocity (ft/sec)		1130	1045	
Test Results	Decrease in Weight	Gms	3.2642	5.7982	
		%	6.0	10.7	
	Density (gm/cc)	Before	1.721	1.705	
		After	1.625	1.531	
	Depth of Erosion (in.)		0.056	0.057	
	Volume of Erosion (in^3)		0.009	0.011	
	Final Back Face Temp $^\circ$F		90	80	
	Final Front Face Temp $^\circ$F		3990	3810	
	Remarks		Moderately severe delamination occurred.	Considerable delamination occurred. Effluent composition = 100% nitrogen.	
	Sample Appearance			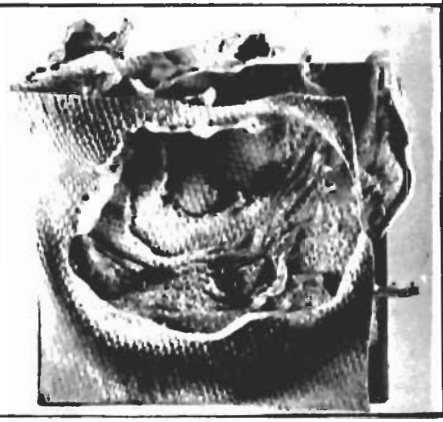	

Table 29

Material			Asbestos Felt with Phenolic Resin and an Inorganic Filler		
Test Conditions	Heat Flux (BTU/ft^2-sec)		493	493	493
	Gas Enthalpy (BTU/lb)		3890	3890	3900
	Test Duration (sec)		24	24	24
	Stagnation Pressure (psig)		0.794	0.794	0.794
	Gas Temperature ($^\circ$F)		7640	7640	7660
	Gas Velocity (ft/sec)		1220	1220	1220
Test Results	Decrease in Weight	Gms	11.4454	11.5201	8.7994
		%	17.9	19.6	12.9
	Density (gm/cc)	Before	1.7543	1.7343	2.0612
		After	1.7010	1.6615	2.0308
	Depth of Erosion (in.)		0.167	0.182	0.150
	Volume of Erosion (in^3)		0.280	0.332	0.357
	Final Back Face Temp $^\circ$F		105	100	100
	Final Front Face Temp $^\circ$F		3690	3690	4060
	Remarks		Filler material: titanium dioxide.	Filler material: potassium titanate.	Filler material: tungsten.
	Sample Appearance		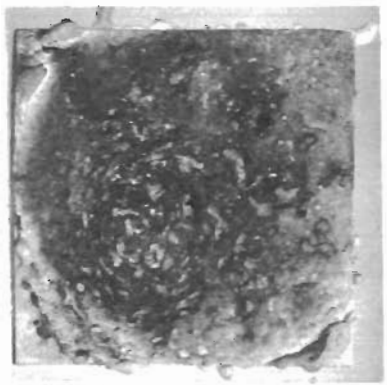	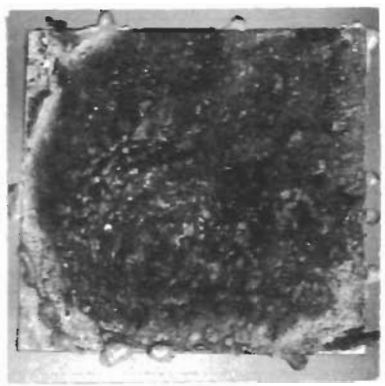	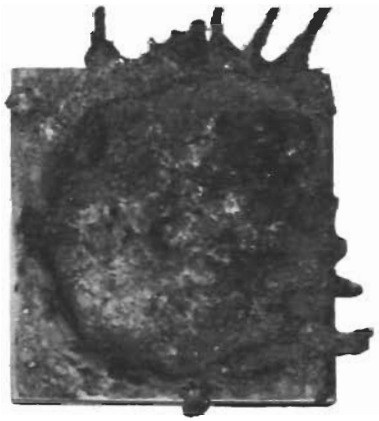

Table 30

	Material		Asbestos Felt with Phenolic Resin and an Inorganic Filler		
Test Conditions	Heat Flux (BTU/ft^2-sec)		500	500	500
	Gas Enthalpy (BTU/lb)		3760	3870	3870
	Test Duration (sec)		64	64	64
	Stagnation Pressure (psig)		0.812	0.812	0.812
	Gas Temperature ($^\circ$F)		7390	7600	7600
	Gas Velocity (ft/sec)		1250	1250	1250
Test Results	Decrease in Weight	Gms	29.3796	30.1209	21.5936
		%	45.1	50.0	29.5
	Density (gm/cc)	Before	1.7604	1.7250	2.0926
		After	1.5920	1.4936	2.0154
	Depth of Erosion (in.)		0.419	0.351	0.299
	Volume of Erosion (in^3)		0.886	0.900	0.571
	Final Back Face Temp $^\circ$F		152	160	136
	Final Front Face Temp $^\circ$F		3670	3700	3850
	Remarks		Filler material: titanium dioxide.	Filler material: potassium titanate.	Filler material: tungsten.
	Sample Appearance		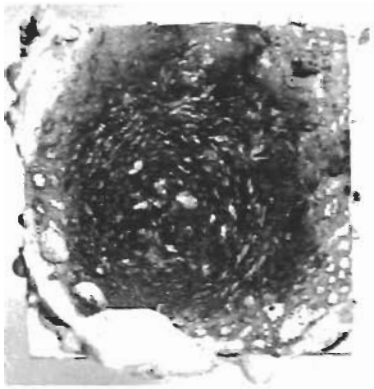	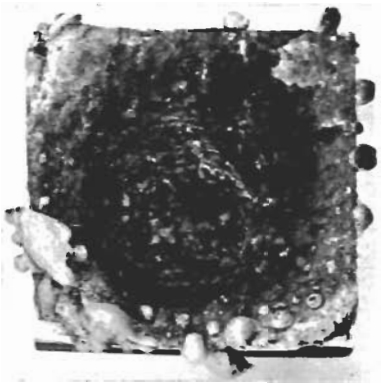	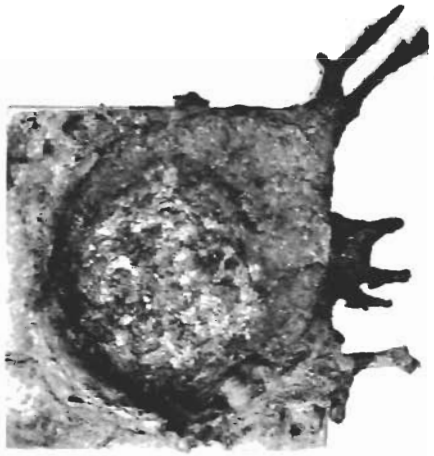

TABLE VI (Cont)

	Material		Asbestos Felt with Phenolic Resin and an Inorganic Filler		
Test Conditions	Heat Flux (BTU/ft^2-sec)		100	100	100
	Gas Enthalpy (BTU/lb)		1260	1260	1260
	Test Duration (sec)		120	120	120
	Stagnation Pressure (psig)		0.357	0.354	0.354
	Gas Temperature ($^\circ$F)		3900	3900	3910
	Gas Velocity (ft/sec)		550	545	545
Test Results	Decrease in Weight	Gms	4.5309	4.8311	4.4703
		%	7.4	8.1	6.2
	Density (gm/cc)	Before	1.7277	1.7226	2.1055
		After	1.6287	1.6055	2.0198
	Depth of Erosion (in.)		0.016	0.021	0.010
	Volume of Erosion (in^3)		0.039	0.029	0.047
	Final Back Face Temp $^\circ$F		150	150	145
	Final Front Face Temp $^\circ$F		2540	2620	2560
	Remarks		Filler material: titanium dioxide.	Filler material: potassium titanate.	Filler material: tungsten.
	Sample Appearance		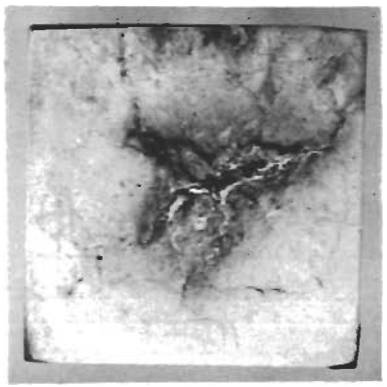		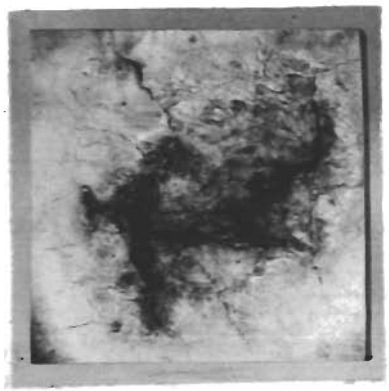

Table 32

	Material		Cermet Plated Graphite	ATJ Graphite	ATJ Graphite
Test Conditions	Heat Flux (BTU/ft^2-sec)		300	300	300
	Gas Enthalpy (BTU/lb)		1940	2325	2080
	Test Duration (sec)		300	40	40
	Stagnation Pressure (psig)		0.487	0.668	0.488
	Gas Temperature (^{o}F)		5210	5640	5400
	Gas Velocity (ft/sec)		750	1030	750
Test Results	Decrease in Weight	Gms	4.3982	1.7651	.5449
		%	6.6	3.5	1.1
	Density (gm/cc)	Before	1.8246	1.624	1.617
		After	2.1736	1.601	1.659
	Depth of Erosion (in.)		nil	0.025	0.013
	Volume of Erosion (in^3)		0.460	0.041	0.066
	Final Back Face Temp ^{o}F		1800	1300	1220
	Final Front Face Temp ^{o}F		2420	2690	2060
	Remarks		Coating showed slight indication of melting at 210 sec.		
	Sample Appearance		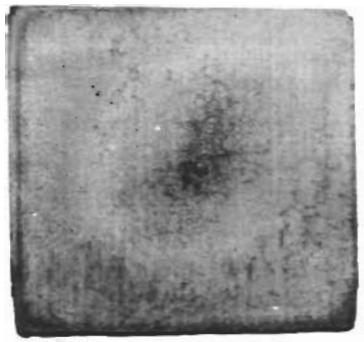		

Table 33

			Material	Cermet Plated Graphite	Cermet Plated Graphite	ATJ Graphite
Test Conditions			Heat Flux (BTU/ft^2-sec)	510	510	465
			Gas Enthalpy (BTU/lb)	3200	3180	3880
			Test Duration (sec)	24	120	24
			Stagnation Pressure (psig)	0.730	0.730	0.836
			Gas Temperature (^oF)	6570	6570	7600
			Gas Velocity (ft/sec)	1125	1125	1350
Test Results		Decrease in Weight	Gms	0.0444	4.7737	1.8376
			%	0.07	7.1	3.3
		Density (gm/cc)	Before	1.8460	1.8402	1.701
			After	2.1339	2.1689	1.726
			Depth of Erosion (in.)	0.001	0.085	0.021
			Volume of Erosion (in^3)	0.310	0.472	0.096
			Final Back Face Temp ^oF	923	2297	1590
			Final Front Face Temp ^oF	2190	3360	---
			Remarks		Coating failed at about 60 sec.	
			Sample Appearance	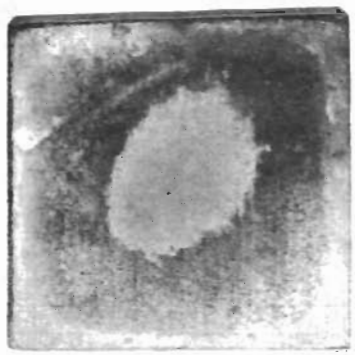	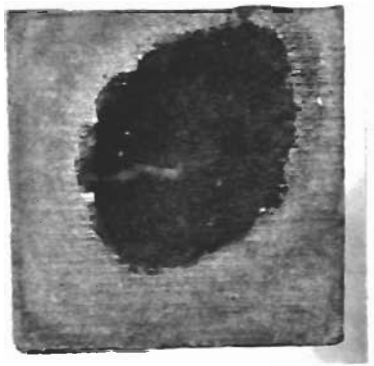	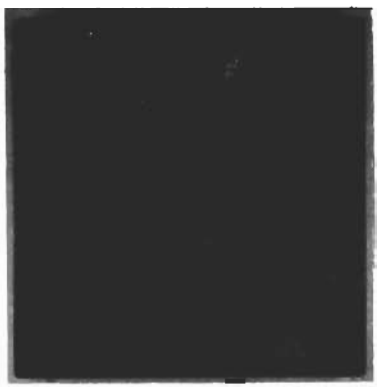

Table 35. Identification and Test Results for Various Sprayed Coatings.

Manufacturer	Coating Identification					Test Results
	Primer	First Gradation	Second Gradation	Third Gradation	Insulating Layer	Cycles to Failure
RMD	0.004" Nichrome				0.010" Rokide Z	1, 1, 1, 2, 2, 2, 4, 4, 6, 7, 8, 10, 12, 14, 15, 16, 18, 19, 19, 20, 20, 26, 43, 54, 55, 55, 55, 65, 80, 90, 90
Plasmakote	0.004" Nichrome				0.010" Rokide Z	11, 16, 24, 32, 39, 46, 53, 53
Plasmakote	0.004" Nichrome				0.010" ZrO_2	33, 33, 35, 35, 55, 55, 63, 69
Plasmakote	0.004" Mo				0.010" Rokide Z	39, 47, 52, 65, 68, 78
Plasmakote	0.004" Mo				0.010"ZrO_2	29, 33, 34, 36, 43, 46
Plasmakote	0.002" Nichrome	0.002" 70% Nichrome 30% ZrO_2	0.002" 30% Nichrome 70% ZrO_2		0.006" ZrO_2	11, 14, 24, 31, 44, 45, 46, 53, 55, 63, 65, 68
Plasmakote	0.002" Nichrome	0.002" 75% Nichrome 25% ZrO_2	0.002" 50% Nichrome 50% ZrO_2	0.002" 75% Nichrome 25% ZrO_2	0.005" ZrO_2	3, 5, 9, 11, 25, 26, 40, 51, 62, 66, 75, 79
Plasmakote	0.002" Nichrome	0.002" 75% Nichrome 25% ZrO_2	0.002" 50% Nichrome 50% ZrO_2	0.002" 25% Nichrome 75% ZrO_2	0.005" ZrO_2 & 1% Ni	12, 17, 19, 22, 23, 35, 39, 43, 54, 58, 58, 63,
Plasmakote	0.002" Mo	0.002" 70% Nichrome 30% ZrO_2	0.002" 30% Nichrome 70% ZrO_2		0.004" ZrO_2	52, 53, 54, 61, 74, 90, 90, 90
Plasmakote	0.002" Mo	0.002" 50% Nichrome 50% ZrO_2	0.002" 10% Nichrome 90% ZrO_2		0.004" ZrO_2	43, 54, 54, 60, 61, 73, 74, 74, 90
Plasmakote	0.002" Mo	0.002" 70% Mo 30% ZrO_2	0.002" 30% Mo 70% ZrO_2		0.004" ZrO_2	31, 33, 55, 59
Plasmakote	0.002" Mo	0.002" 30% Mo 30% ZrO_2	0.002" 30% Mo 70% ZrO_2	0.002" 10% Mo 90% ZrO_2	0.004" ZrO_2	13, 16, 37, 38, 51, 52, 61, 64
Plasmakote	0.002" W	0.002" 70% W 30% ZrO_2	0.002" 30% W 70% ZrO_2	0.002" 10% W 90% ZrO_2	0.004" ZrO_2	16, 19, 21
Plasmakote	0.060" W	0.002" 70% W 30% ZrO_2	0.002" 30% W 70% ZrO_2	0.002" 10% W 90% ZrO_2	0.004" ZrO_2	8, 11, 12
Plasmakote	0.030" W	0.002" 70% W 30% ZrO_2	0.002" 30% W 70% ZrO_2	0.002" 10 % W 90% ZrO_2	0.004" ZrO_2	9, 9, 8, 8, 5

Table 36. Bond Strength of Pure Alumina Coating Arc-Sprayed on an Inconel Substrate Grit Blasted with Various Media

Grit Blasting Media	Bond Strength (psi)	Type Failure
Corundum	590	Metal/Ceramic Interface
Corundum	660	Metal/Ceramic Interface
Corundum	710	Metal/Ceramic Interface
Corundum	960	Metal/Ceramic Interface
Corundum	510	Cohesive in Ceramic
Corundum	580	Cohesive in Ceramic
Corundum	540	Cohesive in Ceramic
Corundum	710	Cohesive in Ceramic
Silicon Carbide	470	Cohesive in Ceramic
Silicon Carbide	560	Cohesive in Ceramic
Silicon Carbide	760	Cohesive in Ceramic
Silicon Carbide	1240	Cohesive in Ceramic
Silicon Carbide	700	Cohesive in Ceramic
Silicon Carbide	690	Cohesive in Ceramic
Silicon Carbide	860	Cohesive in Ceramic
Silicon Carbide	550	Cohesive in Ceramic
Garnet	410	Metal/Ceramic Interface
Garnet	490	Metal/Ceramic Interface
Garnet	530	Metal/Ceramic Interface
Garnet	620	Metal/Ceramic Interface
Garnet	910	Metal/Ceramic Interface
Garnet	610	Metal/Ceramic Interface
Garnet	750	Metal/Ceramic Interface
Garnet	850	Metal/Ceramic Interface
Flint	390	Metal/Ceramic Interface
Flint	510	Metal/Ceramic Interface
Flint	250	Metal/Ceramic Interface
Flint	1030	Metal/Ceramic Interface
Flint	790	Metal/Ceramic Interface
Flint	720	Metal/Ceramic Interface
Flint	660	Metal/Ceramic Interface
Flint	880	Metal/Ceramic Interface

Table 37. Bond Strength of 50% Nickel - 50% Alumina Coating Arc-Sprayed on an Inconel Substrate Grit Blasted with Various Media

Grit Blasting Media	Bond Strength (psi)	Type Failure
Corundum	3100	Metal/Epoxy Bond
Corundum	1760	Metal/Ceramic Interface
Corundum	2030	Metal/Ceramic Interface
Corundum	1550	Metal/Ceramic Interface
Silicon Carbide	2160	Metal/Ceramic Interface
Silicon Carbide	1630	Metal/Ceramic Interface
Silicon Carbide	2020	Metal/Ceramic Interface
Silicon Carbide	1890	Metal/Ceramic Interface
Garnet	3860	Metal/Ceramic Interface
Garnet	1250	Cohesive in Ceramic
Garnet	1140	Cohesive in Ceramic
Garnet	1580	Cohesive in Ceramic
Flint	3246	Ceramic/Epoxy Bond
Flint	2620	Ceramic/Epoxy Bond
Flint	1910	Ceramic/Epoxy Bond
Flint	1800	Ceramic/Epoxy Bond

Table 38. Tensile Bond Strength of Graded Zirconia on 347 Stainless Steel for Two Methods of Sample Preparation.

Specimen Type[2]	Bond Strength psi	Type Failure
A-1	2550	Cohesive in Primer
A-2	2500	Ceramic/Epoxy Bond
A-3	2675	Cohesive in Primer
A-4	2790	Cohesive in Primer
A-5	2720	Cohesive in Primer
A-6	2700	Cohesive in Primer
B-1	3050	Cohesive in Primer
B-2	3410	Cohesive in Primer
B-3	3340	Cohesive in Primer
B-4	2275	Partial Ceramic/Epoxy Bond
B-5	1750	Ceramic/Epoxy Bond
B-6	3400	Cohesive in Primer

[2]Coating consisted of 0.002" Molybdenum Primer
0.002" 70% Nichrome - 30% Zirconia
0.002" 30% Nichrome - 70% Zirconia
0.002" 10% Nichrome - 90% Zirconia
0.004" Zirconia

Type A samples were coated and then ground to 1.0" x 1.0" ± 0.001

Type B samples were coated after substrate was finish ground to 1.0" x 1.0" ± .001

TABLE 39. Results of Constant Exposure Type Test on Manufacturer SY Samples.

Material	Coating Designation	Temperature °F	Time at Temperature	Remarks
Ta-10% W	34[2]	2070	5 min.	
		2240	5 min.	
		2530	5 min.	
		2910	5 min.	
		3230	5 min.	Extensive warpage of sample - No failure
Ta-10% W	34[2]	2550	5 min.	
		2910	5 min.	
		3260	5 min.	
		3340	5 min.	No failure
Columbium	22	2550	5 min.	
		2820	35 sec.	Catastrophic failure
Molybdenum	34S	2550	5 min.	
		2910	5 min.	
		3290	5 min.	
		3450	5 sec.	Catastrophic failure
Molybdenum	34S	2550	5 min.	
		2910	5 min.	
		3200	5 min.	No failure
Tungsten	34S	2750	5 min.	
		2940	5 min.	
		3090	5 min.	
		3260	5 min.	
		3460	17 sec.	Failure due to melting of coating

TABLE 40. Results of Thermal Cycling Tests on Manufacturer SY Samples.

Material	Coating Designation	Temperature °F	Thermal Shock Cycles	Remarks
Ta-10% W	34[2]	2730 2930 3150	15 15 4	 Specimen failed
Ta-10% W	34[2]	2740 2910	15 4	 Specimen failed
Ta-10% W	34[2]	2730 2910	15 11	 Specimen failed
Ta-10% W	34[2]	2730 2930	15 5	 Specimen failed
Ta-10% W	34[2]	2740 2910	15 8	 Specimen failed
Ta-10% W	34[2]	2730 2940	15 8	 Specimen failed
Molybdenum	34S	2730 2910 3090 3270 3450	15 15 15 15 0	 Specimen failed during heating to 3450°F

Table 41. Results of Evaluation Tests on Coated Samples of 2" x 2" x 0.030" Mo-1/2% Ti.

	Oxy-Acetylene Torch Test 30 Minute Heating Cycles at 2960°F[1]		Arc-Plasma-Jet Test Type I - 15 Min Heating Cycles at 3000°F[2]		Arc-Plasma-Jet Test Type II 5 Minute Heating Cycles at Increasing Temperature levels			
Manufacturer and Coating Designation	Coating Thickness Mils	Coating Life Minutes	Estimated Coating Thickness[3] Mils	Coating Life Minutes	Estimated Coating Thickness[3] Mils	Total Exposure Time Minutes	Failure Temperature[2] °F	Time at Failure Temp. Minutes
Boeing Fluidized Bed Silicide	---	---	1.0 1.0	223 90	1.0 1.0	32.3 34.2	3300 3300	2.3 4.2
Boeing Di Sil 1	1.25-1.75	22 24 25	1.0 1.0	2.4 105	1.0 1.0	33.9 36.6	3300 3400	3.9 1.6
Pfaudler PFR-6	2.5	64 66 82	4.1 4.5	240[4] 240[4]	4.6 4.7	35.1 38.9	3400 3400	0.1 3.9
Chromalloy-W-2	2.5	21 24 25	1.5 2.0	25[4] 240[4]	1.7 1.5	25.8 29.0	3200 3200	0.8 4.0
Chance Vought - Vought II and IX	2	60 67 84	2.3 1.9	27.5 96.4	2.6 1.5	26.2 30.8	3200 3300	1.2 0.8

[1] Uncorrected Optical Temperature
[2] Two Color Pyrometer Temperature
[3] Obtained from Measurements of Total Sample Thickness
[4] No Failure

Table 42. Results of 50 Hour Test of Coated Mo-1/2 Ti Panels in Still Air at 2000°F

Manufacturer and Coating Designation	Estimated Coating Thickness (Mils)	Remarks
Boeing Fluidized Bed Silicide	1.0	Edge failure at approximately 25 hours.
Boeing DiSil 1	1.0	Portions of surface flaked and turned from black to tan.
Pfaudler PFR-6	4.0	Slight surface blotching
Chromalloy W-2	1.5	Surface mottled with brown-green spots.
Chance Vought Vought II and IX	2.0	No change in appearance.

APPENDIX

SPECIAL TESTS

1. Ablative Coatings

In certain applications coated refractory alloy structures may be subjected to short periods of extremely high thermal input in excess of the protective capabilities of the coating. To achieve temporary protection during these periods of high thermal input the use of ablative overcoats has been proposed.

To obtain preliminary data relative to the protective ability of an ablative coating on a metallic substrate a series of tests was performed. The materials were selected as being representative of types which might be considered for such an application and included lucite, Teflon, melamine-cotton, melamine-nylon, and an epoxy glass fiber-phenolic microballoon composite. Specimens were cut into 2 x 2 x 1/2 inch flat panels and bonded with an adhesive to 0.067 inch thick Inconel plates. These samples were tested in a plasma-jet effluent of simulated air at heat fluxes of 400 and 100 Btu/ft^2 - sec and orientation angles with respect to the effluent flow of 90^o and 45^o. Tests were also performed at 50 Btu/ft^2 - sec at an orientation angle of 45^o only. Nominal test conditions for the three heat flux levels are shown in Table 43. Tests were conducted for times sufficient to penetrate the ablative coating. Front surface temperatures at the ablative coating - Inconel interface were measured with a Chromel-Alumel thermocouple imbedded in the bond line at the center of the sample. Temperature measurements at this interface provided a means of evaluating the effectiveness of the coating and also served as an indicator of impending coating penetration during test.

The results of these tests are summarized in Table 44. It is interesting to note the similarity of weight loss and erosion volume for any given material despite differences in orientation angle and input heat flux. This would suggest that the pattern of degradation when the sample was allowed to erode to a given depth was relatively independent of heat flux and orientation. Furthermore, the penetration times for each material suggest that this parameter is a function of heat flux but not of orientation angle. Bond line temperature-time histories for several of the systems are shown in Figure 119. The curves illustrate how heat flux and exposure time may influence the behavior of an ablative material. If thermal protection is evaluated strictly as a function of thermal lag, then at 400 Btu/ft^2-sec the phenolic microballoon system performed best with melamine-cotton, melamine-nylon, and Teflon following in decreasing order. At 50 Btu/ft^2 -sec, however, the order of relative performance changes with melamine-nylon providing greatest protection, followed in decreasing order by Teflon, melamine-cotton and the phenolic microballoon system. It should be noted that the evaluation of an ablative system must include factors other than thermal protection such as density and erosion rate and that the selection of a system must, by necessity, be tempered by consideration of the intended application.

2. Insulating Materials

Materials evaluations were also conducted in the low heat flux range and included the testing of three insulating materials in air at a heat flux of approximately 10 Btu/ft^2-sec.

These samples consisted of: 1/8 inch thick cork bonded to 60 mil Inconel sheet, 1/8 inch thick subliming epoxy also bonded to 60 mil Inconel sheet, and a phenolic-asbestos felt composite bonded to a metal honeycomb structure. Thermocouples for the measurement of substrate temperature during test were welded to the back of each Inconel plate and to the back of the honeycomb panel adjacent to the coating. To achieve the desired heat flux, samples oriented at 45° to the arc effluent were positioned 6-3/4 inches from the nozzle exit. All samples were exposed for 180 seconds and duplicate tests were performed for each material. The results of these tests are shown in Table 45. Temperature-time histories of the substrate are shown in Figures 120 and 121, photographs of the samples after test are shown in Figures 122 and 123.

The cork and subliming epoxy coatings were severely degraded in this test. It is doubtful if either material provided any degree of substrate protection after 75 seconds exposure. In contrast, the phenolic-asbestos felt material experienced only a slight decrease in weight, probably due to a loss of phenolic-resin, and was unchanged in appearance after test.

It would appear from the temperature-time histories of these tests that the thermal conductivity of the phenolic-asbestos felt was somewhat higher than the cork or subliming epoxy. However a direct comparison of sample temperatures may not be completely valid due to differences in substrate construction and thermocouple position.

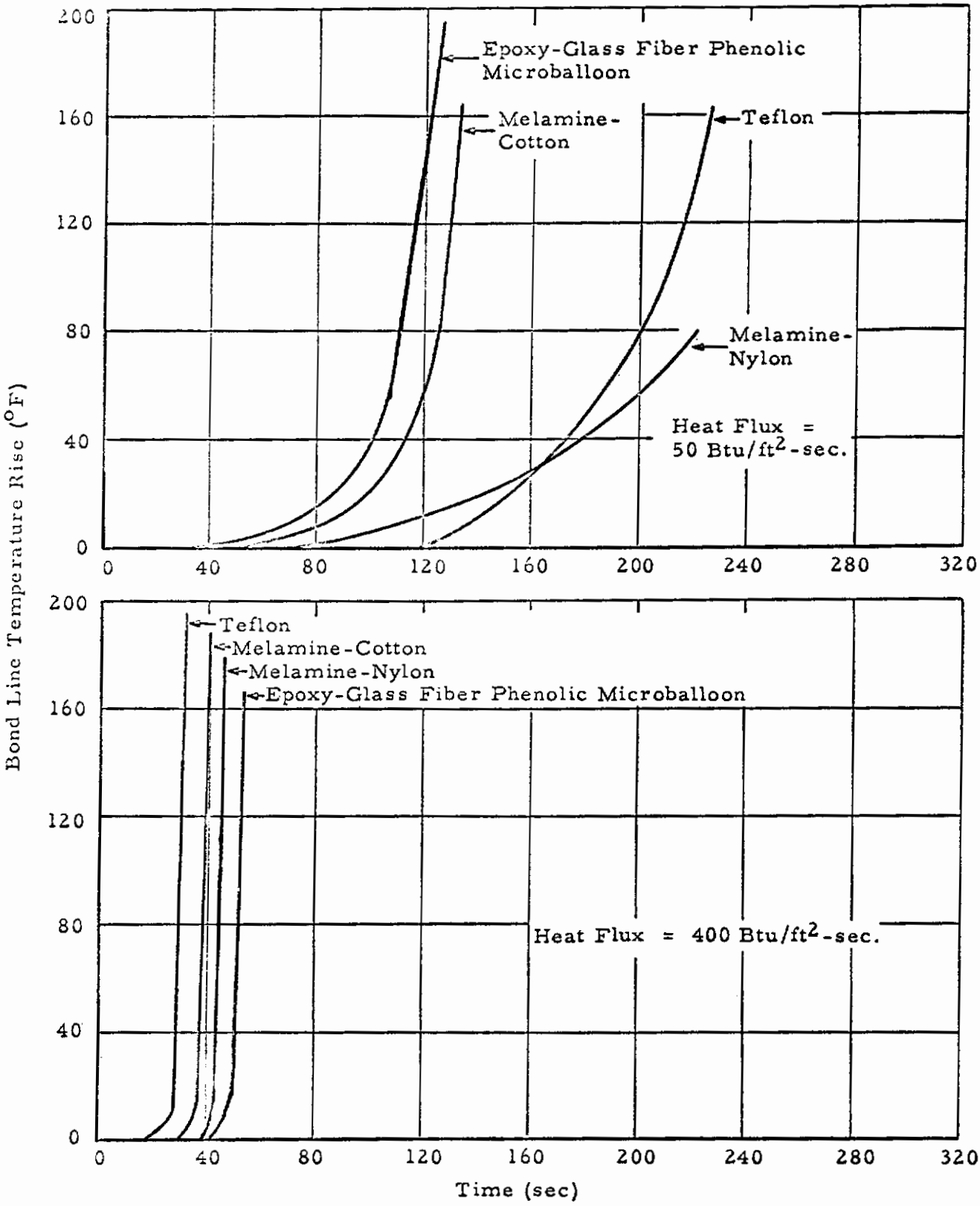

Figure 119. Bond Line Temperature-Time History of Several Ablative Coatings.

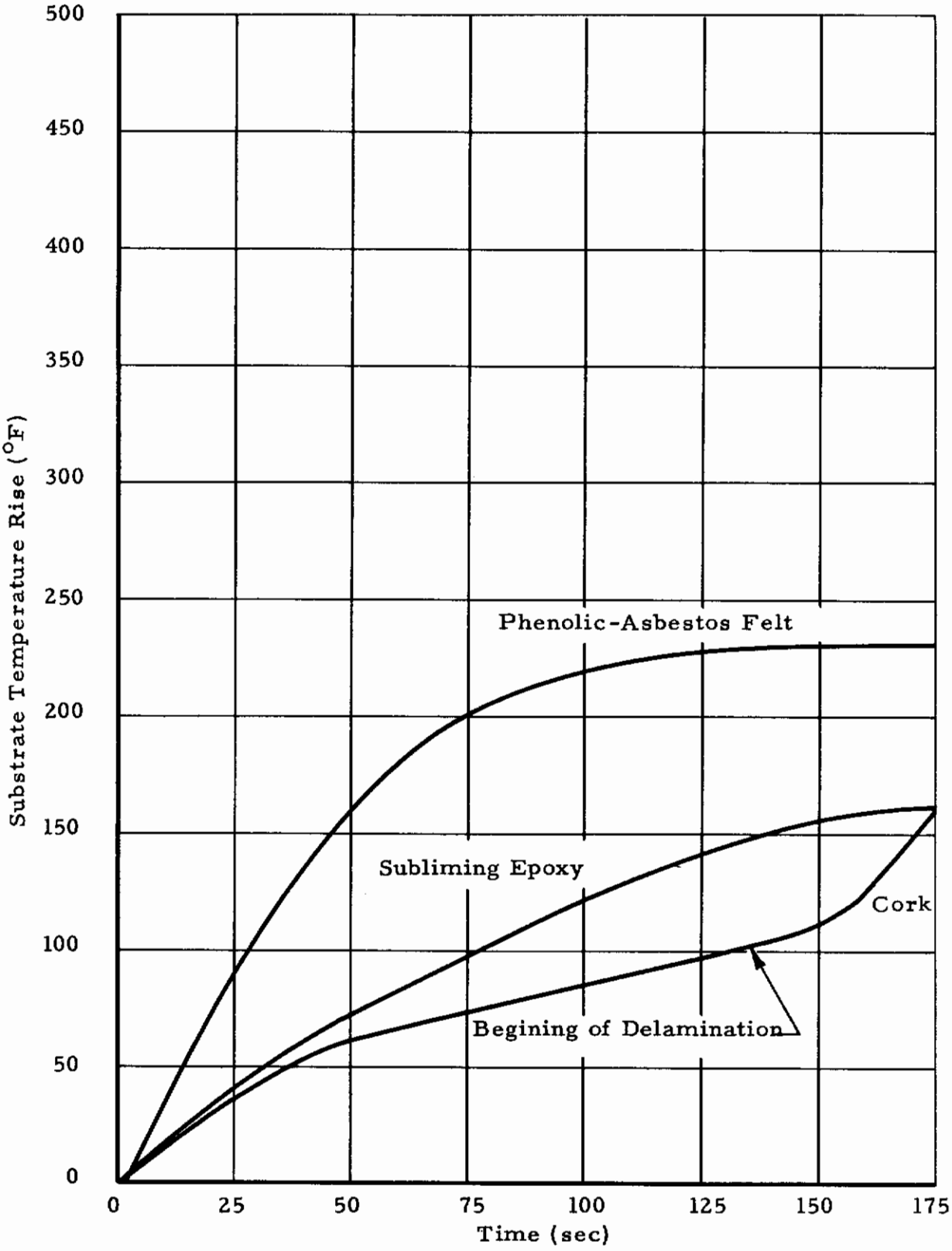

Figure 120. Temperature Time History of Protective Coatings Exposed to a 10 Btu/ft^2-sec Environment (Test 1)

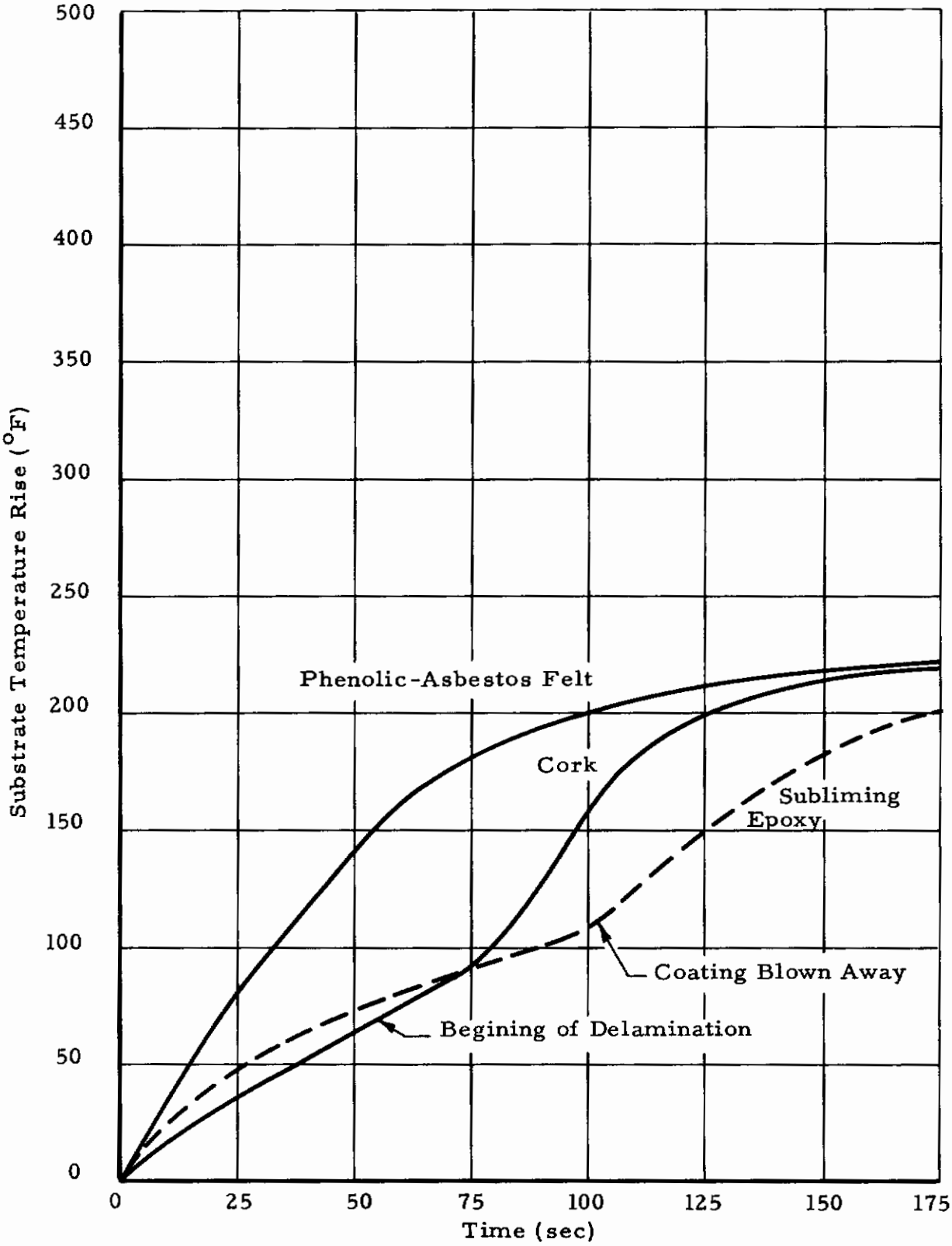

Figure 121. Temperature Time History of Protective Coatings Exposed to a 10 Btu/ft^2-sec Environment (Test 2)

1x

Cork

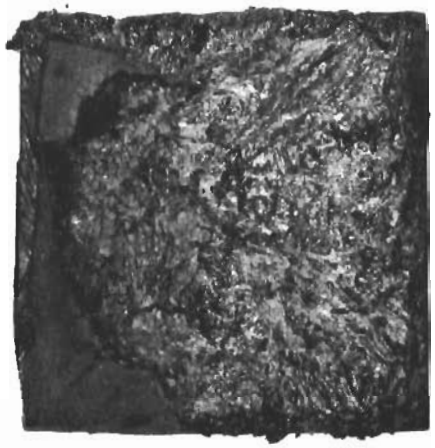

1x

Subliming Epoxy

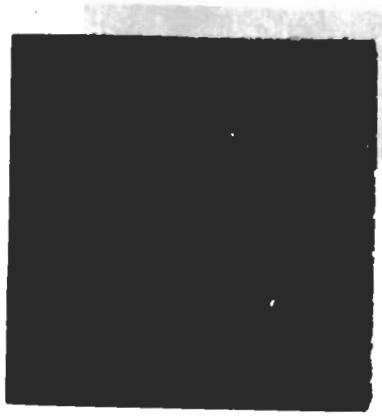

1x

Phenolic Asbestos Felt

Figure 122. Photographs of Protective Coatings after Exposure to a 10 Btu/ft^2-sec Heat Flux Environment (Test 1).

1x

Cork

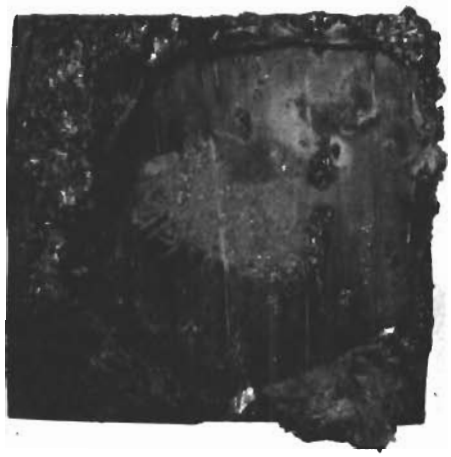

1x

Subliming Epoxy

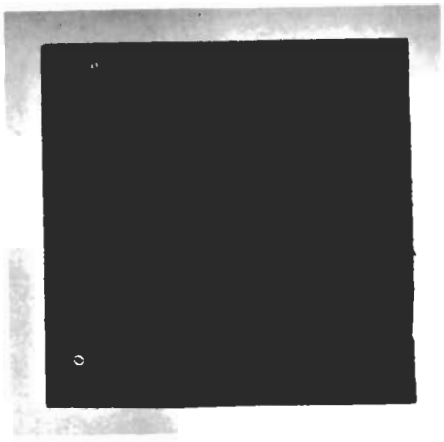

1x

Phenolic Asbestos Felt

Figure 123. Photographs of Protective Coatings after Exposure to a 10 Btu/ft^2-sec Heat Flux Environment (Test 2).

Table 43. Nominal Test Conditions for Ablative Coating Tests.

Heat Flux (Btu/ft^2-sec)	400	100	50
Enthalpy (Btu/lb)	3180	1120	800
Stagnation Pressure (psi)	0.686	0.329	0.235
Effluent Velocity (fps)	1060	510	360
Effluent Mass Flow (lb/sec)	0.0082	0.0082	0.0082
Effluent Composition	79% N_2 21% O_2	79% N_2 21% O_2	79% N_2 21% O_2

Table 44. Summary of Ablative Coatings Tests

Specimen Identification	Heat Flux (Btu/ft^2-sec)	Orientation Angle (Degrees)	Penetration Time (sec)	Density (gm/cc) Before	Density (gm/cc) After	Erosion Volume (cc)	Erosion Depth (in.)	Weight Loss gms	Weight Loss %
Lucite	400	45	22.0	1.22	1.22	17.8	0.503	20.7	53.5
	400	90	20.5	1.22	1.24	17.0	0.506	20.6	52.0
	100	45	35.5	1.22	1.21	16.9	0.499	20.7	52.4
	100	90	35.0	1.22	1.22	16.7	0.502	20.6	52.4
	50	45	55.0	1.22	1.22	17.2		20.9	54.4
Teflon	400	45	34.5	2.10	2.10	16.8	0.536	34.9	58.0
	400	90	30.0	2.10	2.07	15.8	0.536	31.4	52.0
	100	45	87.5	2.10	2.05	14.3	0.536	31.0	51.6
	100	90	89.0	2.10	2.10	15.8	0.536	30.9	51.0
	50	45	222.0	2.10	2.10	12.5		26.3	44.0
55% Melamine 45% Cotton	400	45	42.5	1.52	1.41	18.5	0.528	25.1	47.0
	400	90	45.2	1.52	1.40	18.7	0.528	28.3	54.0
	100	45	89.0	1.52	1.40	16.1	0.528	28.1	55.5
	100	90	85.6	1.52	1.42	17.3	0.528	28.1	55.4
	50	45	129.0	1.52	1.32	16.1	0.528	28.1	55.0
50% Melamine 50% Nylon	400	45	52.0	1.28	1.17	14.0	0.528	21.1	47.0
	400	90	51.2	1.28	1.11	13.4	0.528	20.4	48.0
	100	45	104.0	1.28	1.12	15.0	0.528	22.1	52.0
	100	90	103.5	1.28	1.14	14.9	0.528	21.6	50.5
	50	45	217.0	1.28	1.18	13.1	0.528	18.7	43.6
55% Phenolic 45% Nylon	400	45	63.0	1.16	1.00	17.2	0.542	22.7	56.4
	400	90	61.0	1.16	1.04	16.6	0.542	21.7	53.6
	100	45	90.0	1.16	1.02	15.6	0.542	20.6	51.8
	100	90	90.0	1.16	1.07	18.2	0.542	21.7	52.5
	50	45	116.0	1.16	0.98	15.9	0.542	22.0	56.4
55% Epoxy 10% Glass Fiber 35% Phenolic Microballoons	400	45	57.0	0.68	0.51	16.7	0.435	14.3	62.0
	400	90	49.0	0.68	0.55	14.8	0.382	12.6	54.2
	100	45	110.0	0.68	0.51	19.1	0.524	15.4	68.0
	100	90	156.5	0.68	0.57	18.0	0.524	14.5	63.4
	50	45	138.0	0.68	0.53	19.2	0.524	15.3	65.0

Table 45. Test Conditions and Results for Low Heat Flux Coating Evaluation.

	Material	Heat Flux (Btu/ft^2-sec)	Stagnation Pressure (psi)	Original Weight (gms)	Final Weight (gms)	Remarks
Test 1	Cork	10.9	0.0541	43.9	37.1	Delamination began at 135 seconds
	Subliming Epoxy	10.9	0.0541	45.4	38.9	At 30 seconds coating blistered, partial delamination at 60 sec.
	Phenolic - Asbestos Felt	9.8	0.0541	21.8	20.4	No change in appearance
Test 2	Cork	10.9	0.0541	44.1	37.3	Delamination began at 60 seconds
	Subliming Epoxy	10.9	0.0541	46.9	38.0	Blistering at 15 sec, partial delamination at 60 sec, majority of coating lost at 105 sec.
	Phenolic - Asbestos Felt	10.4	0.0541	21.9	20.6	No change in appearance